



Calhoun: The NPS Institutional Archive
DSpace Repository

Theses and Dissertations

1. Thesis and Dissertation Collection, all items

1990-09

Measurement of the Space Thermoacoustic Refrigerator performance

Adeff, Jay Andrew

Monterey, California. Naval Postgraduate School

<http://hdl.handle.net/10945/30730>

Downloaded from NPS Archive: Calhoun



Calhoun is a project of the Dudley Knox Library at NPS, furthering the precepts and goals of open government and government transparency. All information contained herein has been approved for release by the NPS Public Affairs Officer.

Dudley Knox Library / Naval Postgraduate School
411 Dyer Road / 1 University Circle
Monterey, California USA 93943

<http://www.nps.edu/library>

AD-A241 320



2

NAVAL POSTGRADUATE SCHOOL Monterey, California



DTIC
SELECTED
OCT. 10, 1991
S B D

THESIS

MEASUREMENT OF THE SPACE
THERMOACOUSTIC REFRIGERATOR PERFORMANCE

by

Jay Andrew Adef

September 1990

Thesis Advisor:

Thomas J. Hofler

Co-Advisor:

Steven L. Garrett

Approved for public release; distribution is unlimited.

91-12526



UNCLASSIFIED

SECURITY CLASSIFICATION OF THIS PAGE

REPORT DOCUMENTATION PAGE				Form Approved OMB No 0704-0188	
1a REPORT SECURITY CLASSIFICATION UNCLASSIFIED			1b RESTRICTIVE MARKINGS		
2a SECURITY CLASSIFICATION AUTHORITY			3 DISTRIBUTION AVAILABILITY OF REPORT Approved for public release; distribution is unlimited		
2b DECLASSIFICATION/DOWNGRADING SCHEDULE					
4 PERFORMING ORGANIZATION REPORT NUMBER(S)			5 MONITORING ORGANIZATION REPORT NUMBER(S)		
6a NAME OF PERFORMING ORGANIZATION Naval Postgraduate School		6b OFFICE SYMBOL (If applicable) PH	7a NAME OF MONITORING ORGANIZATION Naval Postgraduate School		
6c ADDRESS (City, State, and ZIP Code) Monterey, CA 93943-5000			7b ADDRESS (City, State, and ZIP Code) Monterey, CA 93943-5000		
8a NAME OF FUNDING SPONSORING ORGANIZATION Naval Research Laboratory		8b OFFICE SYMBOL (If applicable) 8220	9 PROCUREMENT INSTRUMENT IDENTIFICATION NUMBER		
8c ADDRESS (City, State and ZIP Code) 4555 Overlook Avenue Washington, DC 20375-5000			10 SOURCE OF FUNDING NUMBERS		
			PROGRAM ELEMENT NO	PROJECT NO	TASK NO
					WORK UNIT ACCESSION NO
11 TITLE (Include Security Classification) MEASUREMENT OF THE SPACE THERMOACOUSTIC REFRIGERATOR PERFORMANCE					
12 PERSONAL AUTHOR(S) Adeff, Jay A.					
13a TYPE OF REPORT Master's Thesis		13b TIME COVERED FROM _____ TO _____		14 DATE OF REPORT (Year, Month, Day) September 1990	15 PAGE COUNT 241
16 SUPPLEMENTARY NOTATION The views expressed in this thesis are those of the author and do not reflect the official policy or position of the Department of Defense or the U.S. Government.					
17 COSATI CODES			18 SUBJECT TERMS (Continue on reverse if necessary and identify by block number)		
FIELD	GROUP	SUB-GROUP	Space thermoacoustic refrigerator, NASA G-337 (Payload number), heat engine, thermoacoustic stack, helium replaces freon		
19 ABSTRACT (Continue on reverse if necessary and identify by block number) This is the fifth thesis of the Space Thermoacoustic Refrigerator (STAR) project which will be launched aboard the Space Shuttle in 1991 to demonstrate the potential of this technology for cooling satellite electronics and sensors. It describes the design, construction, and testing of the resonator portion of the refrigerator along with its integration with the existing driver and control electronics which were the subject of four previous theses. This resonator incorporates a helium diffusion barrier enabling it to hold ten atmospheres of working gas without leaking. An optimum operating frequency has been chosen based on electroacoustic efficiency measurements and the refrigerator has been allowed to run continuously and autonomously for up to one week at a time to simulate the planned space flight. A lowest temperature of -50°C at a temperature ratio of $T_c/T_h = 0.75$ and a maximum coefficient of performance relative to Carnot of 14 percent has been obtained.					
20 DISTRIBUTION AVAILABILITY OF ABSTRACT <input checked="" type="checkbox"/> UNCLASSIFIED UNLIMITED <input type="checkbox"/> SAME AS RPT <input type="checkbox"/> DTIC USERS			21 ABSTRACT SECURITY CLASSIFICATION UNCLASSIFIED		
22a NAME OF RESPONSIBLE INDIVIDUAL Professor Garrett			22b TELEPHONE (Include Area Code) 408-646-2540	22c OFFICE SYMBOL PH/Gx	

DD Form 1473, JUN 86

Previous editions are obsolete

SECURITY CLASSIFICATION OF THIS PAGE

S/N 0102-LF-014-6603

UNCLASSIFIED

Approved for public release; distribution is unlimited.

Measurement of the
Space Thermoacoustic Refrigerator Performance

by

Jay Andrew Adeff

Submitted in partial fulfillment of the
requirements for the degree of

MASTER OF SCIENCE IN PHYSICS

from the

NAVAL POSTGRADUATE SCHOOL
September 1990

Author;

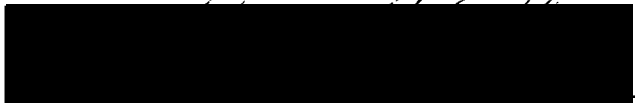


Jay Andrew Adeff

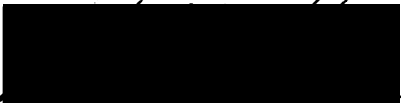
Approved by;



Thomas J. Hofler, Thesis Advisor



Steven L. Garrett, Co-Advisor



K.E. Woehler, Chairman,
Department of Physics

ABSTRACT

This is the fifth thesis of the Space Thermoacoustic Refrigerator (STAR) project which will be launched aboard the Space Shuttle in 1991 to demonstrate the potential of this technology for cooling satellite electronics and sensors. It describes the design, construction, and testing of the resonator portion of the refrigerator along with its integration with the existing driver and control electronics which were the subject of four previous theses. This resonator incorporates a helium diffusion barrier enabling it to hold ten atmospheres of working gas without leaking. An optimum operating frequency has been chosen based on electroacoustic efficiency measurements and the refrigerator has been allowed to run continuously and autonomously for up to one week at a time to simulate the planned space flight. A lowest temperature of -50°C at a temperature ratio of $T_c/T_h=0.75$ and a maximum coefficient of performance relative to Carnot of 14 percent has been obtained.



Accession For	
NTIS GRA&I	<input checked="" type="checkbox"/>
DTIC TAB	<input type="checkbox"/>
Unannounced	<input type="checkbox"/>
Justification _____	
By _____	
Distribution/ _____	
Availability Codes	
Dist	Avail and/or special
A-1	

TABLE OF CONTENTS

I.	INTRODUCTION.....	1
A.	BACKGROUND.....	1
1.	History of Thermoacoustics.....	1
2.	History of STAR.....	4
B.	STAR.....	8
1.	Acoustical Subsystems.....	8
2.	Electrical Subsystems.....	12
3.	NASA Get Away Special Program.....	15
C.	SCOPE.....	17
II.	THEORETICAL ASPECTS OF THERMOACOUSTICS.....	19
A.	INTRODUCTION.....	19
B.	INTUITIVE APPROACH.....	21
1.	Thermodynamics Background.....	21
2.	Acoustic Heat Engine Cycle.....	22
C.	MATHEMATICAL APPROACH.....	26
1.	Single Plate Model.....	26
2.	A More Realistic Model.....	39
III.	RESONATOR.....	44
A.	OVERVIEW.....	44
B.	VERSION ONE.....	48
1.	Design and Description.....	48
2.	Assembly.....	50
3.	Leak Testing.....	54

4.	Instrumentation.....	57
5.	Failure and Recommendations.....	62
C.	VERSION TWO.....	65
1.	Design and Description.....	65
2.	Assembly.....	68
3.	Leak Test.....	70
D.	THERMOACOUSTIC STACK AND HEAT EXCHANGERS.....	70
1.	Stack.....	70
2.	Heat Exchangers.....	75
E.	THERMAL LOSSES.....	83
1.	Heat Leak.....	83
2.	Thermal Vacuum Can.....	84
IV.	STAR DRIVER.....	89
A.	OVERVIEW.....	89
B.	THE DRIVER.....	90
1.	Driver Design and Construction.....	90
2.	Driver Housing.....	92
C.	RESONANCE CONTROL BOARD.....	95
D.	DRIVER HOUSING COOLING SYSTEM.....	101
V.	GAS DISTRIBUTION SYSTEM.....	104
A.	FILLING AND PURGING MANIFOLD.....	104
B.	GAS MIXING MANIFOLD.....	108
C.	GAS ANALYZER.....	110
D.	CONSTRUCTION DETAILS.....	113
E.	FILLING AND PURGING PROCEDURE.....	116

VI. REFRIGERATOR PERFORMANCE.....	120
A. ELECTROACOUSTIC EFFICIENCY.....	120
B. DATA ACQUISITION AND ANALYSIS.....	145
C. NO HEAT LOAD.....	149
D. TEMPERATURE RATIO AND COEFFICIENT OF PERFORMANCE.....	155
E. FAILSAFE PROTECTION.....	162
VII CONCLUSIONS AND RECOMMENDATIONS.....	174
APPENDIX A - DATA ACQUISITION SYSTEM.....	177
APPENDIX B - POWER MEASUREMENT CIRCUIT.....	180
APPENDIX C - THE HOFER TUBE FROM HELL.....	184
APPENDIX D - CONSTRUCTION DRAWINGS.....	189
APPENDIX E - MANUFACTURER'S SPECIFICATIONS.....	217
REFERENCES.....	221
BIBLIOGRAPHY.....	223
INITIAL DISTRIBUTION LIST.....	224

LIST OF FIGURES

I-1	Pulse Tube Refrigerator.....	3
I-2	Hofler Refrigerator.....	5
I-3	Acoustical Subsystems.....	9
I-4	Electrical Subsystems.....	13
I-5	NASA Get Away Special Cannister.....	16
II-1	Prime Mover and Heat Pump.....	20
II-2	Heat Pump Cycle.....	24
II-3	Acoustic Heat Pump Thermodynamic Cycles.....	25
II-4	Single Plate in acoustic Standing Wave.....	27
II-5	Heat Flux Density.....	35
III-1	Three Resonator Geometries.....	45
III-2	STAR Resonator.....	47
III-3	Resonator Foil Soldering Set-Up.....	51
III-4	Resonator Leak Test Set-Up.....	55
III-5	Strip Heater Resistance.....	61
III-6	Modified Resonator Reducer.....	66
III-7	Cold Heat Exchanger Insert and Filler Ring.....	67
III-8	Completed Resonator.....	71
III-9	Stack Winding Loom.....	73
III-10	Completed Stack.....	76
III-11	Heat Exchanger.....	77
III-12	Heat Exchanger Assembly Jig.....	78
III-13	Unplated Heat Exchanger Stack.....	81

III-14	Heat Exchanger Slice.....	82
III-15	Thermal Vacuum Cannister.....	86
III-16	Vacuum Cannister and Diffusion Pump.....	87
IV-1	STAR Driver.....	91
IV-2a	Resonance Control Board Schematic.....	96
IV-2b	Resonance Control Board Schematic.....	97
IV-3	Driver Housing Cooling Band.....	102
V-1	Gas Distribution Panel.....	105
V-2	Gas Analyzer Cross Section.....	112
V-3	Gas Flow Controller Accuracy.....	114
VI-1	Bellows Displacement Versus Frequency.....	122
VI-2	Bellows Displacement Test Comparison.....	123
VI-3	Mechanical Resonance Versus Mean Pressure.....	124
VI-4a	Microphone and Accelerometer Outputs for Helium.....	126
VI-4b	Microphone and Accelerometer Outputs for Helium and 3.71% Argon.....	127
VI-4c	Microphone and Accelerometer Outputs for Helium and 6.42% Argon.....	128
VI-4d	Microphone and Accelerometer Outputs for Helium and 7.94% Argon.....	129
VI-4e	Microphone and Accelerometer Outputs for Helium and 10.1% Argon.....	130
VI-4f	Microphone and Accelerometer Outputs for Helium and 12.4% Argon.....	131
VI-4g	Microphone and Accelerometer Outputs for Helium and 16.0% Argon.....	132
VI-4h	Microphone and Accelerometer Outputs for Helium and 18.9% Argon.....	133
VI-5a	Electroacoustic Efficiency for Helium.....	136

VI-5b	Electroacoustic Efficiency for Helium and 3.71% Argon.....	137
VI-5c	Electroacoustic Efficiency for Helium and 6.42% Argon.....	138
VI-5d	Electroacoustic Efficiency for Helium and 7.94% Argon.....	139
VI-5e	Electroacoustic Efficiency for Helium and 10.1% Argon.....	140
VI-5f	Electroacoustic Efficiency for Helium and 12.4% Argon.....	141
VI-5g	Electroacoustic Efficiency for Helium and 16.0% Argon.....	142
VI-5h	Electroacoustic Efficiency for Helium and 18.9% Argon.....	143
VI-6	Electroacoustic Efficiency Versus Operating Frequency.....	144
VI-7	Warm-Up Data for Resonator 1.....	150
VI-8	Warm-Up Data for Resonator 2.....	152
VI-9	Cool-Down Rate for Medium Power.....	153
VI-10	Cool-Down Rate for Full Power.....	154
VI-11	Temperature Ratio Versus Heat Load at Medium Power.....	158
VI-12	Temperature Ratio Versus Heat Load at Full Power.....	159
VI-13	COPR at Medium Power.....	160
VI-14	COPR at Full Power.....	161
VI-15	Amplifier Relay Circuit.....	163
VI-16	Diffusion Pump Relay Circuit.....	166
VI-17	Failsafe Protection Circuit.....	169
B-1	Power Measurement Circuit.....	183
C-1	Hofler Tube Cross Section (not to scale).....	186

C-2	Photograph of Hofler Tube.....	188
D-1	Resonator Parts Identification Drawing.....	190
D-2	Resonator Flange.....	191
D-3	Resonator Flange.....	192
D-4	Hot Heat Exchanger Insert.....	193
D-5	Top Grip Ring.....	194
D-6	Heat Exchangers.....	195
D-7	Phenolic Sleeve.....	196
D-8	Reducer.....	197
D-9	Cold Heat Exchanger Mounting Ring and Filler.....	198
D-10	Bottom Grip Ring.....	199
D-11	Copper Sleeve.....	200
D-12	Sphere Fitting.....	201
D-13	Trumpet.....	202
D-14	Screw Head Enlargement.....	203
D-15	Stainless Foil Soldering Assembly.....	204
D-16	Thermal Plate.....	205
D-17	Thermal Post.....	206
D-18	Sheet Clamp.....	207
D-19	Assembly Plug.....	208
D-20	Plug With Strip.....	209
D-21	Stainless Sleeve.....	210
D-22	Thermal Sleeve.....	211
D-23	Heat Exchanger Insert Extractor Tool.....	212
D-24	FRP Outer Diameter.....	213
D-25	Vacuum Cannister Base Plate.....	214

D-26	Top View of Feed-Through.....	215
D-27	Vacuum Cannister Flange.....	216

TABLE OF SYMBOLS AND SUBSCRIPTS

SYMBOLS

A	area
c	sound speed
C	centigrade
CFM	cubic feet per minute
COP	coefficient of performance
COPR	coefficient of performance relative to Carnot
c_p	isobaric heat capacity per unit mass
c_v	isochoric heat capacity per unit mass
f	frequency
F	Farad
H	total energy flux
I	electric current
Im	imaginary part of
k	wave number or stiffness
K	thermal conductivity or Kelvin
m	mass or meter
N	Newton
P,p	pressure
PSI	pounds per square inch
PSIA	pounds per square inch, absolute
PSIG	pounds per square inch, gage

\bar{Q}	heat flux
q	heat flux per unit area
R	universal gas constant or resistance
Re	real part of
RMS	root mean square
S	entropy
s	entropy per unit mass
SCCM	standard cubic centimeter per minute
T	temperature
t	time
U	volume velocity
u	velocity
V	volume or voltage
W	Watt
\bar{W}	acoustic power
w	power per unit volume
x	position
Z	impedance
β	thermal expansion coefficient
Γ	normalized temperature gradient
γ	ratio of isobaric to isochoric specific heats
Δx	plate length
δ	penetration depth
ϵ_s	plate heat capacity ratio
η	efficiency

κ	thermal diffusivity
λ	wavelength
μ	dynamic viscosity
ν	kinematic viscosity
Π	perimeter
ρ	density
σ	Prandtl number
τ	period of oscillation or time constant
ϕ	phase angle
Ω	Ohms
ω	angular frequency

SUBSCRIPTS

A	amplitude
ac	acoustic
C	Carnot
c	cold
h	hot
m	mean
s	solid plate
κ	thermal
ν	viscous
1	first order
2	second order

ACKNOWLEDGEMENT

The author would like to thank the following people for their support and assistance in building the STAR resonator and getting the refrigerator running.

Mr. Glenn Harrell, Craftsman Par Excellence of the Naval Postgraduate School, for his unparalleled expertise in machining all of the parts necessary to make the project work.

Mr. David Rigmaiden, of the Naval Postgraduate school, for his unceasing devotion to the task of bringing STAR through the hopelessly complicated maze of NASA certification requirements, and for his relentless pursuit of establishing a proper machining facility for Mr. Harrell.

Mr. Thomas Kawecki, of the Naval Research Laboratories, for his valuable assistance in providing funding, parts, and instrumentation, particularly when all formal NPS channels had been exhausted.

Finally, the author would like to thank his thesis advisors for giving him the strength and courage to do what had to be done.

I. INTRODUCTION

This thesis describes the design, construction, and testing of the resonator for the Space Thermoacoustic Refrigerator (STAR), as well as the integration of the acoustical and electrical subsystems as designed by Harris and Volkert [Ref. 1] and Byrnes [Ref. 2], respectively. Additionally, thermoacoustic improvements by Susalla [Ref. 3] to Hofler's original refrigerator [Ref. 4] are utilized in establishing the actual working heat pump.

A. BACKGROUND

1. History of Thermoacoustics

The earliest known example of thermoacoustics, and acoustical prime movers in particular, is the Sondhaus tube. Glass blowers in the eighteenth century noticed that when a hot glass bulb was attached to a cool glass tube, the tube opening would emit sound. Sondhaus examined the relation between the pitch of the sound and the size of the apparatus while Rayleigh, by 1896, correctly explained the phenomena in a qualitative manner. A second important phenomenon is the Taconis oscillations in which a gas-filled tube, exposed to room temperature on one end and liquid helium temperature (4° K) on the opposite end, oscillates with extremely high

amplitudes. Again, Taconis explained the occurrence in the same qualitative manner as did Rayleigh.

The first example of an acoustic heat pump was the pulse-tube refrigerator in which Gifford and Longworth, by applying low-frequency high-amplitude oscillations to one end of a closed chamber, achieved a temperature ratio of $T_C/T_H=1/2$ with the cold end being at that end where the oscillations were applied (Figure I-1). At about the same time, Merkli and Thomann found that, in an acoustic standing wave in a duct with walls at uniform temperature, heat is transported from the region near the velocity antinode to the region near the adjacent pressure antinode.

A significant improvement to thermoacoustic performance came about in 1962 when Carter found that the Sondhaus effect was augmented by placing a stack of parallel plates within the tube section. This effect is best exemplified by the Hofler Tube (Appendix D) in which very high amplitude oscillations are induced in a quarter wavelength tube by applying a large temperature gradient across a stack of plates located approximately half way between the ends of the tube.

The theoretical explanation of these thermoacoustic effects began with Kirchoff in 1868 when he explained the attenuation of sound waves in a duct due to thermal diffusion between the isothermal duct walls and the gas supporting the sound waves. And while several unsuccessful

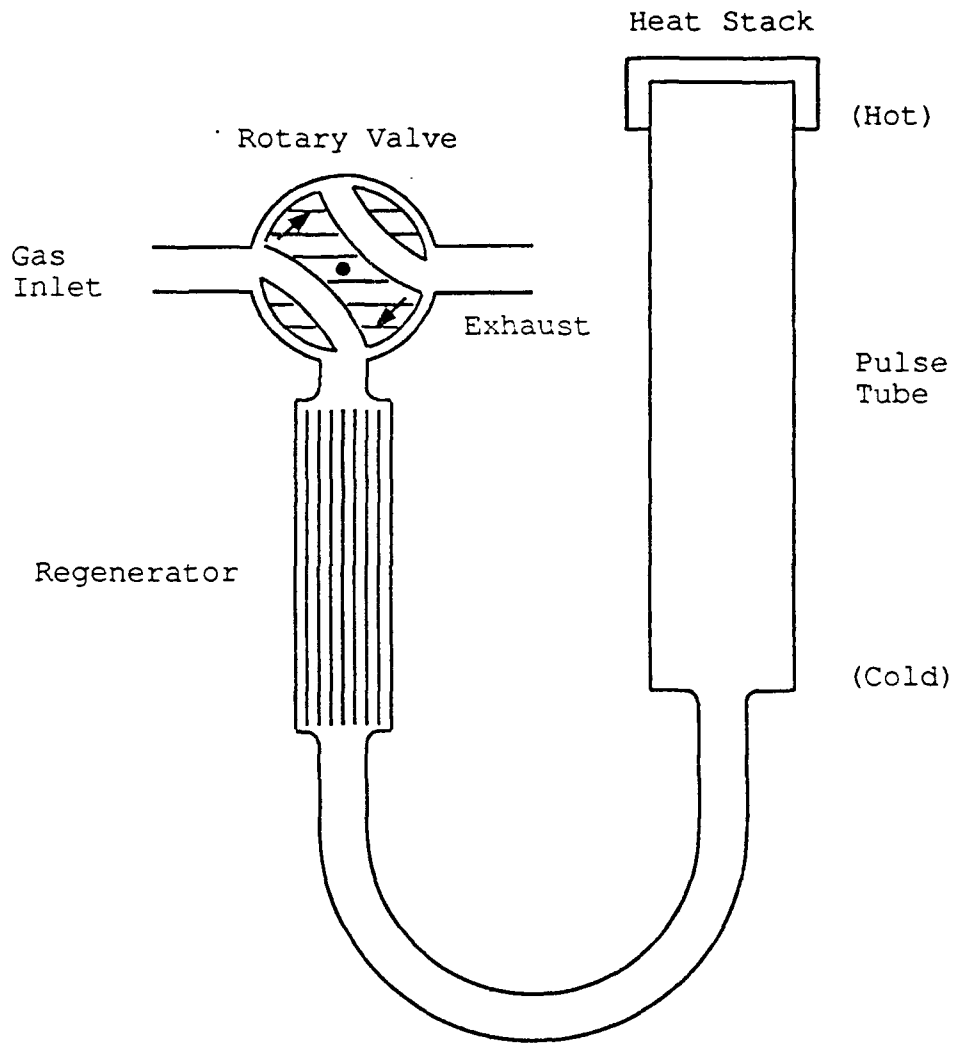


Figure I-1. Pulse Tube Refrigerator

attempts were made by others to further thermoacoustic theory, it was Rott, beginning in 1969, who finally established a complete theory for heat driven oscillations and acoustic heat transport that could be successfully applied to thermoacoustic heat pumps and refrigerators.

Hofler, for his part, was able to numerically solve the Rott equations and apply them to the research being conducted by J.C. Wheatly and Greg Swift and himself as he persued his Doctoral degree at the Los Alamos National Laboratory. Hofler designed and built a working thermoacoustic refrigerator and made measurements of its thermoacoustic efficiency accounting for all energy losses and loads.

2. History of STAR

The history of STAR begins with the Hofler Ph.D thesis refrigerator (Figure I-2). This project provided a means for performing controlled experiments which tested thermoacoustic theory and was a pioneering step toward a practical thermoacoustic cryocooler. This thermoacoustic heat pump consisted of a modified 1/4 wavelength resonator pressurized with ten atmospheres of helium and driven by an electrodynamic loudspeaker at about 500 Hz. It contained a stack of parallel plates with the hot end maintained at room temperature T_h . This stack was actually a long piece of 0.08 mm thick plastic sheet wound spirally around a 1/4 inch diameter rod. Lengths of fishing line where glued

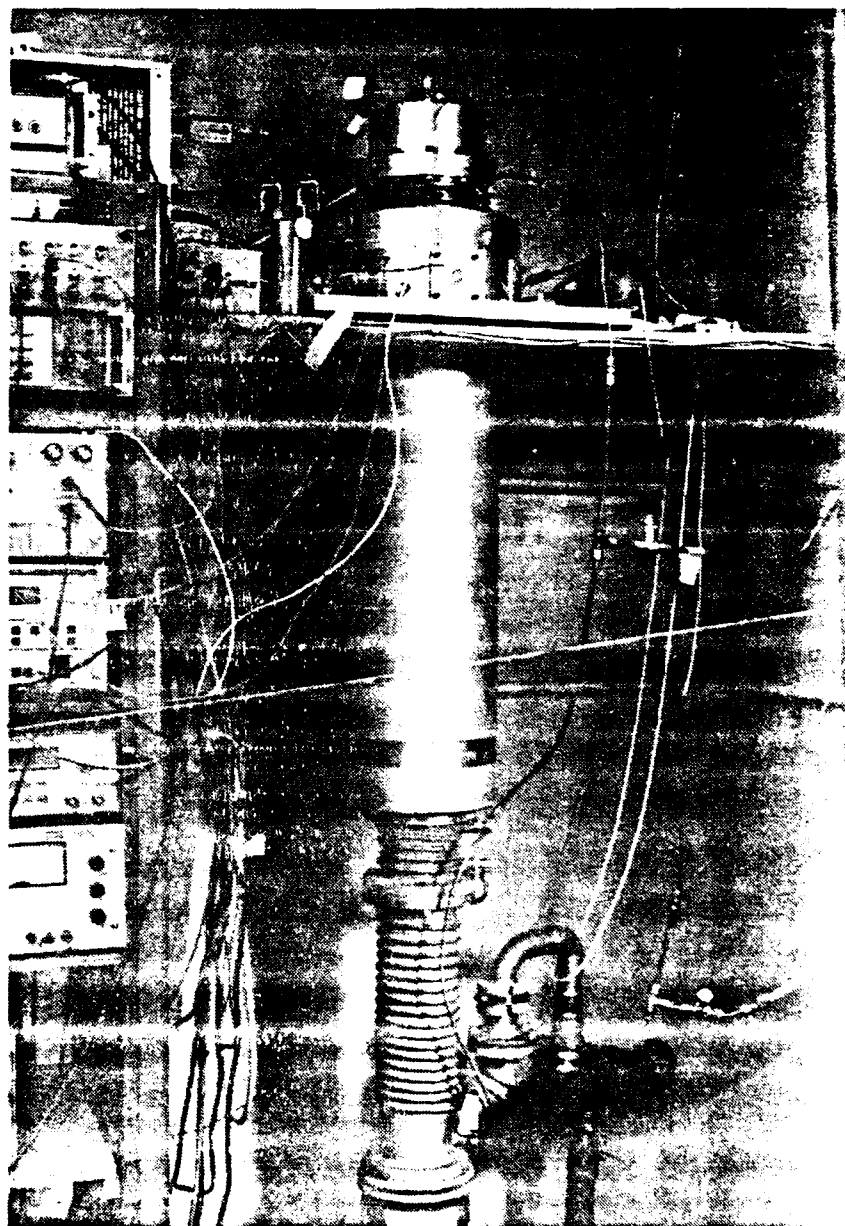


Figure I-2. Hofler Refrigerator

transversely on to the sheet to give a constant spacing. The length and diameter of the stack were 8 cm and 3.8 cm, respectively. The loudspeaker delivered thirteen watts of acoustic power to the resonator with an electroacoustic conversion efficiency of twenty percent. The lowest temperature obtained was $T_C=200^\circ$ K, producing a temperature ratio of $T_C/T_H=0.67$. The highest measured efficiency was twelve percent of Carnot at $T_C/T_H=0.82$ and with an applied heat load of three watts.

Having moved to the Naval Postgraduate school (NPS) to continue his post doctoral studies, Hofler together with Steven Garrett proposed the design and construction of a thermoacoustic cryocooler based on the Hofler thesis refrigerator to be launched aboard the Space Shuttle in a "Get Away Special" (GAS) package. The first two theses, in a succession of theses culminating in this one, were done by Susalla and Fitzpatrick in which several improvements to the Hofler refrigerator were tested. The efficiency of the refrigerator was significantly improved by using a mixture of helium and xenon which lowers the Prandtl number of the working medium and improves the intrinsic thermodynamic performance of the stack. In addition, various stack modifications and variations were explored.

The Fitzpatrick thesis presented a preliminary design for an electrodynamic driver for the proposed space cryocooler, along with a design for the helium tight driver

housing with electrical feed-throughs, microphone, accelerometer, and pressure gauge. A modified JBL 2450J neodymium-iron-boron compression driver was selected because of the considerable weight reduction afforded by this new and highly energetic magnet material. Additionally, Fitzpatrick described techniques for measuring the electrical and mechanical parameters of the driver.

The team of Harris and Volkert took on the task of actually building the flight driver and housing as their thesis. The measured efficiency for the driver with a 1/2 wavelength straight tube resonator was in close agreement with the predicted values. It was found that a maximum electroacoustic efficiency of 50% was obtained when the resonant frequency of the driver matched the resonant frequency of a mock refrigerator-like resonator with stack. A useful observation was that the efficiency decreased by only 10% when the resonator and driver resonance frequencies were off by as much as +/-14%. A design for the flight resonator was also presented along with preliminary tests for a low heat conduction wall for the stack section of the resonator that would hold 10 atmospheres of helium without diffusive losses. This wall consisted of a 0.001 inch stainless steel foil tube soldered at both ends to copper subsections and then wrapped with resin saturated fiberglass tape to provide strength.

B. STAR

1. Acoustical Subsystems

The acoustical subsystems, show in Figure I-3, that will be described in this thesis are the electrodynamic driver, driver housing, resonator, thermoacoustic stack and heat exchangers, thermal isolation vacuum chamber, and gas handling and analysis system. The first two subsystems, while having been designed and built by previous thesis students, will require extensive description both because of the dependence of this thesis on those subsystems and because modifications were made to the original design in the construction of back up units. The remainder of the subsystems as well as the back up units were constructed and tested by the author.

The driver housing does more than simply hold the electrodynamic driver. The considerable mass and size of the housing in relation to the driver serves as a heat sink for the heat generated by the driver and the heat pumped away from the cold end of the resonator. And, while cooling coils will be wrapped around the driver housing for ground based testing, in flight configuration the housing will be bolted to a standard 12 inch bolt circle provided on the GAS cannister lid which will act as a massive radiator/heat-sink. Additionally, the driver housing must be capable of containing ten atmospheres of helium.

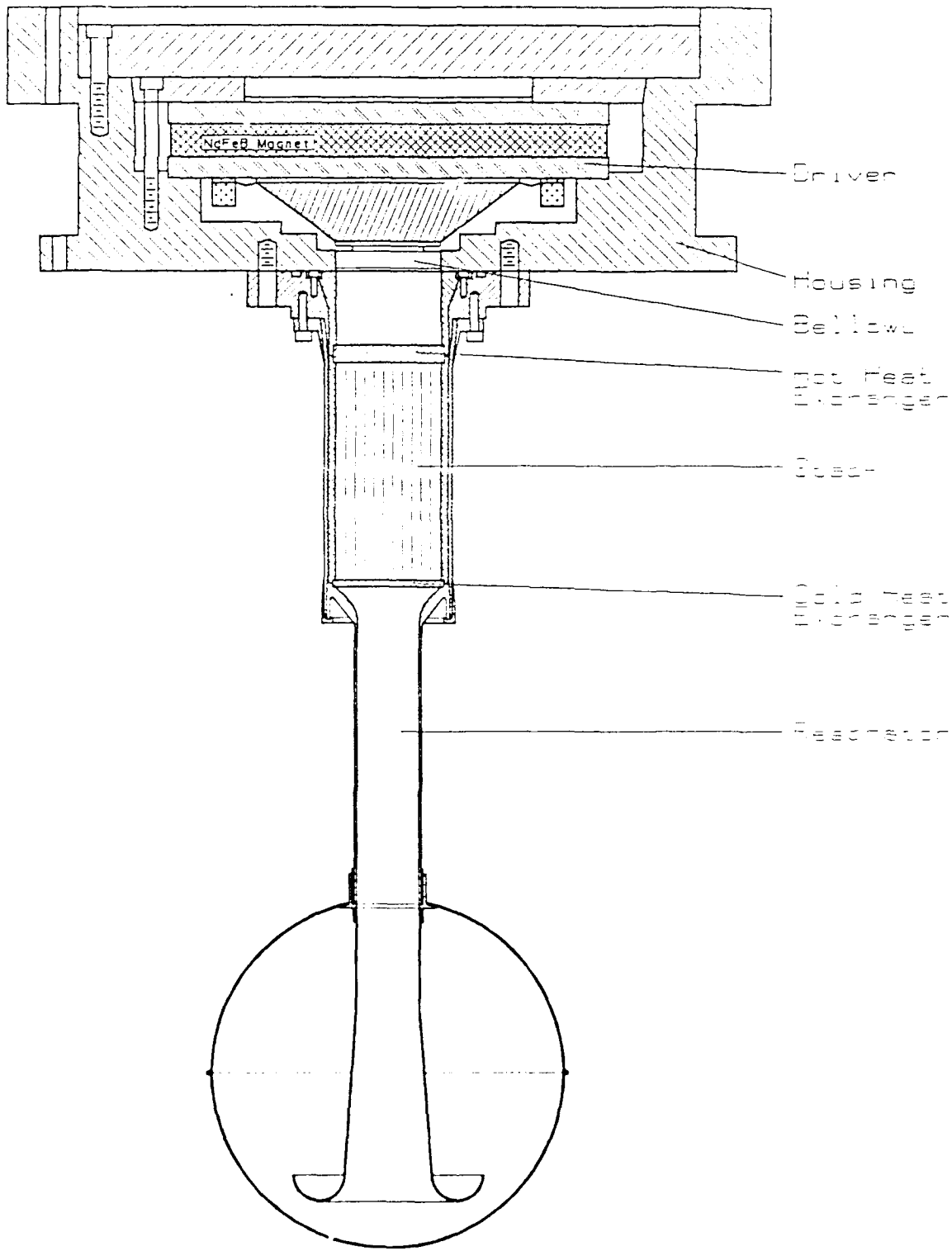


Figure 1-3. Acoustical Subsystems

The driver voice coil is attached to an aluminum reducer cone which is in turn attached to a nickel bellows providing a means of transferring acoustic pressure to the resonator without the need for sliding seals. A miniature Endevco accelerometer is attached to the reducer cone to monitor displacement magnitude and phase relative to the acoustic pressure at the bellows face. The acoustic pressure is monitored by a Valpey-Fisher quartz microphone followed by an Eltec MOSFET impedance converter located directly within the driver housing in close proximity to the microphone. A capillary leak is provided between the housing internal volume and the resonator volume to allow for pressure equalization during operation and for the purging and filling of the entire system through a single port located in the driver housing. There are electrical feed-throughs to provide access to the driver voice coil, microphone, and accelerometer. Finally, there is an Omega PX-80 pressure transducer mounted to the side of the housing to monitor the pressure of the gas mixture.

The resonator is a modified quarter wavelength type with the driver at the closed end. The open end is terminated by a tapered "trumpet" and sealed by a surrounding sphere. Thus, an open termination is simulated while still allowing the resonator to hold ten atmospheres of gas mixture. The thermoacoustic stack and heat exchangers are located in a section of the resonator

designed to allow a minimum of heat conduction back to the cold end. The resonator is instrumented with thermocouples at both the cold and hot ends and wrapped with multiple layers of superinsulation to prevent reheating by reflecting infrared radiation. An electrical heater element is wrapped around the cold end of the resonator reducer neck to permit measurement of refrigerator performance with a variable and quantifiable heat load.

The thermal isolation vacuum chamber surrounds the resonator and seals against the bottom surface of the driver housing with an o-ring. The flight refrigerator will have one port for evacuation of the chamber and an electrical feed through to allow access to the thermocouples and heater. The ground based chamber uses a large mechanical vacuum pump in conjunction with an oil diffusion pump to simulate the vacuum conditions in space. The chamber is instrumented with Granville-Philips thermocouple pressure gauges and an ionization vacuum gauge.

The gas handling system consists of a panel with an arrangement of valves to allow the refrigerator to be evacuated by a small mechanical pump and filled with gas. This panel has a differential pressure gauge and calibrated flow impedance to allow for the monitoring of the flow rate. The gas analysis system consists of a small acoustically resonant cavity and support electronics providing the means

to accurately determine the sound velocity in the gas mixture, and thus, the ratio of helium to xenon or argon.

2. Electrical Subsystems

In order for the refrigerator to operate autonomously, a family of analog and digital electronic subsystems, shown in Figure I-4, are employed to keep the driver running properly and to take useful data. The driver must be kept on resonance, which can change by as much as ten percent over the course of a temperature cycle, and the amplitude must be controlled accurately such that constant conditions exist for the particular experiment at hand.

In addition to measuring the temperatures at the hot and cold ends of the resonator; driver housing pressure and driver parameters such as voice coil current and displacement must be monitored to maintain the health and welfare of the experiment. All of these functions are satisfied by the resonance control board, the multiplexed measurement board, the analog-to-digital board, the pulse width modulated heater board, and the computer/controller and magnetic bubble memory recorder which are described in an NPS Master's thesis by Byrnes. Additional subsystems include the switching power amplifier; designed and built by Instruments Incorporated, and the power distribution system; designed by David Rigmaiden of the NPS Space Systems Group.

The resonance control board receives a signal from the microphone and accelerometer and adjusts the driver

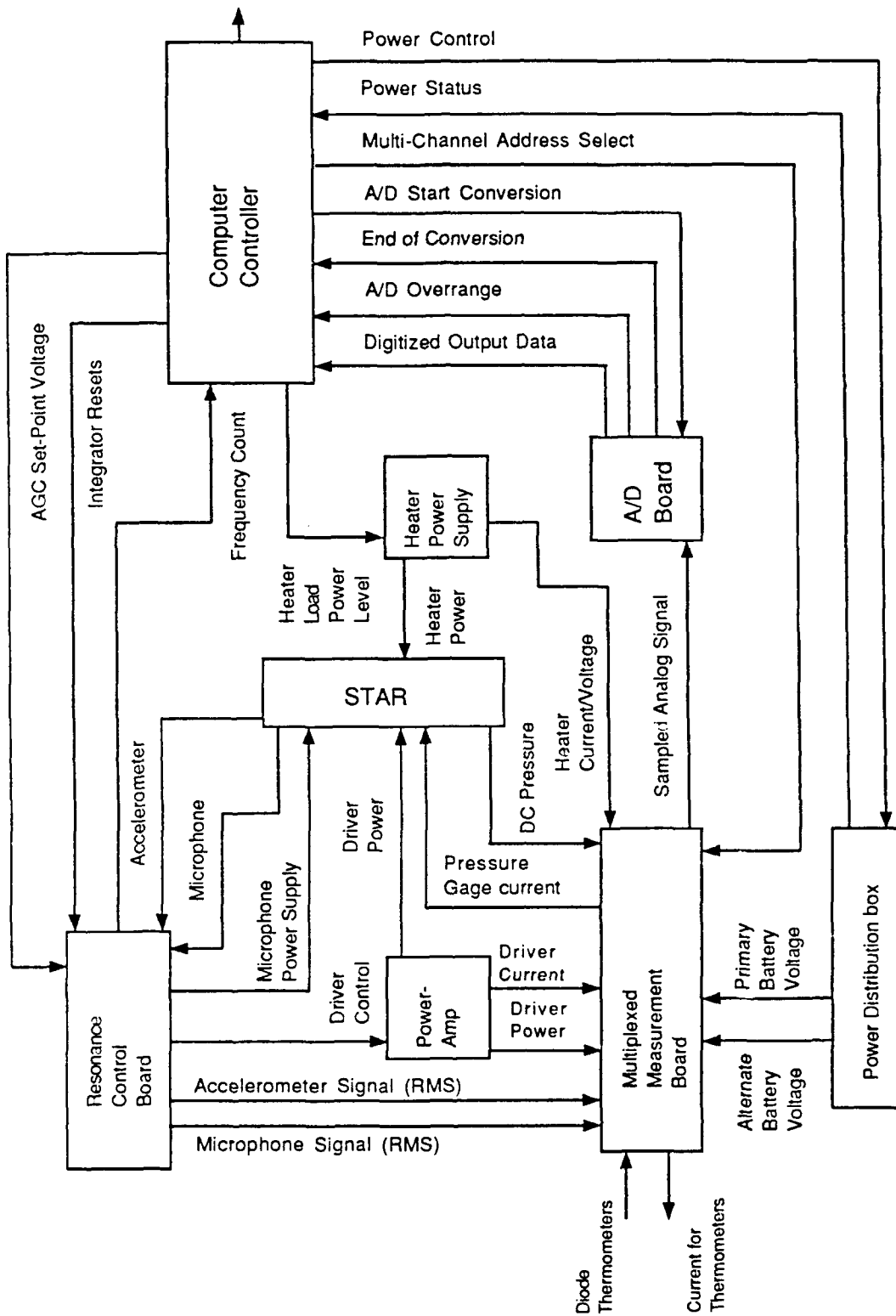


Figure I-4. Electrical Subsystems

operating frequency and amplitude as necessary. These signals are also processed to provide suitable data for the multiplexed measurement board. The resonance control board does not power the driver directly, but rather, sends the sinusoidal drive signal to the switching power amplifier which provides the necessary voltage and current amplification.

The multiplexed measurement board monitors signals from the resonance control board as well as resonator temperatures, and driver housing pressure. The signals are read serially and then sent out as an analog differential voltage signal to the analog-to-digital converter board. This board converts the voltages to a digital signal which can be read by the computer and stored in the bubble memory.

The pulse width modulated heater board provides sixteen possible heater power levels which can be selected by the computer to be sent to the strip heater attached to the cold end of the resonator. Current and voltage through the heater strip are monitored and sent to the multiplexed measurement board.

The computer/controller board contains a microprocessor which will carry out the control program stored in read-only memory. This control program is responsible for changing operating parameters and monitoring the status of the refrigerator. The processor monitors data

from the multiplexed measurement board via the analog-to-digital converter and sends it to the bubble memory.

Finally, the power distribution system provides the necessary voltage to the electronics from an array of batteries consisting of Gates lead-acid rechargeable cells delivering five ampere-hours at two volts each. These batteries were chosen because of the NASA requirement for no outgassing during discharge. Two layers of 42 batteries each provide a total of 840 watt-hours and are configured to provide a 28 volt bus.

3. NASA Get Away Special Program

The NASA Get Away Special provides the opportunity for a small institution to place an experiment in low earth orbit onboard the Space Shuttle. The experiment is housed in a container 28 inches high with a volume of five cubic feet and a maximum capacity of two hundred pounds, (Figure I-5). The experiment must be entirely self contained with autonomous electrical power, control, and data acquisition and storage. NASA's only function during the flight will be to turn the experiment on or off via a switch. The Space Thermoacoustic Refrigerator (STAR) has been assigned a NASA payload number of G-337 and is of particular interest to the agency because of the application possibilities for cooling low-noise high-speed electronics, high T_C superconductors, and infrared imaging systems.

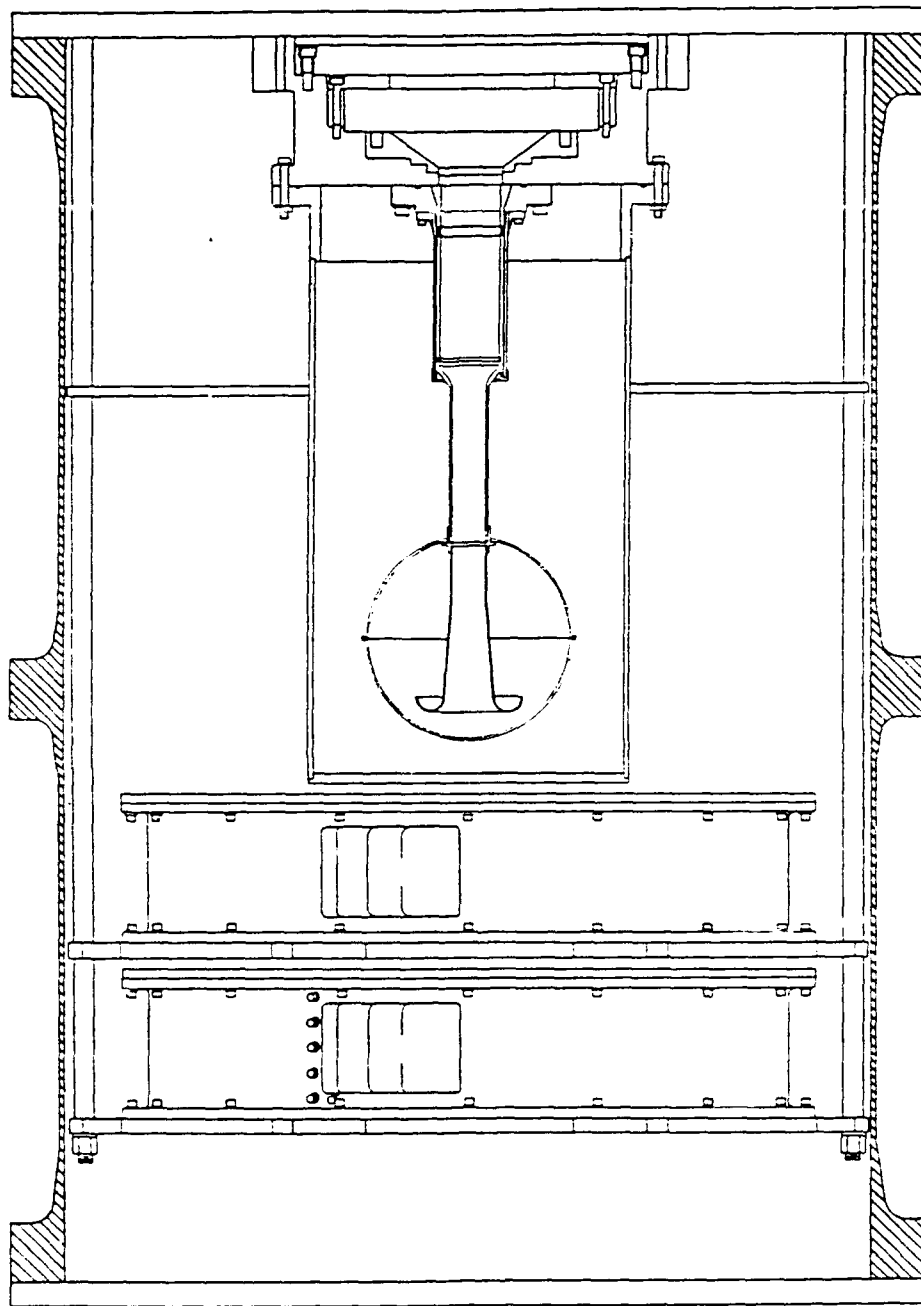


Figure I-5. NASA Get Away Special Cannister

C. SCOPE

This thesis is, in effect, a culmination of all the previous work done on the STAR electronics subsystems, acoustic subsystems, driver design, and thermoacoustic improvements. The author has built the STAR resonator, thermoacoustic stack, thermal vacuum system, gas handling system, and various support circuits for data acquisition and long term testing failsafe protection. But just as important, all of the separate subsystems have finally been brought together to produce a working Space Thermoacoustic Refrigerator.

Chapter two begins with a theoretical approach towards understanding the phenomenon of thermoacoustic heat pumping. Chapter three continues with the design and construction of the STAR resonator, thermoacoustic stack, and heat exchangers, while chapter four gives a short review of the STAR driver and its subsystems and the resonance control board as designed and built by previous students.

Chapter five elaborates on the design and construction of the gas handling system including the filling and purging manifold, the gas mixing apparatus, the gas mixture analyzer, and the proper operating procedures for all of this equipment. Chapter six covers the actual performance of the refrigerator and presents values for the coefficient of performance and temperature ratio as a function of the

applied heat load. The data acquisition system and long term failsafe devices are also described in this chapter.

Chapter seven concludes the thesis by summarizing the results and gives recommendations for the final flight hardware for STAR. Finally, a series of appendices describes the data acquisition program, the power measurement circuit, the driver and resonator construction drawings, the Hofler Tube From Hell, and manufacturer's specifications.

II. THEORETICAL ASPECTS OF THERMOACOUSTICS

A. INTRODUCTION

There are two classes of heat engines; the prime mover and the heat pump as shown in Figure II-1. In a prime mover, heat flows through the engine from a hot reservoir to a cold reservoir so that the engine generates work. In a heat pump, work is done on the engine so that heat flows in the opposite direction from the cold reservoir to the hot reservoir. It is the heat pump which is of primary interest in this thesis.

Thermoacoustics and thermoacoustic heat pumping in particular can be explained by looking at the simple case of a single solid plate in an acoustic standing wave. The plate, small in dimensions, is aligned with its plane parallel to the direction of motion of the fluid or gas particles. While no interesting effects take place in the standing wave alone, save for local temperature oscillations due to adiabatic compression and expansion of the fluid, the presence of the plate modifies the standing wave causing a time-averaged heat flux near the surface of the plate and the absorption or generation of work in the form of sound, also near the surface of the plate.

In this section two approaches toward understanding these processes will be presented. The first is an intuitive Lagrangian approach whereby a parcel of fluid is followed as

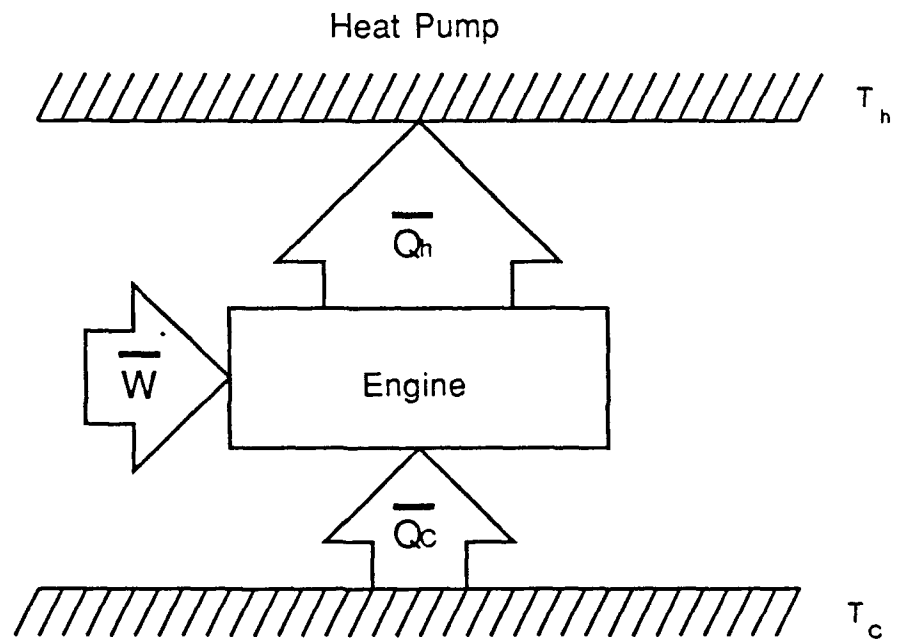
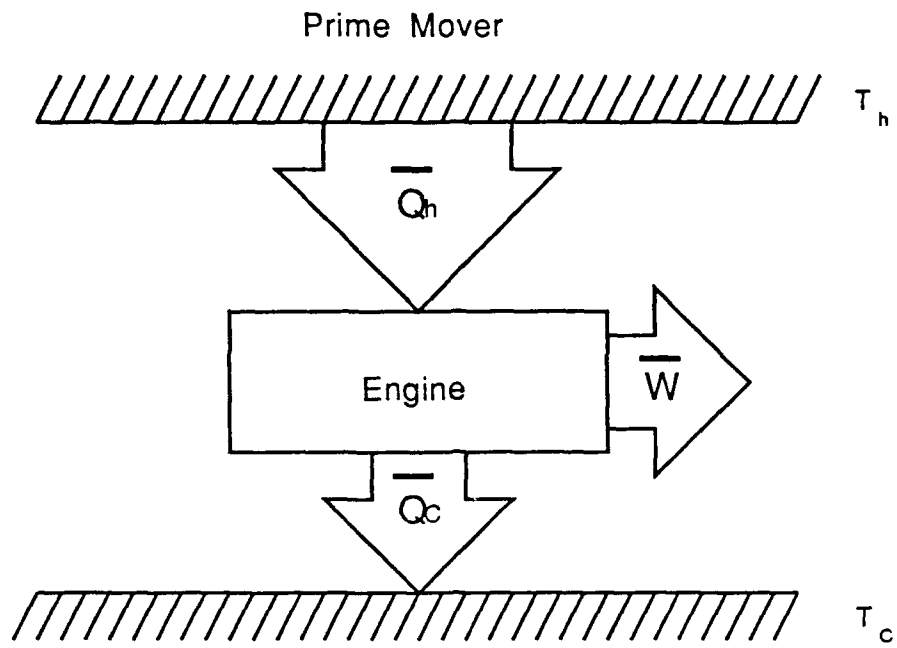


Figure II-1. Prime Mover and Heat Pump

it moves back and forth along the plate. The second is a more mathematically rigorous approach where a given point in space is examined as the fluid passes through it.

B. INTUITIVE APPROACH

1. Thermodynamics Background

An upper limit can be placed on the efficiency of a heat engine by use of the first and second laws of thermodynamics. In Figure II-1 T_h and T_c are the temperatures of the hot and cold reservoirs, \bar{Q}_h and \bar{Q}_c the heat flow rates to and from the reservoirs and \bar{W} is the power flow in or out of the engine. These quantities are all time averaged powers. The first law of thermodynamics is a statement of energy conservation

$$\bar{Q}_h - \bar{Q}_c = \bar{W}. \quad (\text{II-1})$$

The second law of thermodynamics states simply that the net entropy change in any cyclic process must be equal to or greater than zero, or

$$dS = dQ/T \geq 0. \quad (\text{II-2})$$

For the prime mover this can be stated as

$$\bar{Q}_c/T_c - \bar{Q}_h/T_h \geq 0, \quad (\text{II-3})$$

and similarly for the heat pump

$$\bar{Q}_h/T_h - \bar{Q}_c/T_c \geq 0. \quad (\text{II-4})$$

The efficiency of the prime mover is known as Carnot's efficiency $\eta_c = \bar{W}/\bar{Q}_h$, which when combined with equations

(II-1) and (II-3) gives

$$\eta_C = \bar{W}/\bar{Q}_h \leq (T_h - T_c)/T_h. \quad (\text{II-5})$$

For the heat pump the efficiency is known as Carnot's coefficient of performance $\text{COP}_C = \bar{Q}_c/\bar{W}$, or using equations (II-1) and (II-4);

$$\text{COP}_C \leq T_c/(T_h - T_c). \quad (\text{II-6})$$

This determines the maximum coefficient of performance possible. The actual coefficient of performance is usually expressed as a fraction of the Carnot efficiency.

2. Acoustic Heat Engine Cycle

One of the primary wonders of the thermoacoustic heat pump is the lack of moving parts. A traditional refrigerator requires pistons and/or valves operating with specific relative timing to move the working fluid through the necessary thermodynamic cycles. The thermoacoustic refrigerator has no such moving parts. Rather, it relies on the presence of two media, the plate and the fluid, to provide the necessary phasing. As the fluid oscillates back and forth along the plate it undergoes changes in temperature due to the adiabatic compression and expansion from the sound waves. The plate's local temperature also causes temperature changes in the fluid, but not an instantaneous change. The heat flow between the fluid and the plate creates a time delay between the fluid's temperature, pressure, and motion which drives the fluid through the thermodynamic cycle.

Although the oscillations in an acoustic heat pump are sinusoidal, Figure II-2 depicts the motion as a square wave in order to simplify the explanation. The thermodynamic cycle can be considered as consisting of two reversible adiabatic steps and two irreversible constant-pressure steps as in Figure II-3. The plate is assumed to have a mean temperature of T_m and a temperature gradient ∇T , referenced to $x=0$, so that the temperature at the left side of the plate is $T_m - x_1 \nabla T$, and the temperature at the right side is $T_m + x_1 \nabla T$.

In the first step the fluid is transported along the plate by a distance $2x_1$ and heated by adiabatic compression from a temperature $T_m - x_1 \nabla T$ to $T_m - x_1 \nabla T + 2T_1$. Because we are considering a heat pump and work has been done on the fluid, the fluid is now at a higher temperature than the plate. In the second step, at constant pressure, the fluid transfers an amount of heat dQ to the plate so that its temperature drops to that of the plate, $T_m + x_1 \nabla T$. In the third step the fluid is transported back along the plate to position $-x_1$ and cooled by adiabatic expansion to a temperature $T_m + x_1 \nabla T - 2T_1$. In step four the fluid absorbs an amount of heat dQ from the plate, which was previously deposited by an adjacent parcel of fluid, thereby raising its temperature back to that of the plate, $T_m - x_1 \nabla T$. So, the heat dQ has in effect been transported from the cold end of the plate to the warm end.

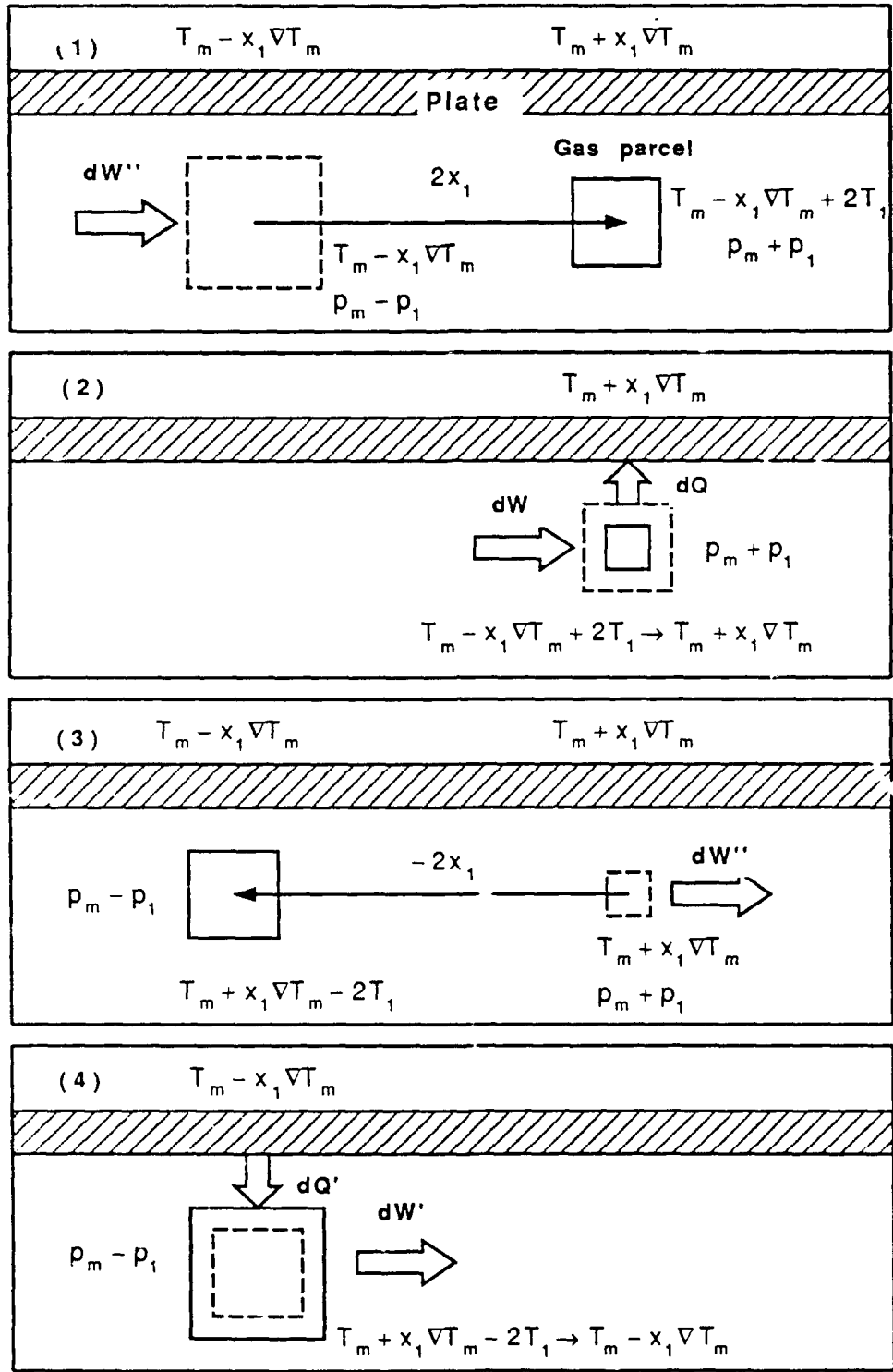


Figure II-2. Heat Pump Cycle

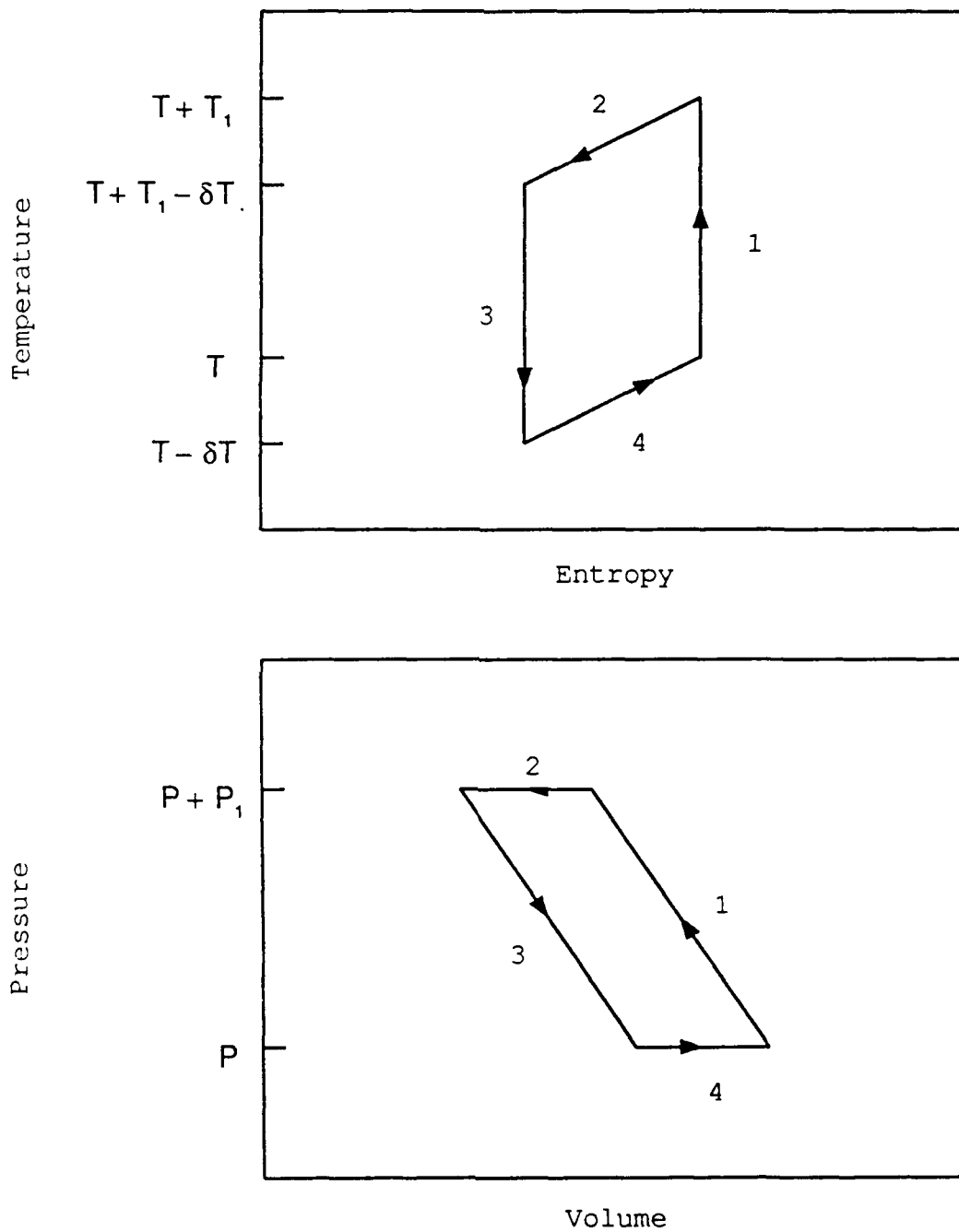


Figure II-3. Acoustic Heat Pump Thermodynamic Cycles

C. MATHEMATICAL APPROACH

1. Single Plate Model

To gain a more detailed understanding of the process of thermoacoustic heat pumping it is necessary to look at the effects produced by the interaction between the sound waves and the solid boundary of the plate. Following the example set by Swift [Ref. 5], except that c is used for sound velocity; consider a plate of length Δx , width $\Pi/2$ and negligible thickness as in Figure II-4. The length Δx of the plate and the acoustic standing wave are both aligned along the x direction. The acoustic pressure is $P_A \sin(kx) \cos(\omega t)$ and the acoustic velocity $U_A \cos(kx) \sin(\omega t)$ or $-(P_A/\rho_m c) \cos(kx) \sin(\omega t)$. Time harmonic quantities will be expressed in complex notation where it should be understood that only the real part represents the actual physical solution, and it is assumed that a first order expansion in the acoustic quantities is sufficient for the following thermodynamic and acoustic calculations.

The pressure p and velocity u are written as

$$p = p_m + P_A \sin(kx) e^{i\omega t} = p_m + p_{1x} e^{i\omega t} \quad (\text{II-7})$$

$$u = i \left(\frac{P_A}{\rho_m c} \right) \cos(kx) e^{i\omega t} = i u_{1x} e^{i\omega t} \equiv u_{1x} e^{i\omega t} \quad (\text{II-8})$$

where p_m is the mean pressure which is a real quantity, $i = (-1)^{1/2}$, and p_{1x} and u_{1x} are the small acoustic quantities which are a function of position and which are in general complex, reflecting their relative time phasing. The time

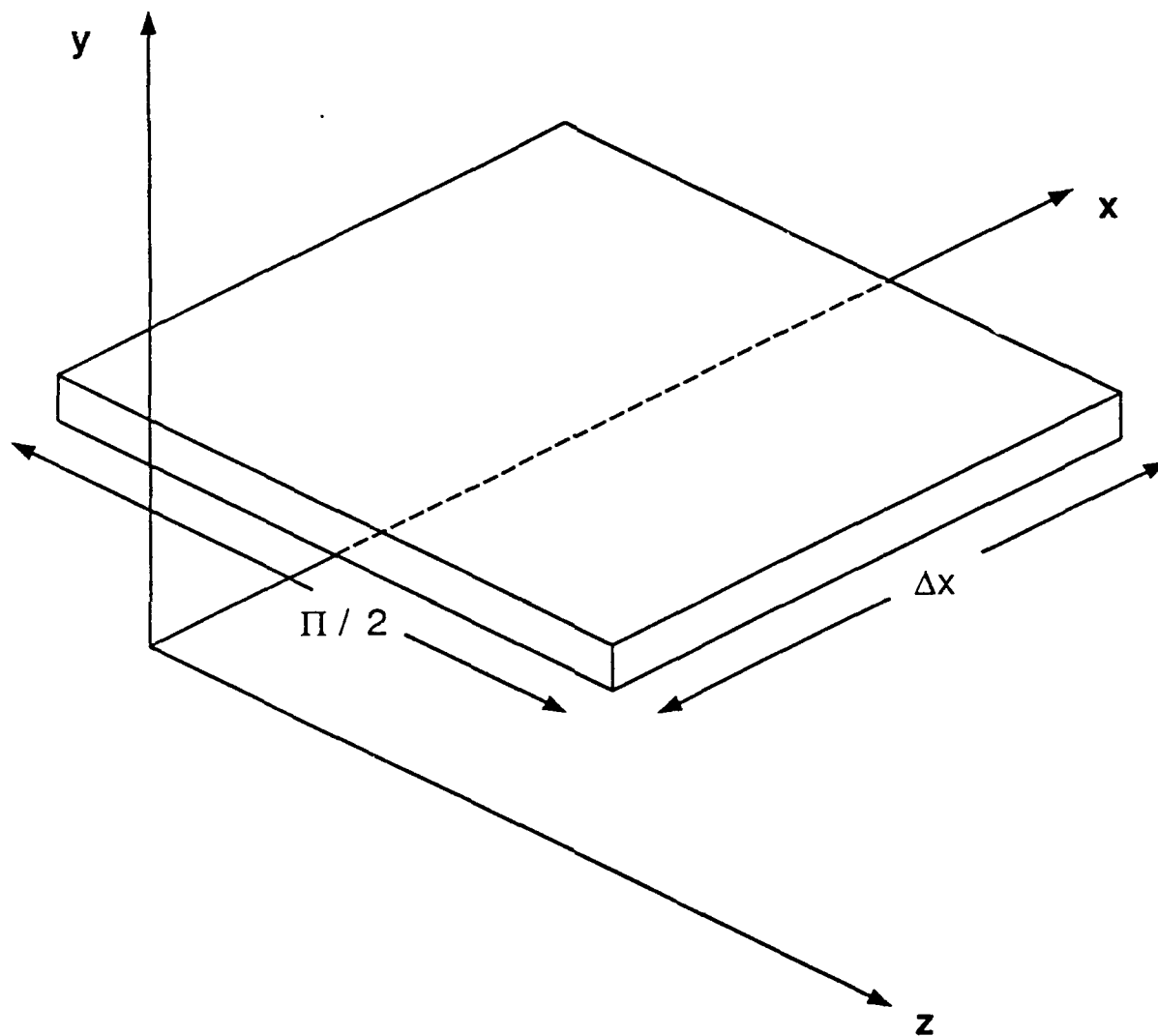


Figure II-4. Single Plate in Acoustic Standing Wave

dependence is expressed in the term $e^{i\omega t}$ and, again, it is understood that the real part is taken to represent the actual physical solution.

The first task is to calculate the oscillating temperature $T = T_m + T_1 e^{i\omega t}$ due to the adiabatic sound waves in the absence of the plate. Using the Maxwell relation

$$(\partial T / \partial p)_S = (\partial V / \partial S)_P \quad (\text{II-9})$$

or

$$(\partial T / \partial P)_S = (1/m) (\partial \rho^{-1} / \partial S)_P = -(m/\rho^2) (\partial \rho / \partial S)_P, \quad (\text{II-10})$$

T_1 may be written as

$$T_1 = (\partial T / \partial P)_S P_1 = -(1/\rho_m^2) (\partial \rho / \partial s)_P p_1 \quad (\text{II-11})$$

where the entropy per unit mass s has been substituted for the traditional extensive entropy S . The temperature may now be expressed as

$$T_1 = -(1/\rho_m^2) (\partial \rho / \partial T)_P (\partial T / \partial s)_P p_1 = [T_m \beta / \rho_m c_p] p_1 \quad (\text{II-12})$$

where $\beta = (1/V) (\partial V / \partial T)_P$ or $(-1/\rho) (\partial \rho / \partial T)_P$ is the volume expansivity or isobaric coefficient of volume expansion $(\Delta V/V)/\Delta T$, and c_p is the heat capacity per unit mass at constant pressure. It is evident from (II-12) that since $(T_m \beta / \rho_m c_p)$ is positive and real, T_1 and P_1 are in phase.

For an ideal gas we have $pV = nRT$. Using the definition for β we can solve for $T_m \beta$;

$$T_m \beta = (T_m / V_m) (\partial V_m / \partial T)_P = (T_m nR / V_m p_m) (\partial T_m / \partial T)_P = 1. \quad (\text{II-13})$$

Now, using $R = (c_p - c_v)$ or $R/c_p = (\gamma - 1)/\gamma$, where $\gamma = c_p/c_v$,

gives

$$\beta = 1/T_m = (\rho_m c_p / p_m) [(\gamma - 1) / \gamma] \quad (\text{II-14})$$

or

$$T_m \beta / \rho_m c_p = (\gamma - 1) (T_m / \gamma p_m) . \quad (\text{II-15})$$

Using (II-15) and (II-12) allows T_1/T_m to be written as

$$T_1/T_m = \beta p_1 / \rho_m c_p = (p_1 / p_m) [(\gamma - 1) / \gamma] . \quad (\text{II-16})$$

Equation (II-16) states that the fractional temperature oscillations are on the order of the fractional pressure variations. For air at 20°C and standard atmospheric pressure and for acoustic pressure amplitudes representative of human speech, T_1 is on the order of 10^{-4} °C so that it is not surprising that thermoacoustic effects are not normally apparent.

The next step is to introduce the plate of Figure II-4 and again calculate the temperature oscillations of the gas near the plate, now expressed as $T = T_m + T_1 e^{i\omega t}$. Several assumptions must be made at this point in order to simplify the calculations. It is assumed that the plate is much shorter than the acoustic wavelength λ and that it is sufficiently far from the pressure and velocity nodes so that p_1 and u_1 may be considered to be constant over the length of the plate. The fluid is assumed to have zero viscosity so that u_1 is independent of y . It is assumed that the plate has a given mean temperature gradient of ∇T_m in the x

direction and the plate's thermal conductivity in that direction is negligible. Also neglected is the thermal conductivity of the acoustic medium. Finally, the mean temperature of the plate and gas are taken as being equal and independent of y .

The general equation of conductive heat transfer is written as

$$\rho T (\partial s / \partial t + \bar{v} \cdot \bar{\nabla} s) = \bar{\nabla} \cdot (K \bar{\nabla} T) + (\text{quadratic terms}), \quad (\text{II-17})$$

where \bar{v} is velocity, K is the thermal conductivity, and the quadratic terms which represent viscose heating will be neglected. This equation states that entropy at a point changes in time because of convective flow of entropy, conduction of heat, and the creation of entropy by the quadratic terms. Thermal heat conduction by the plate along x and by the gas along z will be neglected so that $\bar{\nabla} T$ is just $\partial T / \partial y$ and s will be assumed to have the form $s = s_m(x) + s_1 e^{i\omega t}$. Now, keeping only first order terms, (II-17) becomes

$$\rho_m T_m (i\omega s_1 + u_1 \partial s_m / \partial x) = K (\partial^2 T_1 / \partial y^2). \quad (\text{II-18})$$

In order to express s in terms of p and T , it is necessary to make a series of expansions using the rules of partial derivatives and a Maxwell relation;

$$\begin{aligned} T ds &= T (\partial s / \partial T)_p dT + T (\partial s / \partial P)_T dp \\ &= T (\partial s / \partial T)_p dT - (T / \rho_m V) (\partial V / \partial T)_p dp \end{aligned}$$

$$\begin{aligned}
Tds &= T(\partial s/\partial T)_p dT - T(\partial \rho_m^{-1}/\partial T)_p dp \\
&= T(\partial s/\partial T)_p dT + (T/\rho_m^2) (\partial \rho_m/\partial T)_p dp
\end{aligned}$$

and finally

$$Tds = c_p dT - (T\beta/\rho_m) dp \quad (\text{II-19})$$

where $c_p = T(\partial s/\partial T)_p$ and the previous definition for β have been used. Equation (II-19), upon integration, may be expressed as

$$T_m s_1 = c_p T_1 - (T_m \beta / \rho_m) p_1, \quad (\text{II-20})$$

and when, along with (II-19), inserted into (II-18) gives a differential equation for the unknown $T_1(y)$;

$$T_1 + (i\delta_\kappa^2/2) (\partial^2 T_1/\partial y^2) = (T_m \beta p_1 / \rho_m c_p) + i(\bar{\nabla} T_m u_1/\omega) \quad (\text{II-21})$$

where $\delta_\kappa = (2\kappa/\omega)^{1/2}$ is the thermal penetration depth and

$\kappa = K/\rho_m c_p$ is the thermal diffusivity of the acoustic medium.

This equation can be solved with the help of an integral table to arrive at

$$T_1 = (T_m \beta p_1 / \rho_m c_p - \bar{\nabla} T_m u_{1x}/\omega) (1 - e^{-(1+i)y/\delta_\kappa}). \quad (\text{II-22})$$

Looking at the case far from the plate, $y \gg \delta_\kappa$, where the gas makes poor thermal contact with the plate;

$$T_1 = (T_m \beta p_1 / \rho_m c_p) - (\bar{\nabla} T_m u_{1x}/\omega). \quad (\text{II-23})$$

The first term is identical to (II-12) and is due to adiabatic compression and expansion of the gas. The second term represents the mean temperature gradient of the gas which oscillates back and forth along the plate with

amplitude u_1/ω . As it oscillates back and forth the temperature at a given point oscillates by the amount $\bar{\nabla} T_m u_1/\omega$. Setting (II-23) equal to zero results in the definition for a critical mean-temperature gradient

$$\bar{\nabla} T_{\text{critical}} = T_m (\beta \omega p_1 / \rho_m c_p u_{1x}). \quad (\text{II-24})$$

For such a temperature gradient the temperature oscillations become zero because the temperature changes due to adiabatic pressure oscillations cancel the displacement oscillations. This critical temperature gradient may be considered to be the "border" separating a heat pump from a prime mover.

The y dependent part of equation (II-22) is a complex quantity. The magnitude approaches 1 for $y \gg \delta_k$ and zero for $y \ll \delta_k$. For y equal to δ_k the magnitude is approximately 1.1 but with an imaginary part of 0.27 indicating a 14° phase shift of the oscillating temperature of the standing wave. This phase shift is due to the presence of the plate and leads to a time-averaged heat flux in the x direction as will now be shown.

Heat is transported along x by the hydrodynamic transport of entropy, since regular thermal conduction by the plate along the x direction is being ignored. Swift's expression for the average heat flux per unit area is

$$\overline{q_2} = \rho_m T_m \overline{s_1 u_1}, \quad (\text{II-25})$$

where the subscript 1 denotes a first order quantity and 2 denotes a second order quantity. The average value of the

product of two complex quantities A and B is $\overline{AB} = (1/2) \text{Re} [AB^*]$, and the star denotes complex conjugate. Using equation (II-20) allows (II-25) to be rewritten as

$$\overline{q_2} = \rho_m c_p \overline{T_1 u_1} - T_m \beta \overline{p_1 u_1} \quad (\text{II-26})$$

or

$$\overline{q_2} = \frac{1}{2} \rho_m c_p \text{Re}[T_1 u_1^*] - \frac{1}{2} T_m \beta \text{Re}[p_1 u_1^*]. \quad (\text{II-27})$$

The second term is zero for a pure standing wave because $p_1 u_1^* = -ip_1 u_1$ which is entirely imaginary. The first term, because T_1 is complex, becomes

$$\overline{q_2} = \frac{1}{2} \rho_m c_p u_{1x} \text{Im}[T_m]. \quad (\text{II-28})$$

The heat flux derives its y-dependence, shown in Figure II-5, from the y-dependence of T_1 . It is largest at a distance δ_x and becomes zero at the plate surface and at y equal to infinity.

The total heat flux is now calculated by integrating $\overline{q_2}$ over the y-z plane on both sides of the plate

$$\overline{Q_2} = \int_{\text{upper plate}} \overline{q_2} \, dydz + \int_{\text{lower plate}} \overline{q_2} \, dydz \quad (\text{II-29})$$

where the limits of integration are zero to $\Pi/2$ for z and zero to infinity for y. The result is

$$\overline{Q_2} = \Pi \int_0^{\infty} \overline{q_2} \, dy, \quad (\text{II-30})$$

which is now solved by using (II-22) for T_1 . The integral

becomes

$$\bar{Q}_2 = \frac{\Pi}{2} \rho_m c_p \left[\frac{T_m \beta p_1}{\rho_m c_p} - \frac{\bar{\nabla} T_m u_{1x}}{\omega} \right] \int_0^{\infty} \text{Im} [1 - e^{iy/\delta_k} e^{-y/\delta_k}] dy$$

or

$$\bar{Q}_2 = \frac{\Pi}{2} \rho_m c_p \left[\frac{T_m \beta p_1}{\rho_m c_p} - \frac{\bar{\nabla} T_m u_{1x}}{\omega} \right] \int_0^{\infty} \left[\sin\left(\frac{y}{\delta_k}\right) e^{-y/\delta_k} \right] dy \quad (\text{II-31})$$

which is solved with the use of an integral table to give

$$\bar{Q}_2 = \frac{\Pi}{2} \rho_m c_p \left[\frac{T_m \beta p_1}{\rho_m c_p} - \frac{\bar{\nabla} T_m u_{1x}}{\omega} \right] \frac{\delta_k}{2} \quad (\text{II-32})$$

Now, by making the substitution $\Gamma = \bar{\nabla} T_m / \bar{\nabla} T_{\text{critical}}$, where the gradient of the critical temperature is defined in (II-24), the total heat flux is written as

$$\bar{Q}_2 = -\frac{1}{4} \Pi \delta_k T_m \beta p_1 u_{1x} (\Gamma - 1) \quad (\text{II-33})$$

The heat flux is proportional to the area $\Pi \delta_k$, to $T_m \beta$ which equals one for ideal gases, to $p_1 u_1$ which equals zero at a standing wave pressure or velocity node, and to the temperature gradient factor $\Gamma - 1$. It has its maximum value of $p_1 u_1 = (P_A)^2 / 2 \rho_m c$ exactly half way between the pressure and velocity nodes. When $\bar{\nabla} T_m = \bar{\nabla} T_{\text{critical}}$, $\Gamma - 1 = 0$ so that there is no heat flux. When $\bar{\nabla} T_m > \bar{\nabla} T_{\text{critical}}$, $\Gamma - 1 > 0$ so that the heat flux is toward the pressure node. And when $\bar{\nabla} T_m < \bar{\nabla} T_{\text{critical}}$, $\Gamma - 1 < 0$ so that the heat flux is away from the pressure node.

Turning now to the acoustic power; the work dw done by a volume of gas in a free expansion is $dw = pdV$. The power

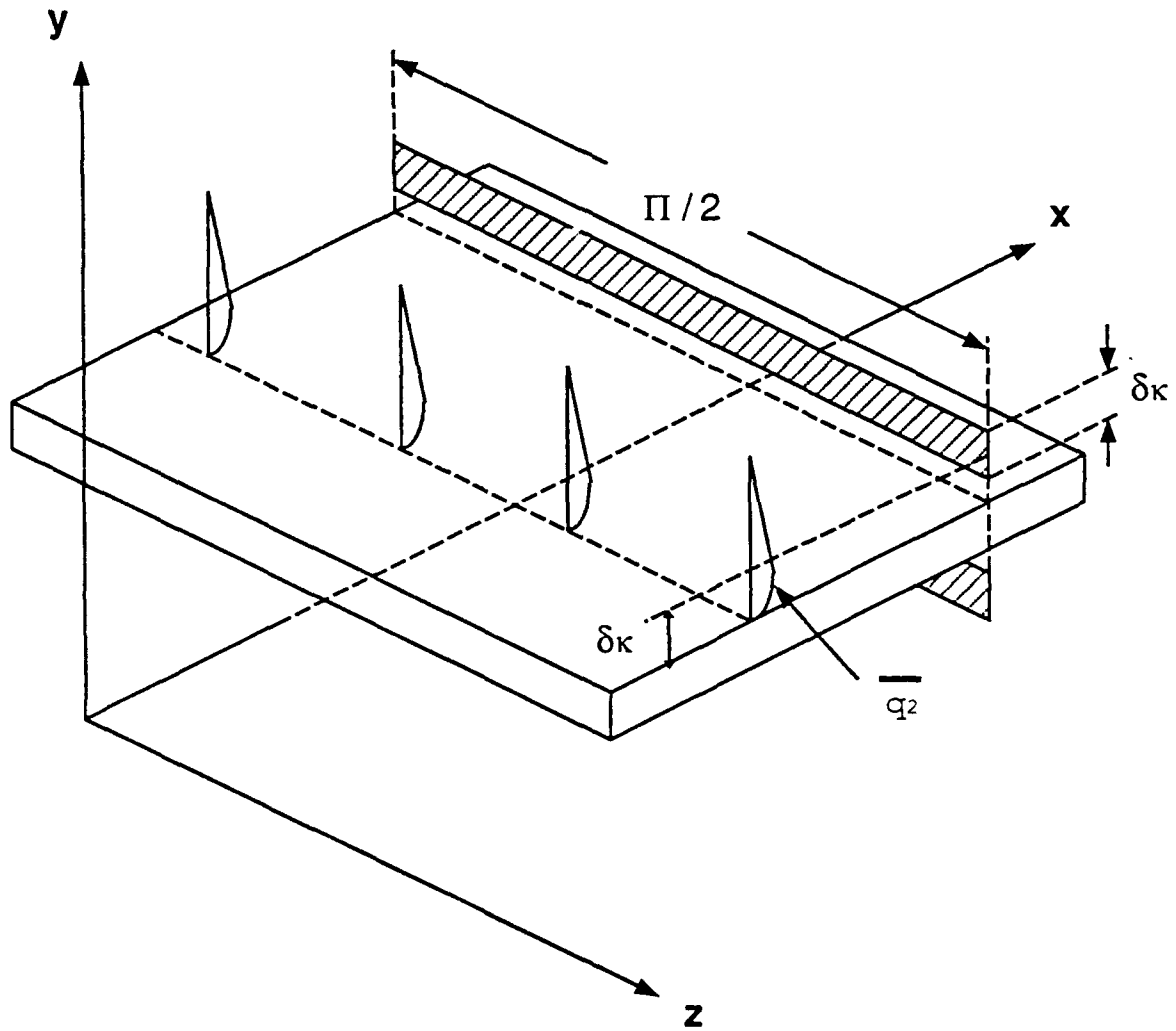


Figure II-5. Heat Flux Density

per unit volume \bar{w} is

$$\bar{w} = (p/V) dV/dt = -(p/\rho) dp/dt \quad (\text{II-34})$$

where $p = p_m + p_1 e^{i\omega t}$, $\rho = \rho_m + \rho_1 e^{i\omega t}$, and

$$\begin{aligned} dp/dt &= \partial p/\partial t + (\partial p/\partial x) (dx/dt) = \partial p/\partial t + u (dp/dx) \\ &= i\omega p + u_1 (d\rho_m/dx). \end{aligned} \quad (\text{II-35})$$

Substituting (II-35) and the definition for p into (II-34) gives

$$-(p/\rho_m) dp/dt = (-1/\rho_m) (p_m + p_1 e^{i\omega t}) [i\omega p_1 + (u_1) d\rho_m/dx] \quad (\text{II-36})$$

which separates into four terms. It should be understood that since power is being calculated the average value must be taken;

$$\begin{aligned} -(p/\rho_m) dp/dt &= \{ -(p_m/\rho_m) \omega \overline{ip_1} - (\omega/\rho_m) \overline{ip_1 \rho_1 e^{i\omega t}} \\ &\quad - (p_m/\rho_m) (\partial \rho_m/\partial x) \bar{u}_1 - (1/\rho_m) (\partial \rho_m/\partial x) \overline{p_1 u_1 e^{i\omega t}} \}. \end{aligned} \quad (\text{II-37})$$

The first, third, and fourth terms of (II-37) are zero, and the second term may be solved by expressing ρ_1 and T_1 in terms of p_1 by using

$$dp = (\partial p/\partial T)_p dT + (\partial p/\partial p)_T dp = -\rho\beta dT + (\partial p/\partial p)_T dp \quad (\text{II-38})$$

which, upon integration, yields

$$\rho_1 = -\rho_m \beta T_1 + (\partial p/\partial p)_T p_1. \quad (\text{II-39})$$

The second term of (II-37) now becomes

$$-(p/\rho_m) dp/dt = \bar{w}_2 = (\omega/\rho_m) \left[\rho_m \beta \overline{ip_1 T_1} + \left(\frac{dp}{dp} \right) \overline{ip_1 p_1} \right] \quad (\text{II-40})$$

or

$$\overline{w}_2 = (\omega\beta p_1) \text{Re}[iT_1^*] + (\omega/\rho_m) (\partial\rho/\partial p) \text{Re}[ip_1 p_1^*]. \quad (\text{II-41})$$

The second term of (II-41) is zero because p_1 is real, and the first term becomes

$$\overline{w}_2 = (\omega\beta p_1/2) \text{Im}[T_1] \quad (\text{II-42})$$

which is similar to (II-28) for the heat flux density. The imaginary part of T_1 is the only part that contributes to the acoustic power per unit volume.

The total acoustic power, \overline{W}_2 , is found by integrating (II-42) over all space with the use of (II-22) for T_1 ;

$$\begin{aligned} \overline{W}_2 &= \frac{-1}{2} \omega\beta p_1 \left(\frac{T_m \beta p_1}{\rho_m c_p} - \frac{\overline{\nabla T_m u_{1x}}}{\omega} \right) \int_0^{\Delta x} \int_0^{\infty} \int_0^{\pi/2} \text{Im}[1 - e^{-y/\delta_\kappa} e^{-iy/\delta_\kappa}] dx dy dz \\ &= \frac{-\pi}{4} \Delta x \omega\beta p_1 \left(\frac{T_m \beta p_1}{\rho_m c_p} - \frac{\overline{\nabla T_m u_{1x}}}{\omega} \right) \int_0^{\infty} e^{-y/\delta_\kappa} \sin\left(\frac{y}{\delta_\kappa}\right) dx \\ &= \frac{-\pi}{4} \Delta x \omega\beta p_1 \left(\frac{T_m \beta p_1}{\rho_m c_p} - \frac{\overline{\nabla T_m u_{1x}}}{\omega} \right) \frac{\delta_\kappa}{2} \end{aligned} \quad (\text{II-43})$$

where this result is actually multiplied by two since the power being calculated is over both sides of the plate. By substituting $\Gamma = \overline{\nabla T_m} / \overline{\nabla T}_{\text{critical}}$ and the definition for the critical temperature gradient, (II-43) can be made to look like

$$\overline{W}_2 = \frac{-\pi}{4} \delta_\kappa \omega \Delta x T_m \frac{\beta^2 p_1^2}{\rho_m c_p} [\Gamma - 1] \quad (\text{II-44})$$

which shows that the total acoustic power is proportional to

the volume $\Pi \delta_x \Delta x$ of gas that is one thermal penetration depth from the plate surface. It is also proportional to $(p_1)^2$, hence quadratic relative to the acoustic pressure and zero at the pressure nodes. And it is proportional to $(\Gamma-1)$, as was dQ/dt , so that when the temperature oscillations of the gas match that of the plate there is also no acoustic power absorbed. Acoustic power is produced when the mean temperature gradient is larger than the critical temperature gradient. But when the mean temperature gradient is less than the critical temperature gradient, acoustic power is absorbed at the plate surface and the heat flux as given by (II-33) is in the positive x direction or up the temperature gradient. The work absorbed causes a heat flux from the colder end to the warmer end so that the heat engine acts as a heat pump.

The final step is to calculate the efficiency of the heat pump. Carnot's coefficient of performance COP_C was defined in (II-6) as $T_c/(T_h-T_c)$ and the heat pump's efficiency or coefficient of performance is $COP = \overline{Q_C}/\overline{W}$. Substituting (II-33) for $\overline{Q_C}$ and (II-44) for \overline{W} gives

$$COP = - \frac{u_{1x} \rho_m c_p T_m}{\Delta x \beta \omega p_1 T_m} , \quad (II-45)$$

and using the definition for the critical temperature gradient gives

$$COP = \frac{T_m}{\Delta x \nabla T_c} . \quad (II-46)$$

Now, using the definition for Γ , a final expression for COP can be arrived at by the following progression;

$$\begin{aligned} \text{COP} &= \frac{\Gamma T_m}{\nabla T_m \Delta x} \\ &= \frac{\Gamma T_m}{\Delta T} \\ &= \Gamma \frac{T_c}{T_h - T_c} \\ &= \Gamma \text{COP}_C \end{aligned} \tag{II-47}$$

Since Γ is less than one for the heat pump, the efficiency is less than Carnot's efficiency.

In this section, a simplified explanation of the thermoacoustic heat engine has been presented. Many assumptions were made in order to avoid obscuring the important results. These results are that the presence of a stationary plate in the acoustic standing wave causes a heat flux along the plate approximately one thermal penetration depth from the plate, and that acoustic power is either absorbed or produced by the gas near the plate depending on whether the engine is a prime mover or a heat pump.

2. A More Realistic Model

The next step in deriving a more realistic model of the thermoacoustic heat engine would be to include viscosity effects, longitudinal thermal conductivity, finite plate heat capacity, and multiple plates. This derivation has been carried out by Swift but is far beyond the scope of this thesis to be presented here. It is useful, however, to cite

the results as they figure prominently in the design of a practical thermoacoustic heat pump for space applications.

The equations that result from Swift's derivations are long, complicated and generally difficult to interpret. Having already made the boundary-layer approximation where it is assumed that the thermal penetration depth is much less than half the separation between adjacent plates, and the short-stack approximation where it is assumed that the stack is not long enough to perturb the acoustic standing wave; Swift further limits the discussion to the case for lowest order in viscosity, or $\sqrt{\sigma}$. In addition, he assumes $y_0 \approx \delta_k$ so that $\delta_v/y_0 \approx \sqrt{\sigma}$, claiming that this is the case for the most realistic applications.

The total enthalpy flux, a second order quantity, is simplified to the following expression;

$$\overline{H_2} = \frac{1}{4} \Pi \delta_k \frac{T_m \beta p_1 i \langle u_{1x} \rangle}{(1 + \epsilon_s)(1 - \sqrt{\sigma})} (\Gamma - 1) - \Pi (y_0 K + 1 K_s) \frac{dT_m}{dx} \quad (\text{II-48})$$

where $\langle u_1 \rangle$ is the mean x velocity, or

$$\langle u_1 \rangle = \frac{1}{y_0} \int_0^{y_0} u_1 dy = i \langle u_{1x} \rangle, \quad (\text{II-49})$$

and is purely imaginary, $\sigma = c_p \mu / K = \nu / \kappa$ is the Prandtl number of the gas, and $\epsilon_s = (\rho_m c_p \delta_k / \rho_s c_s \delta_s)$ is the gas to plate heat capacity ratio. The kinematic viscosity ν and the dynamic viscosity μ are related by $\nu = \mu / \rho_m$, and the subscript s refers to the solid plate so that δ_s is the thermal penetration depth of the plate, c_s is the heat capacity of the plate, and K_s is the thermal conductivity of the plate.

Inspection of (II-47) reveals that the first term is the same as the hydrodynamic heat flux derived in (II-33) except for the factors $1/(1+\epsilon_s)$ and $1/(1-\sqrt{\sigma})$. The first factor reduces the hydrodynamic heat flux because of the plate's finite heat capacity, while the second factor increases it because the velocity at a distance δ_k from the plate, which is where the convective entropy transport occurs, is higher than the mean velocity $\langle u_1 \rangle$ by just that amount. The second term in (II-47) is the conduction of heat down the temperature gradient by the gas and by the plate, where Πy_0 is the cross sectional area of the gas and Πl is the cross-sectional area of the plate.

The total acoustic power, also a second order quantity, is

$$\overline{W}_2 = \frac{1}{4} \Pi (k\Delta x) (\rho_m c) \left\{ \delta_k \left(\frac{\gamma-1}{\gamma} \right) \frac{\Gamma-1}{1+\epsilon} \left(\frac{p_1}{p_m} \right)^2 - \delta_v \gamma \left(\frac{u_1}{c} \right)^2 \right\} \quad (\text{II-50})$$

where $\delta_v = (2\nu/\omega)^{1/2}$ is the viscous penetration depth in the gas. This expression differs from Swift in that the relation $\rho_m c^2 = \gamma p_m$ has been used to rearrange the terms. The first term is simply the acoustic power derived in (II-44), except for the factor $1/(1+\epsilon_s)$ which reduces the acoustic power just as the total energy heat flux was reduced in (II-47). The second term represents the dissipation of power due to viscous shear.

Although it would appear from (II-47) that lowering the Prandtl number serves only to decrease the total energy

flux; these losses due to viscosity can be reduced if one considers the definition of the Prandtl number as the square of the ratio of the viscous penetration depth to the thermal penetration depth

$$\sigma = \left(\frac{\delta_v}{\delta_\kappa} \right)^2. \quad (\text{II-51})$$

The effects of a lower Prandtl number on the coefficient of performance of a thermoacoustic refrigerator have been explored by Susalla and Hofler and the reader is referred to the Susalla thesis for further information.

Several other important conclusions can be reached by manipulating these simplified equations, the mathematics of which is not important here. The first is that the acoustic power density is proportional to $(P_A)^2$, indicating that the acoustic pressure amplitude must be kept as high as possible. This dependence may be understood if one notices that both the acoustic power and the energy flux are proportional to $p_1 u_1$. Secondly, the power is proportional to the perimeter Π , so that obviously as much plate area as possible is desired.

To summarize, it has been shown that the inclusion of viscosity, longitudinal thermal conductivity by the plates and the working gas, and finite plate heat capacity serve only to reduce the efficiency of the heat engine as would have been expected. But several improvements can also be made to the heat engine such as using a working gas with a lower Prandtl number to reduce viscous losses, and keeping

the acoustic pressure amplitude as high as possible to increase the acoustic power density. It is also assumed by now that the reader understands that the portion of the resonator containing the plate would actually house many parallel plates spaced on the order of a few thermal penetration depths apart to maximize the heat pumping effect.

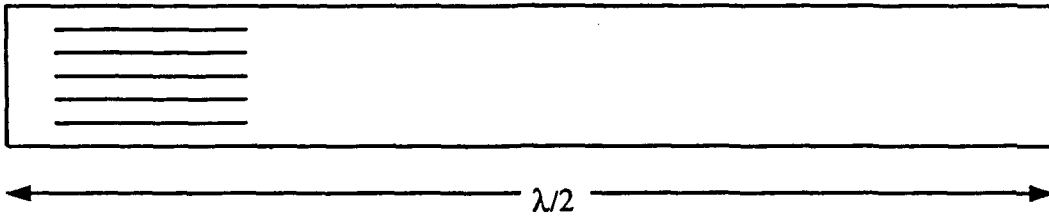
III. RESONATOR

A. OVERVIEW

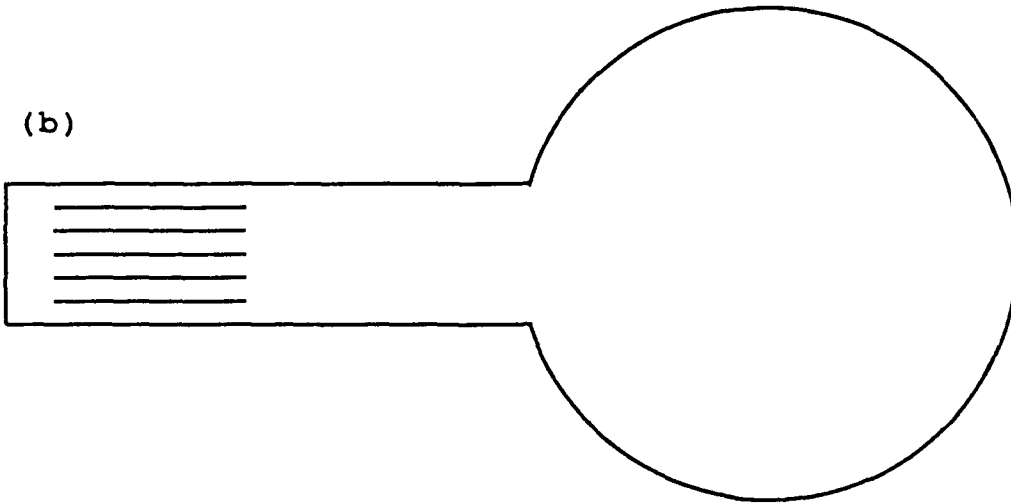
The resonator is a vessel that contains and helps to generate the standing wave in which the thermoacoustic stack and associated heat exchangers are to reside. This standing wave possesses the time phasing of particle velocity and acoustic pressure necessary for acoustic heat pumping to occur. The simplest resonator geometry as shown in Figure III-1A [Ref. 6] is a $1/2$ wavelength hollow straight tube with the transducer at a pressure anti-node, and the cold end of the stack away from the driver. The dissipation in this geometry is highest because fluid within a penetration depth of the resonator wall is dissipative. Thus, almost all of this resonator's surface area contributes toward dissipation which is a substantial heat load on the cold end of the stack.

The second possible geometry is shown in Figure III-1B [Ref. 6]. Here, the resonator tube is reduced to a $1/4$ wavelength resonator with a sphere attached to the open end. This termination simulates an open termination while still allowing pressurization of the vessel. In a simplistic case, if the sphere volume is assumed infinite, the particle velocity and acoustic pressure in the sphere are zero so that there are no dissipative losses associated with the

(a)



(b)



(c)

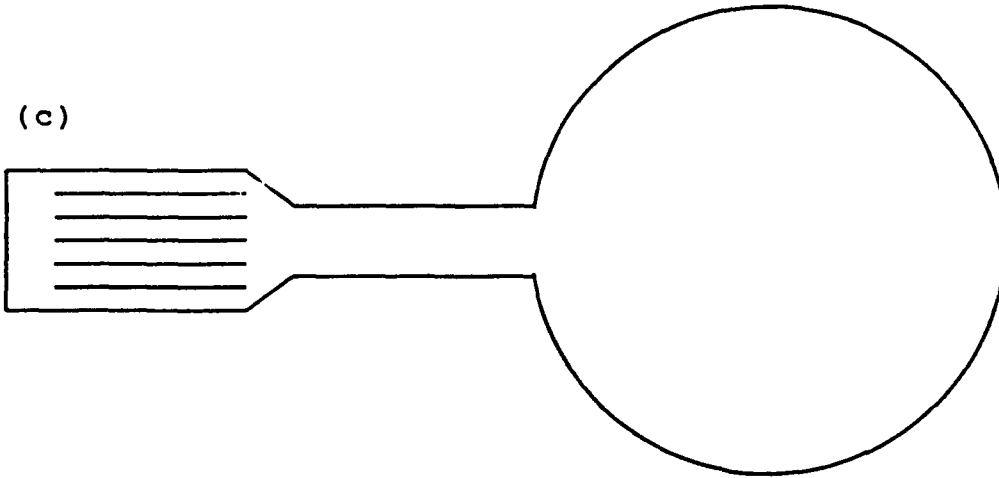


Figure III-1. Three Resonator Geometries

surface area of the sphere. The total dissipative losses would now be somewhat less than half that of the straight tube resonator. Hofler improved on this geometry with the resonator shown in Figure III-1C [Ref 6]. This resonator has lower losses because for small decreases in the length and diameter of the straight portion of the tube, the decrease in dissipative losses due to the reduction in surface area is more than the increase in losses due to increased particle velocities.

Another intuitive explanation of the effectiveness of this geometry emerges if we consider the resonator as being made up of three sections. In the stack section, fluid within a penetration depth is involved in the transport of heat along the stack from the cold end to the hot end. In the rest of the resonator, fluid within a penetration depth of the walls is involved in the dissipative losses while the remainder of the volume holds fluid that simply stores energy. This resonator design works best because the losses on the cold portion are lower.

The final resonator used by Hofler was modified slightly from the third geometry described above by the inclusion of a taper at the transition from the straight portion of the resonator to the sphere to reduce losses due to turbulence. This taper was replaced by a trumpet in the STAR resonator (Figure III-2).

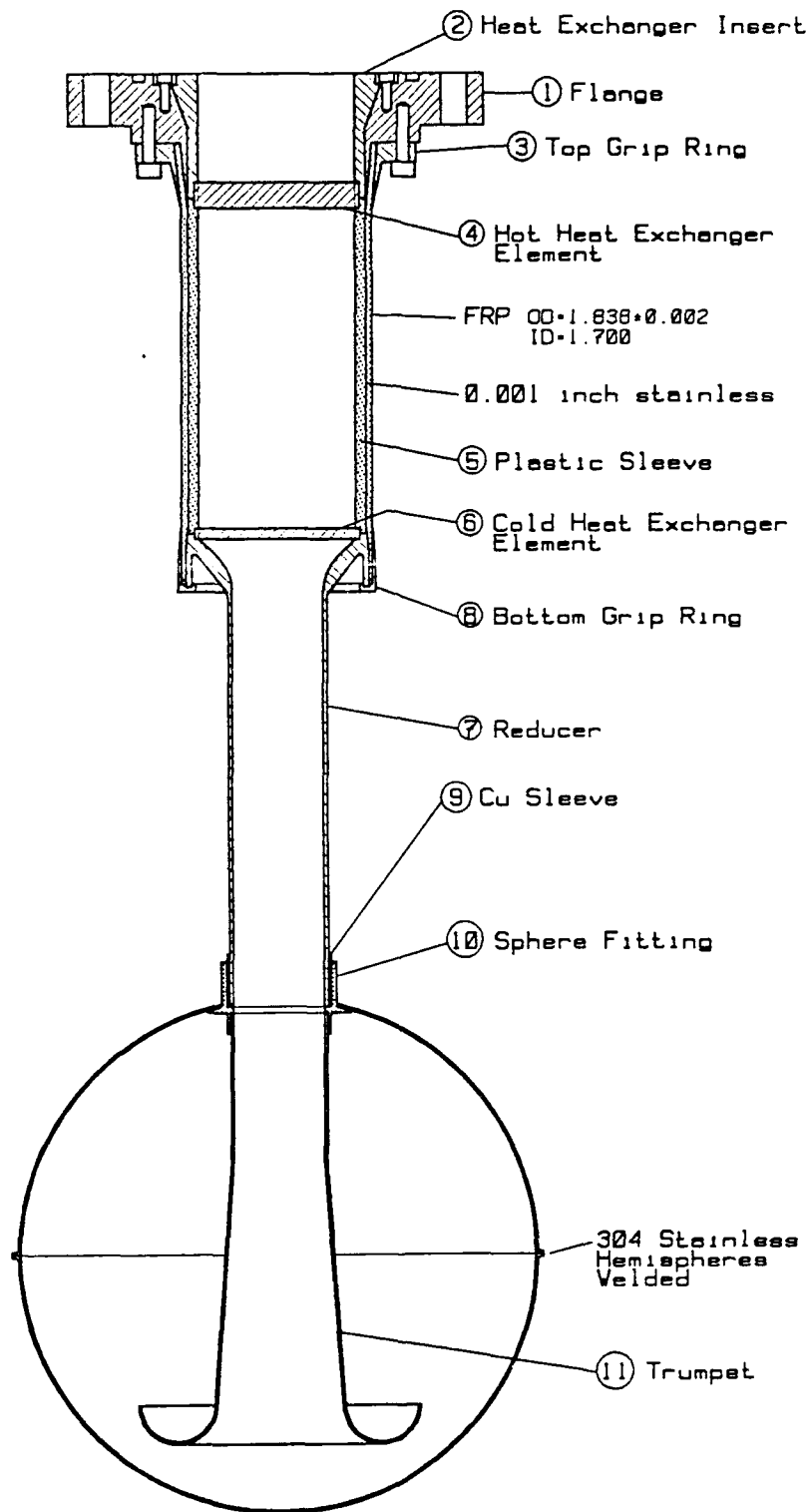


Figure III-2. STAR Resonator

The vessel which is to support the 1/4 wavelength standing wave and house the stack and heat exchangers must be capable of maintaining helium pressurized to 150 psi. The original goal was to hold such a pressure on a time frame to be measured in years. Clearly, this is useful in building a space bound experiment, it being most likely that the completed and packaged experiment will sit unattended at a NASA facility for a lengthy period of time awaiting a Space Shuttle manifest. The resonator design as presented in Figure III-2 was penned by Hofler based on the resonator he built for his Ph.D. thesis refrigerator. Several concessions have been allowed for in an effort to simplify the fabrication, as well as making the device more capable of withstanding the rigors of space flight.

B. VERSION ONE

1. Design and Description

The parts of the resonator assembly are as follows. The flange (1), taken from a solid piece of oxygen free copper, is the mounting point for the resonator to the driver housing. This material was chosen based on its high thermal conductivity since heat conducted away from the cold end of the resonator will flow through this part to reach a heat sink. This flange has two o-ring grooves in the mounting face; one for a rubber o-ring and one for a lead o-ring to seal the resonator against the driver housing.

Within the base is mounted a hot heat exchanger insert (2) to hold the hot heat exchanger (4) in a non-permanent fashion within the resonator. This insert has a 20 degree taper to mate with a similar taper in the flange. The surface finish of the tapers is very smooth (20 to 25 micro-inch) and the two parts are assembled with a layer of heatsink grease to provide the lowest possible resistance to heat flow.

The stack is contained in the area between the two heat exchangers. This cavity is lined with a layer of 0.001 inch stainless steel foil to act as a diffusion barrier against helium. A removable plastic sleeve (5) is inserted into the stack cavity within which resides the actual stack. Opposite the hot end of the stack is the cold heat exchanger (6) which is permanently soldered to the reducer neck (7), also made of copper.

A copper trumpet (11) and a stainless steel sphere are attached to the end of the reducer neck. The purpose of the sphere is to load the resonator in such a manner as to simulate an open termination, while still allowing for the pressurization of the resonator. The trumpet further enhances this termination by reducing excessive velocities and turbulence in the oscillating gas mixture.

In order to give structural integrity to the stack cavity wall, layers of fiberglass tape saturated with epoxy are wrapped around the stainless steel foil, overlapping

onto the copper flange and reducer neck to insure strength. Two grip rings (3 & 8) are glued over the fiber reinforced plastic (FRP) wrap, and another layer of FRP wrap is applied over the works to give added strength.

Dexter-Hysol epoxy (part number 9396) was chosen based on its high strength over a wide range of service temperatures and good resilience particularly at low temperatures. This particular epoxy may be cured at room temperature or at elevated temperatures of up to 82° C. The latter method was chosen because it reduced the curing time from several days down to 30 minutes, and because of the manufacturer's claim that the tensile lap shear strength in the temperature range of -55° C to +150° C was highest after such a cure.

The layers of fiberglass tape should be applied in an advancing helical patterns with each subsequent layer in the opposite direction in the same manner as that of a bias belted automobile tire. A longitudinal layer should also be inserted between pairs of spiral layers to give added strength.

2. Assembly

The assembly of the STAR resonator is of a complicated and delicate nature and deserves further description. Figure III-3 illustrates the assembly rig for soldering the stainless steel foil to the copper flange and reducer neck.

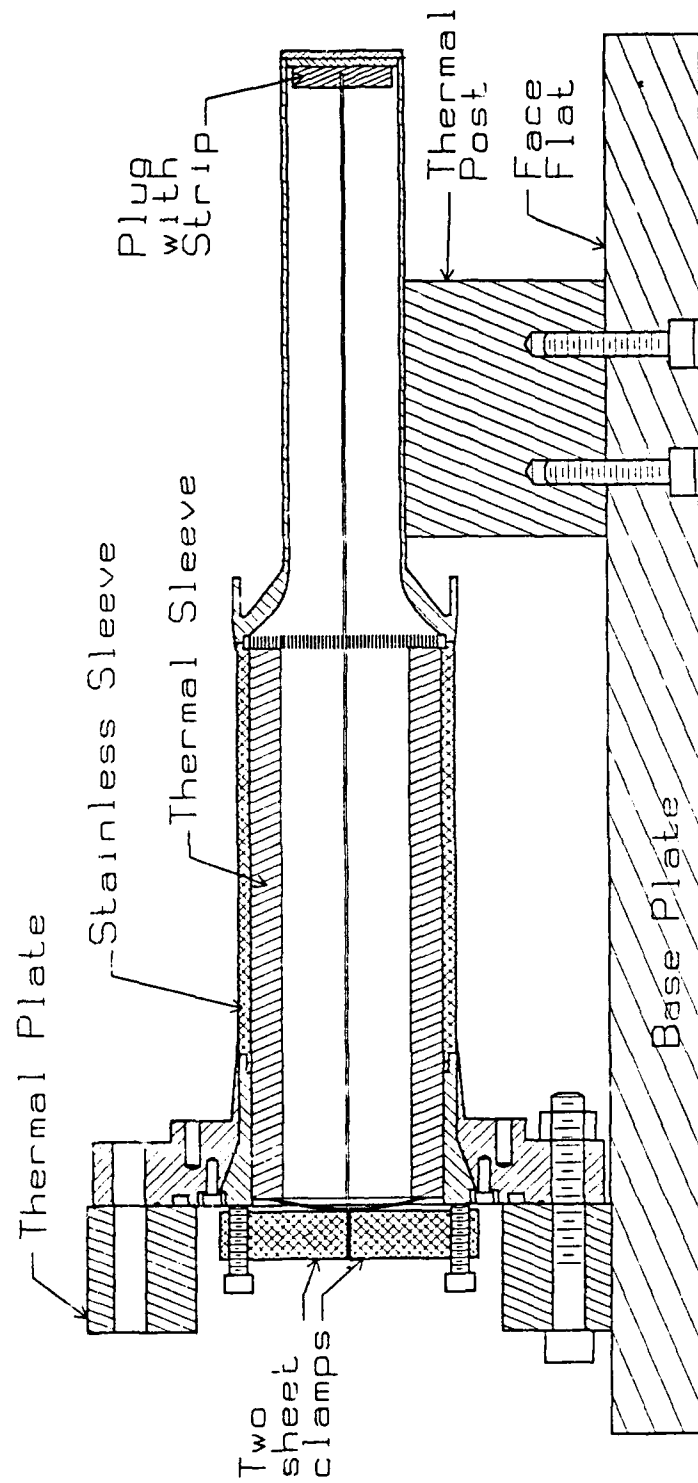


Figure III-3. Resonator Foil Soldering Set-Up

A sheet of stainless steel foil measuring 3.190 +/-0.025 inches by 5.50 +/-0.05 inches was pre-tinned taking great care not to splatter excessive amounts of soldering flux onto the foil as this would encourage corrosion, particularly in places where impurities might be embedded in the foil. This pre-tinned stainless foil was then wrapped tightly around a stainless mandrel (1), identical to the plastic stack sleeve in its dimensions. Now, having previously soft soldered the cold heat exchanger into the reducer-neck and having pre-tinned the inner faces of the flange and reducer-neck knife-edges, the latter two parts were slipped onto the ends of the stainless foil/mandrel.

It was imperative that all the parts be as clean as possible and that all traces of solder flux be removed to reduce the risk of soldering the stainless steel sleeve to the resonator. This resonator sub-assembly, with all its pieces in proper relation to each other, and with an aluminum thermal sleeve inserted inside of the stainless steel sleeve, was held together in tension by a plug with strip and two strip-clamps. The entire setup was bolted to a square thermal plate and placed horizontally on the base plate/thermal post.

This resonator sub-assembly could now be heated up to such a temperature as would cause the solder on all the pre-tinned mating surfaces to melt and flow into each other. By judiciously applying small dabs of flux-dipped solder

along the joints, a good fillet of solder could be deposited to complete the soldering process and form a leak tight seal. Only copper flux was used at this point so that if any flux found its way into the resonator it would not be possible for the solder to flow onto the stainless steel sleeve. A small thin strip of aluminum was placed over the longitudinal seam of the foil and held in place by wrapping a thin wire spirally around the resonator sub-section to keep the seam flat and to insure a good solder joint.

After preliminary leak testing, repairs were done to the stainless steel foil as described in the following section, and the FRP wrap was layed down. As an aid to this step, an aluminum mounting boss was bolted to the resonator flange to allow the structure to be placed in a lathe chuck for easy turning about its longitudinal axis. Each successive coating of FRP was first cured in an oven at 85 degrees centigrade and then sanded to prepare it for the next layer. After two opposite spirals layers, then one longitudinal layer, and finally two more opposite spiral layers had been layed down, the FRP was machined to a diameter of 1.838 inches with a 4.9 degree taper at the hot end. This taper corresponds to the taper in the hot end grip ring and is illustrated in Figure III-2. The copper grip rings could now be glued and bolted into place, and the final two opposite spiral layers of FRP applied.

At this stage, the resonator sub-assembly was strong enough that the assortment of clamps and mandrels could be removed allowing it to stand on its own. The trumpet and sphere were hard soldered together with an intermediate sphere fitting (Figure III-2, #10), and then soft soldered to the end of the copper reducer neck. The final step was to solder the hot heat-exchanger (Figure III-2, #4) into the heat-exchanger insert (Figure III-2, #2). By attaching a special adapter with a rubber o-ring to the flange of the completed resonator assembly, leak testing could now commence.

3. Leak Testing

The leak test of the resonator was performed on an Alcatel ASM 110 Turbo CL leak tester. Figure III-4 illustrates the physical set-up for these tests. The leak testing was actually done at two stages of the assembly. First, after the stainless foil had been soldered in place; and second, after the FRP wrap had been applied and the resonator/trumpet attached. The procedure for leak testing the resonator was to first evacuate the interior of the resonator with the Alcatel's built in roughing pump until the pressure was brought below 10^{-1} mBar. The turbo-molecular pump could then be used to further reduce the pressure to below 10^{-5} mBar. The helium mass spectrometer could then be used to detect any helium that might enter the

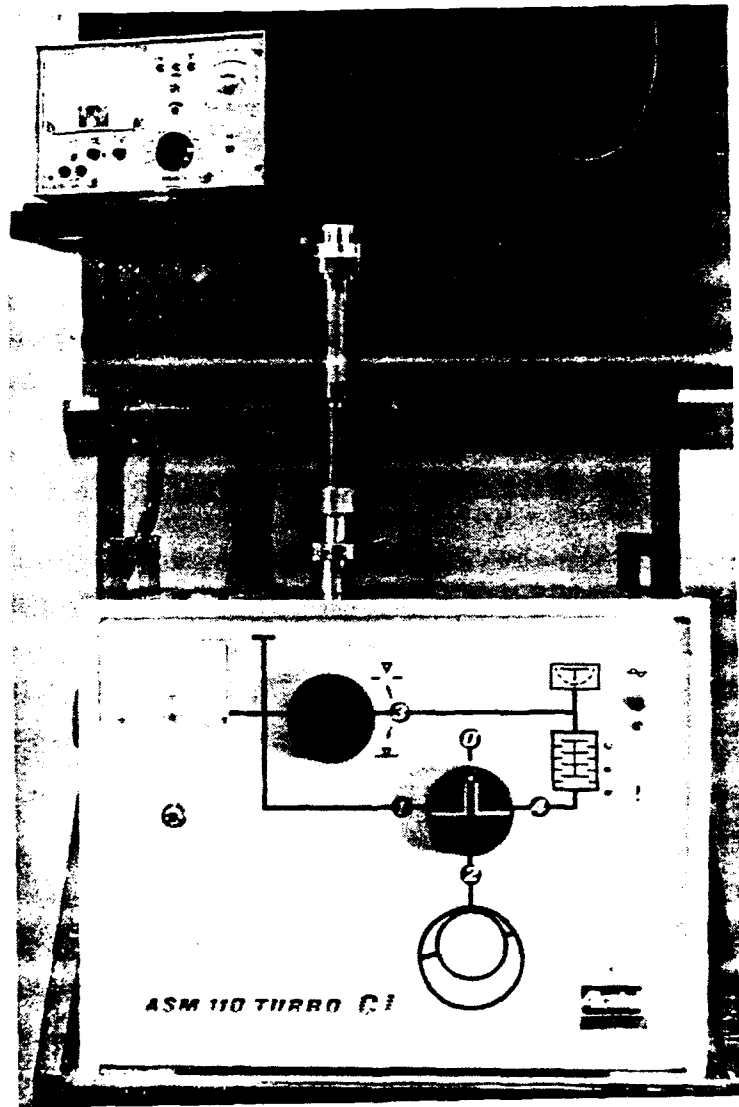


Figure III-4. Resonator Leak Test Set-Up

system through a leak by applying a spray of helium to the exterior of the resonator.

The first leak test of the resonator sub-assembly (as described in the assembly section) allowed for the pinpointing of small repairable leaks in the stainless steel foil solder joints. After exposing and touching up several small leaks with a soldering iron, the final result was that with a pressure inside the resonator below 10^{-5} mBar and with a healthy stream of helium applied to the outside, a leak rate of less than 2×10^{-8} standard cubic cm./sec. was measured. The background leak rate with no helium applied was 1.5×10^{-9} standard cubic cm./sec. It was decided at this point that further attempts to touch up the solder joints would probably make the leak rate worse.

The second leak test could not be performed by spraying the evacuated resonator with helium as the FRP wrap would greatly lengthen the diffusion time. This long diffusion makes it virtually impossible to pinpoint a specific leak. It was more important at this point to establish a base leak rate to determine if the resonator was holding up or if new leaks were forming as the resonator cold end was pressurized and temperature cycled. It was now necessary to wrap a plastic bag around the resonator in order to displace all the air with helium. With a vacuum in the resonator below 10^{-5} mBar and with same bathed in one atmosphere of helium, no leak rate beyond the background

rate of 1.5×10^{-9} standard cubic cm./sec. was detected after one hour. Letting the test stand for two more hours eventually produced a response from the leak detector on the order of twice the background leak rate; or 3×10^{-9} standard cubic cm./sec.

4. Instrumentation

There are three devices mounted to the exterior of the resonator, the first two being thermocouples and the third, a resistive heater strip. The two thermocouples are for monitoring the hot and cold temperatures, and are mounted on the largest diameter of the flange and on the smallest diameter of the reducer close to the cold heat exchanger. The heater strip provides a heat load of up to ten watts to determine the coefficient of performance of the refrigerator. It is mounted next to the cold thermocouple but opposite the cold heat exchanger.

For this first version of the resonator, E-type thermocouples were applied to make use of existing E-type thermometers and thermocouple amplifiers. A thermocouple is produced when two dissimilar metal wires are brought into contact, resulting in an open circuit voltage across the two wires known as the Seebeck-voltage. This voltage is a function of the temperature of the junction of the two metals and of their composition. It is therefore desirable that only thermocouple wire (chromel/constantan in this case) be used from the thermocouple to the thermometer

because any additional junctions between a thermocouple wire and a non-thermocouple wire will create additional thermoelectric circuits in series with the original thermocouple. For the temperatures of interest in STAR, the Seebeck-voltage is on the order of minus three to plus three millivolts.

Thermocouple thermometers have connectors made of thermocouple metal and incorporate a cold-junction compensation circuit to insure that the temperature reading is accurate and referenced to zero degrees centigrade. If copper wire is used between the thermocouple and the thermometer, the temperature reading will be erroneous. The first potential problem in this application, therefore, was the need to bring the thermocouple leads out of the hermetically sealed vacuum cannister and into a temperature reading device without effecting the accuracy.

It is actually permissible to have extra non-thermocouple junctions in the thermocouple wire line under certain conditions. The law of intermediate metals states that if one of the lines is interrupted by a different type of wire; so long as both new junctions are at the same temperature the overall voltage will not be effected. For example, if the chromel line is interrupted by a length of copper line; as long as both new chromel/copper junctions are at exactly the same temperature, the overall reading will not be effected. This is useful because it means that

the thermocouple wires can be brought out through the vacuum canister wall via a hermetic feed-through, and then continue on to the thermometer with proper thermocouple wire. The two new junctions at the feed-through are so close to each other that they may be considered to be at the same temperature. The temperature readings will thus remain accurate.

There are two methods for reading the thermocouple voltage directly on a voltmeter to simplify data acquisition. The first method, used for the cold thermocouple, is the simplest and involves the use of a thermocouple DC millivolt amplifier with a built-in cold junction compensator and a voltage gain of 100. The output of this device, under ideal conditions, is the Seebeck-voltage multiplied by a factor of 100 which can be converted to a temperature reading through the use of a thermocouple table or a polynomial equation approximating the table. An Omega Omni-Amp IIB battery operated thermocouple amplifier with built in E-type cold junction compensation fulfilled this requirement.

The second method, used for the hot thermocouple, does not require cold junction compensation hardware. Instead, it uses a computer to perform a software compensation. A Hewlett-Packard thermistor is used in conjunction with a HP 3457A multimeter to measure the temperature of the thermocouple wire to copper junction at

the vacuum canister electrical feed-through. The multimeter has built into it the necessary mathematical function to convert the temperature dependent resistance of the thermistor into a centigrade temperature. The temperature is then recorded by a HP 9836 computer which is interfaced with the 3457A through the HP-IB line. The computer uses a fifth order polynomial fit to the Seebeck-voltage versus temperature function for the E-type thermocouple to convert this temperature into an equivalent thermocouple voltage. It then adds this voltage to the voltage from the hot thermocouple which has been measured directly with the HP 3457A. This new voltage is now proportional to the temperature of the hot thermocouple referenced to zero degrees centigrade, and by reversing the above calculation can be converted back into a degrees centigrade reading.

The resistive heater strip (Minco HK5232R45.8112a1-7) has a manufacturer specified resistance of fifty ohms and is powered off of a DC power supply. The voltage drop across the heater was monitored on a hand-held multimeter and recorded manually. The amount of heat delivered to the cold end of the resonator was easily calculated , for DC voltages, as the power in watts equal to the voltage squared divided by the resistance of the heater. Since the resistance of the heater is proportional to the temperature, this dependence was measured and is plotted with a linear best fit in Figure III-5.

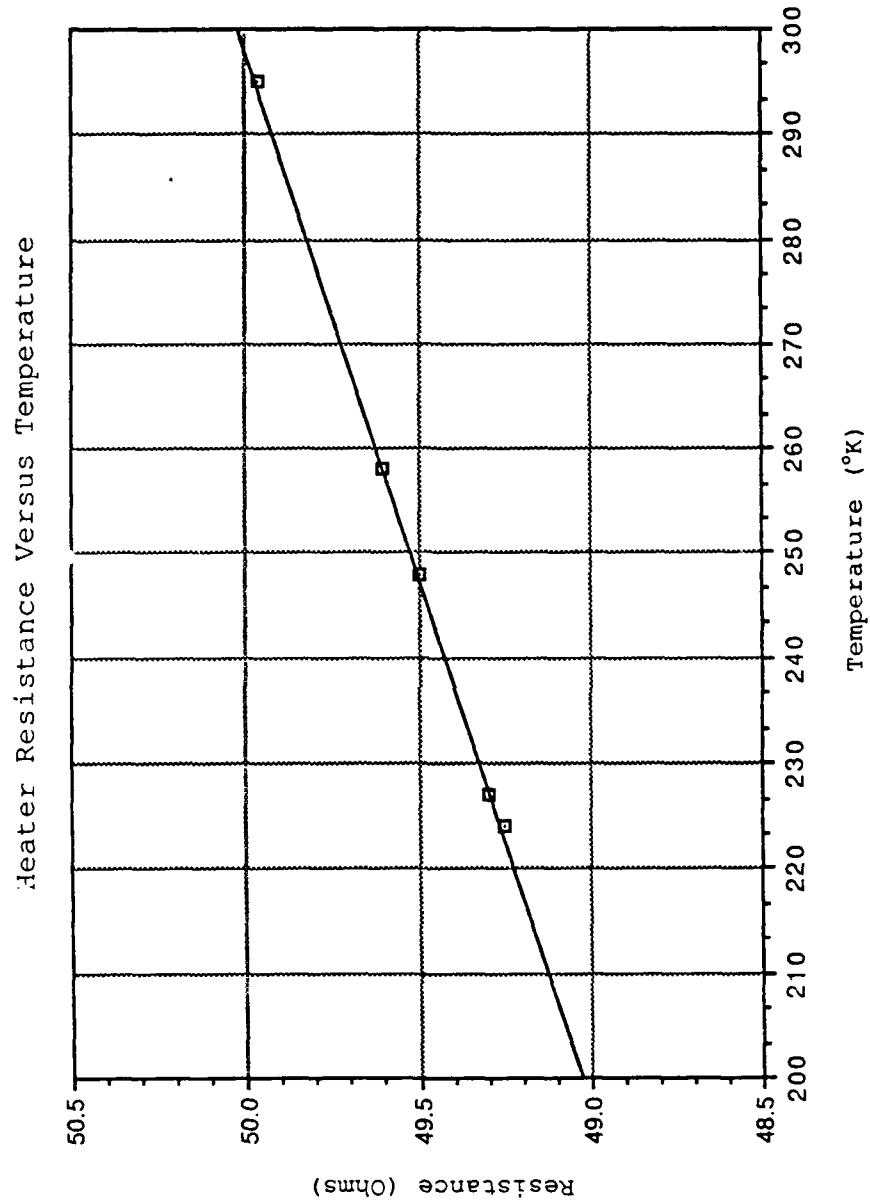


Figure III-5. Strip Heater Resistance

5. Failure and recommendations

Version one of the resonator began to leak after the first temperature cycle. The cold temperature reached was minus forty degrees centigrade, while the hot temperature was thirty degrees centigrade for a temperature span of seventy degrees. The leak was found to be located at the cold end where the FRP wrap meets the copper reducer. The "moat" area in the reducer neck was filled with Emerson-Cummings 2850FT epoxy, allowed to cure, and then leak tested again to confirm that the leak had indeed been stopped. At room temperature, the resonator now appeared to be capable of holding ten atmospheres of helium indefinitely. This state of affairs , however, did not last beyond the succeeding temperature cycle.

Several factors must have contributed to the resonator's inability to withstand a temperature cycle. The first candidate for blame was the method used for curing the Dexter-Hysol 9396 epoxy FRP wrap. Each individual layer of FRP was cured in an oven at a temperature of 85 degrees centigrade. Such an elevated temperature must surely have caused the copper parts to expand, while the epoxy cured to these larger dimensions. Add to this the contraction of the copper reducer that occurred when the cold end of the resonator was brought down to minus forty degrees, and one may surmise that the FRP wrap easily delaminated from the

copper and stainless foil possibly tearing the foil thereby producing the leak.

A second possible cause of the leak was in the stainless steel vapor shield. This 0.001 inch foil was subjected to a temperature of 175 degrees centigrade for a rather long period of time while it was soldered to the copper pieces. It is entirely possible that if any impurities existed in the foil, the extreme heat could have vaporized them, especially if splattered by the corrosive soldering flux. In fact, under the extreme heat, just the soldering flux itself could have caused pin-hole leaks to have formed by oxidizing the stainless steel. It is also possible that an air bubble could have formed between the stainless steel foil and the FRP wrap. If so, each time the driver housing/resonator was evacuated the air bubble would have expanded and could have possibly torn the foil.

To solve the first problem of the FRP delaminating from the copper sub-components, it would be necessary, first of all, to cure the epoxy at as close to the service temperature as possible. While it is impossible to cure the EA9396 at minus forty degrees centigrade, it is possible to cure it at room temperature. The advantage to an elevated cure temperature is that a less tacky surface finish is obtained, and the tensile lap shear strength is increased slightly. A compromise can be reached by first curing the epoxy at twenty to thirty degrees centigrade until hard, and

then placing it an oven at forty to fifty degrees to provide a smoother surface finish. Such a surface finish is desirable because it makes sanding, machining, and preparation for succeeding layers easier. Baking the epoxy also helps hasten the outgasing that takes place with any such material.

The fundamental cause for the delamination of the FRP from the copper reducer still remains however, and that is the contraction of the copper at a different rate from the epoxy impregnated fiberglass tape at low temperatures. The classic method employed in cryogenics when two materials with dissimilar thermal expansion coefficients are joined at liquid helium temperatures is to make the joint flexible by using long thin knife-edges to "feather" the transition between the two materials. Returning to Figure III-2 it can be seen that the existing 0.050 inch long knife-edge must be made longer.

Finally, the question of the stainless steel vapor shield must be addressed. Probably the most overwhelming cause of problems in soldering the foil to the copper sub-components was the author's lack of experience in performing such a delicate operation. The second try would undoubtedly be more successful in that much less time would be required to achieve even better results, thus reducing the foil's exposure to extreme temperatures. In addition, exposure to corrosive soldering flux must also be minimized.

C. Version Two

1. Design and Description

Structurally, version two of the resonator has one difference from the first version. The reducer neck has been modified to provide a longer knife edge where it meets the stainless steel foil. Figure III-6 shows an enlarged cross-section illustrating how material was removed from the existing design to lengthen the knife edge to 0.150 inches, or three times the length of version one. Consequently, to keep the relationship between the reducer and the cold heat exchanger identical, it was necessary to add a cold heat exchanger holder as shown in Figure III-7A. A loose fitting filler ring (Figure III-7B) occupies the gap created by the inner knife-edge wall and the heat exchanger holder. This ring must be loose enough that the knife edge will be free to bend with the FRP wrap as the cold end of the resonator is temperature cycled.

Other ideas were explored but not employed, such as making the grip rings out of aluminum instead of copper and finding a different epoxy. An aluminum grip ring might possibly keep the FRP wrap from delaminating because the ring would contract more than the copper reducer and thus pinch the epoxy layer down against the underlying surface. This idea, however, was left as a last resort in the event that version two did not hold up. On the other hand, it is

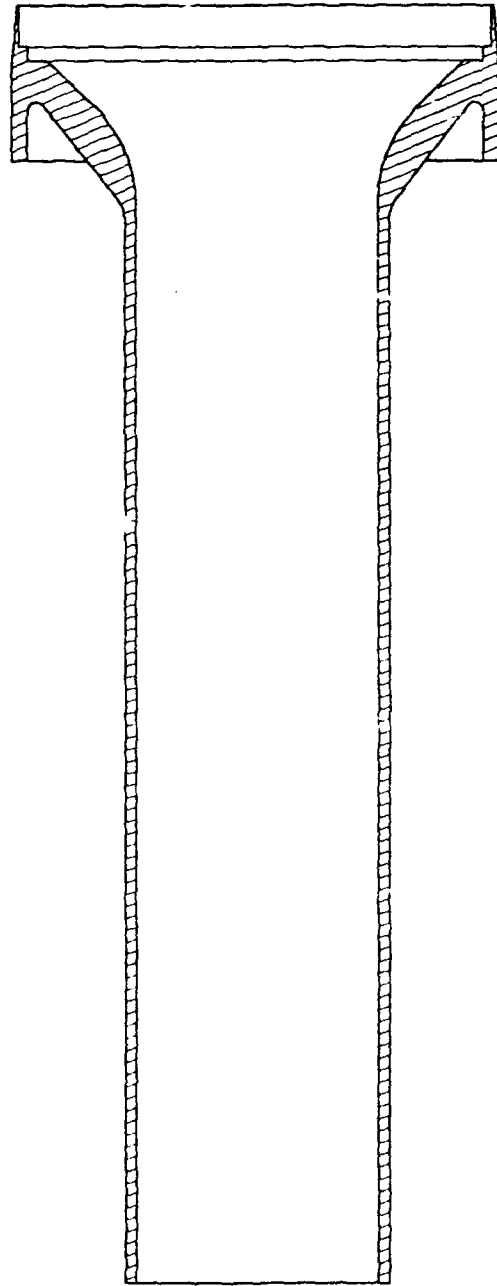
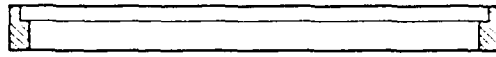


Figure III-6. Modified Resonator Reducer

a. Cold Heat Exchanger
Mounting Ring



b. Filler Ring
1 Req'd Copper



Figure III-7. Cold Heat Exchanger Insert and Filler Ring

possible that there exists a different epoxy better suited to cryogenic temperatures.

The first thermoacoustic refrigerator built by Hofler used Stycast 1266 epoxy for the FRP layer [Ref. 8]. This two part epoxy has a high degree of plasticity at low temperatures and has yet to delaminate after years of operation. Stycast 1266, unfortunately, is not suitable for STAR because of the possibility of exposure to high temperatures which would severely soften this epoxy. NASA has recommended the use of 3M Scotchweld 2216. This is an epoxy that, while not at the forefront of materials technology, has been used extensively for space applications. This information arrived too late to be of use for resonator number two, but will be explored for subsequent flight resonators.

2. Assembly

The procedures for assembling resonator number two are mostly identical to the first version. Some important differences do exist, however. The first important alteration came in the very first step of soldering the stainless steel foil to the copper sub-parts. The strategy was, firstly, to lessen the trauma imparted to the delicate foil by not exposing it to extreme high temperatures for an unnecessarily long period of time, as was done the first time around. Secondly, the stainless foil was covered as

much as possible with aluminum foil to prevent flux from spattering onto it and oxidizing a hole into it.

Rather than heating the entire resonator until the solder would flow, and subsequently losing control of the situation because solder would drip out of one joint as another was worked on, the resonator was heated in sections. First, the reducer section was placed directly over the hot plate and heated until the solder just softened. A tiny amount of solder, pre-flattened to a knife edge and wetted with copper flux, was applied to the joint until a good fillet was produced. The resonator assembly was immediately moved so that the opposite end was now directly over the hot plate. In this manner, the solder joint just completed was allowed to cool before the solder could flow down and collect underneath. As the other joint reached soldering temperature, it could be worked on without fear of ruining the first joint. The seam along the length of the stainless foil was completed with a soldering iron while the resonator was still quite hot, but not hot enough for solder to flow. Thus, the mandrel beneath the foil was prevented from acting as a massive heat sink which would render the meager power of the soldering iron to be insignificant.

The modifications to the FRP layup have already been described, but it must be stressed at this point that it is very important to insure that there are no air bubbles in between the stainless foil and the first layer of FRP.

Attaching the sphere/trumpet assembly was done at NPS by the author instead of at the Naval Research Center (NRL) as with resonator number one. Extra caution was taken to keep the body of the resonator from being overheated while the sphere assembly was soft soldered onto the end of the reducer neck.

3. Leak Test

The second resonator (Figure III-8) was tested in a manner identical to the first. Also like the first resonator, it did not pass the test the first time around. Small leaks in the copper to stainless foil interface were easily touched up with a soldering iron. The foil seam was, however, much more elusive and required repeated attempts at obtaining a leak tight joint. Finally, a leak rate so small was achieved that the leak detector would only register on the most sensitive scale after the resonator had been enclosed in a plastic bag and smothered with helium gas for upwards of thirty minutes.

D. THERMOACOUSTIC STACK AND HEAT EXCHANGERS

1. Stack

The so called "heart" of the thermoacoustic refrigerator, the (thermoacoustic) stack, is an arrangement of parallel plates spaced on the order of a thermal penetration depth apart. A strictly parallel plate arrangement is rather difficult to manufacture when resources are limited. Thus, an elegantly simple solution

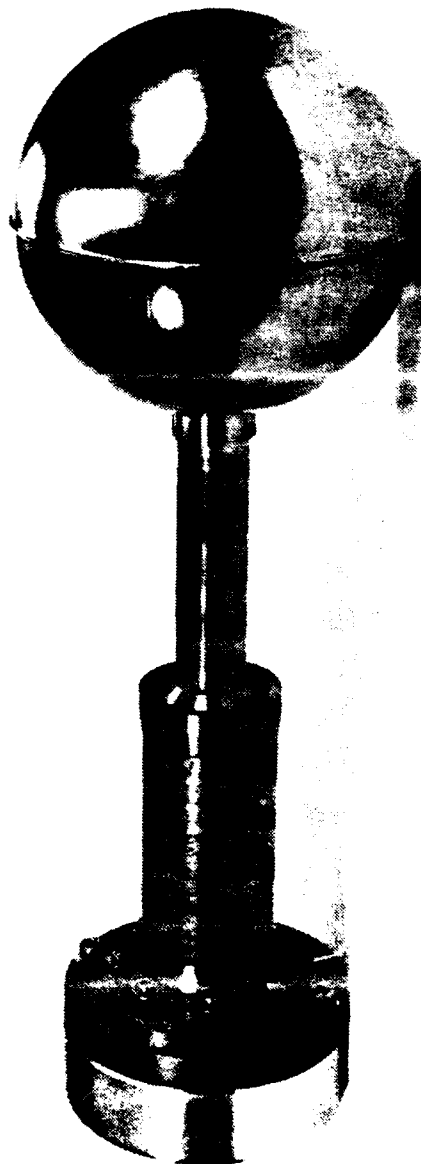


Figure III-8. Completed Resonator

was devised by Hofler [Ref.9]. A close approximation to the parallel geometry could be produced by winding a long sheet of 0.003 inch thick polyester film, with spacers at predetermined intervals, spirally around a plastic rod. The spacers consist of 0.015 inch diameter monofilament fishing line glued laterally onto the plastic sheet using 3M type 77 spray adhesive.

The polyester film was cut on a paper shear to a width of 3.090 +/-0.005 inch by holding it against a length of masking tape that was layed down 3.090 inches from the cutting edge. In order to provide accuracy, repeatability, and ease of construction an aluminum loom was used to locate the monofilament fishing line. Two looms were used, one with a filament separation of 0.200 inches and the other with a spacing of 0.125 inches. Narrow spacing was used on the inside of the spiral to insure that the plastic film did not collapse on itself, and then the wider spacing was used once the curvature of the the stack had decreased sufficiently.

The fishing line was strung onto the loom as illustrated in Figure III-9. A continuous length was strung side to side between a series of hooks and grooves which provided about six inches of parallel filament that was exposed both front and back. It was important not to wind the filament too tightly as this would cause it to curl up once glued onto the film and released from the loom. A mask

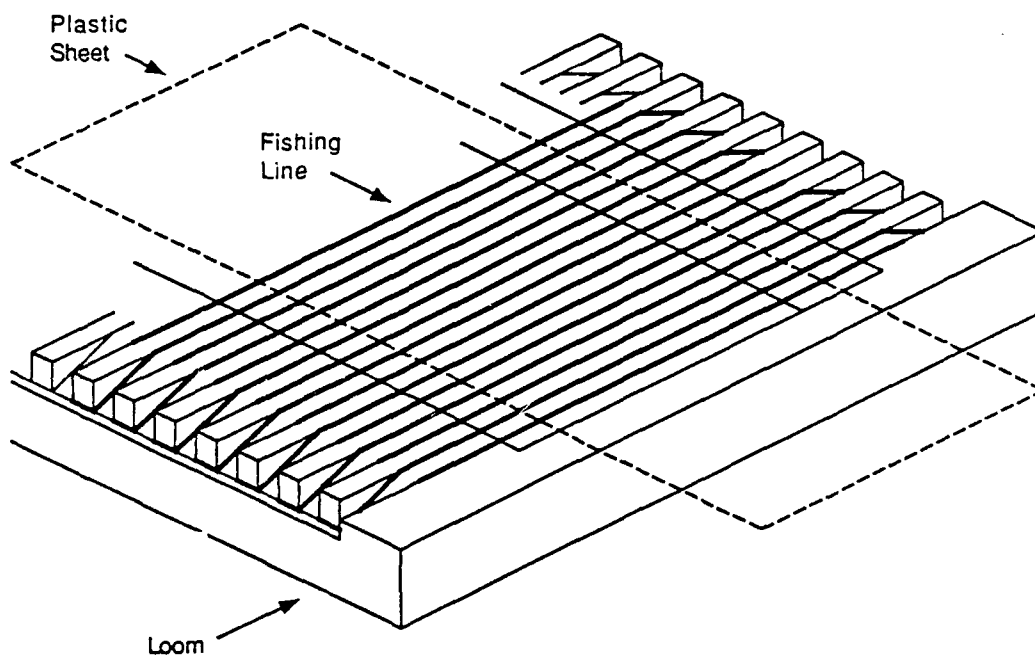


Figure III-9. Stack Winding Loom

was placed around the strung filament to cover the loom and glue was sprayed onto one side of the filament. The assembly was then lowered onto the film using, as a guide, lines drawn onto a piece of paper placed underneath a sheet of translucent Teflon. A Teflon wrapped aluminum block, slightly smaller than the opening of the loom was used to press the monofilament against the film. Having allowed the glue to dry for a few minutes, the filament hangover could then be cut with a scalpel blade and the loom lifted off of the film. Although the glue would set rather quickly (one to two minutes), it would not cure for at least one hour, so it was necessary to handle the newly completed sections carefully.

Once a sufficient length of film had been prepared, it was wound onto a nylon rod 0.25 inches in diameter and no more than 3.090 inches in length. The stack was wound with one end against a flat surface and periodically checked for uniformity to insure that the stack would not have uneven end faces. This technique eliminated any need to make adjustments to the completed stack. If one edge of the roll began to run ahead of the other the stack would become lopsided and begin to form kinks and uneven spacing. A small amount of tension was necessary to keep the roll uniform and to maintain a cylindrical outline, but too much tension would create non-uniform spacing and would also introduce the risk of rolling the filament off of the film.

Once the roll was completed it was held together by a piece of Mylar tape (Figure III-10). The diameter of the stack could be adjusted by simply cutting off some material until the dimension was as desired.

2. Heat Exchangers

The heat exchangers provide the means by which heat is conducted away from the walls of the cold end of the resonator to the cold end of the stack and then, subsequently, from the hot end of the stack to the walls of the hot end of the resonator. These heat exchangers, a series of parallel copper plates, look simple in form, but are rather complex in their multi-stage fabrication (Figure III-11). The method of "lost aluminum" was used in the manufacturing of these elements.

To begin, cold-roll soft-temper copper sheet of 0.010 inch thickness and 1100 series half-hard aluminum sheet of 0.020 inch thickness were cut into squares measuring 1.55 by 1.55 +/-0.005 inches on a sheet-metal shear. These dimensions were critical because the squares would be stacked and pressed alternately into a precision machined rig with epoxy in between each sheet (Figure III-12). Before this could be done, however, the squares had to be properly prepared. Each square was examined, and any that had dimples or creases were discarded. The good squares were then very carefully deburred first with a jeweler's file, and then with aluminum-oxide wet/dry sand

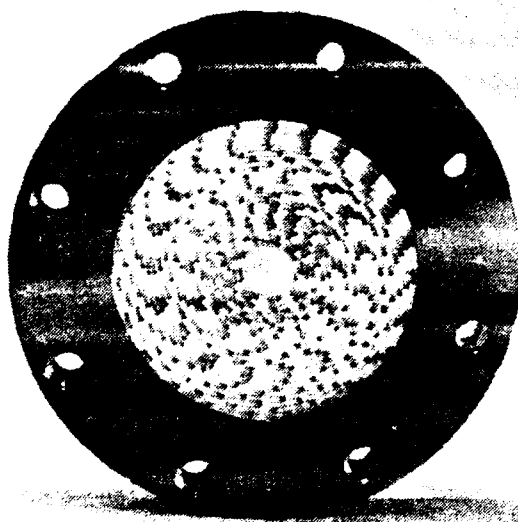


Figure III-10. Completed Stack

Faint, illegible text, possibly bleed-through from the reverse side of the page.

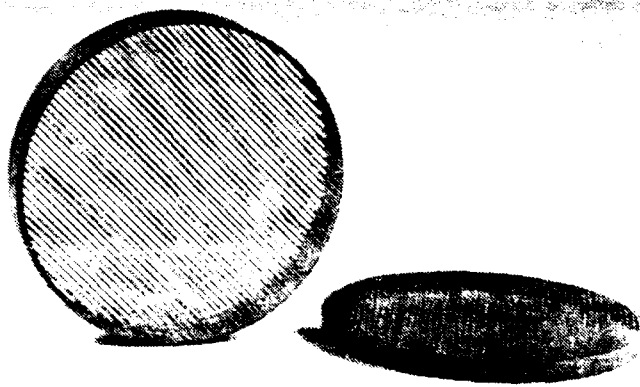


Figure III-11. Heat Exchanger

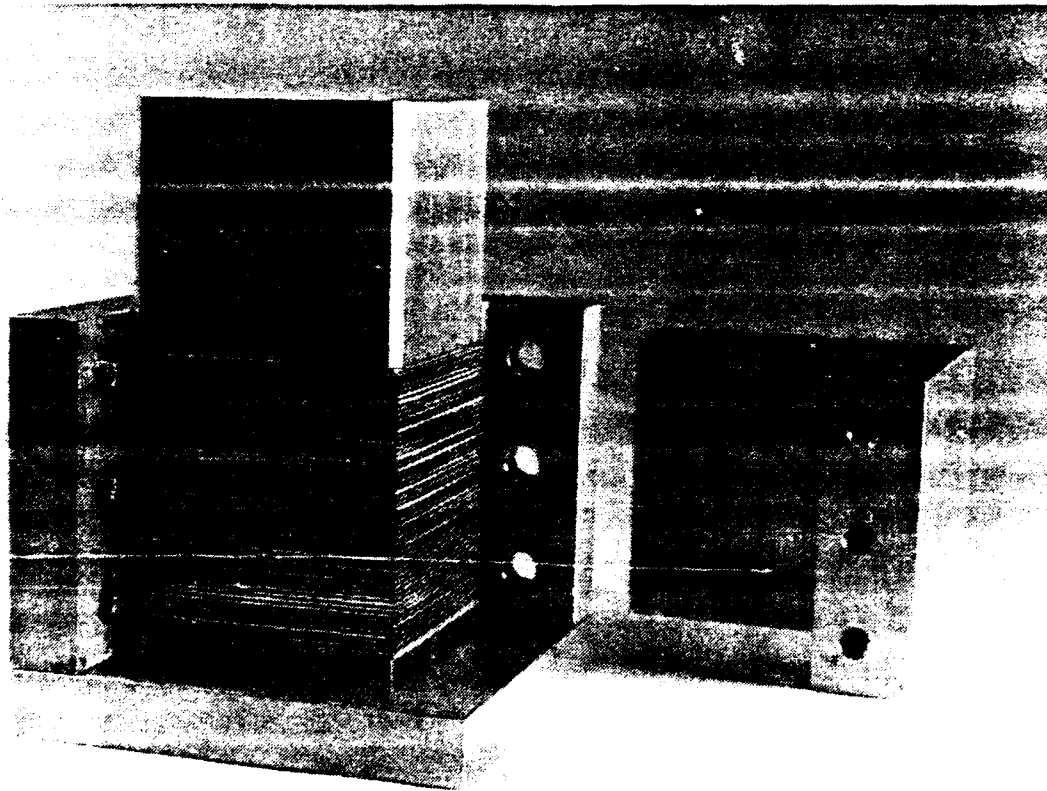


Figure III-12. Heat Exchanger Assembly Jig

paper. The squares were then checked for flatness against a granite laboratory standard flat surface and bent carefully by hand until they were as flat as could be achieved. The plates were then soaked in an acetone bath overnight and wiped with lint-free cloth to remove all traces of oil and grease. Finally, the plates were pressed, all at once, in between two machined aluminum slabs for several days to remove any remaining hints of curvature.

The plates were then assembled into the aluminum jig. The jig was slowly filled, alternating between aluminum and copper plates, with a layer of Stycast 1266 epoxy in between each plate. After ten plates had been placed in the jig, a block of aluminum was inserted and pressed into the jig with the aid of a ten ton hydraulic press to squeeze the plates together. Grooves cut into the inside walls of the jig and pressing block allowed the excess epoxy to escape. This procedure was continued until the jig was filled and all the plates compressed. The hydraulic press was then replaced with a C-clamp and the walls of the jig removed. This assembly could then be allowed to set overnight if one trusted the mold release applied to the contact surfaces of the jig base and press block. On the other hand, by being very careful, the C-clamp could be removed long enough for the remainder of the jig parts to be replaced by clean aluminum plates coated with fresh mold release. This procedure was used since the

risk of glueing the sandwich of plates to the jig was quite real.

Once the sandwich had set, it was released from compression and carefully machined on a lathe into a cylindrical rod as shown in Figure III-13. This was certainly the most critical step as the sandwich could very easily delaminate under the forces created by the cutting tool on the plates. It was necessary for the master machinist to stop the lathe after each 0.005 inch cut to manually debur the leading edge of the sandwich with a file thus preventing the cutting tool from catching one of the plates and tearing the laminated block apart. The final diameter of the laminated cylinder was 1.50 inches.

The sandwich of copper and aluminum plates was then electroplated with copper to a thickness that would provide sufficient material to allow it to be machined into a cylindrical rod with a diameter of 1.588 +/-0.001 inches. Now, the rod could be sliced, deli-style, into wafers of 0.250 inch and 0.100 inch thickness for the hot and cold heat exchangers, respectively. The cutting was done on a wire electro-discharge machine (E.D.M.), and the wafers were actually cut 0.003 inch over-size to allow for sanding to remove the surface roughness caused by this cutting method (Figure III-14). The final step was to remove the aluminum from the wafers by soaking them in hydrochloric acid. The epoxy was sufficiently softened by the acid that most of it

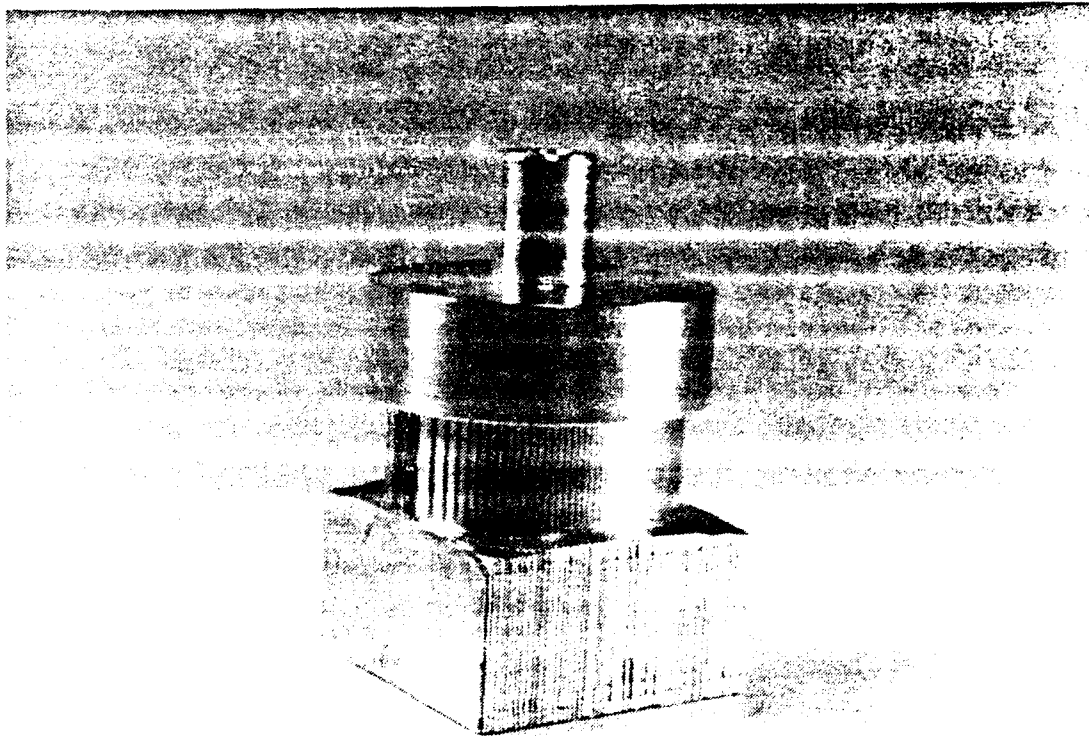


Figure III-13. Unplated Heat Exchanger Stack

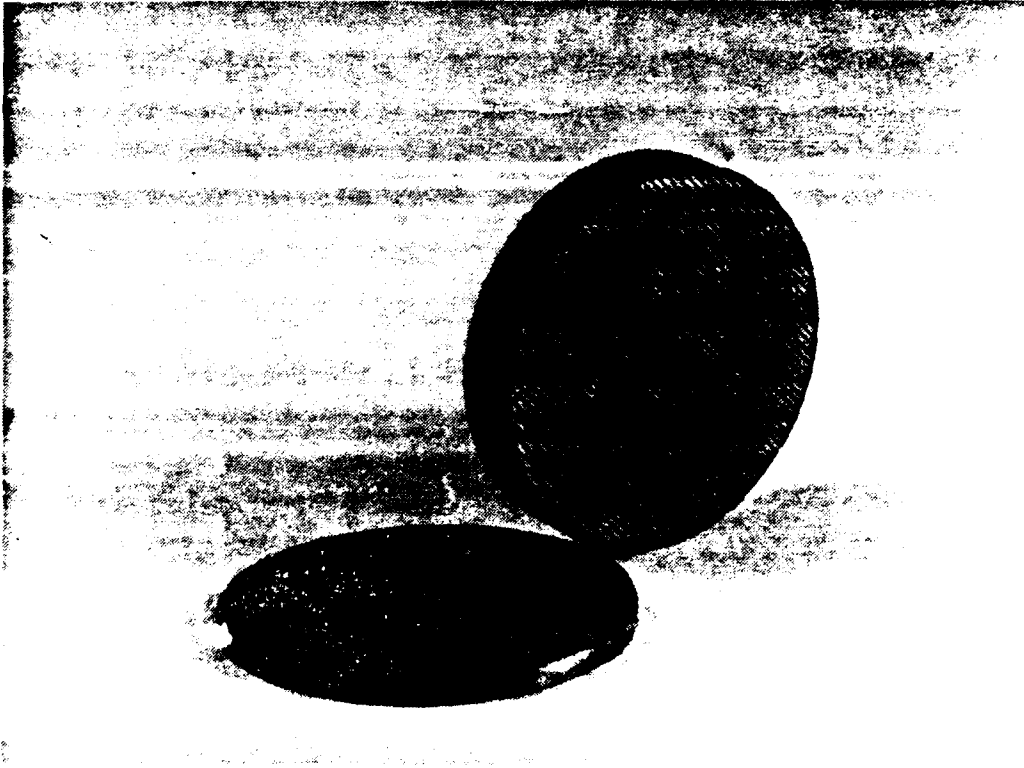


Figure III-14. Heat Exchanger Slice

fell out and the rest could be removed with an ultrasonic cleaner or manually with a sharp probe.

E. THERMAL LOSSES

1. Heat Leak

Heat can leak back to the cold end of the resonator by at least four methods. The first, and most serious, is by simple convection due to the air surrounding the resonator. This source is eliminated, as described in the following section, by enveloping the resonator in a vacuum. The second cause of heat leakage is by infrared radiation. The walls of the vacuum can are necessarily at ambient temperature and thus will radiate energy toward the resonator. This problem is solved by wrapping the structure with a form of insulation affectionately referred to as "super insulation." This material consists of alternating layers of 0.0005 inch aluminized mylar and ultra fine glass fiber blanket. The glass fiber blanket serves, primarily, to separate the layers of aluminized mylar. A minimum of five layers should be applied but it is preferable that ten layers be used.

The remaining two methods whereby heat may leak back to the cold end of the resonator are essentially losses that have already been minimized as much as possible. The first is by conduction due to the cables leading to the cold end thermocouple and resistive heater strip. These sources are

of small enough magnitude that they may be considered to be negligible. The second source is the resonator itself. Heat will inevitably leak down the FRP tube separating the cold end of the resonator from the hot end.

Providing that the resonator has been well insulated as described previously, and that a good vacuum has been achieved in the thermal vacuum canister, a good estimate of the heat leak along the FRP tube can be calculated by cooling the refrigerator down close to its lowest temperature and then shutting it off and measuring the warm up time. Combined with an estimate of the heat capacity of the cold end subsection of the resonator including the reducer, trumpet, sphere, cold heat exchanger, and sphere flange the heat leak in Watts can be calculated from the relation

$$\text{heat leak} = (\text{heat capacity}) / \tau \quad (\text{III-1})$$

where the heat capacity is expressed in joules/°K and the thermal time constant τ is derived from fitting the warm up data ($T_h - T_c$ versus time) to a logarithmic curve of the form

$$T_h - T_c = A e^{-t/\tau} \quad (\text{III-2})$$

where A is a constant and t denotes the time in seconds.

2. Thermal Vacuum Can

In order to eliminate convective heat transport, the entire resonator will be surrounded by a vacuum cannister which has been designed by Harris and Volkert [Ref. 10]. The cannister has an external length of fifteen inches and a

diameter of eight inches. It is welded together from three parts machined from 6061-T6 aluminum.

The mounting flange of the cannister (Figure III-15) is 9.86 inches in diameter and seals to the resonator side of the driver housing with a Parker 2-174 rubber O-ring. A port is milled into the side of the flange to accept a pre-fabricated six-pin electrical feed-through (Hermetic Seal Corp. SS7201-10B-6P mod 1). This feed-through provides access to the hot and cold heat-exchanger thermocouples and the resistive strip heater which is mounted on the cold end of the resonator. The cannister body was cut from a prefabricated aluminum tube with a 1/8 inch wall, and was capped by a 1/4 inch thick base plate.

The ground based cannister is evacuated by a combination of a 15 CFM mechanical roughing pump and an oil diffusion pump. The diffusion pump is separated from the base plate of the cannister by a cold trap (Figure III-16). This device has two staggered baffles in series to prevent oil vapor from entering the cannister both under normal operation and especially in the event of a sudden loss of vacuum due to a power blackout. The outlet of the diffusion pump is connected to the mechanical pump via a large bellows type valve. This valve allows the vacuum to be drawn gradually so as to prevent the thermal insulation on the resonator from being torn off.

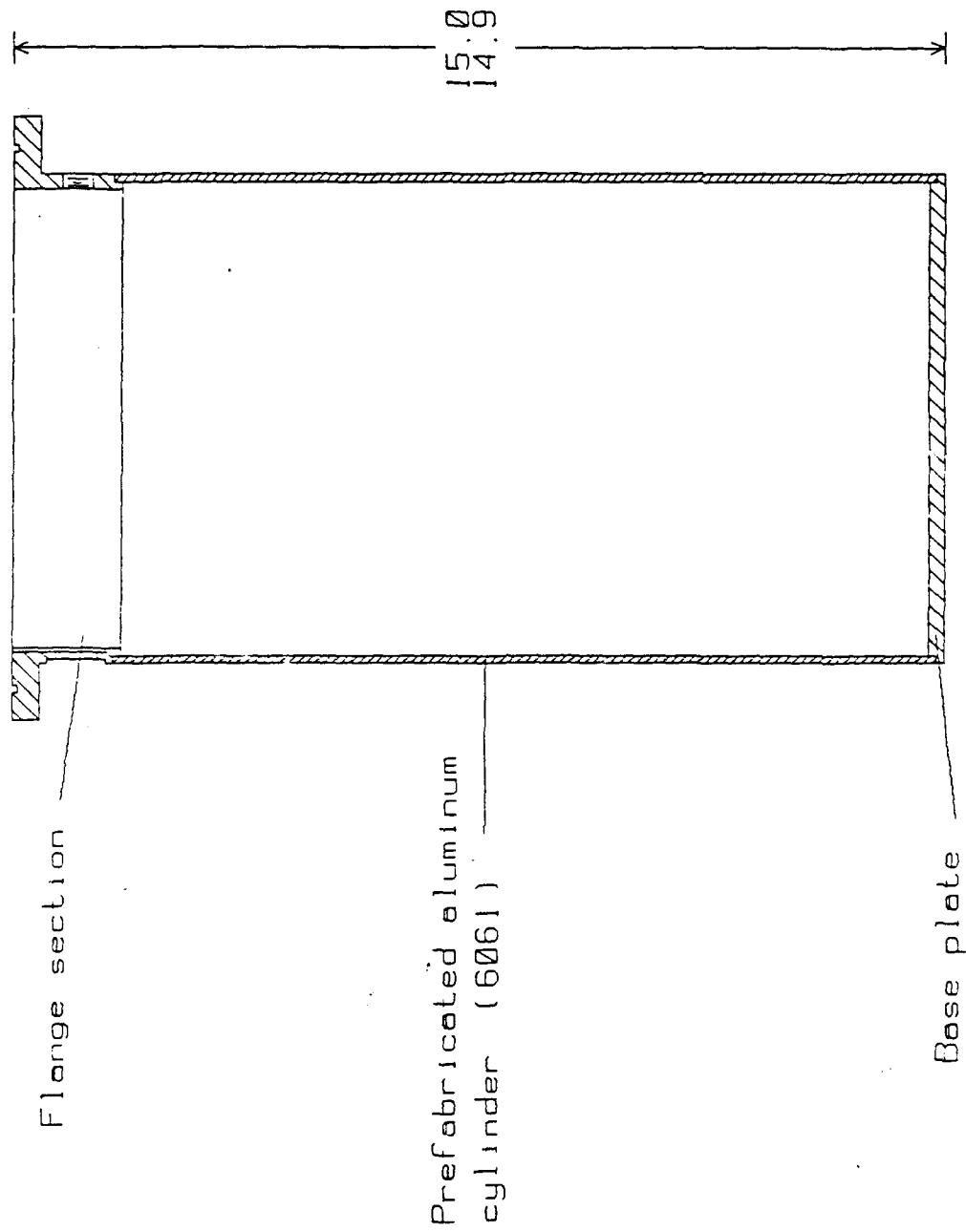


Figure III-15. Thermal Vacuum Cannister

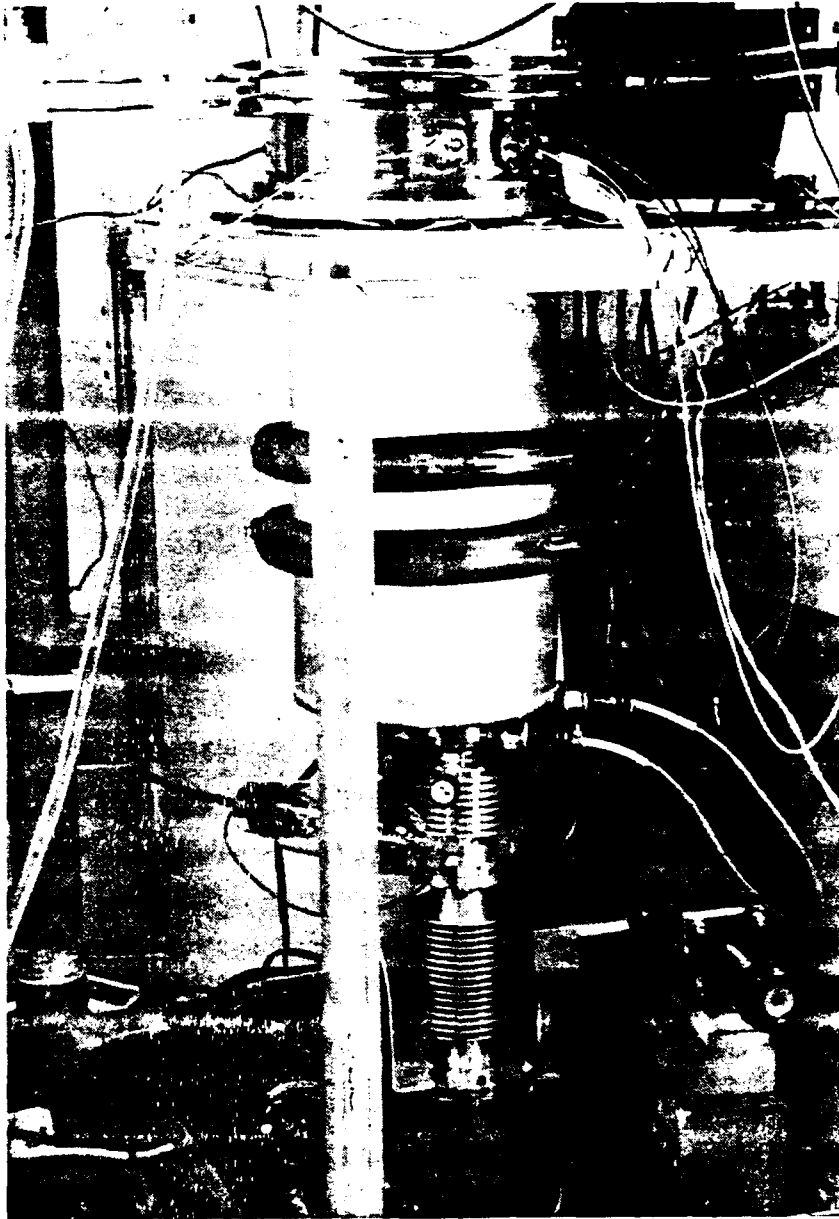


Figure III-16. Vacuum Cannister and Diffusion Pump

The vacuum in the canister is monitored with a Granville-Philips model 270 ion gauge controller. This device uses two thermocouple gauges to measure pressure from one torr down to 10^{-3} Torr, and an ionization gauge to measure pressure from 10^{-3} Torr down to 10^{-8} Torr. All three gauges are mounted on the vacuum can base plate. The ionization gauge circuitry comes pre-adjusted from the manufacturer, but the thermocouple gauge must be zeroed by the user. This was done simply by connecting the thermocouple gauge to an Alcatel leak tester and drawing a vacuum until the controller meter had bottomed out (indicating that the pressure was lower than the thermocouple gauge could resolve), at which point the controller meter was set to zero. The thermocouple gauge serves to notify when the pressure is low enough to allow operation of the diffusion pump. The diffusion pump then pulls the vacuum cannister pressure down to an operating level below 10^{-5} Torr.

The diffusion pump is operated using a silicon based oil in place of an organic oil, allowing it to be turned on at a higher pressure (100 microns of Hg instead of 50 microns). This is convenient because the oil also tends to outgas rather severely as the pump warms up to operating temperature. An organic oil, because it oxidizes easily, requires cycling the pump on and off many times initially to prevent the pressure from rising above 50 microns.

IV. STAR DRIVER

A. OVERVIEW

The design of the driver and its housing was first presented by Fitzpatrick [Ref. 11]. The construction and testing was then described in a joint Master's thesis by Harris and Volkert [Ref. 1]. A thorough description is in order here so as to allow the reader to fully appreciate the integration of the driver with the resonator and control electronics.

The sole purpose of the driver is to excite a standing wave in the resonator by providing a sinusoidal pressure variation. The driver housing must hold this transducer and must provide a central mounting point for the resonator and vacuum canister. The housing also hosts the acoustic pressure sensor, diaphragm acceleration sensor, and the static pressure sensor. The refrigerator will operate at a pressure of ten atmospheres and will generate enough heat to raise the temperature of the housing by at least fifteen degrees centigrade. The housing must be capable of withstanding these conditions and be strong enough to tolerate the forces experienced during a shuttle launch.

B. THE DRIVER

1. Driver Design and Construction

The heart of the driver, depicted in Figure IV-1, is a commercially available JBL 2450J compression driver with a neodymium-iron-boron magnet, a titanium dome and suspension and a four inch diameter voice-coil. The dome has been cut away from the suspension/voice-coil assembly and an aluminum reducer cone attached in its place. This reducer cone translates the diameter of the voice coil down to the one and one-half inch diameter of the bellows and resonator barrel. The reducer cone was machined from a block of 6061-T6 aluminum and has lightening holes drilled into it to bring the mass in below eleven grams. These lightening holes act also as a free passage for the gas to circulate in order to reduce the stiffness effect that would be imparted to the driver by trapped gases.

A flexible lightweight electroformed nickel bellows is glued to the end of the reducer cone and sealed against the resonator opening of the driver housing. In this manner, a flat radiating surface is presented to the pressure antinode of the 1/4 wavelength resonator. This radiating surface operates without the need for a sliding seal.

An Endevco Picomin model 22 microminiature piezoelectric accelerometer is attached to the underside of the reducer cone to provide a means for monitoring the

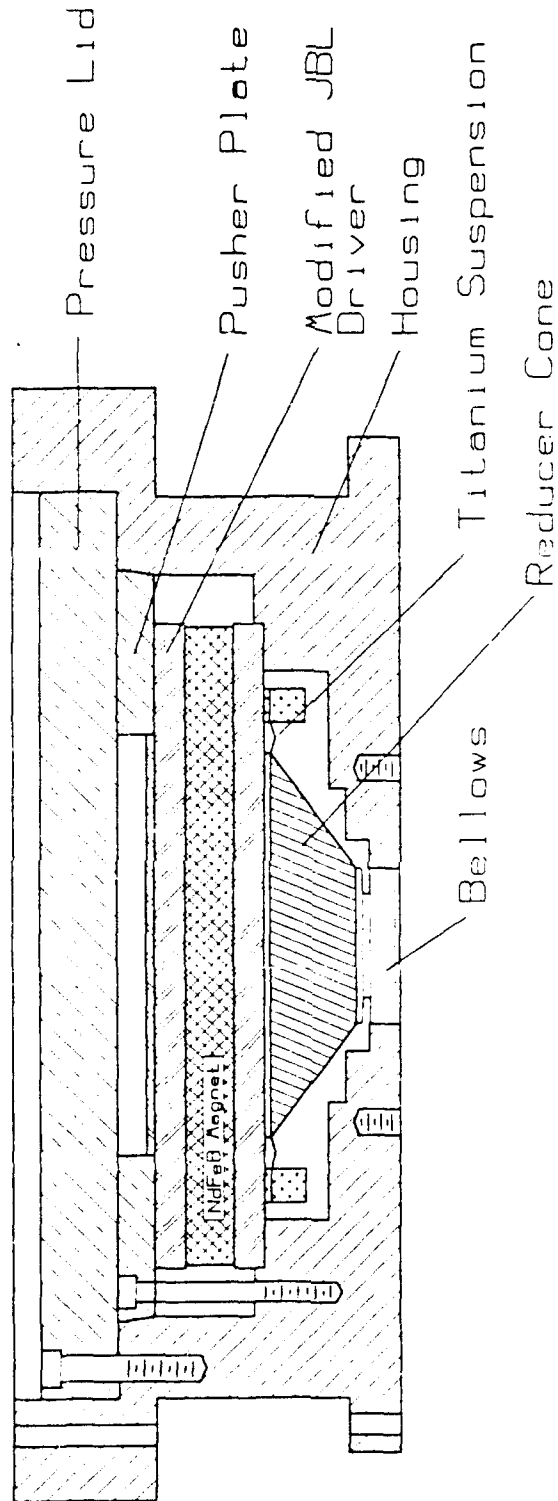


Figure IV-1. Star Driver

bellows displacement as well as the particle velocity phase relative to the acoustic pressure at the radiating surface. The acoustic pressure is measured by a Valpey-Fisher Y-cut quartz disk microphone placed as close as possible to the radiating surface. The microphone is connected to an Eltec impedance converter located in the driver housing next to the microphone. The impedance converter, having a very high impedance input and a low impedance output, is capable of driving a coaxial cable outside of the driver housing leading to the resonance control board without degradation of the signal. Of particular importance, since the acceleration of the radiating surface and the acoustic pressure must maintain a specified phase relationship for the resonator to be at resonance, is that the impedance converter does not shift the phase of the microphone signal by more than 0.5 degrees between 200 and 500 Hz.

2. Driver Housing

The driver housing consists of a housing shell, pressure lid, pusher plate, DC pressure transducer support plate with strain relief, and electronics access plug all machined from 6061-T6 aluminum. The dimension of the housing itself are constrained because it must bolt on to an existing 9.5 inch diameter hole pattern on the pressure lid of the NASA/GAS canister. Aluminum was the obvious choice for the material because of its light weight, high strength, and good heat conducting properties. The result is a

housing with a maximum diameter of 10.80 inches and a height of 3.75 inches. To simplify and reduce the amount of work and fabrication necessary, the driver was designed with interchangeability in mind. Any resonator or thermoacoustic stack used on the Hofler refrigerator will attach to the STAR driver housing.

The interior of the driver housing shell is machined to accept the driver magnet and hold it in proper relation to the resonator entrance port. There is a 1/32 inch hole in the bottom of the housing in which is placed a 0.8 inch length of 0.010 inch inner diameter copper-nickel capillary tubing to provide a static pressure equalization between the driver housing volume and resonator. It is through this capillary leak that the resonator is purged and filled with gas. The housing exterior has two flanges; the upper flange for mounting to the NASA Get Away Special cannister lid, and the lower flange providing a sealing surface for the vacuum can o-ring and bolt pattern.

The refrigerator is connected to the purging and gas distribution system through a Teflon wrapped Swagelok fitting screwed into a 1/8 NPT threaded hole on the side of the driver housing. The pressure is monitored by an Omega PX-80 piezo-resistive pressure transducer. The PX-80 is held in its own port by a support plate which has a strain relief tower attached to it to prevent damage to its delicate leads and to house the external compensation

resistors. A lead o-ring is used to seal the transducer against the port.

The electronics access plug has three coaxial and three single conductor feed-throughs. The coaxial connections are for the nine volt microphone supply, the microphone signal, and the accelerometer signal. Two of the single conductor feed-throughs are for the driver voice coil while the third is a spare. In order to make these feed-throughs as helium leak tight as possible the annular cross section area to depth ratio was kept as small as possible and a glass filled epoxy (Emerson and Cummings' Stycast 2850FT) was used both to fill the narrow gap between the feed-through wire and the surrounding wall of the hole and to act as electrical insulation. As with the pressure transducer, the electronics plug is sealed against the driver housing with a lead o-ring.

The driver magnet assembly is held in place by the pusher plate. Some of the voice coil heat is also conducted away from the driver through this plate. A ten degree taper along the outer circumference matches a taper in the driver housing as a method for obtaining close contact without scraping off the heat sink grease compound which was used to further increase the efficiency of heat conduction.

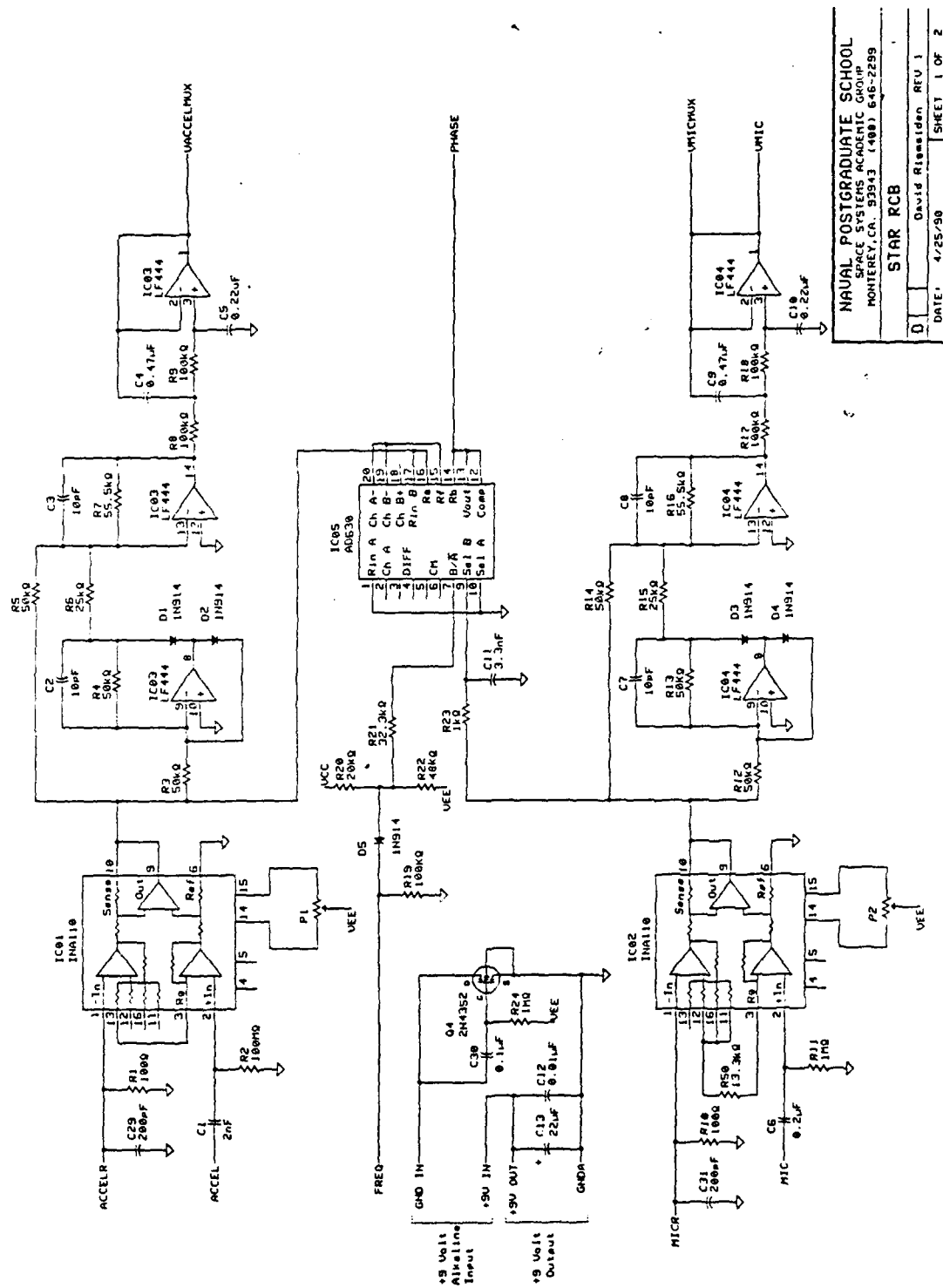
The top of the driver housing is sealed off by the pressure lid. This 3/4 inch thick aluminum lid is held in place by twelve 1/4-20 high-strength carbon-steel bolts

which are capable of withstanding forces far in excess of those which the lid will normally experience. The lid is sealed against the driver housing by two o-rings. The outer seal is a 1/32 inch thick lead o-ring while the inner seal is a back up rubber o-ring.

It should be stressed at this point that lead o-rings were necessary since STAR will most likely be filled with helium before it is delivered to NASA and will then sit unattended for up to six months before being launched. A non-metallic seal would allow excessive amounts of helium to diffuse out of the refrigerator and create a need for constant monitoring and possible refilling which is not allowed by NASA.

C. RESONANCE CONTROL BOARD

The Resonance Control Board (RCB) is considered the heart of the STAR electronics package and is depicted schematically, with corrections, in Figures IV-2a and IV-2b [Ref. 12]. This board monitors the acoustic pressure and bellows acceleration and keeps the driver operating at the gas resonance of the resonator. It also monitors the amplitude at which the driver is operating and makes the necessary adjustments to the oscillator output to keep the refrigerator running at an acoustic pressure to mean pressure ratio of $P_o/P_m=2\%$ or 3% depending on the experiment being conducted. What follows is a description of the RCB



NAVAL POSTGRADUATE SCHOOL
 SPACE SYSTEMS ACADEMIC GROUP
 MONTEREY, CA 93943 (408) 646-2299
STAR PCB
 DATE: 4/25/90 | SHEET 1 OF 2
 David Rasmussen REV 1

Figure IV-2a. Resonance Control Board Schematic

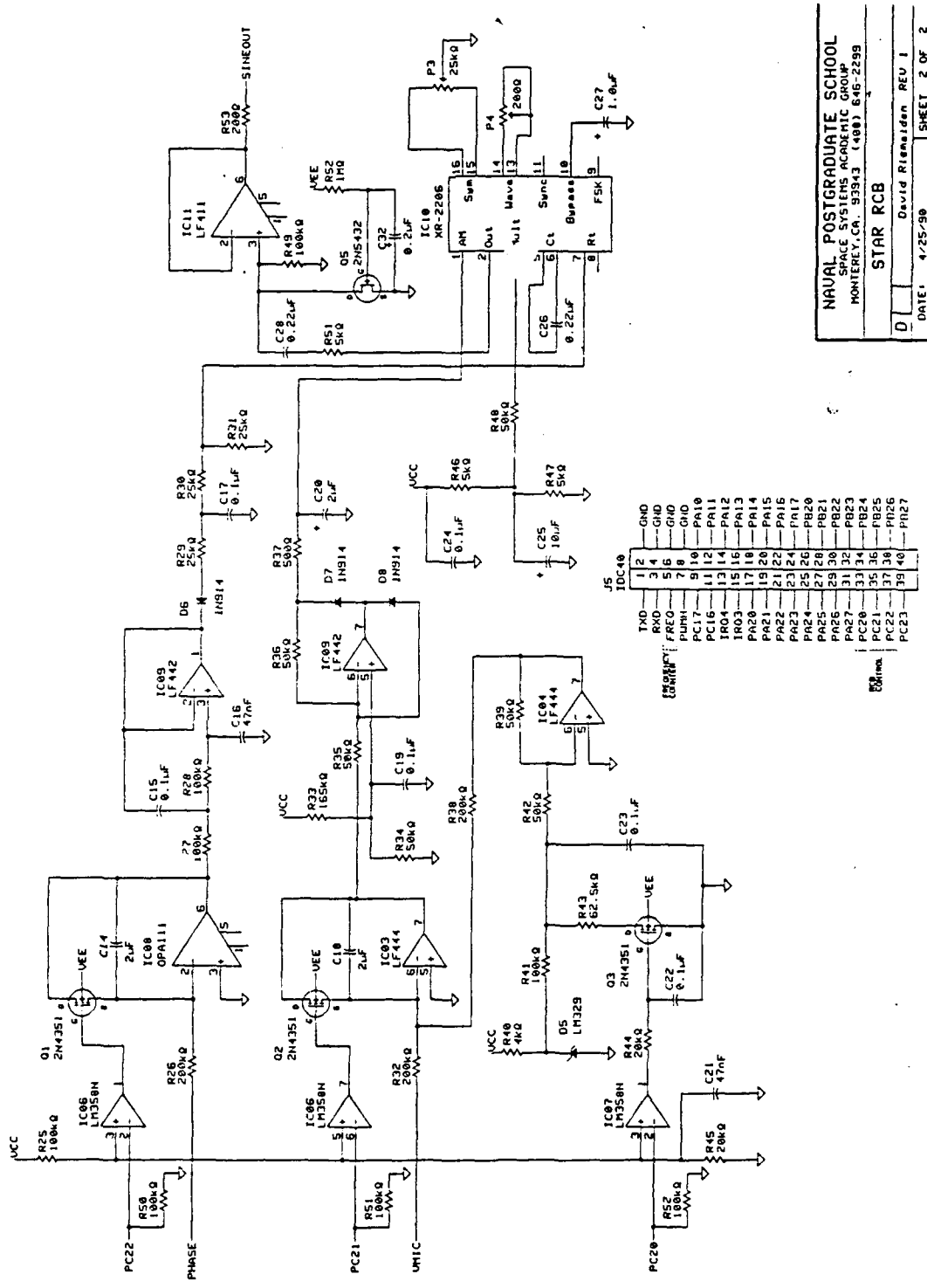


Figure IV-2b. Resonance Control Board Schematic

NAVAL POSTGRADUATE SCHOOL
 SPACE SYSTEMS ACADEMIC GROUP
 MONTEREY, CA. 93943 (408) 646-2299
STAR PCB
 DATE: 4/25/90 SHEET 2 OF 2

paraphrased from Byrnes [Ref. 13], with notes about the modifications that were eventually made when the RCB was actually interfaced with the STAR driver/resonator.

The first stage of the RCB is the input from the microphone and accelerometer. The microphone signal has already been buffered by an Eltec impedance convertor within the driver housing. The two signals are here amplified by a pair of instrumentation amplifiers. These differential amplifiers feature a high common mode rejection ratio, very low noise, high input impedance and low output impedance, and were originally set for a gain factor of ten. However, after preliminary full power operation of STAR it was decided that the gain setting for the microphone would have to be lowered. The original RCB circuit had been designed with the assumption that the microphone and accelerometer signals would have a magnitude on the order of $0.25 V_{\text{RMS}}$ and $0.3 V_{\text{RMS}}$, respectively. The actual microphone signal turned out to be on the order of $0.5 V_{\text{RMS}}$ while the accelerometer signal was on the order of $0.1 V_{\text{RMS}}$. Because the amplified signals have to remain below five volts to interface properly with the data acquisition circuits, an amplified microphone signal of five volts is just too close to the limit for comfort. The gain was not, however, simply lowered to an arbitrary value. This will be explained later in a discussion of the automatic gain control (AGC).

The condition for resonance is that the acoustic pressure be in phase with the bellows velocity. But since only the acceleration and pressure signals are given, and since the acceleration is 90 degrees out-of-phase with the velocity, resonance conditions can be satisfied by keeping the accelerometer signal in phase quadrature with the acoustic pressure signal. This is done by the RCB with a phase locked loop (PLL) circuit. The sinusoidal pressure and acceleration signals are multiplied or mixed by a comparator and a polarity switcher.

The pressure and accelerometer signals can be represented mathematically, when they are in phase quadrature, as

$$P(t) = P_0 \cos(\omega t) \quad (IV-1)$$

$$a(t) = a_0 \sin(\omega t) \quad (IV-2)$$

or more generally when they have an arbitrary phase difference (ϕ) between them as

$$P(t) = P_0 \sin(\omega t) \quad (IV-3)$$

$$a(t) = a_0 \sin(\omega t - \phi). \quad (IV-4)$$

The result of multiplying these two signals together is

$$P(t) * a(t) = P_0 a_0 [\sin^2 \omega t * \cos(\phi) - \sin 2\omega t * \sin(\phi) / 2] \quad (IV-5)$$

where the first term in the brackets is essentially a combination of a harmonically varying AC voltage with a constant DC voltage, and the second term is an AC harmonic of the original signal. The AC components can now be filtered out with a low pass filter leaving only the $\cos(\phi)$

term which varies with the phase angle between the two original signals. This voltage is used as an error signal which is integrated to drive the frequency of the voltage controlled oscillator (VCO) toward the resonance frequency.

It is interesting to point out at here that because the absolute phase of the microphone relative to the accelerometer was not known (they could either be 90 degrees out of phase or 270 degrees out of phase), there was the possibility that when the RCB was first hooked up to the driver, that it would try to lock the driver to anti-resonance. That is, it would try to keep the two signals 270 degrees out-of-phase with each other. This, in fact, is what did happen and it was easily corrected by reversing the polarity of the microphone input to the phase comparator.

The rms level of the amplified microphone and accelerometer signals is converted to an equivalent DC voltage for purposes of data acquisition and automatic gain control (AGC). In the AGC section, the microphone rms level is compared to a voltage equivalent to the rms level when STAR is operating at $P_o/P_m=0.02$ or 0.03 . A DC error signal is created when the two voltages are not equal which causes the VCO to adjust the amplitude of its output. Since the RCB was designed without a priori knowledge of the actual microphone rms signal level under operating conditions, an "equivalent" voltage of $2.3 V_{rms}$ for three percent operation and $1.5 V_{rms}$ for two percent operation was chosen. Rather

than changing the microphone voltage gain to an arbitrary value and then adjusting these equivalent voltages to match, it was simpler to adjust the gain such that it equaled the equivalent voltage divided by the actual voltage. The actual microphone signal at $P_o/P_m=0.03$ was $0.540 V_{rms}$, so the correct gain is $2.3/0.54$ or 4.26 .

The RCB also has a microphone power supply to provide nine volts DC separately from the battery pack that powers STAR. While this feature will probably be located somewhere other than on the final flight RCB, it is worth noting that the original design was incorrect and has been replaced with a new design as shown in Figure IV-2.

D. DRIVER HOUSING COOLING SYSTEM

Preliminary operation of the refrigerator at full power revealed that the driver housing is massive enough to allow unloaded operation without a heat dissipation system because the housing temperature did not exceed thirty degrees centigrade. However, in order to make good laboratory measurements, it is desirable to hold the normally variable driver temperature fixed.

The chosen method for cooling the driver housing was a recirculating water system. A round "cooling band", shown in Figure IV-3, was made of $1/32$ inch brass plate with two $1/4$ inch outer diameter copper tubes soft-soldered along the outer perimeter and joined at both ends by brass manifold

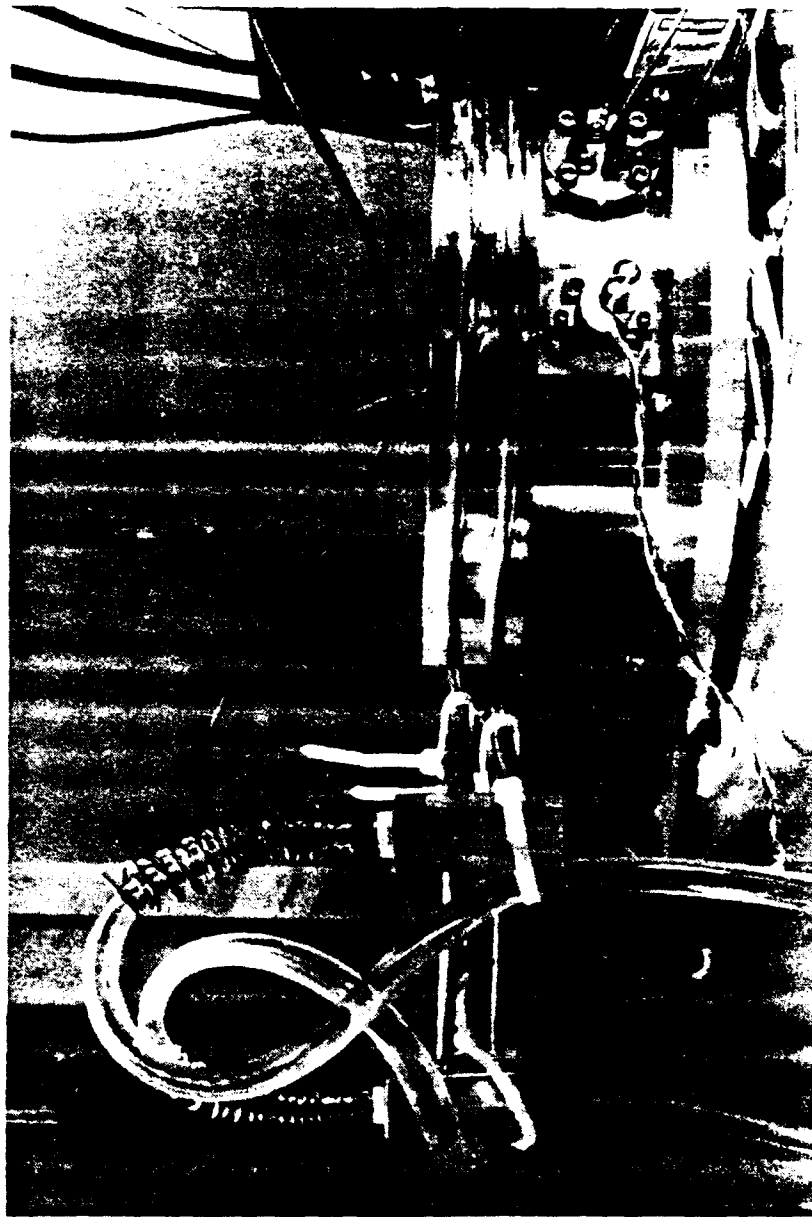


Figure IV-3. Driver Housing Cooling Band

blocks. The band is clamped around the largest diameter of the driver housing and connected to a Neslab Endocal RTE-110 refrigerated bath recirculator, allowing the housing to be kept at a constant temperature. The two copper coils running around the driver housing are run in parallel rather than in series so as to decrease the flow restriction presented to the recirculator pump.

V. GAS DISTRIBUTION SYSTEM

A. FILLING AND PURGING MANIFOLD

The filling and purging manifold is the hub of the gas distribution system. It is from here that the operator selects whether the refrigerator will be purged or filled and at what rate. A schematic diagram of the panel is shown in Figure V-1 with all of the valves indicated by letters or numbers. However, before describing the operation of the panel it is important to elaborate on the need to control the purging and filling rate. The resonator mounting face of the STAR driver housing has a small capillary tube of 0.010 inch inner diameter to equalize the static pressure between the driver back volume and the resonator volume. Because the capillary is the only connection between the two volumes, and because the refrigerator is connected to the gas supply lines exclusively through a fitting on the driver side of the housing, it is important to insure that the refrigerator not be purged or filled too rapidly as this would cause a large differential pressure across the bellows. This differential pressure would push the reducer cone beyond the excursion limits of the delicate titanium suspension.

A practical upper limit may be placed on the differential pressure permitted across the bellows by

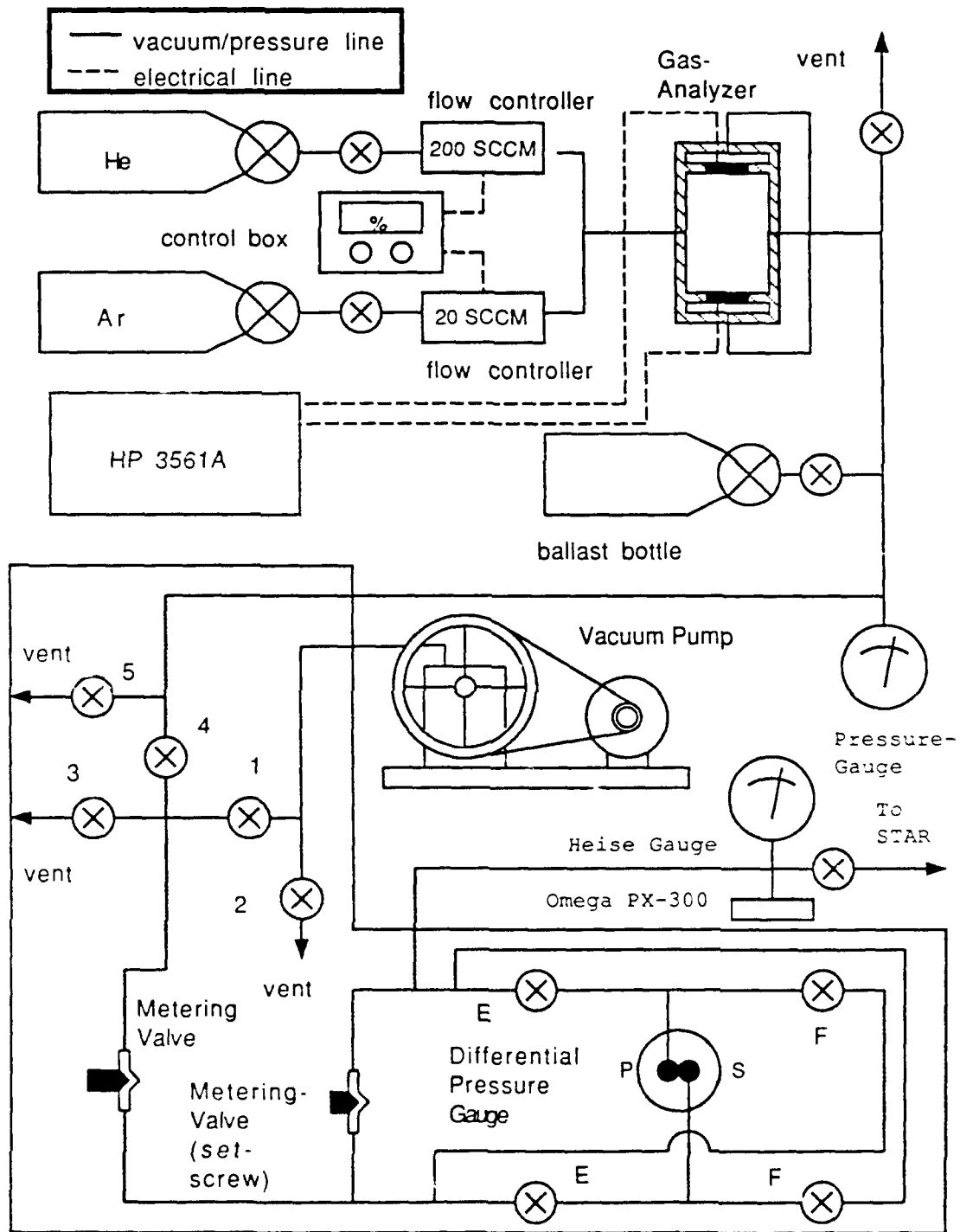


Figure V-1. Gas Distribution Panel

calculating the force per unit area needed to displace the voice coil by a safe amount. From the Harris and Volkert thesis [Ref. 14], the driver/bellows stiffness is $k=6.83 \times 10^4$ N/m and the effective bellows diameter is approximately 1.25 inches or 0.032 meters. If the maximum allowable bellows displacement is 0.010 inches or 0.000254 meters; the corresponding pressure differential is easily calculated as 3.2 PSI.

There are several ways to insure that a differential pressure of 3.2 PSI is not exceeded. The simplest is to insert a capillary identical to the one inside the driver housing into the distribution panel and in series with the line between the gas supply and the driver housing inlet. A differential pressure gauge would be used to monitor the pressure drop across the capillary while a metering valve between the gas supply and the capillary would regulate the flow to maintain a safe pressure differential. However, to allow for the possibility of different driver housings with different size capillaries, a metering valve with a set screw was used to approximate the flow rate of the capillary. The need for the differential pressure gauge and regulating valve remains unchanged.

Returning to Figure V-1; the positive-reading differential pressure gauge is designed to always have a higher pressure on the "P" inlet and a lower pressure on the "S" inlet. It is therefore necessary to reverse the

connections to the gauge depending on whether the refrigerator is being drained or filled. Four shut-off valves, to be opened and closed in pairs, are used to reverse the pressure gauge connections. When the driver is purged, the two valves marked "E" are opened while the two valves marked "F" are closed. The status of the valves is reversed when the driver is filled.

A small 1.5 CFM mechanical vacuum pump is used to evacuate the panel and the driver/resonator. It is closed off from the panel by valve 1. A venting valve (2) is placed on the pump side of cutoff valve one since the inlet of the vacuum pump should not be exposed to a vacuum when it is shut off as this would cause oil to be sucked into the vacuum lines.

Together with valve 1 and the metering valve, valves 3 and 4 create a central chamber to allow selection of either the vacuum pump or the gas supply line. Valve 3 vents this chamber, while valve 4 closes off the gas supply. Valve 5 vents the gas supply line.

The panel is instrumented with three pressure gauges. A Heise CM-96728 200 PSIA mechanical unit with 0.5 PSI subdivisions is placed between the outlet of the panel and the driver housing inlet. This gauge was calibrated against a mercury column converted to PSI. The second pressure gauge is an Omega PX-304-300AV pressure transducer connected to a ten volt DC supply source and mounted opposite the

Heise gauge. The zero to one-hundred DC millivolt output signal is monitored on a voltmeter. The third gauge is the differential pressure gauge mounted across the set-screw metering valve. This unit is a Wallace and Tiernan gauge reading in units of inches of water up to 200".

B. GAS MIXING MANIFOLD

Since the selection of the exact gas mixture to be used depends on the acoustical characteristics of the driver and resonator and their interaction, the ability to mix the two gases in the desired ratio while filling the refrigerator was a requisite towards simplifying the process of selecting the operating frequency.

The simplest method allowing for the most accurate control of the mixture and the highest rate of repeatability was to use a commercially available mass flow control system. An Omega FMA-114 mass flow controller rated for a maximum of 200 standard cubic centimeters per minute (SCCM) was used to control the flow of helium while an FMA-111 controller rated for a maximum flow rate of 20 SCCM was used to control the flow of the second gas. These two mass flow controllers are actually calibrated for nitrogen (N_2), but are easily corrected for helium, argon, and xenon by multiplying the flow rate by a correction factor of 1.45. The two controllers are, therefore, actually rated for a

maximum flow rate of 290 SCCM and 29 SCCM for these three gases.

An Omega FMA-2DPV dual channel electronic control box was used to operate the two mass flow controllers. This box controls any two Omega series FMA-100 units, each of which is independently adjustable from zero to one-hundred percent of its rated flow capacity. In addition, pin-outs are provided to allow override of the valves which force them fully open or closed regardless of the control box settings.

Referring again to Figure V-1; the two mass flow controllers feed into a "T" connection where the gases combine and flow through a gas mixture analyzer (section C). The gas then enters a ballast bottle of one liter displacement before entering the filling manifold. The ballast bottle serves several purposes: First, since the refrigerator must be filled at a slow rate, it is easier to first fill the ballast bottle at the maximum rate allowed by the mass flow controllers, and then fill the refrigerator from the ballast bottle. This allows for a more accurate and consistent gas mixture. Second, different gas mixtures are easily mixed and tested by filling the ballast bottle and then checking the sound velocity with the gas analyzer. A Weksler 200 PSIG pressure gauge is located opposite the ballast bottle to monitor the gas pressure.

C. GAS ANALYZER

Analysis of the gas mixture is performed by an acoustic gas analyzer consisting of a resonant chamber with a piezo-electric ceramic transmitter at one end and a similar receiver at the other end. The device is depicted in the sectional drawing of Figure V-2 which may be attributed to Hofler and Garrett [Ref. 15]. With pure helium, the chamber has a fundamental mode frequency of approximately 26 kHz, corresponding to a half wavelength. The mass of a mixture of helium and argon, for instance, can be calculated by measuring the frequency at which the chamber resonates. The sound velocity is simply given by

$$c = \lambda f \quad (V-1)$$

where f is the resonant frequency and λ is the wavelength which is equal to twice the effective length of the chamber since it is a closed-closed resonator.

The mass of the gas mixture is calculated from the relation

$$c^2 = \gamma RT/m \quad (V-2)$$

where γ is the ratio of specific heats for the gas, R is the universal gas constant, T is the temperature in Kelvin and m is the molecular mass. Since the sound velocity and atomic weight of helium are already known, the mass of the unknown mixture is more easily found by the relation

$$(c_1/c_2)^2 = m_2/m_1 \quad (V-3)$$

where the subscript 1 refers to helium and the subscript 2 refers to the unknown gas mixture. This relation is accurate provided that the temperature has been kept constant. The concentration of argon or xenon present may now be calculated from the following expression;

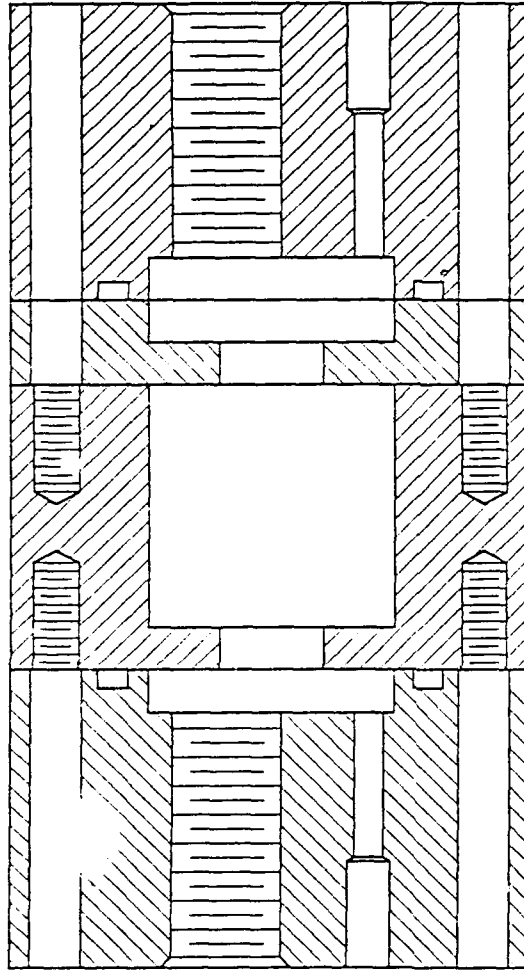
$$m_2 = X m_{\text{Ar/Xe}} + (X-1) m_{\text{He}} \quad (\text{V-4})$$

where X is the mole fraction of argon or xenon and $m_{\text{Ar/Xe}}$ is the mass. Armed with these formulas it is possible now to either analyze the composition of an unknown mixture, or working backwards, to arrive at a mass ratio for a desired sound velocity.

The analyzer was operated with a HP 3561A dynamic signal analyzer which provided a periodic or random noise signal with an amplitude of one volt RMS to the transmitter. The receiver signal was fed back into the analyzer to track the resonant mode. The resonant peaks were at least 20 dB above the "noise floor" allowing for easy detection.

Once a desired sound speed had been selected and the mass ratio calculated, the Omega FMA-2DV control box could be set so that the ratio of the mass flows was equivalent to the mass ratio of the desired gas mixture. This is not strictly correct because these units measure volume flow in standard cubic centimeter per second, but worked well as will be shown presently.

Some amount of error in the actual gas mixtures obtained is to be expected since the mass flow controllers have their



Part #1

Part #2

Part #3

Same as
Part #1

Figure V-2. Gas Analyzer Cross Section

limits of accuracy. The Omega series FMA-110 units have a specified accuracy of +/- 2 percent of full scale between 5° C and 50° C and between 5 PSIG and 150 PSIG. In fact, the expected error is actually greater than this because the pressure at the inlet to the controllers was kept at 200 PSIG. This saved refilling time by allowing the ballast bottle to be filled to 190 PSI. The filling had to be stopped at 190 PSI because the pressure regulators on the gas supply bottle could not be expected to match each other to within better than five percent. The graph of Figure V-3 shows a comparison of the mass ratio of different mixtures versus frequency as indicated by the Omega FMA-2DV and as calculated by equations (V-3) and (V-4). The agreement is close enough that a fair amount of repeatability is possible.

D. CONSTRUCTION DETAILS

The distribution panel is made up of one-quarter inch outer diameter copper tubing soldered together. All of the valves have brass Swagelok compression fittings making assembly quite easy and allowing for multiple reconnections. These compression fittings must be used according to the manufacturer's directions since they are easily damaged by overtightening. Due to the convoluted nature of the manifold, it was at times necessary to do some soldering after a valve had been inserted into the assembly. Great

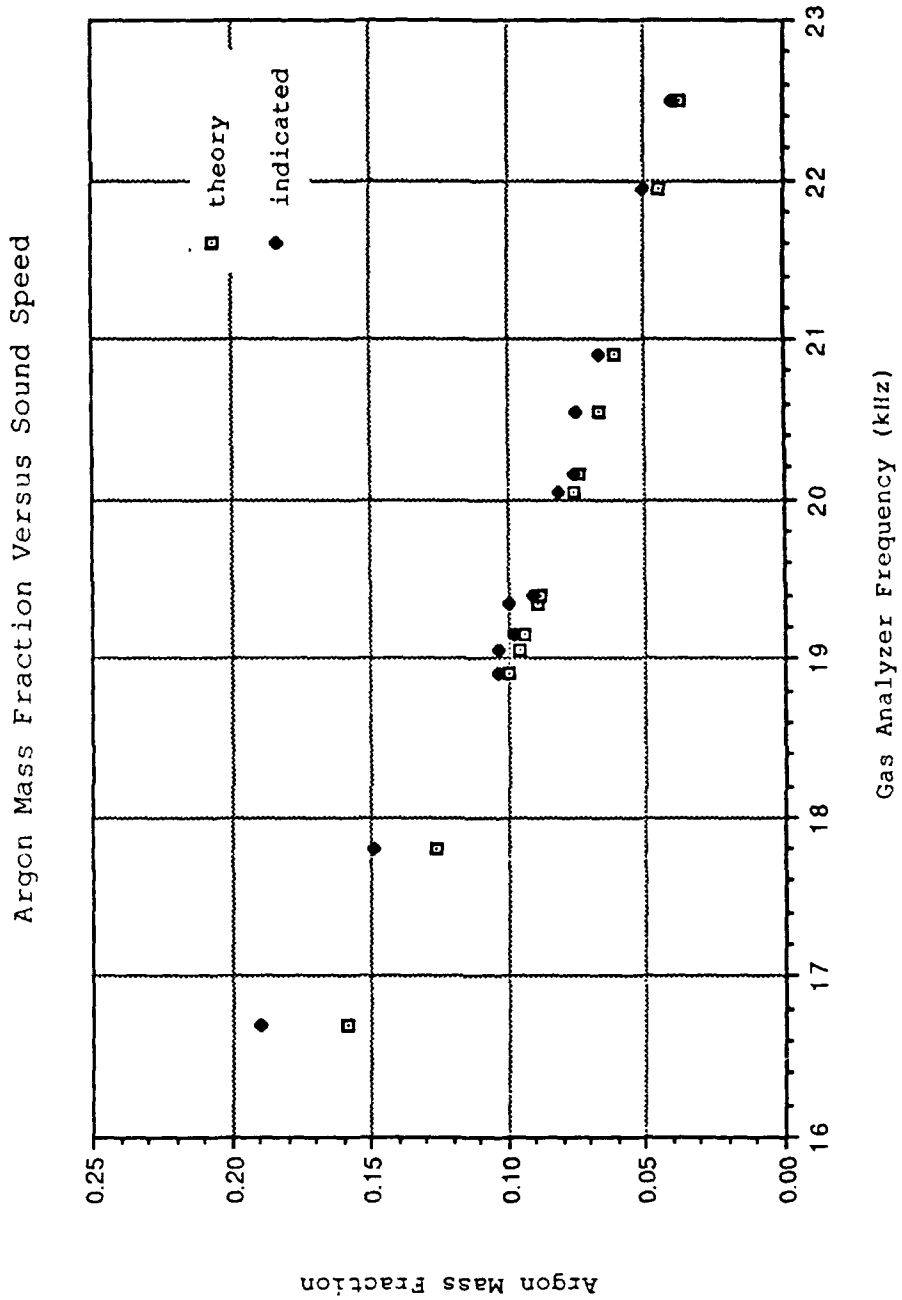


Figure V-3. Gas Flow Controller Accuracy

care was taken not to overheat and damage the valve seats by wrapping them with wet towels to absorb the excess heat.

Valves 1 through 5 are Nupro "JN" series screwed-bonnet needle valves with Teflon seats rated to 600 PSI while the "F" and "E" valves are Whitey "1G" series toggle valves with Viton o-rings and Teflon stem-tips rated for 200 PSI. The metering valve is a Whitey SS-22RS4 Micro-Metering valve with a micrometer handle, Viton o-ring, stainless steel needle and Teflon packing and 0.020" orifice. The set-screw metering valve is a Nupro "S" series fine metering valve with Viton o-ring and stainless steel stem rated for 2000 PSI.

The entire assembly was leak tested on the same Alcatel helium leak detector as used for the resonator leak tests. The panel, at first, had so many leaks that it could not be pumped down far enough to allow use of the helium mass spectrometer. Instead, the suspected leaking joints were doused with acetone, which has a high vapor pressure, resulting in the Alcatel pressure gauge jumping as the acetone entered the leak detector. The gross leaks were detected and repaired in this manner while the smaller leaks were subsequently located by spraying helium around the joints and allowing the helium spectrometer to function. It must be stressed, again, that when soldering repairs were performed near a valve, a wet towel was wrapped around the valve to absorb excess heat thus preventing damage to the

valve seats. Additionally, all adjacent solder joints were wrapped to prevent the solder from melting and creating a new leak.

E. FILLING AND PURGING PROCEDURE

The proper sequence of operations for purging and filling the refrigerator driver/resonator deserves some mention here in order to stress the delicate nature of the driver system. First, to remove all traces of air from the inside of STAR, it is necessary to alternately evacuate and then fill the driver/resonator with helium at least twice, but preferably three times.

Starting with all the panel valves closed except for valve 1, the vacuum pump is turned on and allowed to stabilize. Now, having opened the two "E" valves, the metering-valve is slowly opened until the differential pressure gauge indicates that the maximum allowable pressure drop across the capillary-like metering-valve has been reached. The metering-valve may now be left at its present setting unattended without the danger of the filling rate increasing. The diminution in the mass flow through the capillary-like valve due to the drop in the absolute pressure causes the bellows pressure differential to decrease as well. To expedite the process, the metering-valve may be continuously adjusted to allow for the maximum evacuation rate. Eventually, however, the metering-valve

will have been opened entirely, whereas the pressure differential will continue to decrease. When the absolute pressure has dropped below the permissible bellows pressure differential, the "F" valves may be opened to allow the flow path to bypass the capillary-like metering-valve.

Once the Heise gauge has bottomed out, one is left only with the question of how long to allow the vacuum pump to continue to draw on the driver housing. A zero PSI reading on the Heise gauge is obviously no guarantee of a good vacuum since it will resolve, at best, to within a tenth of a PSI. This leaves only the Omega PX-80 transducer for monitoring small changes in the driver housing pressure at low absolute pressure. Since no zero-offset calibration was performed on this specific transducer prior to insertion in the driver housing, the best that can be done is to continue to pump down on the refrigerator until the PX-80 voltage has very nearly stopped changing.

Once an acceptable vacuum is attained, the refrigerator must be filed with helium and the whole process repeated one to two more times. If one is simply exchanging one gas mixture for another, it is only necessary to perform the evacuation once. This step was eliminated when the second resonator was brought into operation and, instead, the refrigerator was filled with gas and then depressurized three to four times to insure that there were only trace amounts of air in the system. This change was made in an

attempt to minimize damage to the delicate stainless foil vapor shield. In any event, the metering-valve must first be closed followed by valve 1 and the two "E" valves. The two "F" valves must remain opened. Filling the driver with pure helium is simple and requires only that the helium mass controller be opened fully to fill the ballast bottle. Or, if the refrigerator is to be filled with a gas mixture, the mass controller electronics box must be set to the appropriate value for each mass controller, and the ballast bottle filled.

With the ballast bottle full and the "F" valves open, valve 4 is opened to join the gas mixing apparatus to the fill manifold, and the metering-valve opened until, once again, the pressure drop across the capillary-like metering-valve has reached the maximum allowable. As when evacuating, the valve may remain unattended since the gradual decrease in the pressure difference from the gas well to the refrigerator will reduce the mass flow through the capillary and cause a gradual diminution of the pressure drop across the capillary. The metering-valve may, again, be continually adjusted to hasten the process. However, since the ballast bottle has a smaller volume than the driver/resonator, the pressure between the two will equalize at a lower than desired level. The metering valve must now be closed off, the ballast bottle refilled, and the process repeated until the refrigerator is filled to the desired

pressure. Two refills of the ballast bottle are necessary to fill STAR to 150 PSI.

The steps described in this section are necessary to protect the driver suspension and bellows from being subjected to overextension as caused by a large pressure differential between the resonator side and the driver housing side of the bellows. It is advisable that the status of each and every valve be double checked before any change is made to prevent a catastrophic accident.

VI. REFRIGERATOR PERFORMANCE

A. ELECTROACOUSTIC EFFICIENCY

The first test performed on STAR, once the resonator had been mated to the driver, was to measure the electroacoustic efficiency as a function of frequency for a variety of gas mixtures ranging from pure helium to a mixture of helium with an 18.85% concentration of argon. It was expected that the electroacoustic efficiency would be maximized if the fundamental ("operating") frequency of the resonator was matched to the mechanical resonance of the driver; the reason being that at resonance the driver can deliver the largest voice-coil displacement for the least amount of electrical power.

The mechanical resonance of the driver in a vacuum was measured as being approximately 358 +/- 1 Hz. However, it must be pointed out that the output impedance of the device which is driving STAR has a substantial effect on what is perceived to be the mechanical resonance of the driver. It is customary to test a dynamic loudspeaker using an instrument such as the HP 4192A impedance analyzer which has a built in oscillator with a relatively high output impedance. The driver, however, will be powered by a Crown PS-100 power amplifier with an output impedance of less than 0.01 ohms at 400 Hz. This has the effect of causing the

electrical damping characteristics of the driver's voice coil to be non-negligible relative to the mechanical damping effects of the suspension and bellows. In fact, even the output impedance of the HP 4192A is not high enough that some electrical damping was not evident.

Because the driver's resistance was less than 50 ohms, however, a 10,000 ohm resistor could be inserted in series with the power amplifier to transform it into essentially a constant current supply, thereby eliminating the electrical damping effects. The accelerometer output plot of Figure VI-1 shows the "true" mechanical resonance with all electrical, gas, and resonator effects eliminated.

Strictly for comparison, Figure VI-2 shows the accelerometer output when driven by the HP 4192A and, conversely, when driven directly off of the PS-100 power amplifier. The effect of an amplifier on a moving coil loudspeaker is commonly observed in a home audio system where the electrical damping properties of the power-amplifier/voice coil are used to control the excessive motion of the low frequency driver at its resonant frequency.

Figure VI-3 shows that the resonance remained essentially constant as the refrigerator was pressurized to 150 PSI with helium. However, under these circumstances, the resonator's fundamental frequency was at 560 Hz, far enough from the driver's resonance that they did not

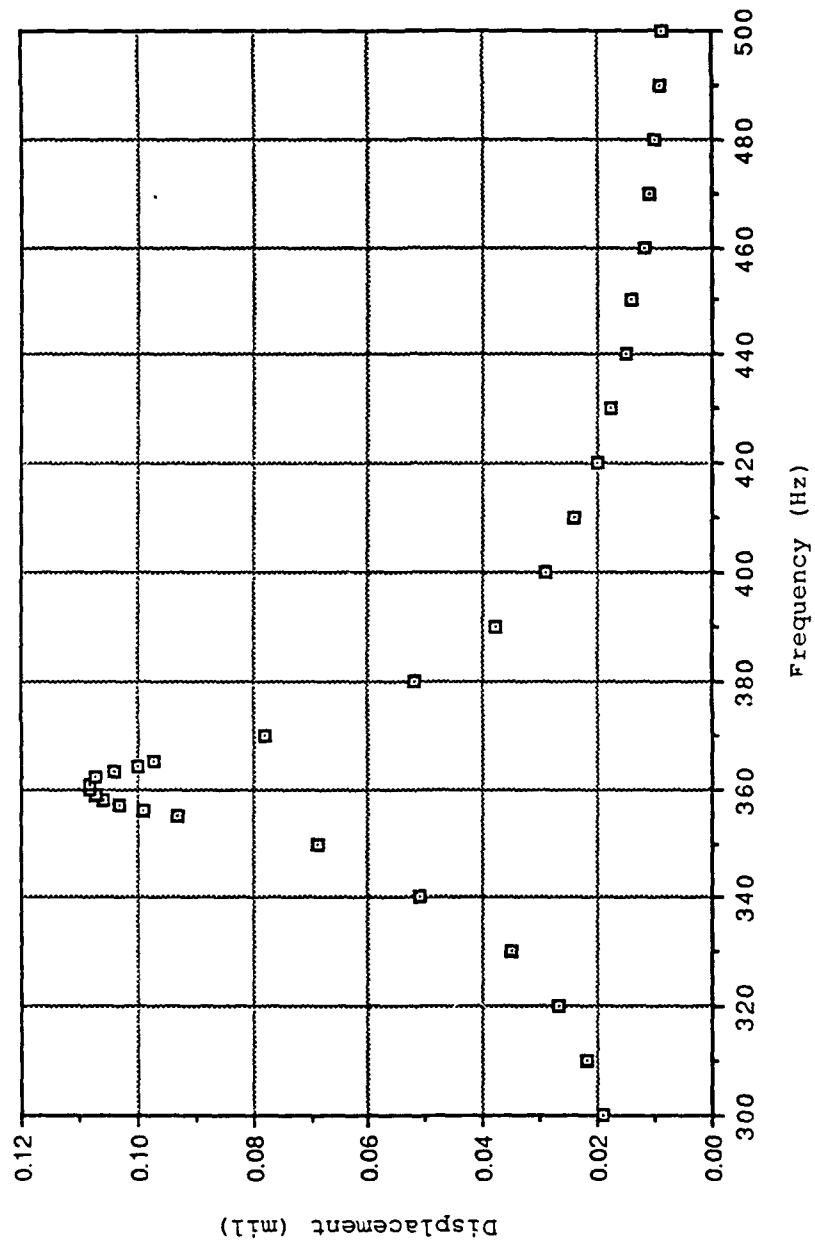


Figure VI-1. Bellows Displacement Versus Frequency

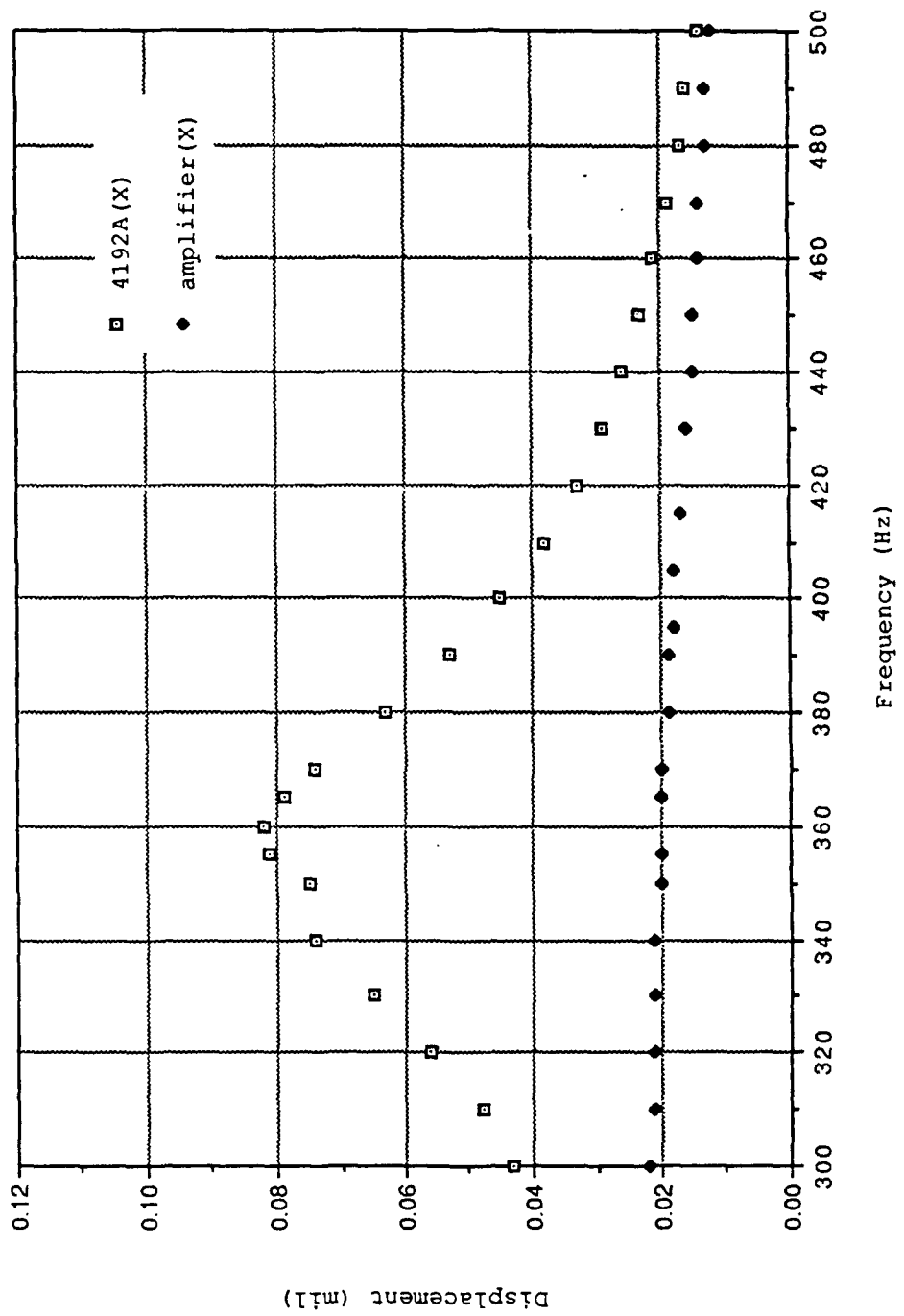


Figure VI-2. Bellows Displacement Test Comparison

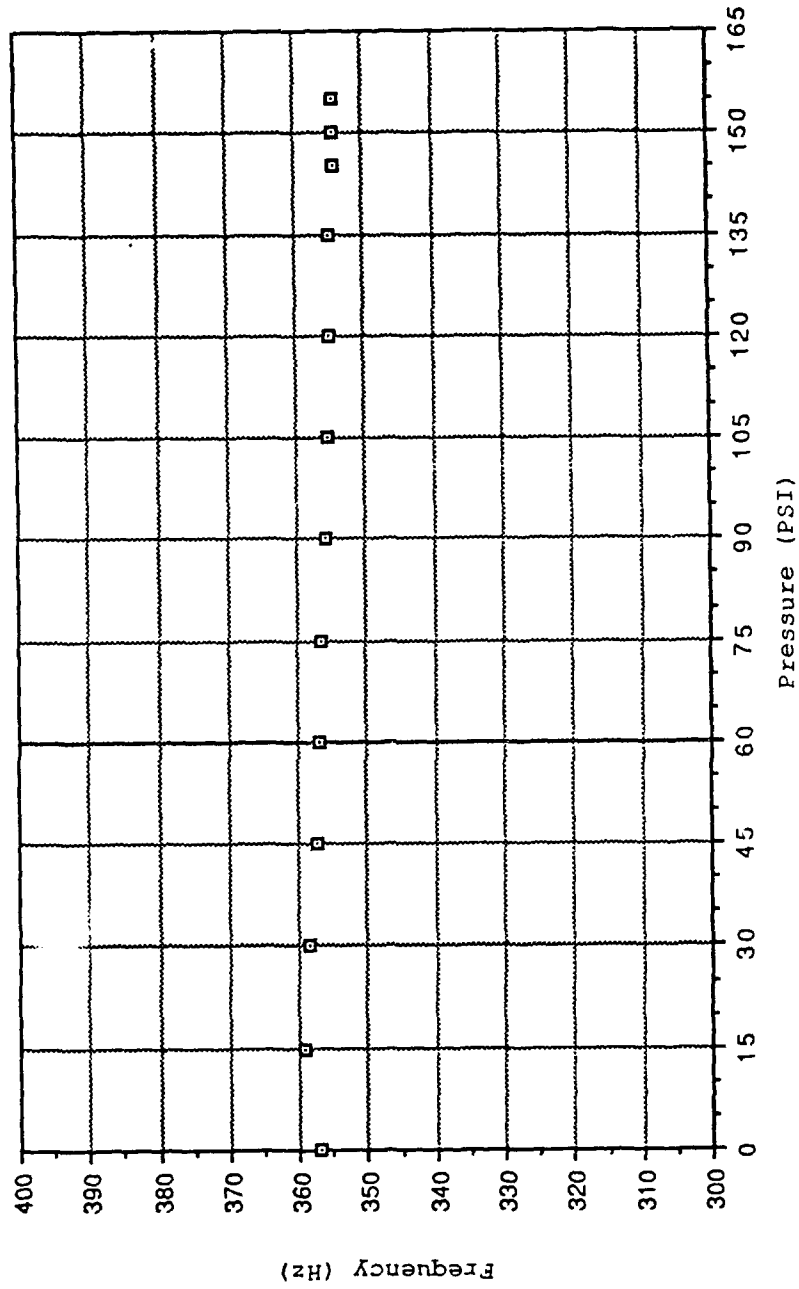


Figure VI-3. Mechanical Resonance Versus Mean Pressure

measurably effect one another. Such behavior was not observed when the gas mixture was changed in order to move the resonator's fundamental closer to that of the driver's. Here are, essentially, two harmonic oscillators which, as their fundamental frequencies become more coincident, are no longer decoupled.

Eight different gas mixtures were tested, ranging from pure helium to a mixture of helium with 18.85% argon. Although these tests were conducted with the refrigerator driven at conservative power levels, the amount of electrical power being delivered to the voice coil had to be high enough that the voltages measured by the power measurement circuit would be at least two to three orders of magnitude above its DC offset. The chosen power level was roughly 200 milliWatts of electrical power delivered to the driver. This corresponded to an acoustic pressure at the microphone of about 0.25 percent of the mean pressure, which was 150 PSIA.

Upon investigation of the accelerometer and microphone outputs (Figures VI-4a through VI-4h) for each of the various helium/argon gas mixtures, it may be seen that the resonator fundamental occurs at the peak of the microphone response, or approximately at a relative minimum for the accelerometer response, as expected. Also, as mentioned previously, the mechanical resonance of the driver and the fundamental of the resonator appear to repel each other as

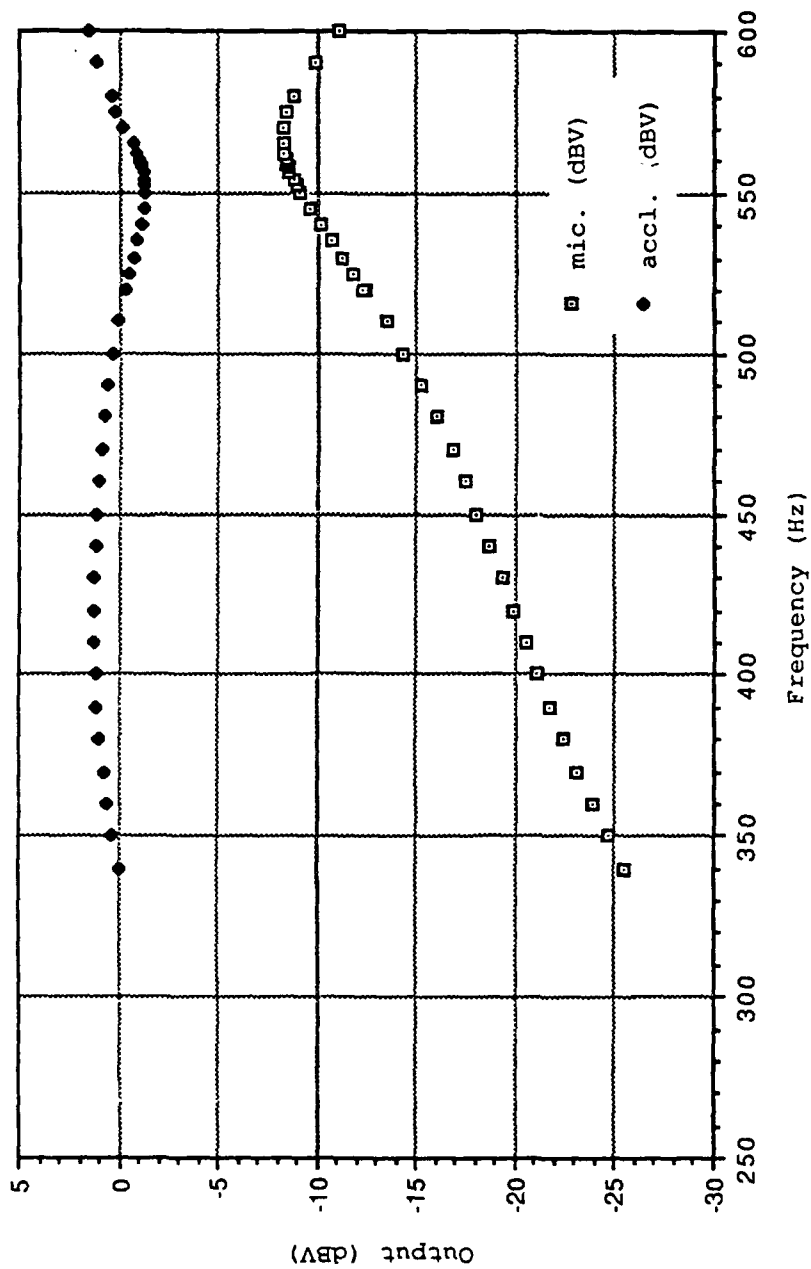


Figure VI-4a. Microphone and Accelerometer Outputs for Helium

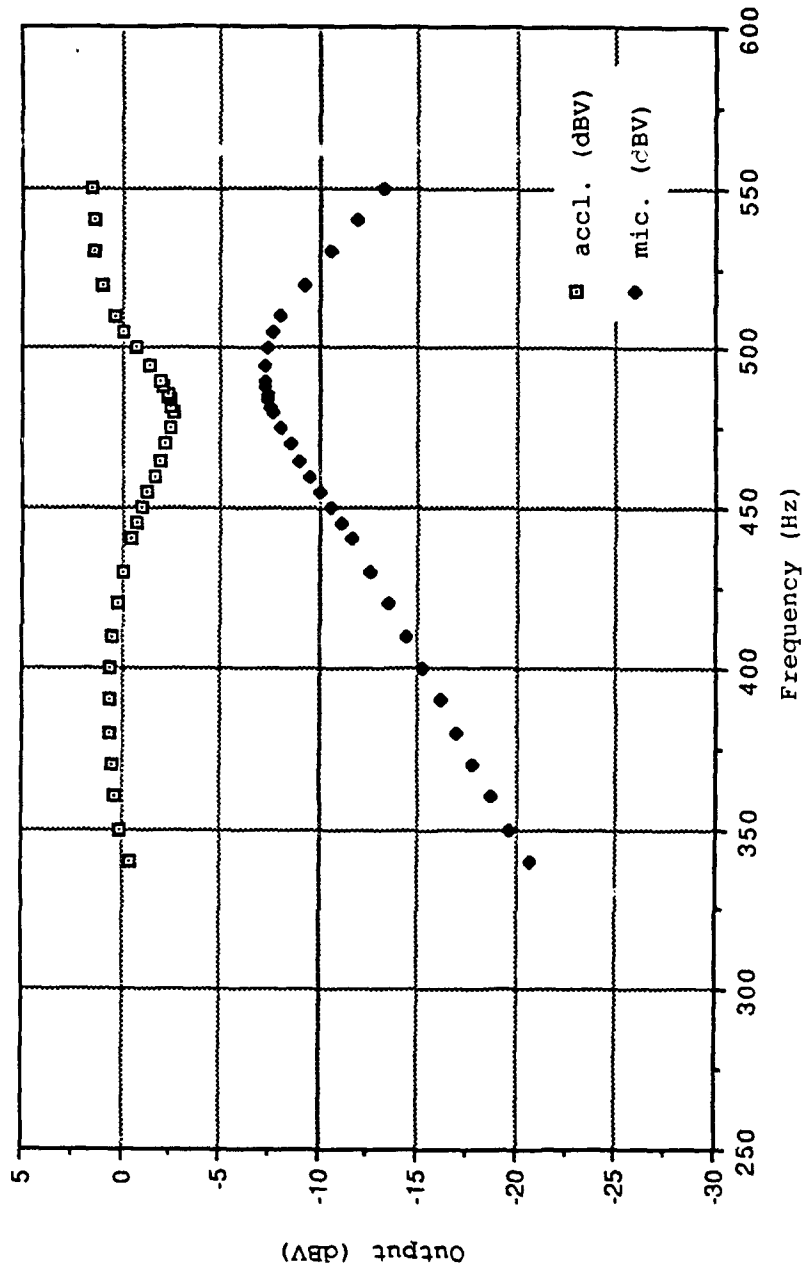


Figure VI-4b. Microphone and Accelerometer Outputs for Helium and 3.71% Argon

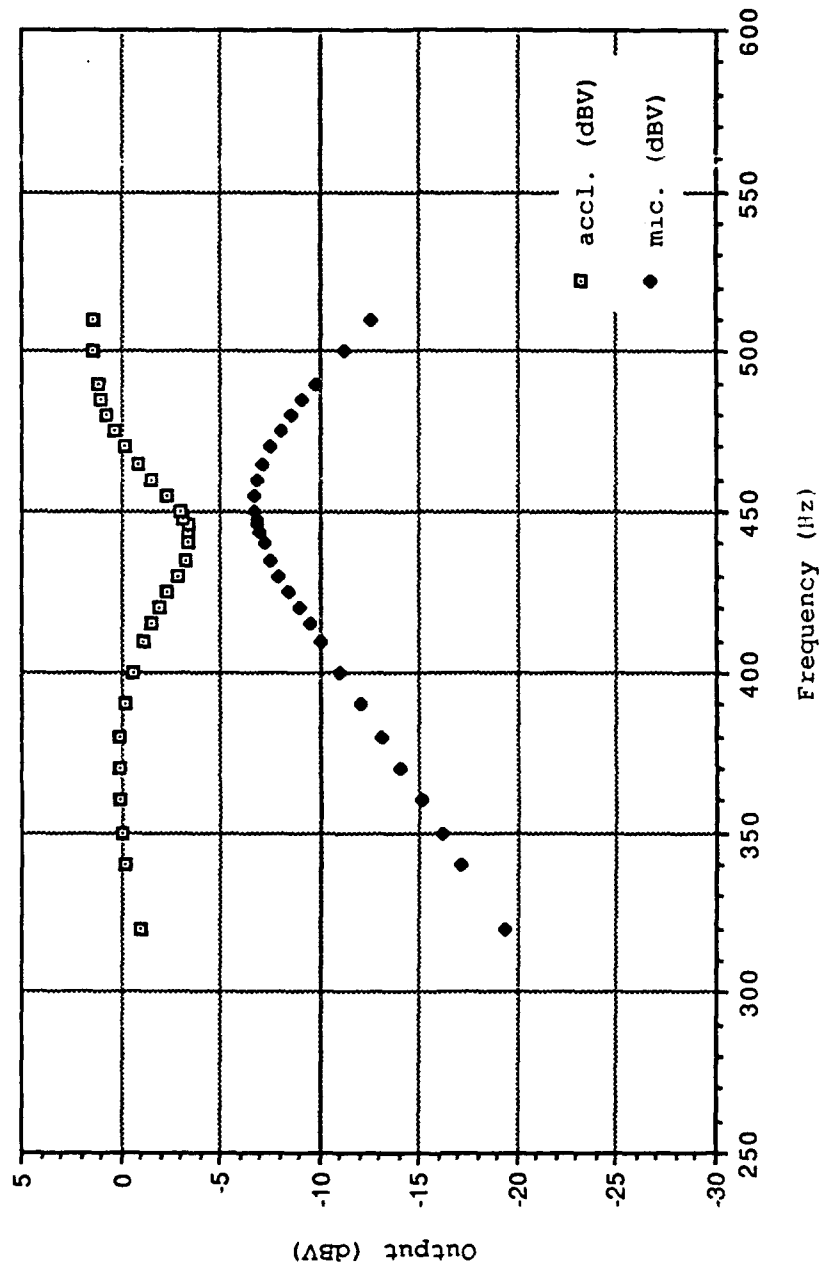


Figure VI-4c. Microphone and Accelerometer Outputs for Helium and 6.42% Argon

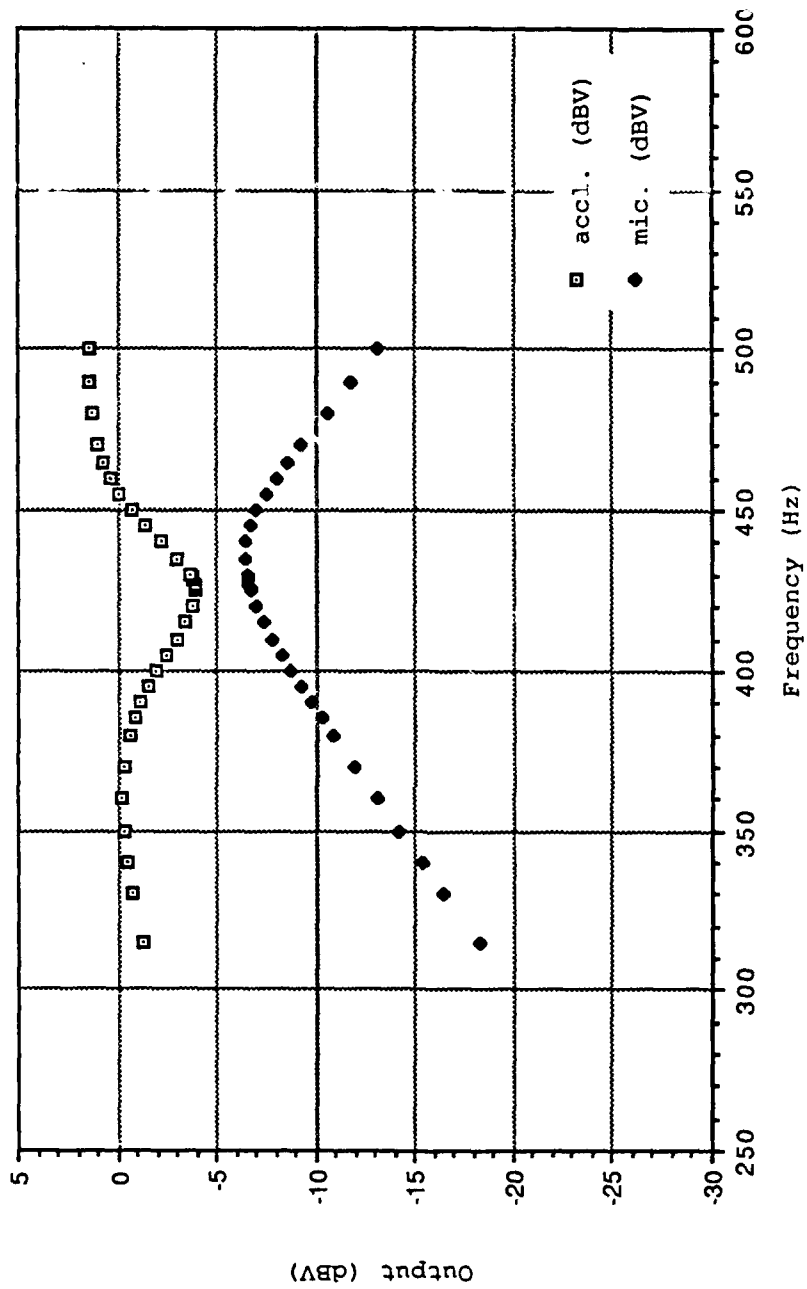


Figure VI-4d. Microphone and Accelerometer Outputs for Helium and 7.94% Argon

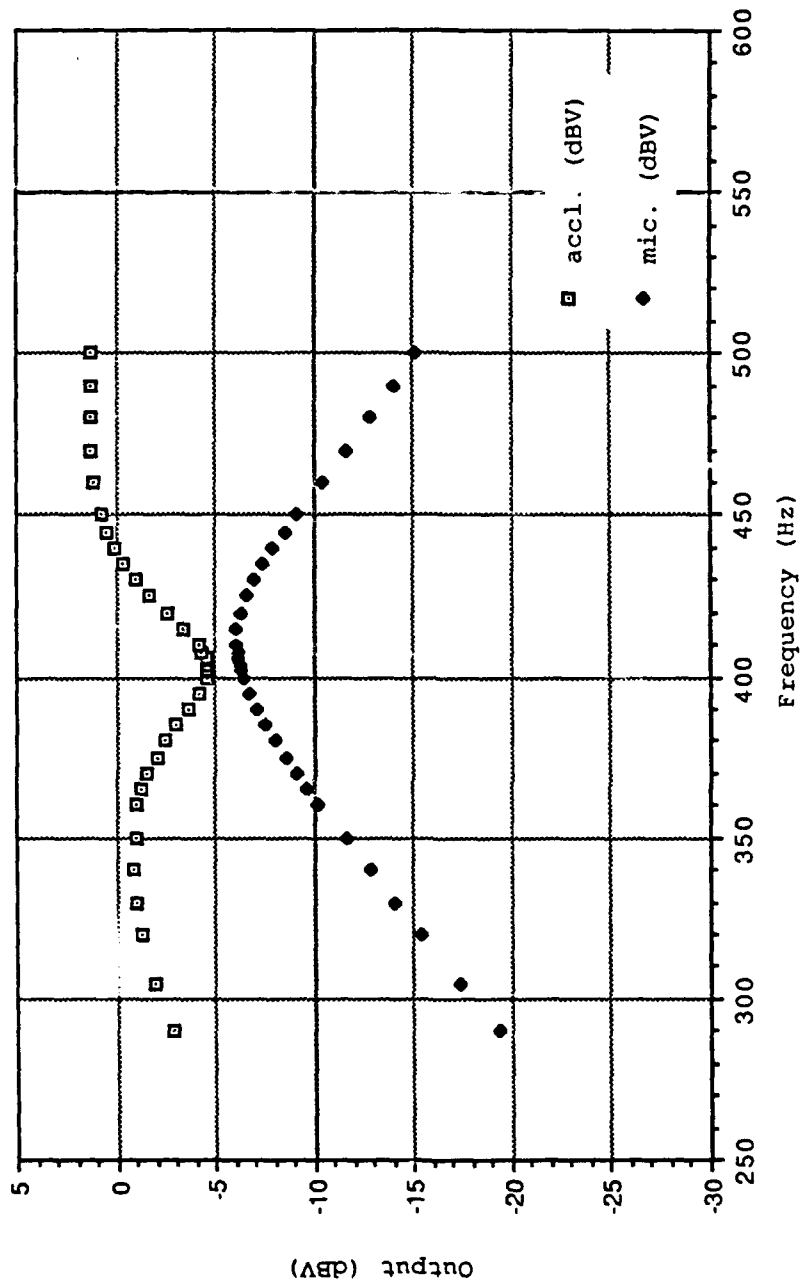


Figure VI-4e. Microphone and Accelerometer Outputs for Helium and 10.1% Argon

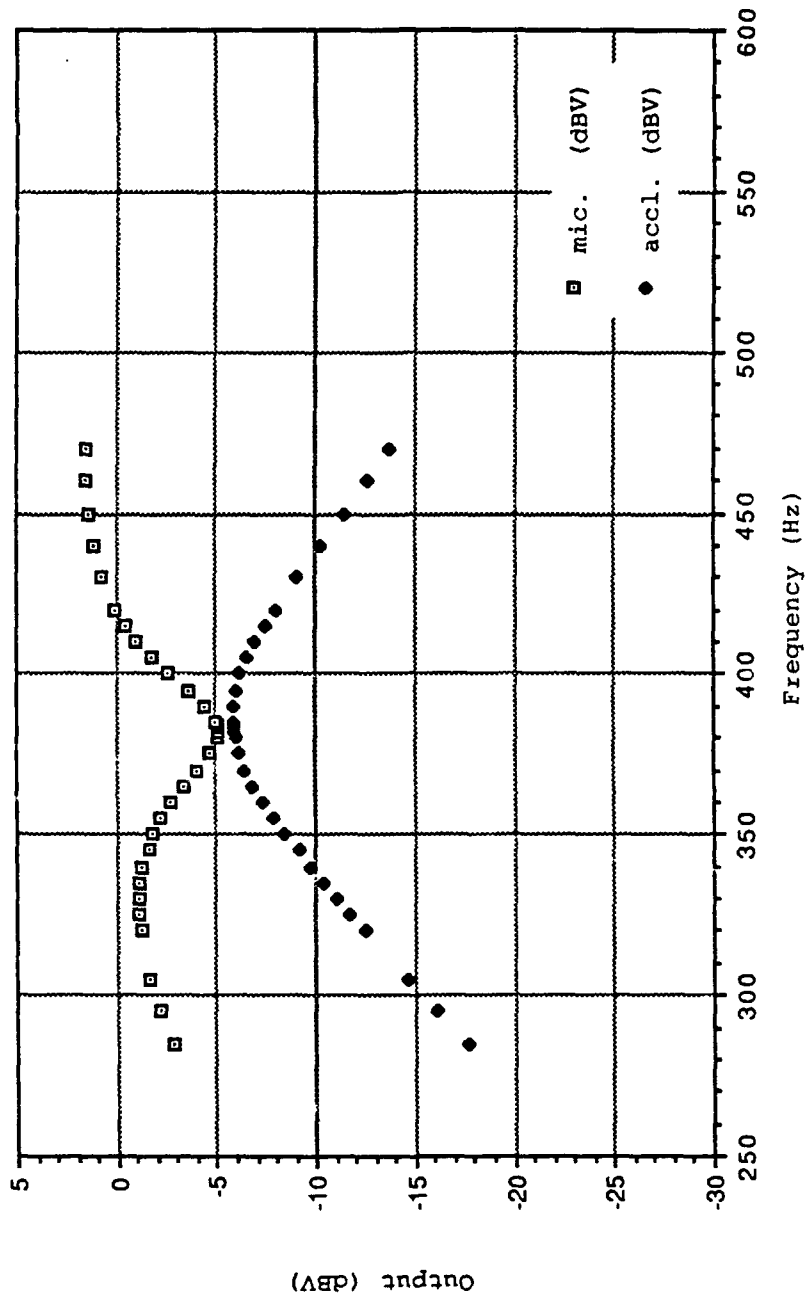


Figure VI-4f. Microphone and Accelerometer Outputs for Helium and 12.4% Argon

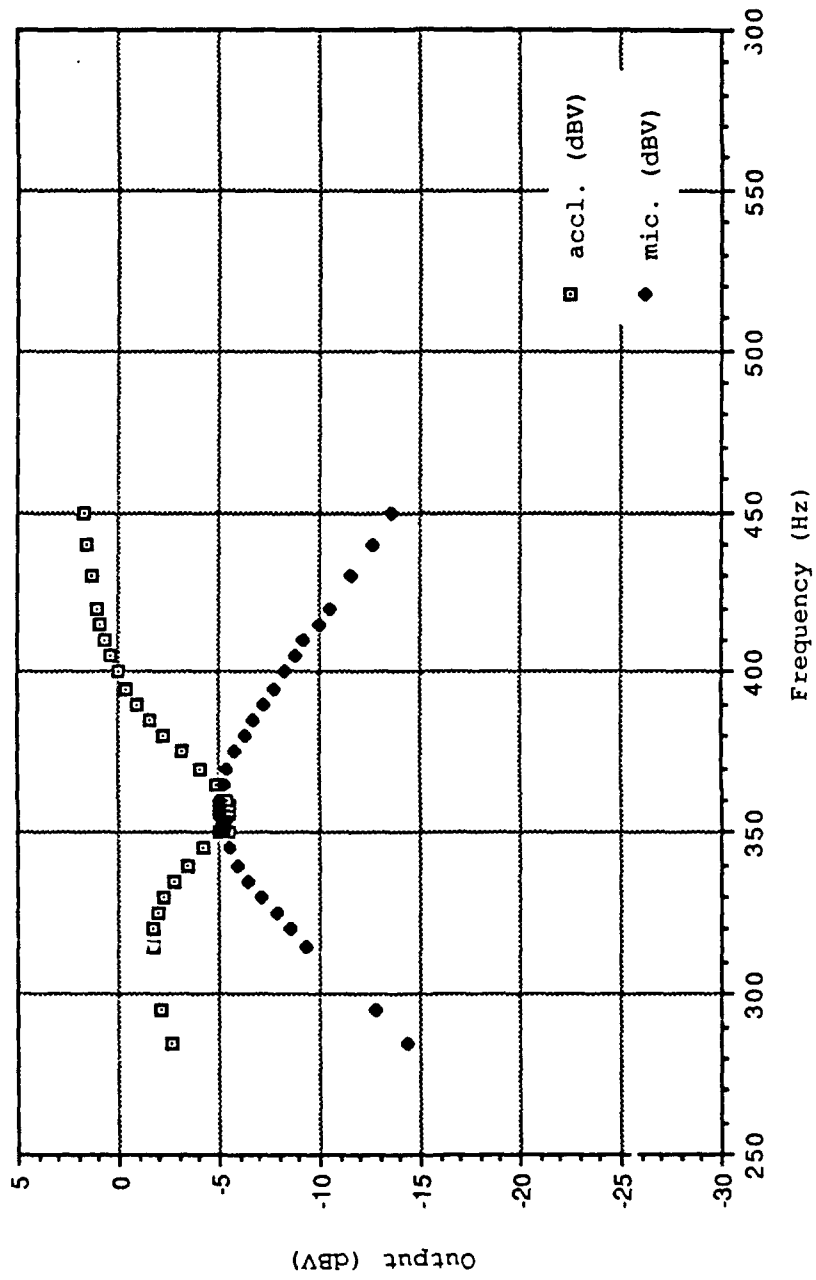


Figure VI-4g. Microphone and Accelerometer Outputs for Helium and 16.0% Argon

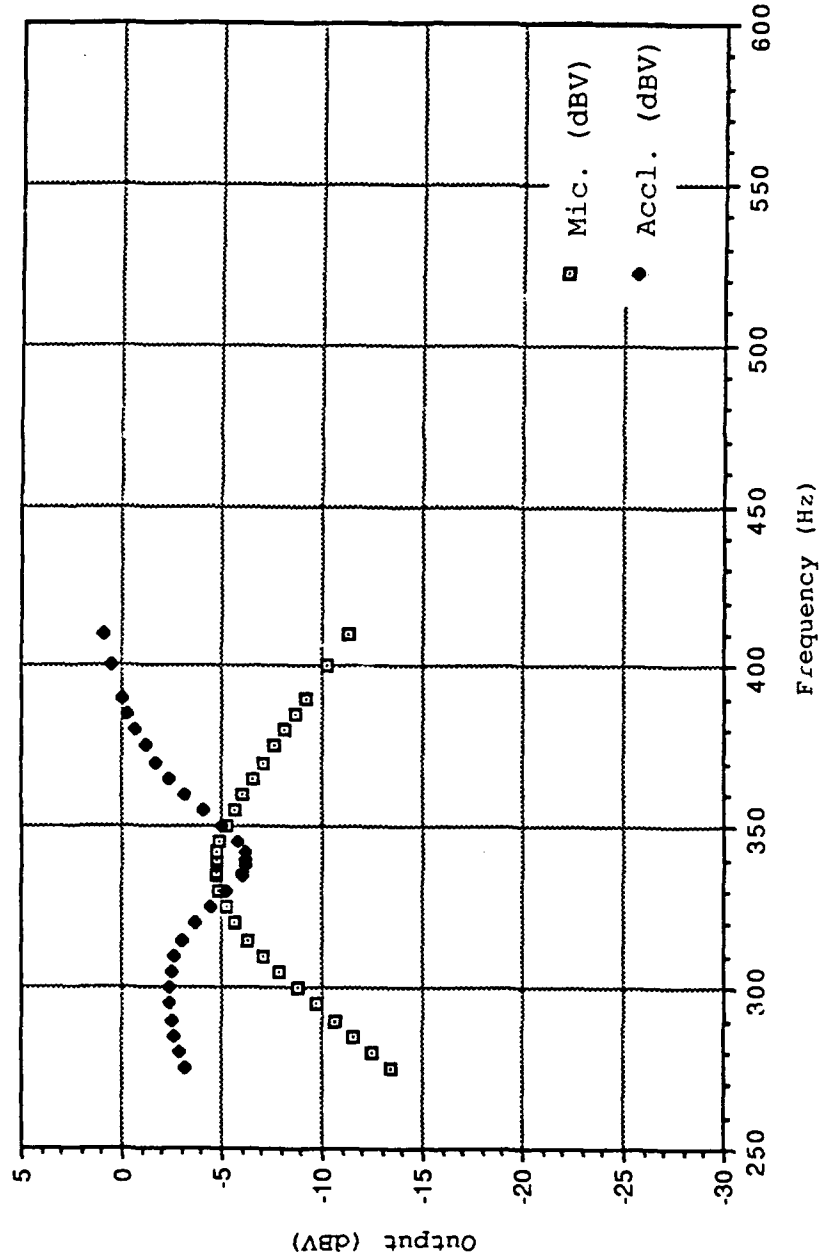


Figure VI-4h. Microphone and Accelerometer Outputs for Helium and 18.9% Argon

they are brought closer together. It is obviously not safe to assume, then, that one has merely to set the gas mixture such that the resonator fundamental coincides with the mechanical resonance of the driver; for where indeed is the driver's mechanical resonance when so many factors such as electrical damping and resonator interactions cloud the picture? Returning to the original impetus for these tests, it is clear that the gas mixture must be set for a maximization of the electroacoustic efficiency.

Given the frequency at which the refrigerator is driven, the electrical power P_{elec} delivered to the voice coil, the volume velocity U and acoustic pressure p at the bellows' radiating surface and the phase angle ϕ between them, the electroacoustic efficiency is easily calculated as outlined in Volkert and Harris [Ref. 16]. The acoustic power P_{ac} delivered to the resonator is

$$P_{ac} = p U \cos(\phi). \quad (VI-1)$$

Or using the measured data;

$$P_{ac} = (V_{mic}/M_{mic})(V_{acc}/\omega M_{acc}) \cos(\phi) \quad (VI-2)$$

where M_{mic} and M_{acc} are the voltage sensitivities of the microphone and accelerometer respectively, and ω is the angular frequency. The electroacoustic efficiency η_{ea} is now simply

$$\eta_{ea} = P_{ac}/P_{elec}. \quad (VI-3)$$

The individual efficiency curves are presented in Figures VI-5a through VI-5h, and the efficiency as a function of the

resonator fundamental is shown in Figure VI-6. The data is summarized in Table VI-1 where F_0 is the fundamental or "operating" frequency of the resonator and F_{peak} is the frequency of maximum efficiency.

ELECTROACOUSTIC EFFICIENCY				
% argon	F_0 (Hz)	eff.(%)	F_{peak} (Hz)	eff.(%)
0	560	23.0	570	26.0
3.71	485	32.4	500	38.9
6.42	446	36.4	465	45.8
7.94	428	38.0	450	49.3
10.05	406	39.8	435	50.5
12.42	384	39.7	415	51.8
15.96	358	38.0	400	47.6
18.85	340	36.3	385	42.6

Table VI-1

The final consideration in picking the actual gas mixture to be used is the anticipated drop in sound speed (or operating frequency) due to the drop in temperature as the refrigerator cools down. And, while it would appear that only the "cold" portion of the resonator experiences this temperature drop; that is where most of the particle velocity is, so that the gas temperature can essentially be taken to be that of the cold end of the resonator.

Given that the speed of sound in an ideal gas is related to the temperature by

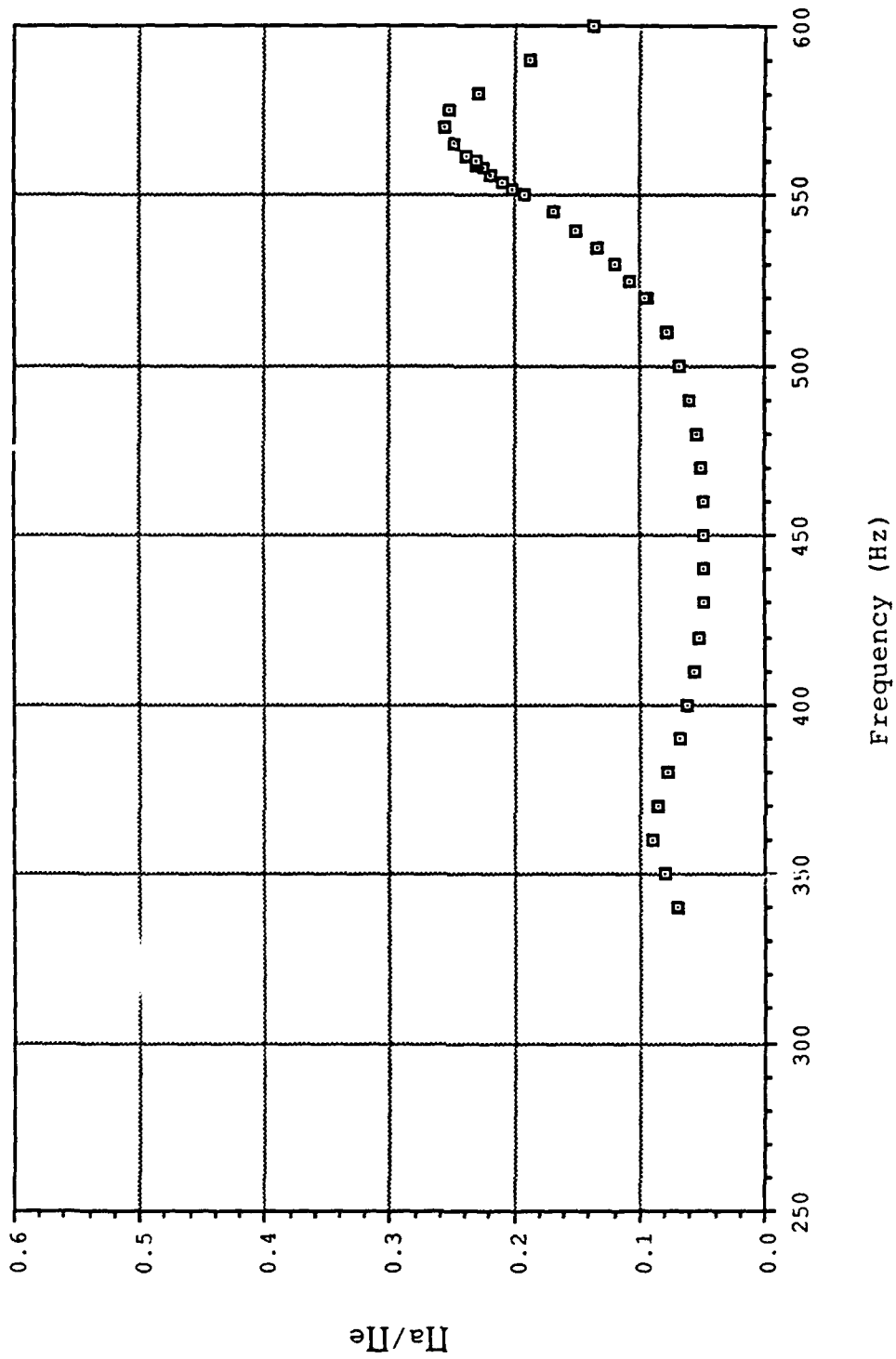


Figure VI-5a. Electroacoustic Efficiency for Helium

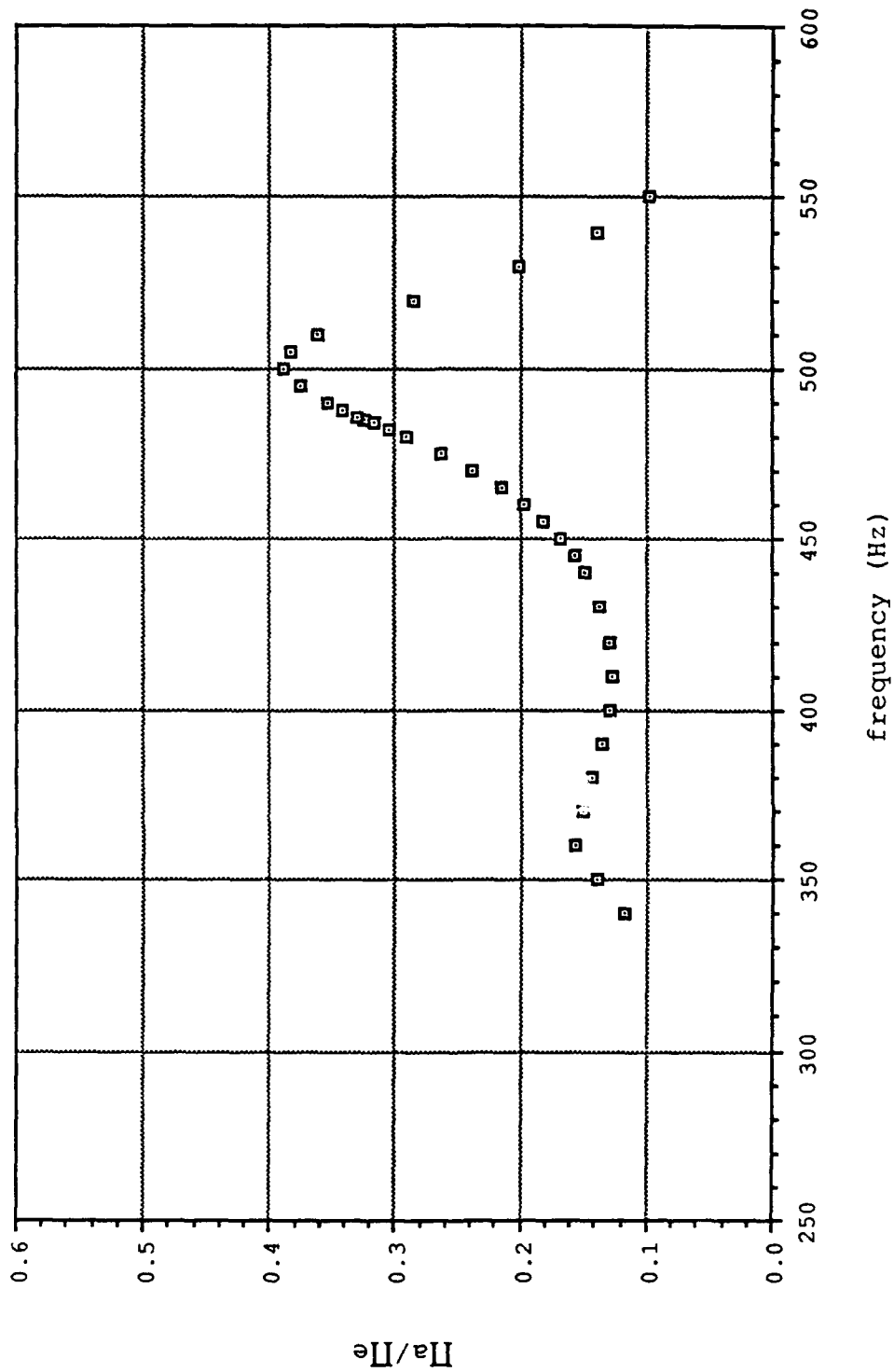


Figure VI-5b. Electroacoustic Efficiency for Helium and 3.71% Argon

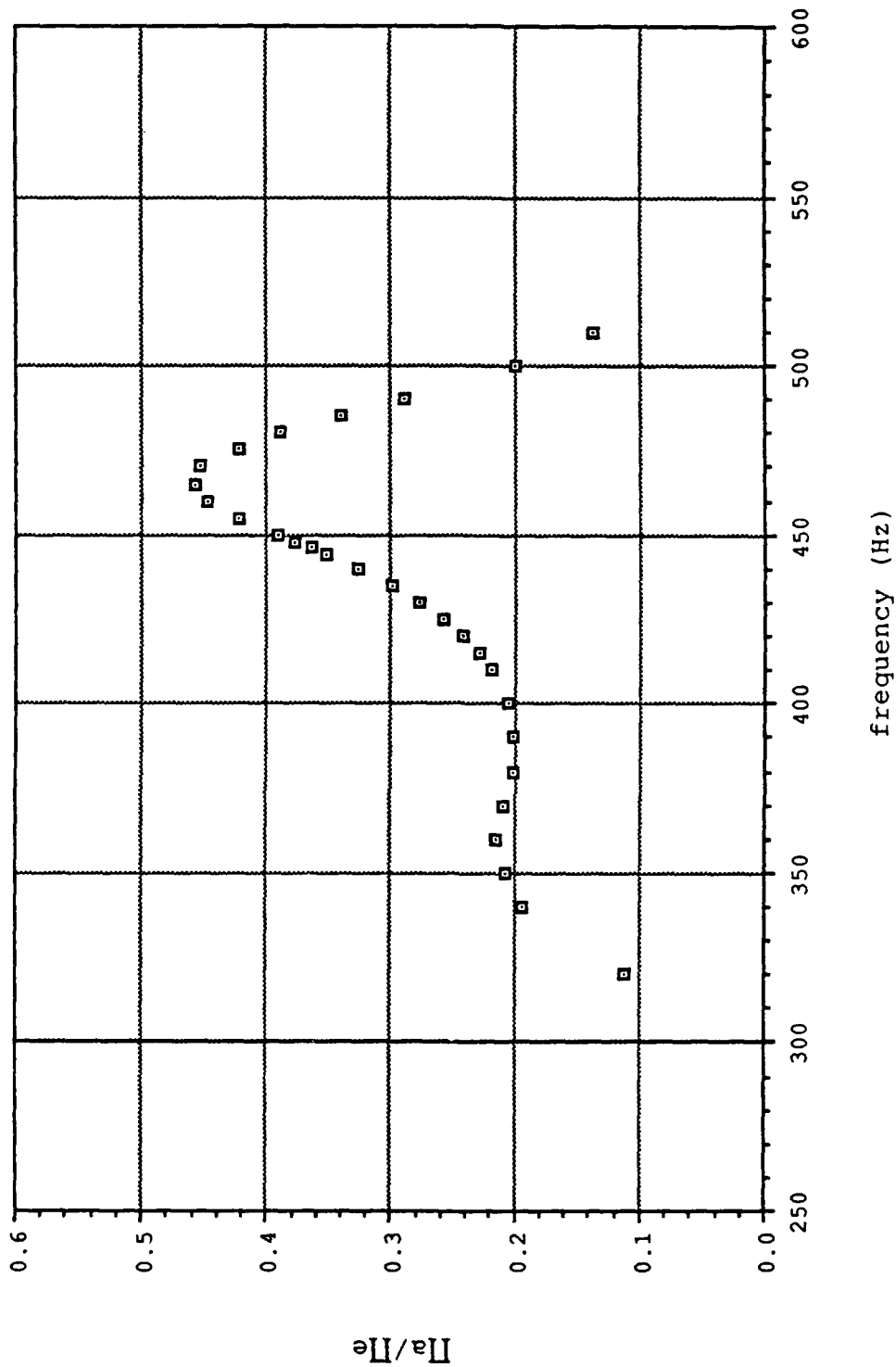


Figure VI-5c. Electroacoustic Efficiency for Helium and 6.42% Argon

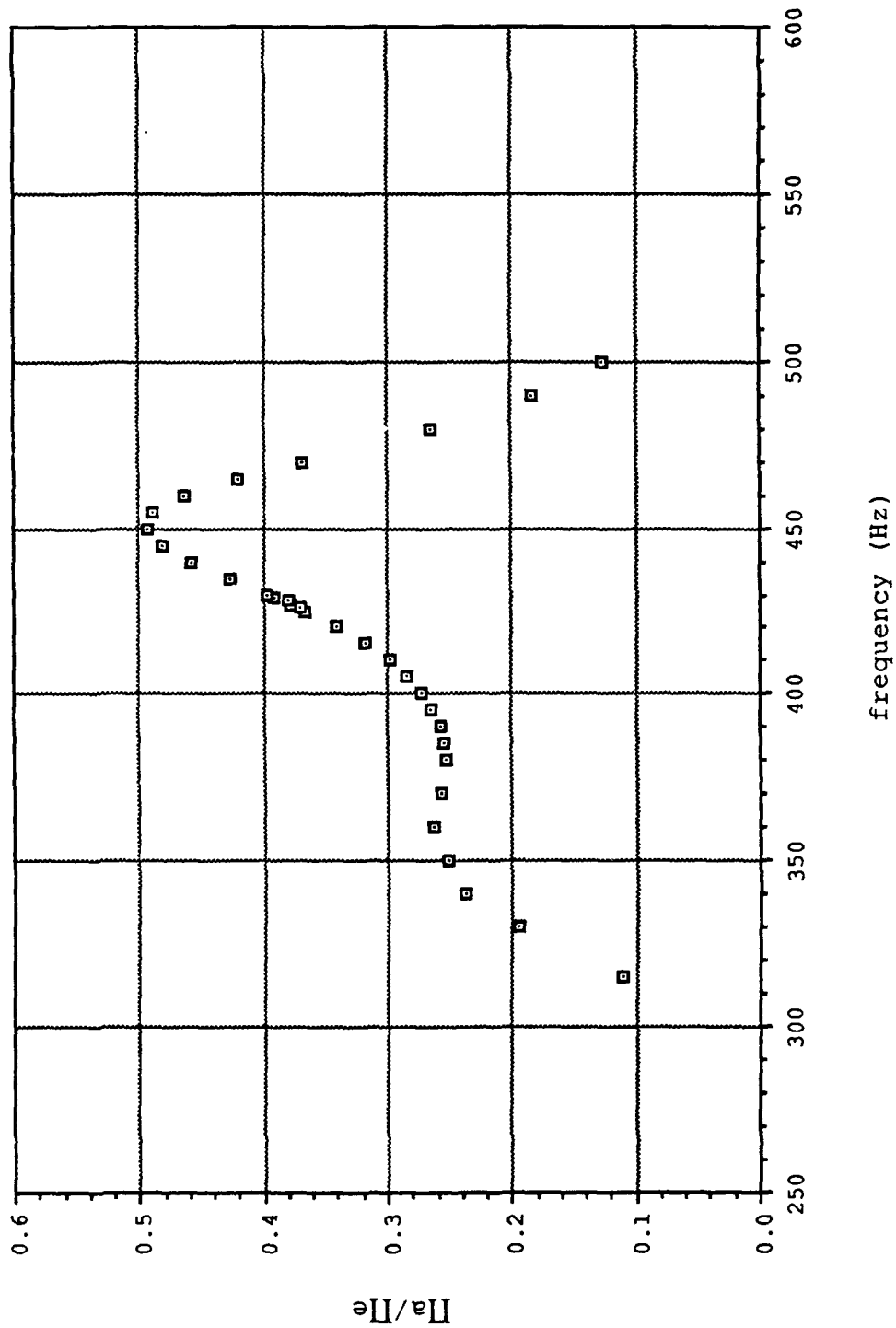


Figure VI-5d. Electroacoustic Efficiency for Helium and 7.94% Argon

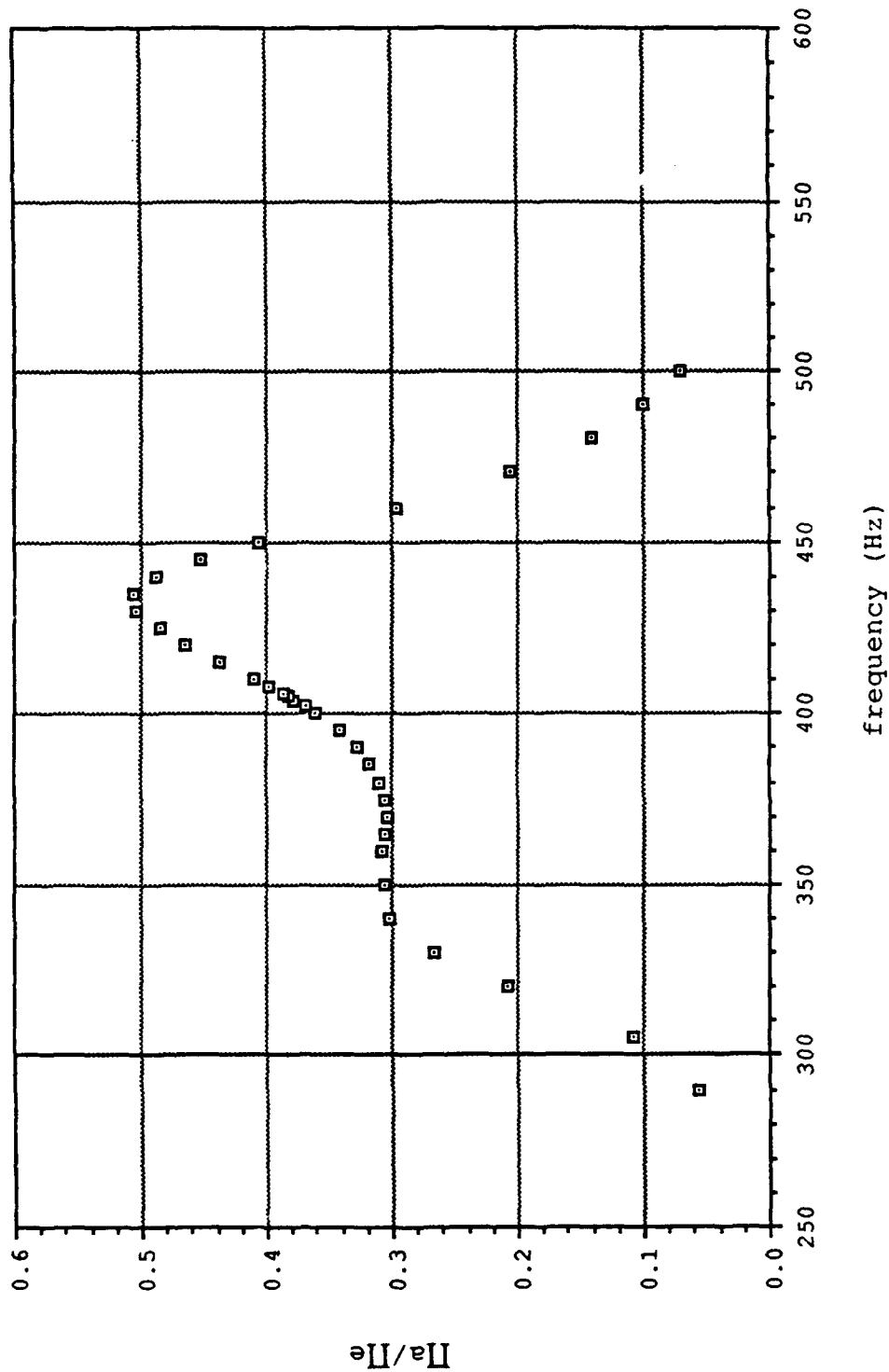


Figure VI-5e. Electroacoustic Efficiency for Helium and 10.1% Argon

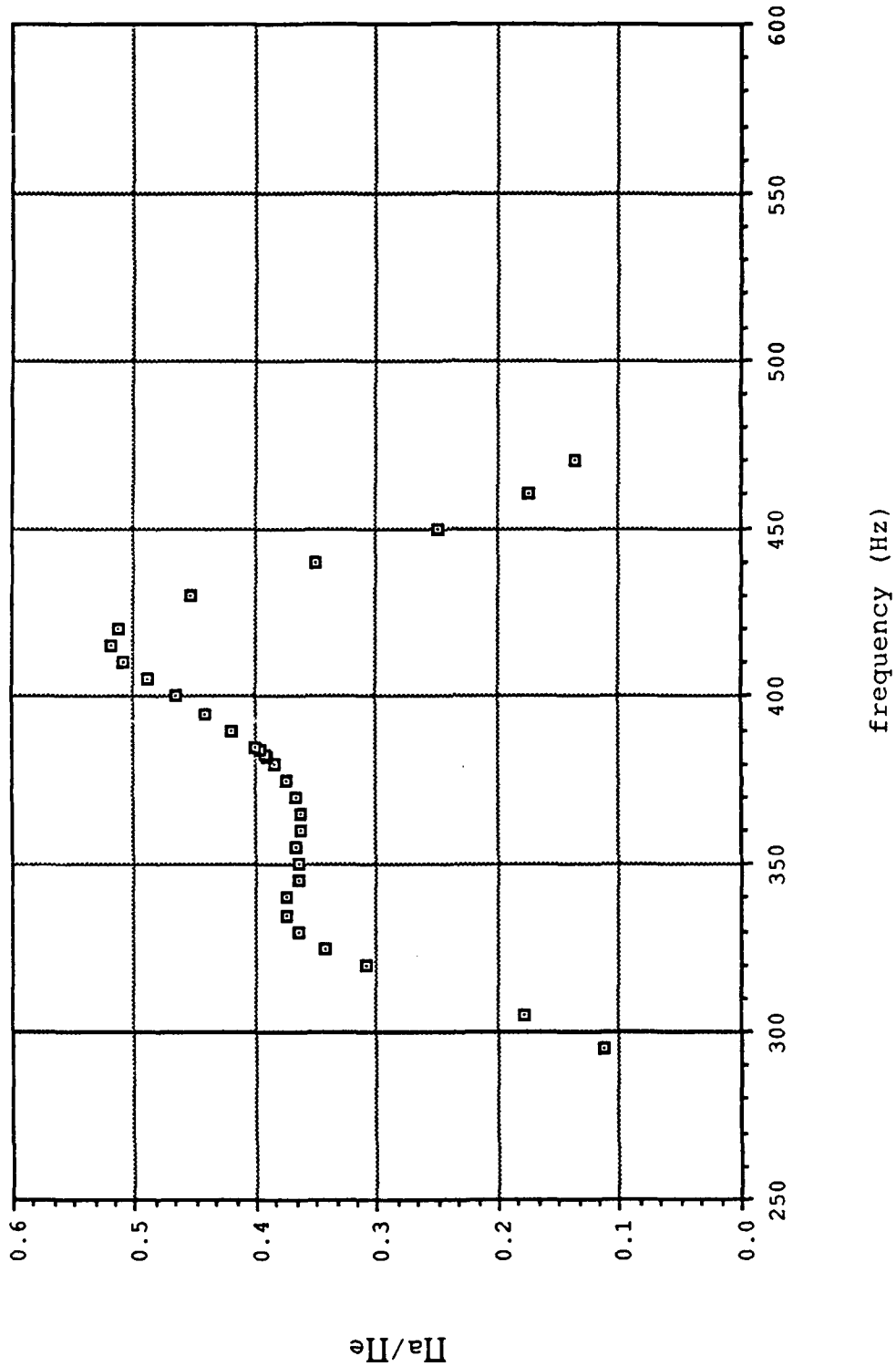


Figure VI-5f. Electroacoustic Efficiency for Helium and 12.4% Argon

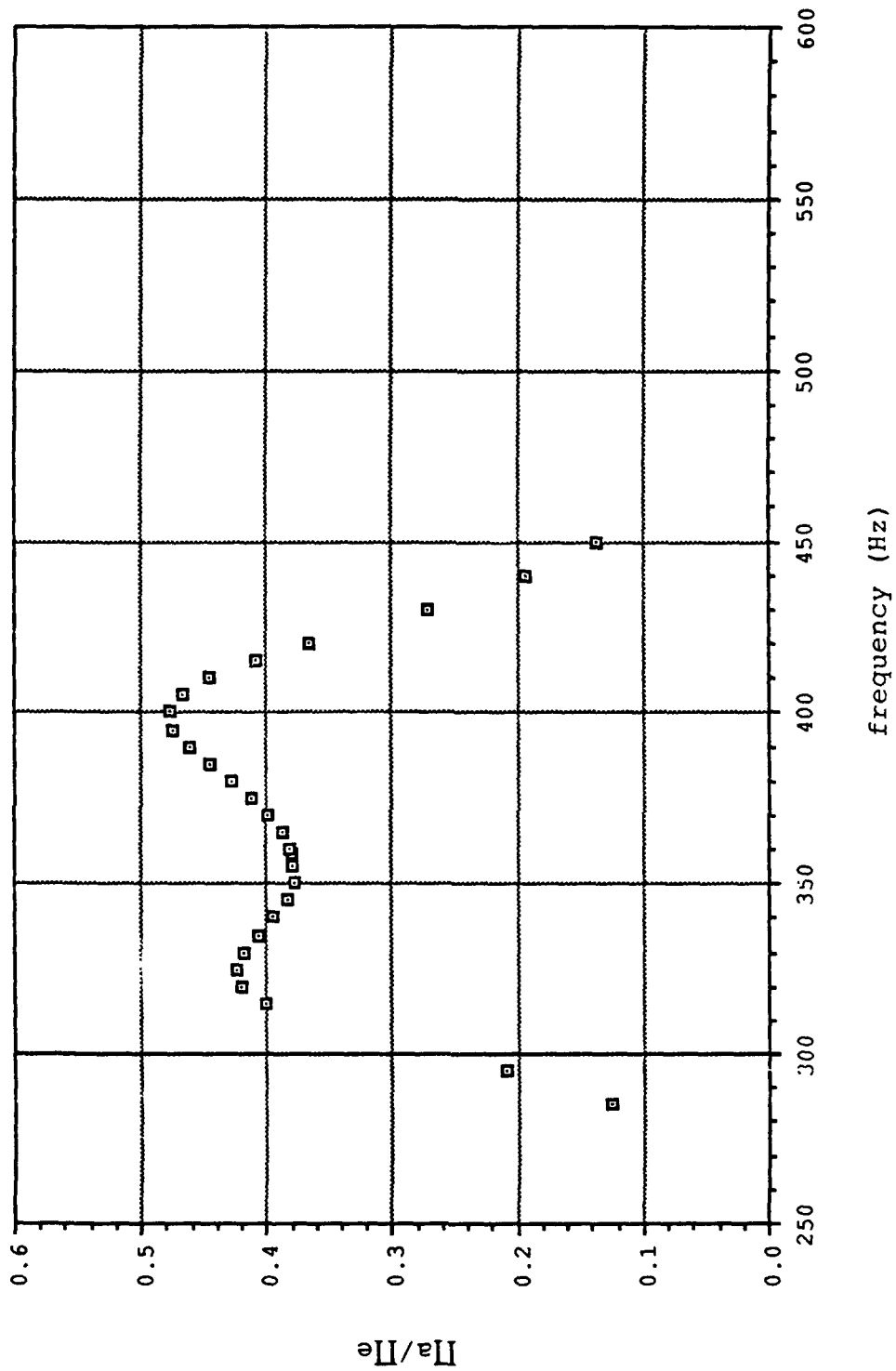


Figure VI-5g. Electroacoustic Efficiency for Helium and 16.0% Argon

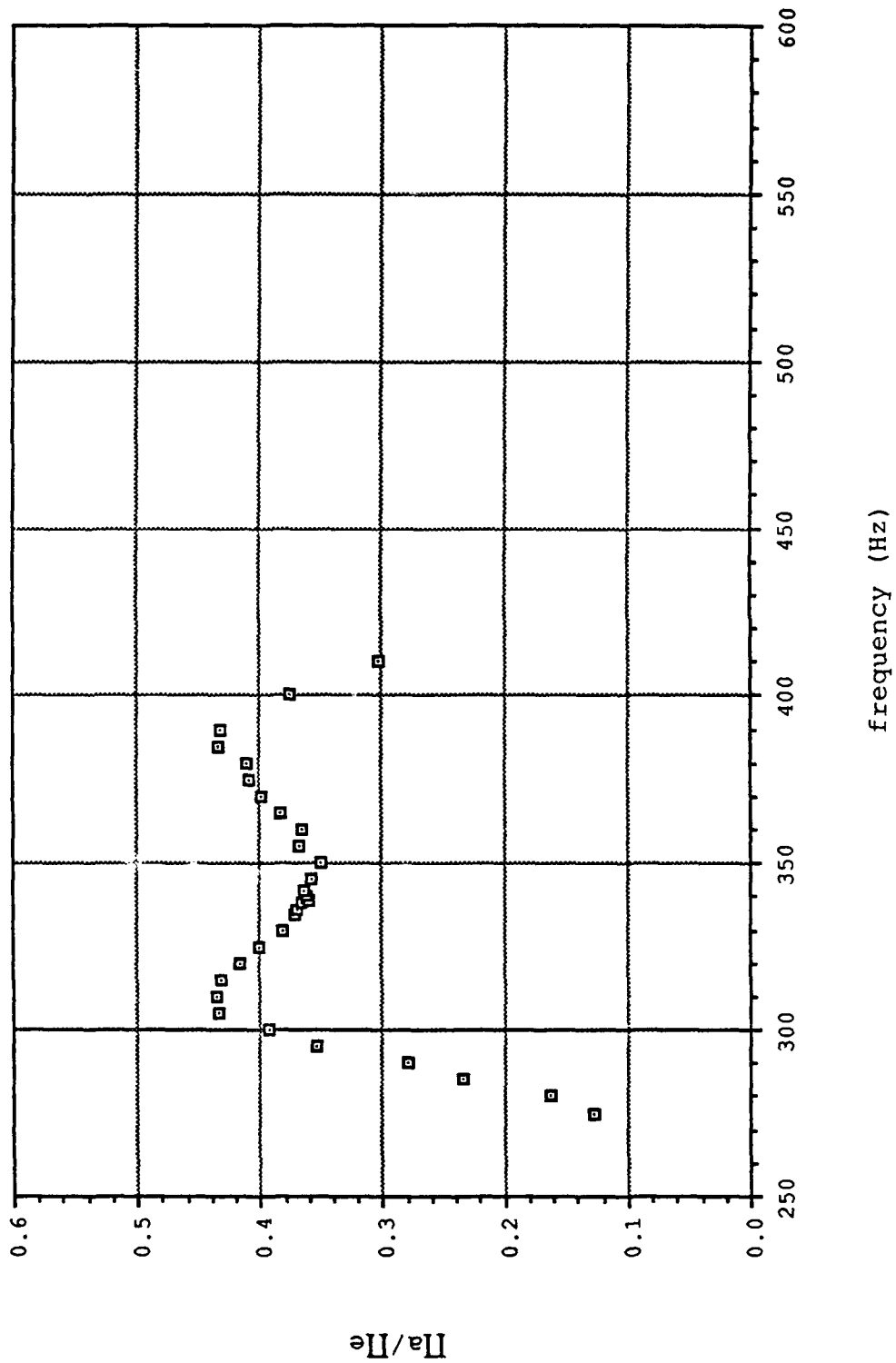


Figure VI-5h. Electroacoustic Efficiency for Helium and 18.9% Argon

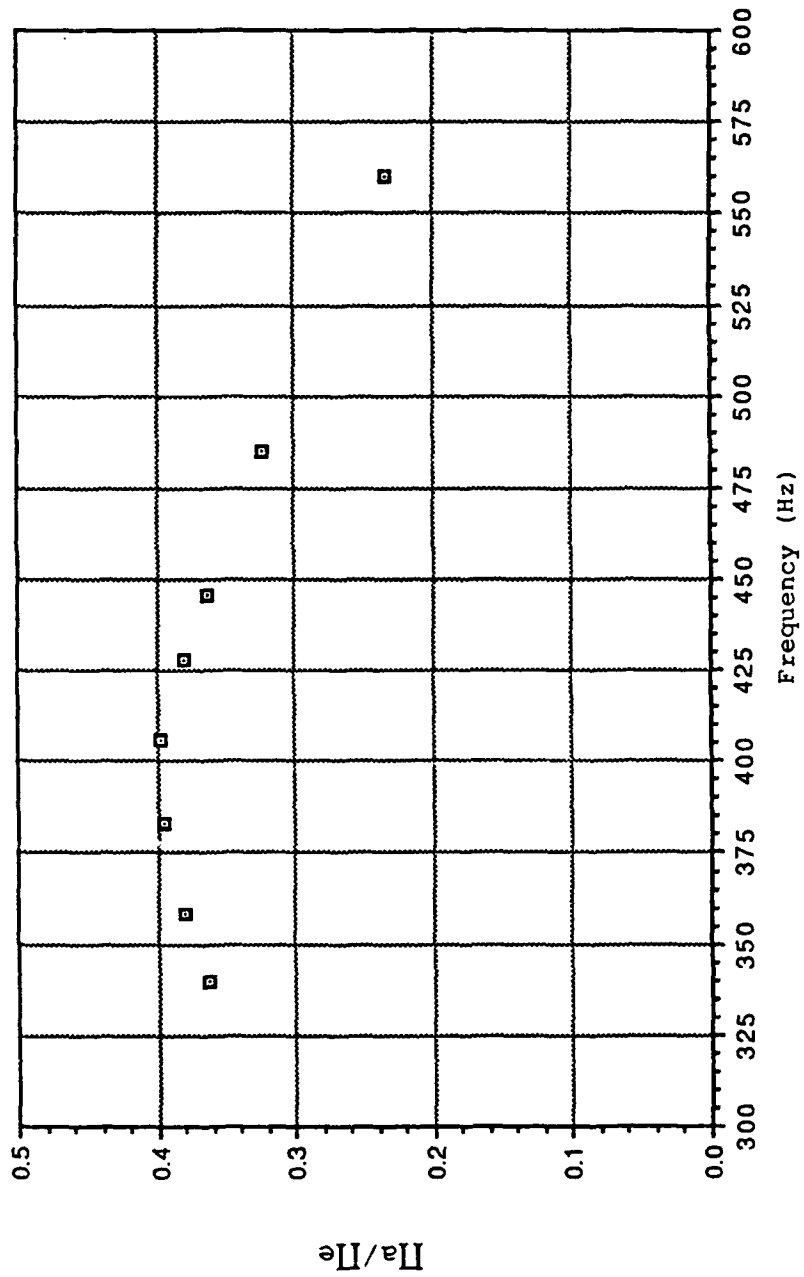


Figure VI-6. Electroacoustic Efficiency Versus Operating Frequency

$$c^2 = \gamma RT/m, \quad (\text{VI-4})$$

and guessing that on the first run the refrigerator would reach a cold temperature of at least 233° K (-40° C), an operating frequency of 410 Hz at 293° K (20° C) was chosen which would drop to about 366 Hz with the drop in temperature. This selection appeared to straddle the efficiency curve nicely, and would hopefully allow the refrigerator to run at its most efficient frequency when a heat load was applied; that frequency being somewhere between 366 Hz and 410 Hz. The starting frequency was eventually adjusted to 420 Hz as lower temperatures were attained.

B. DATA ACQUISITION AND ANALYSIS

In order to operate STAR safely at full power for days at a time and to amass useful data, some sort of protocol for powering up and operating the refrigerator had to be established. The first step, after completely purging the system of air, was to fill the driver/resonator with the appropriate gas mixture. Because this step could take up to three hours, it was prudent to start up the vacuum pumps for the thermal vacuum canister at the same time since it took two to three hours just to achieve a minimum acceptable vacuum of at least 10^{-4} Torr. In fact, it was common to begin drawing the vacuum 24 hours in advance of operation of STAR.

Once the refrigerator was pressurized and a good vacuum was achieved, starting up was quite easy thanks to the Resonance Control Board (RCB). With the data acquisition system, power amplifier, and ancillary monitoring electronics equipment powered up, the resonance control board was turned on with the frequency and amplitude resets on and the operating level switch set to the two percent position.

The power amplifier was first set to a low gain level so that the RCB board would be receiving a microphone and accelerometer signal. The frequency reset was then disconnected to allow the RCB to track towards the fundamental frequency of the resonator. Once the refrigerator was at the proper operating frequency, the power amplifier gain was increased to a level that had already been experimentally determined to give the Automatic Gain Control section of the RCB proper control of the driver at full power. At this point the driver was still operating at a substantially reduced power level. Turning off the amplitude reset was all that remained to bring the refrigerator up to full operating status.

Once the refrigerator was operating, two types of data were accumulated. The first was simply status data which were recorded by a combination of a HP 3457A data acquisition unit and a HP 9836 computer as outlined in Appendix A. The second data set were single points taken

when the refrigerator had reached equilibrium after some change had been made to the heat load imposed upon it. Status data was taken at intervals of anywhere from 30 seconds to 20 minutes depending on how fast things were changing, and was useful for charting how fast events occurred or simply for monitoring the vital signs of STAR. The single data points were used for analysis of the temperature ratio and coefficient of performance (COP) of the refrigerator.

The status points monitored where the hot and cold temperatures of the resonator, the electrical power and current being delivered to the driver, the mean pressure within the driver housing, the microphone and accelerometer RMS output voltages, the operating frequency, and of course the time at which the data were taken. The single data points taken were the elapsed time, the hot and cold temperatures, the mean pressure, the DC voltage applied to the resistive heater strip, the microphone and accelerometer RMS voltages, and the operating frequency.

Three tests were of interest once the refrigerator was running at full power. The first, simply out of curiosity, was to measure how fast the refrigerator would cool down to its lowest temperature. The second, for determining the magnitude of the nuisance heat leak, was how fast the refrigerator warmed up again after the power was shut off. The third, requiring long term operation, was to allow the

refrigerator to reach its lowest temperature, record the data, and then change the heat load at the cold end of the resonator and take data after it had been allowed to equilibrate again. Data for the first and third tests were taken by the automated data acquisition system (ADAS) because of its accuracy and reliability. Data for the second test, while actually recorded by the ADAS, was simultaneously annotated by hand in a lab book.

The raw data for the refrigerator cool down and warm up will be presented in a graph of temperature versus time. The analyzed performance data will be presented in the form of a graph of the temperature ratio (T_C/T_H) versus total heat load and the coefficient of performance relative to Carnot (COPR) versus the total heat load. The total heat load includes the heat applied via the resistive heater strip and the nuisance heat leak from the resonator itself. Because the analysis of the data was relatively straightforward and there was not a large number of data points, these calculations were done by hand on a HP 15C programmable calculator. All of the formulas may be found elsewhere in this thesis.

Some mention should be made at this point about the accuracy of the temperature data taken. First of all, the temperatures measured with the Omega E-type thermocouples are specified by the manufacturer as being accurate to within the greater of 1.7°C or $\pm 1\%$ of the temperature as

referenced to 0°C. This error was somewhat compounded for the cold thermocouple by the millivolt thermocouple amplifier. The DC offset at the output of this unit tended to drift after several hours and in any event could not be reduced below about 0.2 millivolts, which translates to as much as three degrees centigrade. The cold temperature data annotated by hand was subsequently read on an Omega 450 AET E-type thermocouple thermometer. This eliminated the errors extraneous to the specified accuracy of the thermocouple.

C. NO HEAT LOAD

Because of the time constraints involved, it was decided that performance data at medium-power ($P_o/P_m=2\%$) would be taken with resonator number one, leaks and all, while version two was being constructed. The first important data was actually the last taken. The warm up data was used to calculate an estimate of the heat leak back to the cold end of the refrigerator. The graph of Figure VI-7 is an exponential fit of the temperature difference (T_h-T_c) versus time. The computer graphics program used was Cricket Graph which can calculate a base 10 logarithmic fit which is easily converted to a natural logarithmic formula of the form

$$\text{Temperature Difference} = 68.5 e^{-0.00005t}. \quad (\text{VI-5})$$

Following the procedure outlined in Chapter III, the heat leak was calculated as being approximately 0.0118 Watts/°K

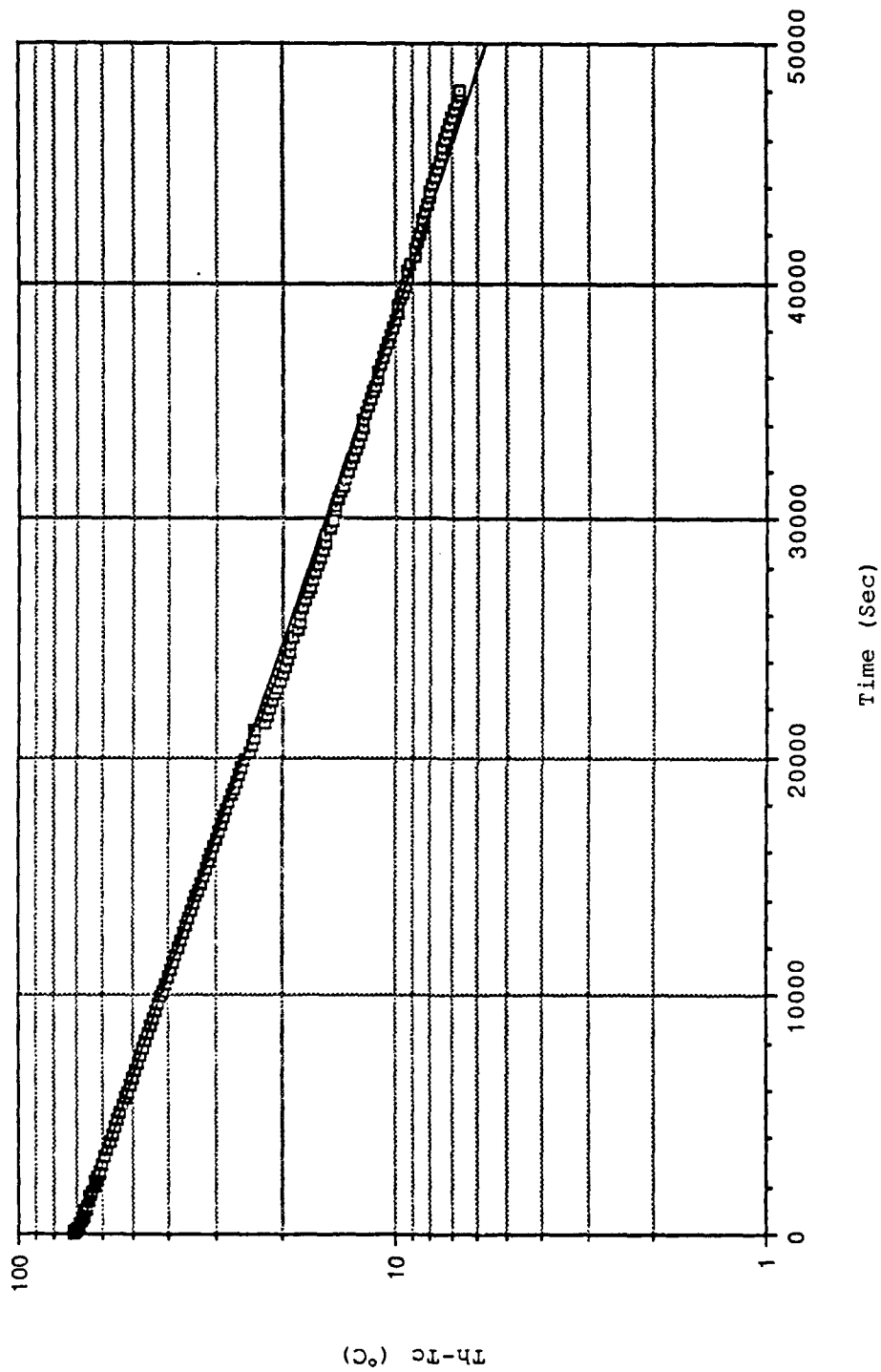


Figure VI-7. Warm-Up Data for Resonator 1

for resonator number one. As per Susalla [Ref. 17], an allowance of 0.0024 Watts/°K was made for thermal conduction due to the stack and gas which reduced the nuisance heat leak to 0.0094 Watts/°K.

Resonator number two faired better than the first because it remained leak tight throughout the full-power performance tests. It also had a minimum of ten layers of super-insulation around the sphere, and as much as 15 layers around the reduced portion of the resonator barrel. The warm-up data is presented in the graph of Figure VI-8 and leads to a heat leak of 0.010 W/°K from which 0.0024 W/°K is subtracted to arrive at 0.0076 W/°K.

While not being of any particular use for this thesis, it is of interest to look at the cool-down rate of the refrigerator. This data will be needed at a future date by whomever will be programming the microprocessor that will control STAR while it is in orbit aboard the Space Shuttle. Figures VI-9 and VI-10 show the temperature in degrees centigrade versus time, of the cold end of resonator number two, for medium-power (2%) and full-power (3%), respectively. The full power data begins at -17° C because the driver voice coil is displacement limited at temperatures above this. It can be seen that while the temperature drops more quickly with the refrigerator running at full-power, the lowest ultimate temperature is reached

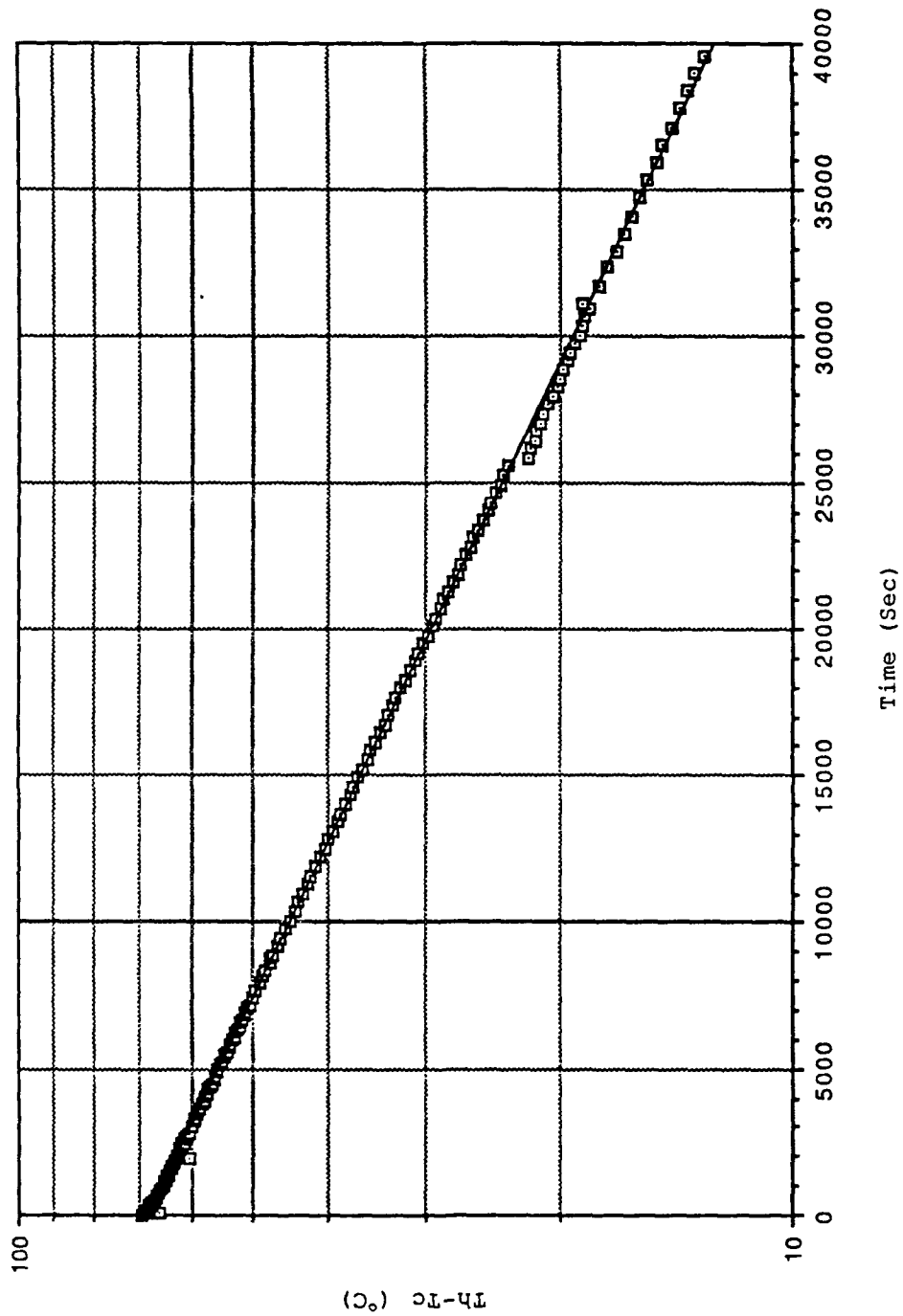


Figure VI-8. Warm-Up Data for Resonator 2

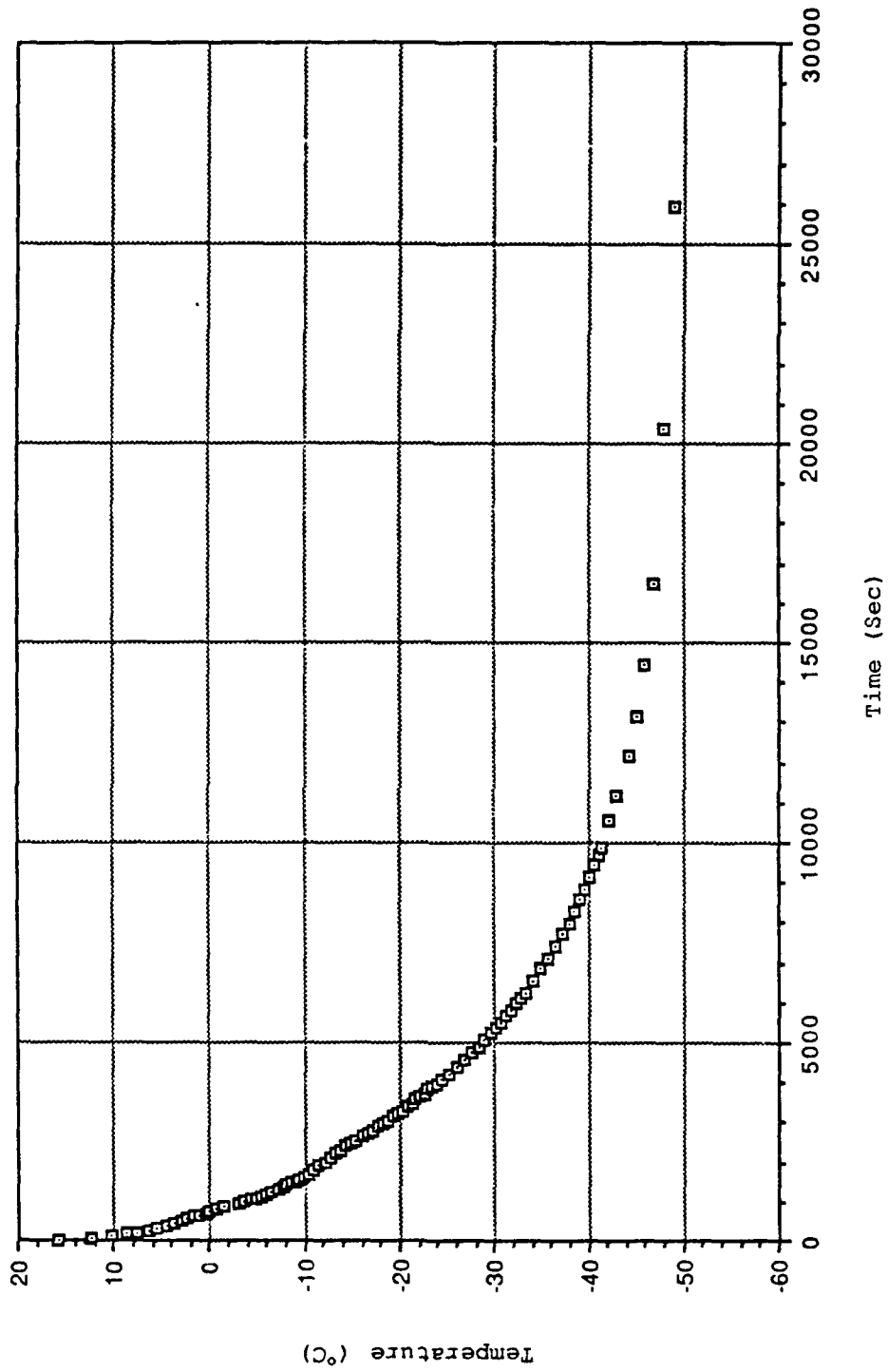


Figure VI-9. Cool-Down Rate for Medium Power

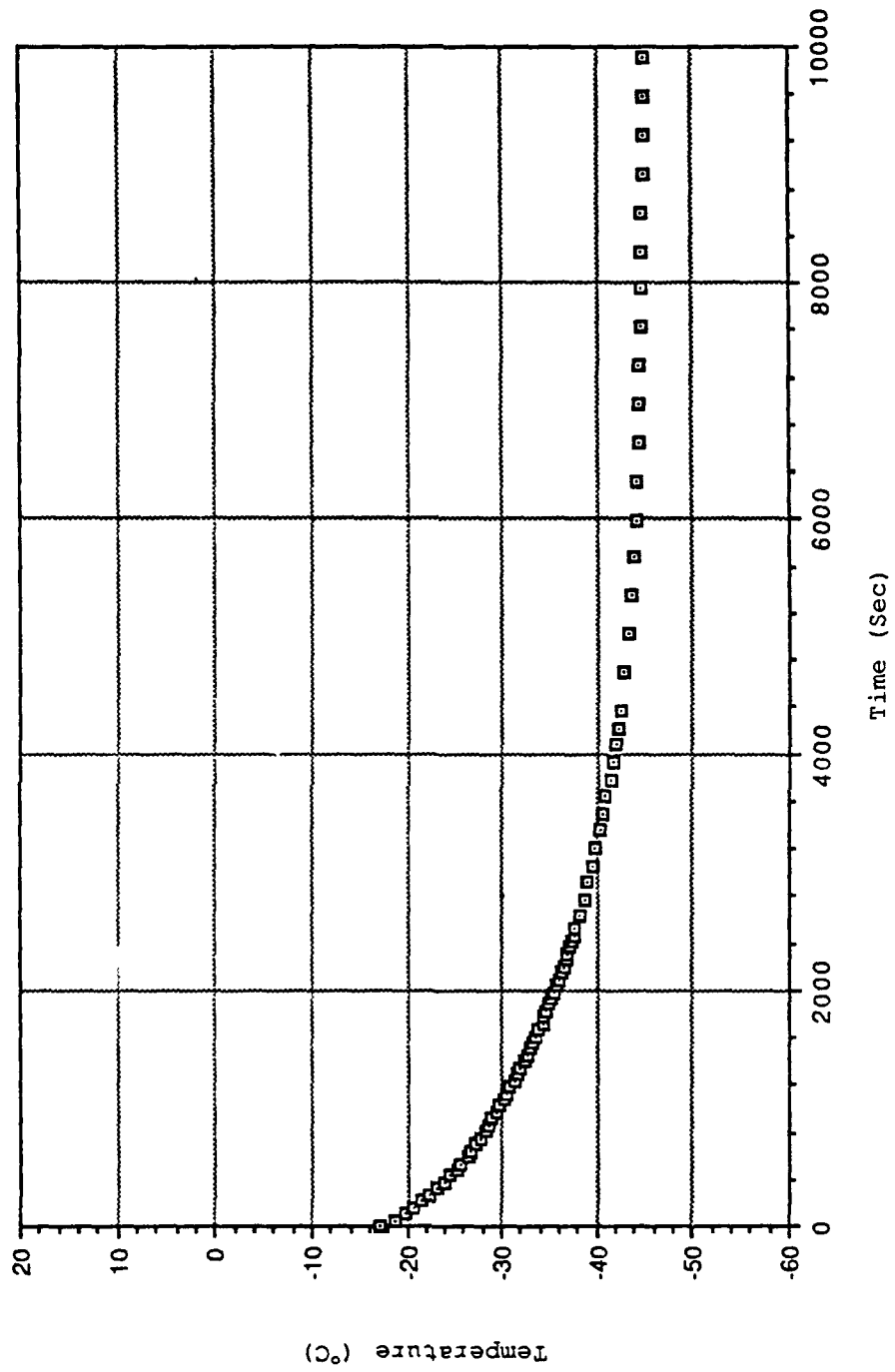


Figure VI-10. Cool-Down Rate for Full Power

under medium-power operation. This behavior is identical to that of Hofler's original research refrigerator [Ref. 18].

D. TEMPERATURE RATIO AND COEFFICIENT OF PERFORMANCE

The first long term run of the refrigerator, using resonator number one, was conducted at an acoustic pressure to mean pressure ratio of 2 percent. Gas was continuously added to the resonator/driver as it cooled down because of the anticipated pressure drop as the gas cooled. However, once the heat load tests were begun, the refrigerator should have been able to reach equilibrium from within 12 hours of each heat load change. But because of the rather large leak in the resonator, about one PSI per hour, it was necessary to first overpressurize the refrigerator to 155 PSIA when the heat load was increased, and then allow it to equilibrate for 12 hours. Then the refrigerator was refilled to 155 PSIA and allowed to equilibrate for another 12 hours at which point another data point was taken. By then, the mean pressure had typically dropped to about 145 PSIA and in fact, all of the data points were taken at this pressure to insure consistency.

The previously described procedure was necessary because the first 12 hour interval would allow the refrigerator to get within two degrees of equilibrium, while the second 12 hour interval was needed because topping off the refrigerator introduced warm gas into the resonator which

threw it off equilibrium by three to four degrees. By the end of the second 12 hour interval, if the temperature was found to not change by more than a tenth of a degree over a span of one hour, it was safe to conclude that it was within less than one percent of its equilibrium value.

Matters improved considerably when the second resonator was installed. Once the refrigerator had reached its lowest temperature, the mean pressure having been maintained at 150 PSIA, a heat load could be introduced and the refrigerator allowed to equilibrate without the need to add any more gas to it. In fact, it was necessary to bleed off about one PSI of gas within the first 30 minutes as the refrigerator warmed up to within one degree of its final value.

Throughout the full-power tests conducted with resonator number two, the vacuum cannister pressure remained below 10^{-6} Torr and no leaks developed. Subsequently, equilibrium was usually reached within three to four hours when the heat load was increased by one-half of a Watt, and within five to eight hours when it was increased by one Watt.

Unlike previous theses where variables such as gas composition or stack design were changed in order to analyze their effect on the performance of the thermoacoustic refrigerator, this thesis concerns itself solely with the performance of a thermoacoustic refrigerator modified to withstand the rigors of space flight. Here, then, are the results for the Space Thermoacoustic Refrigerator.

The graphs of Figures VI-11 and VI-12 show the temperature ratio T_C/T_h versus the total heat load in Watts for medium power and full-power, respectively. There are no surprises in that there is a linear relation between the temperature ratio and heat load as was seen previously by Hofler [Ref. 19] and Susalla [Ref. 20]. Also similar to Hofler [Ref. 21] is how the lowest temperatures were obtained at medium-power when no heat load existed. When a heat load was applied, however, the lowest temperatures were obtained at full-power.

Turning to the coefficient of performance relative to Carnot (COPR), the results for medium-power are presented in Figure VI-13 while the results for full-power appear in Figure VI-14. Again, the data shows a trend that was fully expected at the outset. The refrigerator has the highest COPR for low heat loads (two Watts) when operated at medium-power, but the highest COPR for larger heat loads (four to five Watts) when operated at high-power.

Quantitatively speaking, the results for the full-power runs are disappointing. While it was expected that the ultimate COPR at full-power would be slightly lower than for medium-power, it was not expected to be 29 percent lower. The two sets of COPR data were taken with two separate resonators, and it was clear from the start that the refrigerator was not operating properly when resonator

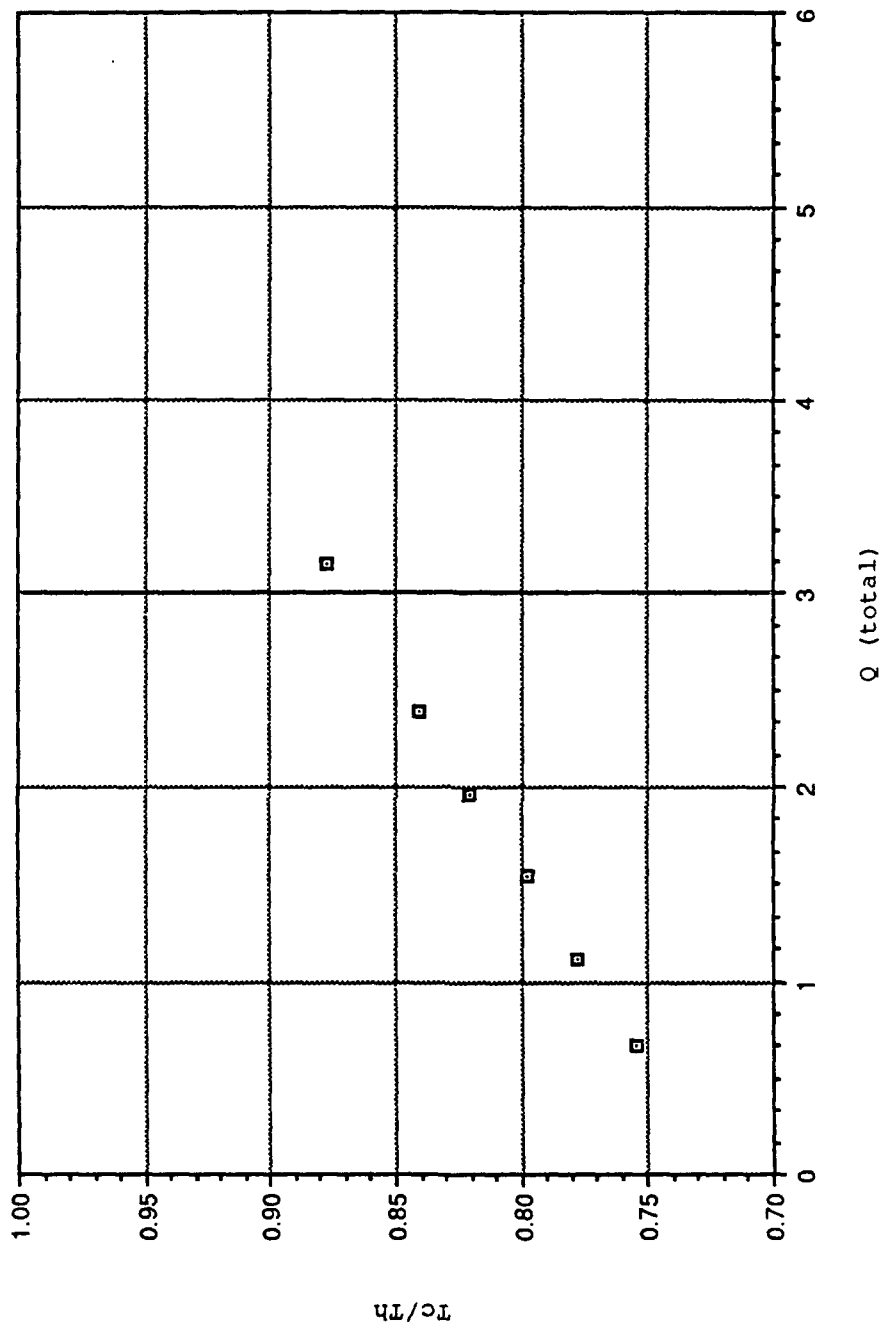


Figure VI-11. Temperature Ratio Versus Heat Load at Medium Power

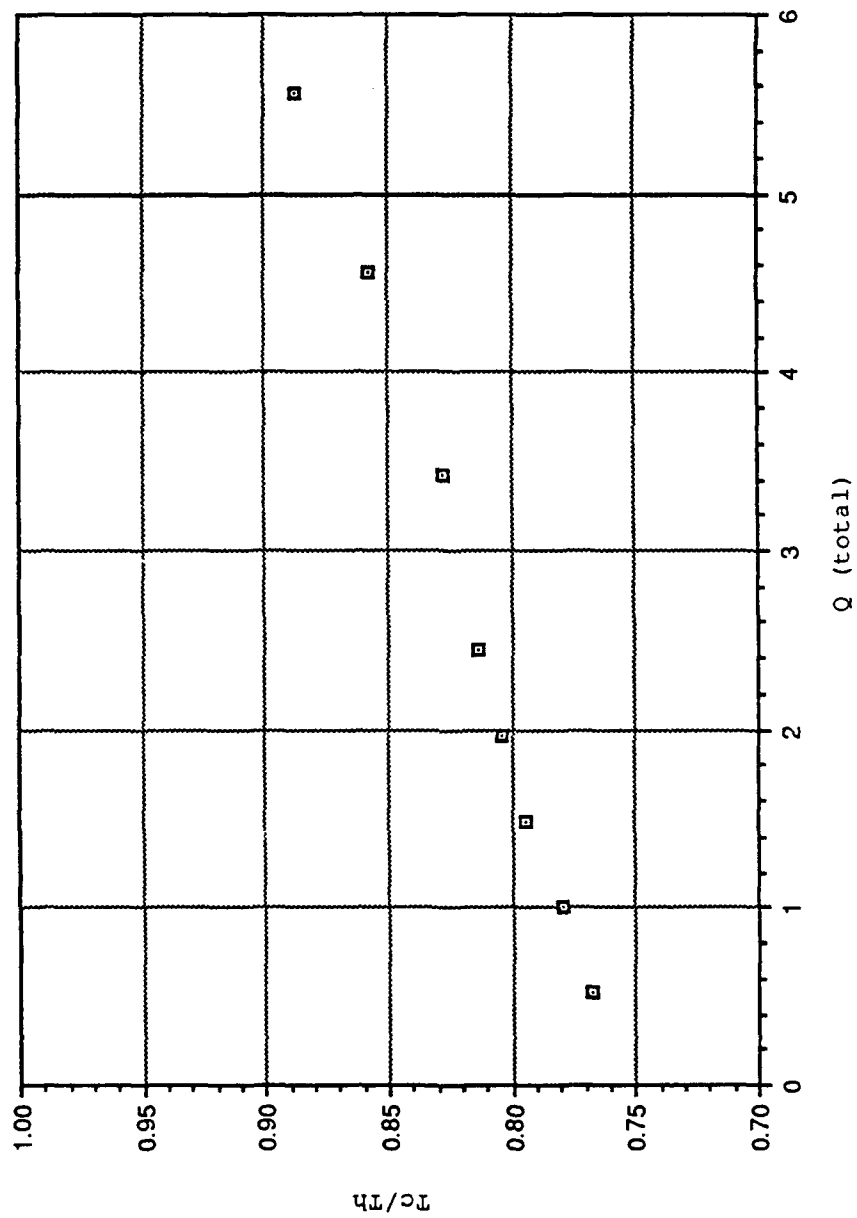


Figure VI-12. Temperature Ratio Versus Heat Load at Full Power

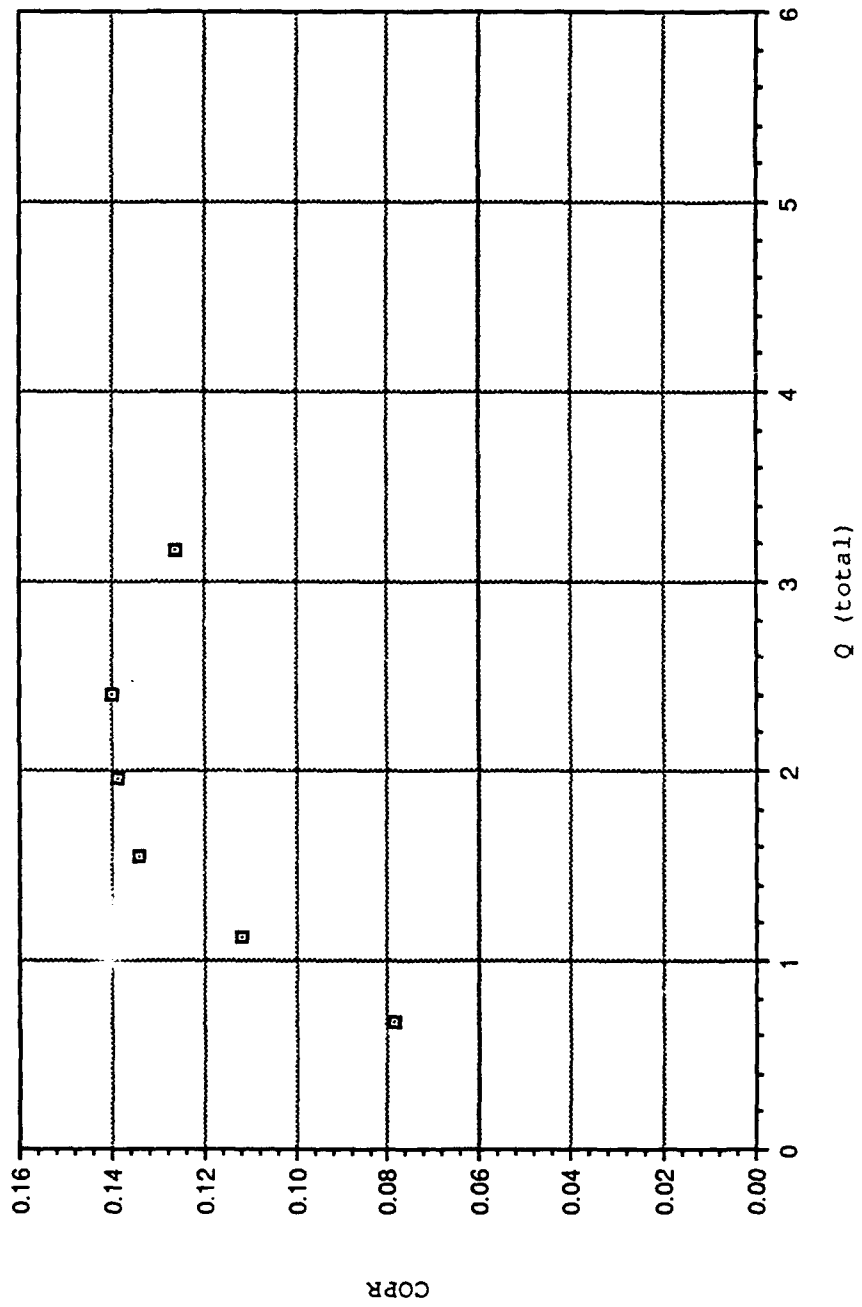


Figure VI-13. COPR at Medium Power

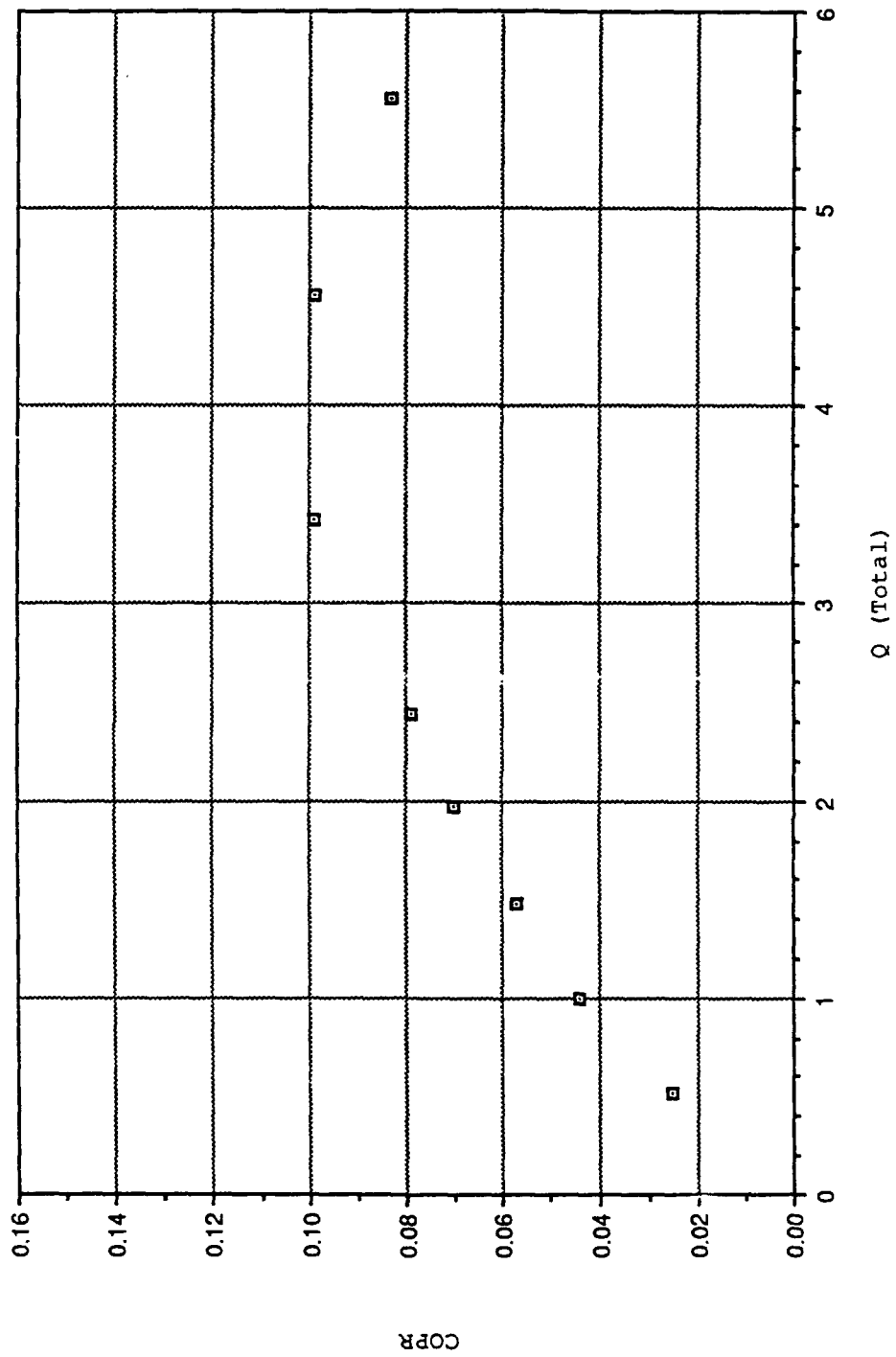


Figure VI-14. COPR at Full Power

number two was used. Several possible problems that may have existed will be explored in chapter seven.

E. FAILSAFE PROTECTION

To allow STAR to be run for long periods of time unattended, an automated shut-down system was designed based on three failure scenarios. First, was the possibility of a sudden loss of power. In this case it was desirable that STAR be prevented from trying to start up again when power was restored. The second case was that of a sudden loss of vacuum in the thermal vacuum cannister, in which case the diffusion pump should automatically shut itself off and not be allowed to restart unless the pressure in the cannister dropped below a specified level. Additionally, the diffusion pump should stay off after a power black out. The third possibility was driver failure. In this case it was desirable to try and detect a failure early on and shut down the experiment before irreparable damage was done to the driver, without the ability to automatically restart.

The first failure scenario was addressed with a simple relay circuit to control the 120 volt supply line to the power amplifier. Figure VI-15 shows how a double pole single throw mechanical relay was wired so that a momentary contact switch would energize the relay. Once energized, the first relay contact would continue to supply the relay coil with current while the second contact would supply

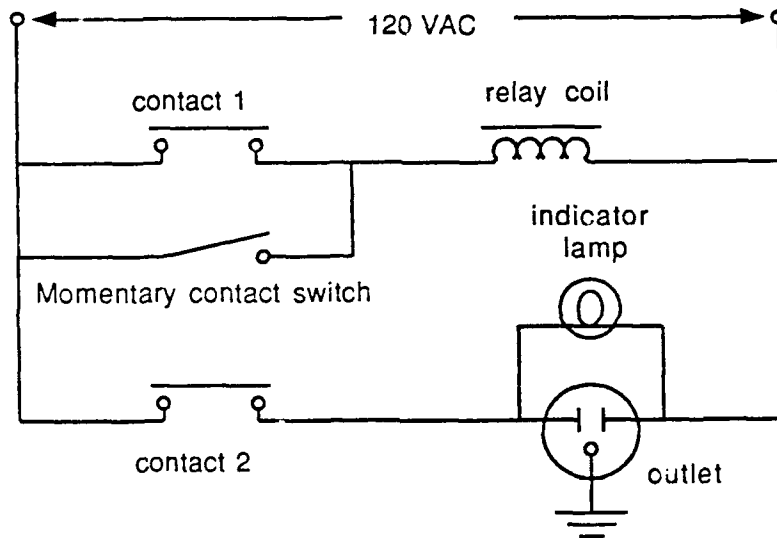


Figure VI-15. Amplifier Relay Circuit

power to an accessory outlet for the power amplifier. If power to the relay were suddenly lost, as with a power black out, the relay would shut off and not be able to re-energize unless the momentary contact switch was manually closed by the experiment's operator. Thus, the refrigerator driver would remain silenced to prevent damage to the voice coil.

The second failure scenario was dealt with in a manner similar to the first. The Granville-Philips ionization gauge controller used to monitor the pressure in the vacuum canister has a single pole double throw relay contact for each of the two thermocouple gages. Each relay has a continuously variable set point adjustable from a vacuum level of 10^{-3} Torr up to 0.2 Torr. The diffusion pump is specified as having a 360 watt heater element, and while the contacts on the two relays are rated at four amperes at 115 volts AC, it was decided to use a separate high capacity mechanical relay to supply the actual current to the diffusion pump heater to insure safety.

The simplest circuit, ignoring safety problems, would have been to simply allow a thermocouple relay to energize the diffusion pump relay once the mechanical roughing pump had dropped the pressure to below a specified level, and then turn it off if the pressure rose above the same level. This, however, would not be practical because the mechanical pump requires a lengthy amount of time to drop the pressure below 35 microns of Hg. And, while the diffusion pump may

be turned on at a pressure level as high as 50 to 100 microns of Hg, it must be cycled two to three times to allow the oil to outgas properly. To further complicate the issue, the auto shut off point should be kept below ten microns of Hg so that the oil in the diffusion pump has an opportunity to cool off before the pressure increases enough to cause the oil to oxidize and create a mess. All of this means that the current supply setup for the diffusion pump must have a manual override switch to energize the relay, but that the thermocouple relay be able to take over control of the diffusion pump once the pressure has dropped below the specified level. This eliminates the need for the experiment operator to remember to disable the override switch and makes for an essentially idiot proof system.

The circuit used to power the diffusion pump is shown in Figure VI-16. A second mechanical relay is used to control the power to the first relay, which actually switches the current to the pump heater element. The power box is enabled by first energizing relay number two with momentary contact switch number two. To turn on the diffusion pump, momentary contact switch number one is used to energize relay one. Once the pressure in the vacuum cannister has dropped below the set point of ten microns of Hg, thermocouple switch number one automatically transfers the current supply for relay number one directly to the 120 volt

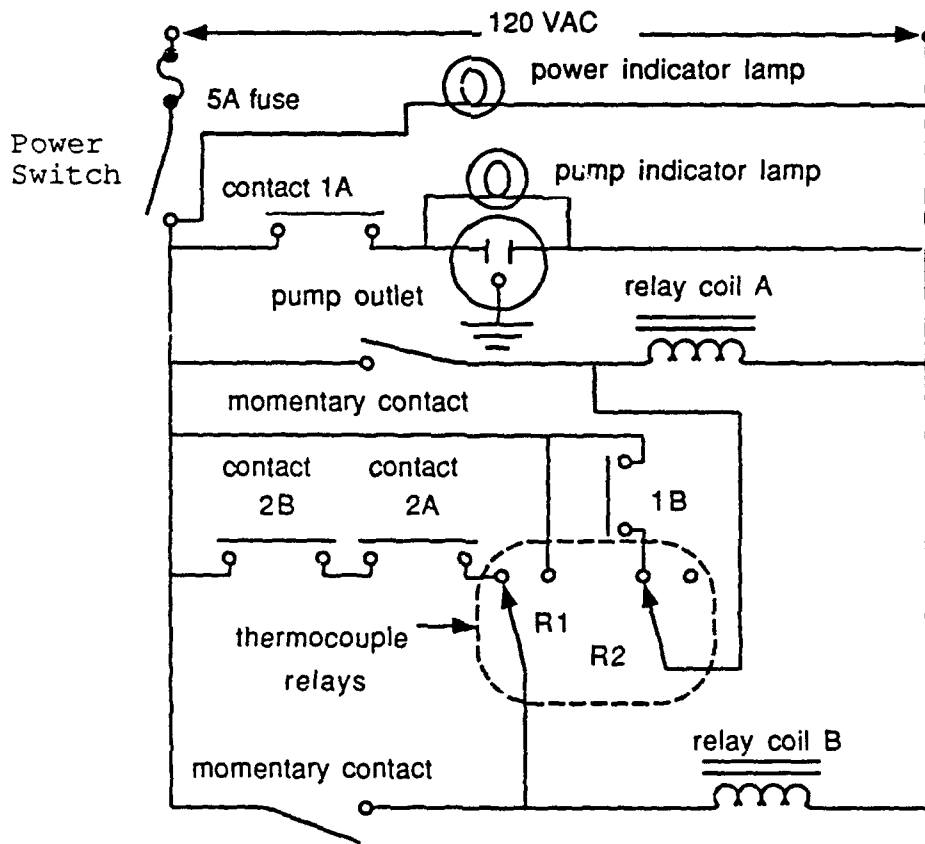


Figure VI-16. Diffusion Pump Relay Circuit

AC line, and thermocouple switch number two automatically de-energizes relay number two.

If the pressure should rise above the set point, thermocouple switch number one would transfer the current supply for relay number one back under the control of relay number two which is now de-energized. The diffusion pump will remain off and only come back on if the operator turns it on, or if the pressure in the vacuum canister drops below ten microns of Hg. Additionally, the operator has the option of turning the diffusion pump on or off at will, regardless of the state of the thermocouple relay switches.

The third failure scenario requires a much more subtle approach. The driver must be monitored to detect the possibility of a failure before it actually occurs. The two best indicators are the amount of current passing through the voice coil, and the displacement of the reducer cone/bellows. Once the refrigerator has reached a state of equilibrium, the two parameters just mentioned should remain fairly constant. For example, when STAR is running properly and operating at an acoustic pressure to ambient pressure ratio of three percent with no applied heat load, the current drawn through the voice coil does not exceed 1.25 amperes and its displacement does not exceed 0.009 inches RMS. These are actually the harshest conditions under which the driver will operate.

The philosophy behind this failsafe protection is to use an electrical circuit to monitor the previously mentioned parameters, compare them to a safe limit, and then shut down the experiment if the limit is exceeded. Such a circuit was designed and is shown in Figure VI-17. When an unsafe condition is reached, the comparison section of the circuit grounds the input of a timer IC whose output latches from ground to five volts long enough to close the contacts of a Triac. The Triac shorts the driver voice coil leads together causing the power amplifier to blow out a protection fuse. This permanently disconnects the power amplifier from the driver.

Both peak current and RMS current are important parameters. It is easy to see that an excessive amount of RMS current through the coil would severely damage it if not burn it out entirely. But spikes in the current wave form, while not necessarily showing up on the RMS current level, and while not damaging to the voice coil individually, could have a cumulative effect of damaging the voice coil by slowly heating it up. Since the RMS current is directly related to the peak current when no spikes are present, a peak sensing circuit may be used to monitor both the RMS current and any transient current anomalies.

The current level is monitored by measuring the voltage drop across a 0.1 ohm resistor which is in series with the driver voice coil. This sinusoidal waveform "signal" may

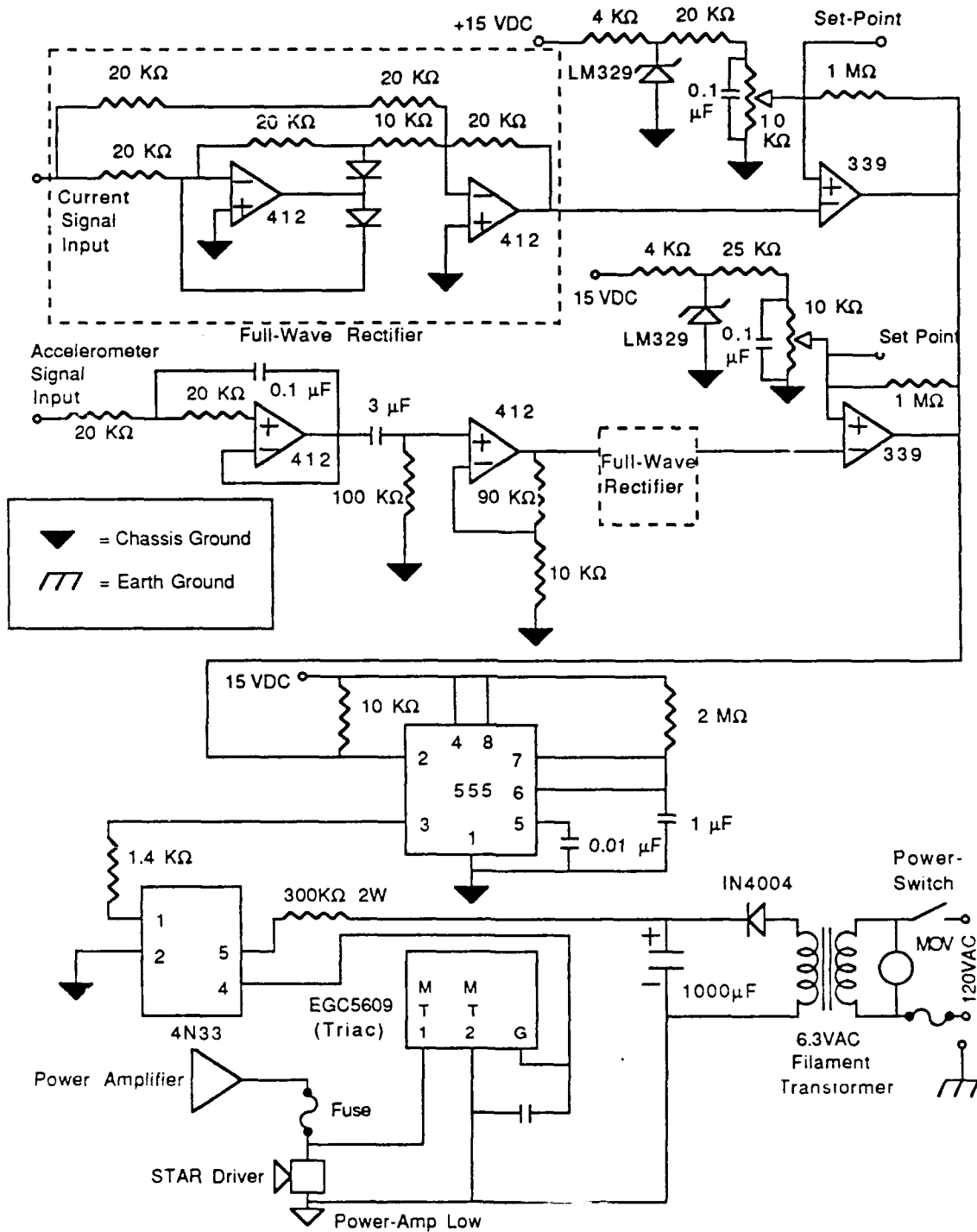


Figure VI-17. Failsafe Protection Circuit

actually be taken off of the power measurement circuit where an INA-110 instrumentation amplifier buffers and amplifies it by a factor of ten. In order to use a voltage comparator to compare the amplitude of this waveform to a specified safety limit, the signal is full wave rectified. This rectified signal is then sent to a comparator for comparison to a DC set point voltage. Since the amplitude of the waveform from the INA-110 scales as one volt equal to one ampere, the set point voltage is simply adjusted to the maximum peak current level that would be acceptable. When the actual peak current exceeds the desired limit, the comparator changes state and the voltage at its output terminal drops from 15 volts DC to ground. For example, if the RMS current is not to exceed 1.3 amperes, the set point voltage is adjusted to $(2^{1/2}) \times (1.3) = 1.84$ volts DC.

The displacement monitoring circuit uses the signal from the accelerometer which is mounted to the back side of the reducer cone. For a sinusoidal waveform, displacement can be calculated from a double integration of the acceleration or by the relation

$$X = a/\omega^2 \quad (\text{VI-1})$$

where X is the displacement, ω is the angular frequency, and a is the acceleration. This sort of signal processing can be done by passing the accelerometer signal through a second order low pass filter with an attenuation rate of 12 dB per octave (a voltage transfer function proportional to $1/f^2$).

A second-order filter equivalent to two first-order Butterworth filters cascaded together with a -6dB point of 80 Hz is used as shown in the schematic. If the knee of the filter is too low in frequency, the accelerometer signal will be attenuated too much to be relied upon accurately. On the other hand, if the knee of the filter is too high in frequency, the attenuation rate in the stop band will not be -12dB per octave at the frequency of interest, which ranges from 370 Hz to 420 Hz.

As an example of all this processing, a preliminary full power run of STAR indicated that at an operating frequency of 377 Hz, the equilibrium displacement was about 0.0082 inches (0.21mm) RMS. Choosing a maximum allowable displacement of 0.009 inches RMS (0.23 mm RMS), and working backwards from the voltage calibration of the accelerometer, the expected voltage output amplitude would be

$$V_a = (80 \times 10^{-6} \text{ volts sec}^2/\text{meter})\omega^2 X \quad (\text{VI-2})$$

where V is in volts and X has been converted to meters. This gives $V=0.103$ volts RMS at 377 Hz. The signal is amplified by a factor of ten before reaching the failsafe circuit, and is then passed through the second order low-pass filter with the voltage transfer function

$$V_{out} = V_{in} (80/f)^2. \quad (\text{VI-3})$$

Taking $V_{in}=(0.103 \times 10)$ and $f=377$ Hz gives $V_{out}=46.4$ mV.

The signal is then AC coupled to remove any DC offset and amplified by a another factor of ten giving $V_{out}=464$ mV.

The accelerometer signal is full wave rectified before it gets to the voltage comparator. Since the comparator will be set change state at a peak level, the accelerometer RMS value is converted to peak voltage;

$$V_{out} = (2)^{1/2} (464 \text{ mV}) = 656 \text{ mV.} \quad (\text{VI-4})$$

When the accelerometer peak level is in excess of 656 mV the voltage comparator's output will drop from 15 volts DC to ground.

To check these calculations we can pick a different frequency such as 350 Hz, from which we obtain

$$V_a = (80 \times 10^{-6} \text{ V sec}^2/\text{m}) (2\pi)^2 (350)^2 (0.000229) \quad (\text{VI-5})$$

or $V_a=88.6 \text{ mV}$. This arrives at the circuit amplified by ten to give 886 mV and is then double integrated by the filter and amplified again by ten to give

$$V_{out} = (0.886) (80/350)^2 \quad (\text{VI-6})$$

or $V_{out}=463 \text{ mV}$. This agrees with the previous voltage to within 0.2 percent.

The outputs of the two comparators are tied together in an "or" configuration to the input of a timer (LM555) such that either comparator can pull the timer input to ground and cause it to trigger. The timer has an adjustable reset delay that is determined by a capacitor and resistor. A reset of half a second was chosen so that the timer output would remain high for at least half a second regardless of the timer input.

The timer output is connected through an opto-isolator (GE 4N23) to the gate of a Triac (ECG 5609). When the Triac gate sees 5 volts it causes pins MT1 and MT2 to be conducting, which shorts the voice coil of the driver and causes the power amplifier to blow out a 1.25 Ampere "slow-blow" type protection fuse. Now, regardless of what may happen, the power amplifier is disconnected from the driver and the experiment is terminated.

The opto-isolator is used to electrically isolate the STAR driver power circuit from the failsafe circuit. To maintain this isolation, it was necessary to provide a separate DC supply line to the opto-isolator. A simple six volt DC power source was built using a 6.3 volt filament transformer, a diode (IN4004), and a capacitor. This setup steps down the available 120 volt 60 Hz supply, and then half-wave rectifies and AC filters it to give about nine volts DC.

To allow for easily adjustable set-points, a 6.9 volt reference was taken from an LM329 and split by a potentiometer. The set-point can be adjusted to whatever value suits the experiment being conducted.

The only problem not addressed at this point is that if the driver is disconnected by the crow-bar circuit, the heat load at the cold end (from the resistive strip heater) should be shut off to prevent overheating the resonator. This must be corrected before further tests are run.

VII. CONCLUSIONS AND RECOMMENDATIONS

The objective of this thesis has been to design, build, and test the resonator for the Space Thermoacoustic Refrigerator, and to arrive at a fully operational flight ready unit by integrating all the work that has been done by previous thesis students in thermoacoustic improvements, and driver and electronics design and construction. The rigors of space flight have necessitated several extensive structural modifications to the original thermoacoustic refrigerator which was designed and built by Hofler. These changes will give the device more overall efficiency, and make it stronger in order to withstand the launch aboard the Space Shuttle, the mission itself, and the return to Earth.

The refrigerator has been shortened by allowing the end of the resonator termination to protrude into the stainless steel sphere. In addition, a stainless steel vapor shield of 0.001 inch thickness has been placed beneath the fiberglass reinforced resin layer to keep helium from diffusing out of the refrigerator, without introducing a serious heat leak from the flange to the cold end. By using the classical cryogenic techniques of a knife edge transition between dissimilar construction materials, a very low leak rate on the order of 10^{-8} standard cubic centimeters per second has been achieved. Most importantly,

the resonator has proven capable of operating at full power and at low temperatures without producing a leak. The basic design has been pressure tested to four times the working pressure by NRL and found to be fully capable of withstanding a large overpressurization without failure.

The resonator was not only successfully mated to the STAR driver, but also integrated with the Resonance Control Board to provide a refrigerator capable of operating autonomously without the need for an operator to keep it on resonance or at the proper acoustic pressure amplitude.

Although there were no expectations of surpassing the performance levels achieved by Susalla and Hofler with the prototype thermoacoustic refrigerator, and although a COPR of 0.14 at medium-power was encouraging, a value of 0.10 at full-power should have been about 30 percent higher. The disappointing results for full-power are likely attributable to defects in the trumpet/sphere assembly in the form of a small dent in the sphere. This dent was, unfortunately, exactly at the point where the trumpet has its closest approach to the sphere. This defect could possibly have created turbulence which would have heated the working gas enough to down-grade the operation of the refrigerator.

Another possible cause that must be investigated is the fit of the thermoacoustic stack and thermal sleeve within the resonator. If the fit were loose, the cooling efficiency might be reduced because the high gas velocities

would cause these parts to vibrate. Additionally, the gas may be driven acoustically in and out of small gaps created by the loose fitting thermal sleeve which could cause acoustic losses and heating.

The refrigerator has been operated continuously at full-power now for periods of up to one week, without incident. Under these circumstances, the only service performed by the experimental investigator has been to change the heat load. Otherwise, the device is fully capable of running itself unattended. One can only conclude that the design, construction, testing, and finally the certification by NASA of the Space Thermoacoustic Refrigerator has been an enormous success and a valuable education.

APPENDIX A

DATA ACQUISITION PROGRAM

In this section, the data acquisition program is reproduced verbatim. No explanations will be given for the commands save that the program is written in HP BASIC for use with the HP 9836 computer which is interfaced, via the HP-IB, with the HP 3457A programmable multimeter. This multimeter has one front panel input and eight rear panel input channels. The Program, in addition to commanding the multimeter to take the required data at the desired intervals, also converts the thermocouple voltages to degrees centigrade temperature; converts the power measurement circuit outputs to watts and amperes; converts the pressure transducer output voltage to a PSI reading; and converts the microphone and accelerometer to RMS voltage.

```
2 PRINT DAT$(TIMEDATE)
10 PRINT "TIME", "Tc"; "    "; "Th"; "    "; "POWER(W)", "CURR(A)",
"PRESS (PSI)", "MIC (VRMS)", "ACCL (VRMS)", "FREQ"
20 OUTPUT 722; "RESET"
30 OUTPUT 722; "NDIG 4"
40 OUTPUT 722; "NPLC 10"
50 OUTPUT 722; "CHAN 2"
60 OUTPUT 722; A
```

```
70 OUTPUT 722;"CHAN 3"  
80 OUTPUT 722;B  
90 OUTPUT 722;"CHAN 0"  
100 ENTER 722;C  
110 OUTPUT 722;"CHAN 1"  
120 ENTER 722;D  
130 OUTPUT 722;"CHAN 4"  
140 ENTER 722;E  
150 OUTPUT 722;"CHAN 5"  
160 ENTER 722;F  
170 OUTPUT 722;"CHAN 6"  
180 ENTER 722;G  
190 OUTPUT 722;"CHAN 7"  
192 OUTPUT 722;"FREQ AUTO"  
193 OUTPUT 722;"ACBAND 300"  
194 ENTER 722;H  
195 OUTPUT 722;"TERM FRONT"  
196 OUTPUT 722;"OHM"  
197 OUTPUT 722;"ARANGE OFF"  
198 OUTPUT 722;"MATH CTHRM"  
199 ENTER 722;N  
200 A=A*10  
210 I=A*3.25536E-4+7.57757E-4  
220 I=I*A+1.81301E-2  
230 I=I*A+2.687857E-1  
240 I=I*A+1.705659E+1
```

```
250 I=I*A+1.380078E-2
251 P=N*1.652E-12+2.351E-10
252 P=P*N+9.625E-8
253 P=P*N+5.178E-5
254 P=P*N+0.0586
255 P=P*N+5.664E-4
260 B=B*1000
261 B=B+P
270 J=B*3.25536E-4+7.57757E-4
280 J=J*B+1.81301E-2
290 J=J*B-2.687857E-1
300 J=J*B+1.705659E+1
310 J=J*B+1.380078E-2
320 K=G/10
330 L=F/4.2
340 M=E*1000-6.3022
350 M=M/1.621
360 C=C*10
400 PRINT
400 PRINT TIME$(TIMEDATE);DROUND(I,4);DROUND(J,4);DROUND
(C,4);DROUND(D,4);DROUND(M,4),DROUND(L,4),DROUND(K,4),
DROUND(H,3)
410 WAIT 60
420 GOTO 20
430 END
```

APPENDIX B

POWER MEASUREMENT CIRCUIT

An electrical circuit was designed and built to monitor the electrical power and current being delivered to the STAR driver. This data is useful for monitoring the status of the driver and for calculating the electroacoustic efficiency of the driver/resonator system. This circuit also provides the emergency shut down crowbar circuit with the necessary driver current data. A schematic of the circuit is shown in Figure B-1. It is housed in the same cabinet with the failsafe protection circuit (Chapter VI-E).

The current being delivered to the driver voice coil is easily measured by inserting a "current sensing" resistor of known value in series with the voice coil and power amplifier and measuring the voltage drop across it. The current through the resistor, and thus the voice coil, is simply the voltage drop divided by the value of the resistor. Because AC sinusoidal wave forms are employed, it is assumed that all voltages and currents are RMS unless otherwise stated.

A resistor value of 0.1 ohms was chosen to minimize the amount of power wasted. Since it was anticipated that the driver would have about 1 to 1.5 amperes of current passed through it at full power, a 0.1 ohm resistor would only

dissipate 100 to 225 milliwatts of electrical power. Unfortunately, a resistor value this small would also have a small voltage drop of about 100 to 150 millivolts across it at full power, and much less at lower power levels. The voltage drop is therefore amplified by a factor of ten by a high accuracy instrumentation amplifier (INA-110). This factor of ten cancels the one tenth of an ohm in the equation

$$V = I * R \quad (B-1)$$

such that the scaling factor between the resistor voltage drop and the current is exactly one. The RMS value of the sinusoidal waveform is measured by a true RMS to DC converter integrated circuit (AD536) which returns a DC voltage equivalent to the RMS level of the waveform.

The average electrical power P_{Average} being delivered to the driver is given simply by the expression

$$P_{\text{Average}} = \overline{V(t) \cdot I(t)} \quad (B-2)$$

where the bar denotes the time average of the quantity. A combination of a four quadrant multiplier and a low pass AC blocking filter is used to multiply the two voltage and current signals and give the average value.

The IC multiplier multiplies two differential voltages and divides by a scale factor of 10 giving $V_{\text{out}} = V_1 V_2 / 10$, where the harmonic time dependance of V is suppressed for convenience. Letting $V_1 = V_{\text{driver}}$ and $V_2 = 10V_{\text{resistor}}$ gives $V_{\text{out}} = V_d(10V_r) / 10$. The low pass filter gives

$V'_{out} = V_{out}/2 = V_d V_r / 2$, and substituting $V_r = I_d R = I_d (0.1)$ gives $V'_{out} = (V_d I_d / 2) / 10$ or $P_{RMS} / 10$. Thus, $P_{RMS} = 10(V'_{out})$. This is useful for measuring low power levels of one watt or less. For higher power levels where the voltage drop across the voice coil exceeds 10 volts RMS, a voltage divider is placed at the input to the multiplier to prevent the circuit from being saturated and returning erroneous data. The voltage divider allows the input of the multiplier to see $V_{driver}/10$ such that the RMS power is now $P_{RMS} = 100(V'_{out})$. Of course, the voltage divider could be left in for low power measurements, but the magnitude of V'_{out} would be on the order of a couple of millivolts which is perilously close to the DC offset of the circuit.

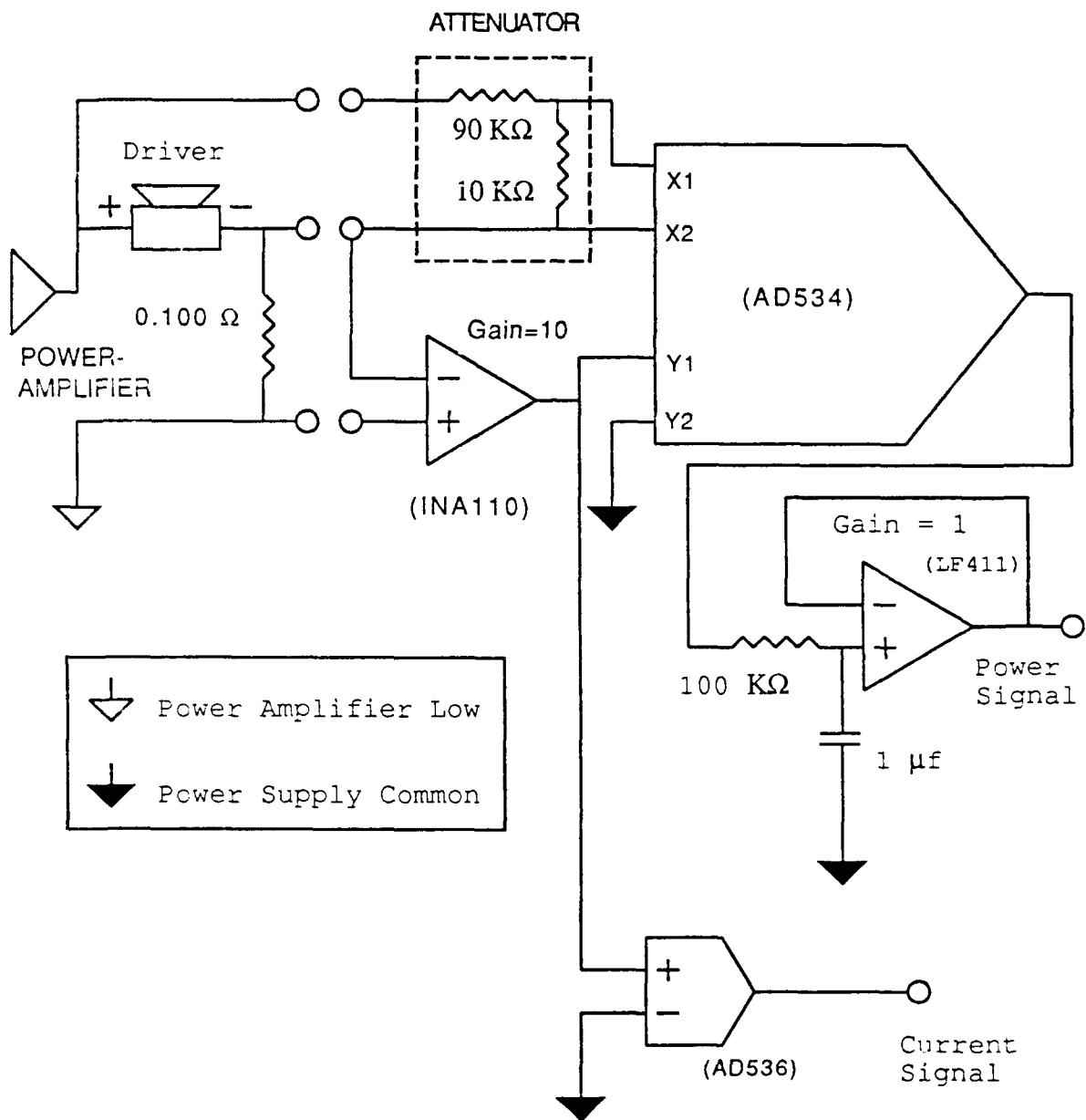


Figure B-1. Power Measurement Circuit

APPENDIX C

THE HOFLEER TUBE FROM HELL

The thermoacoustic effects described in chapter II were focused primarily on those of the heat pump. A very simple example of a prime mover exists, however, which can actually aid in the understanding of how a thermoacoustic refrigerator operates. Tom Hofler built such a device, affectionately known as the Hofler tube, to show his Ph.D. candidacy committee at the University of California, San Diego.

Recalling that the thermoacoustic heat pump becomes a prime mover when a large heat gradient is placed across the thermoacoustic stack: the Hofler tube consists of a quarter-wave length copper "organ pipe" with a series of parallel fiberglass plates located in the middle acting as the thermoacoustic stack and parallel copper strips glued to the edges of these plates to act as hot and cold heat exchangers. It is capable of resonating at a considerable sound intensity level when the stack is exposed to a substantial temperature ratio T_h/T_c greater than 2. This is done by immersing the open end in liquid nitrogen while the closed end is held at room temperature. The resonance is entirely self-exciting and requires no loudspeaker to start it, as just the slightest perturbation is enough to get it

going. Indeed, the only way to stop it is to stuff a towel in its mouth until it warms back up.

The author, along with Mr. Glenn Harrell of the Naval Post Graduate School Space Systems Precision Fabrication Facility, built a second generation Hofler tube employing the same stack and heat exchanger manufacturing methods as used in STAR, albeit with a much shorter stack. Figure C-1 shows a cross sectional view of the Hofler Tube which uses a spirally wound stack 0.550 inches in length and of the same diameter as the STAR stack. The heat exchangers are identical to the STAR units except for their length which is 0.125 inches for both the hot and cold heat exchanger.

The tube is actually divided into three parts. The center section is a stainless steel tube with flanges which houses the stack and has relatively poor thermal-conductivity. The two outer sections are made of copper (having better thermal-conductivity) with copper flanges, and have the heat exchangers soft-soldered into them such that they are flush with the flange surface. The stack is inserted into the center section and the three sections are bolted together with a small amount of heat-sink compound between the mating surfaces of the copper and stainless steel flanges.

A photograph of the completed Hofler Tube is shown in Figure C-2. It is capable of borderline painfully loud sound intensities and is considerably more efficient than

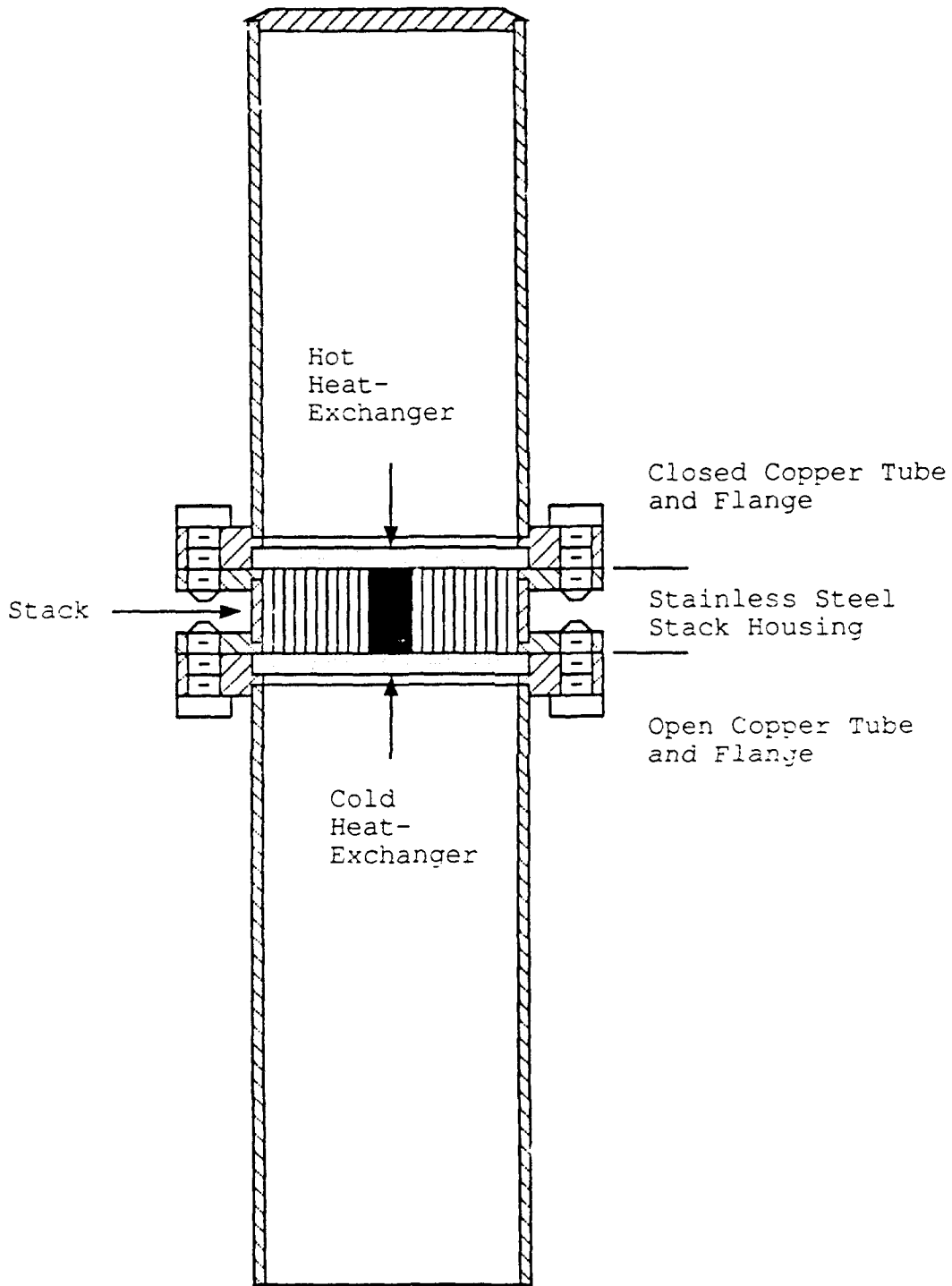


Figure C-1. Hofler Tube Cross Section (not to scale)

the original Hofler tube. The superior properties of helium as a working medium are easily demonstrated by injecting helium into the tube while it is running. As expected, since the velocity of sound in helium is approximately three times as fast as for air, the resonant frequency triples, or increases by about one and one-half octaves. The sound intensity also increases considerably since the radiation efficiency for a simple sound source, where the wave-length is much larger than the diameter of the radiator, increases with frequency.

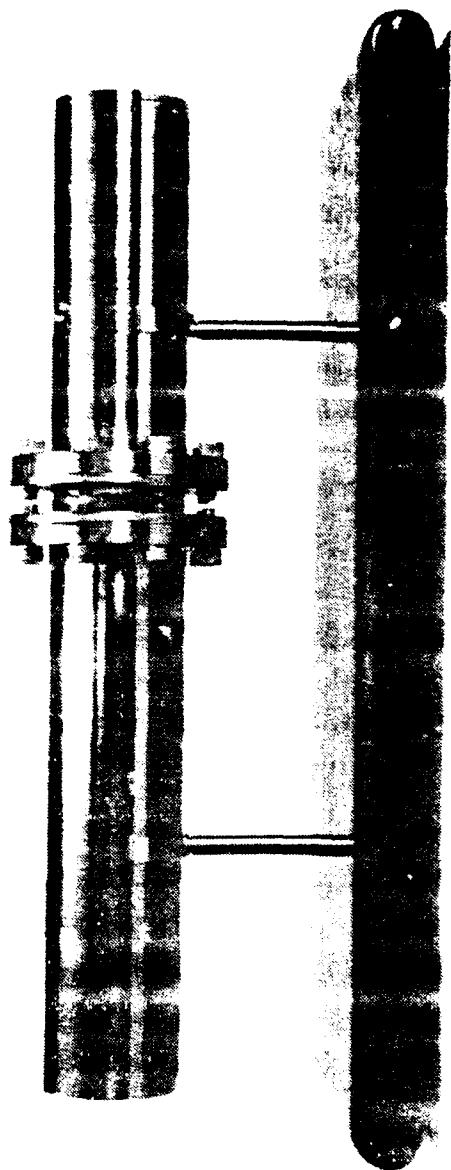


Figure C-2. Photograph of Hofler Tube

APPENDIX D

CONSTRUCTION DRAWINGS

This section contains construction drawings for the resonator, the stainless foil soldering assembly and the thermal vacuum cannister. The first two sets of drawings were done by Professor T.J. Hofler but include the modifications to the resonator reducer which were designed by the author. The third set of drawings are from Harris and Volkert [Ref. 1].

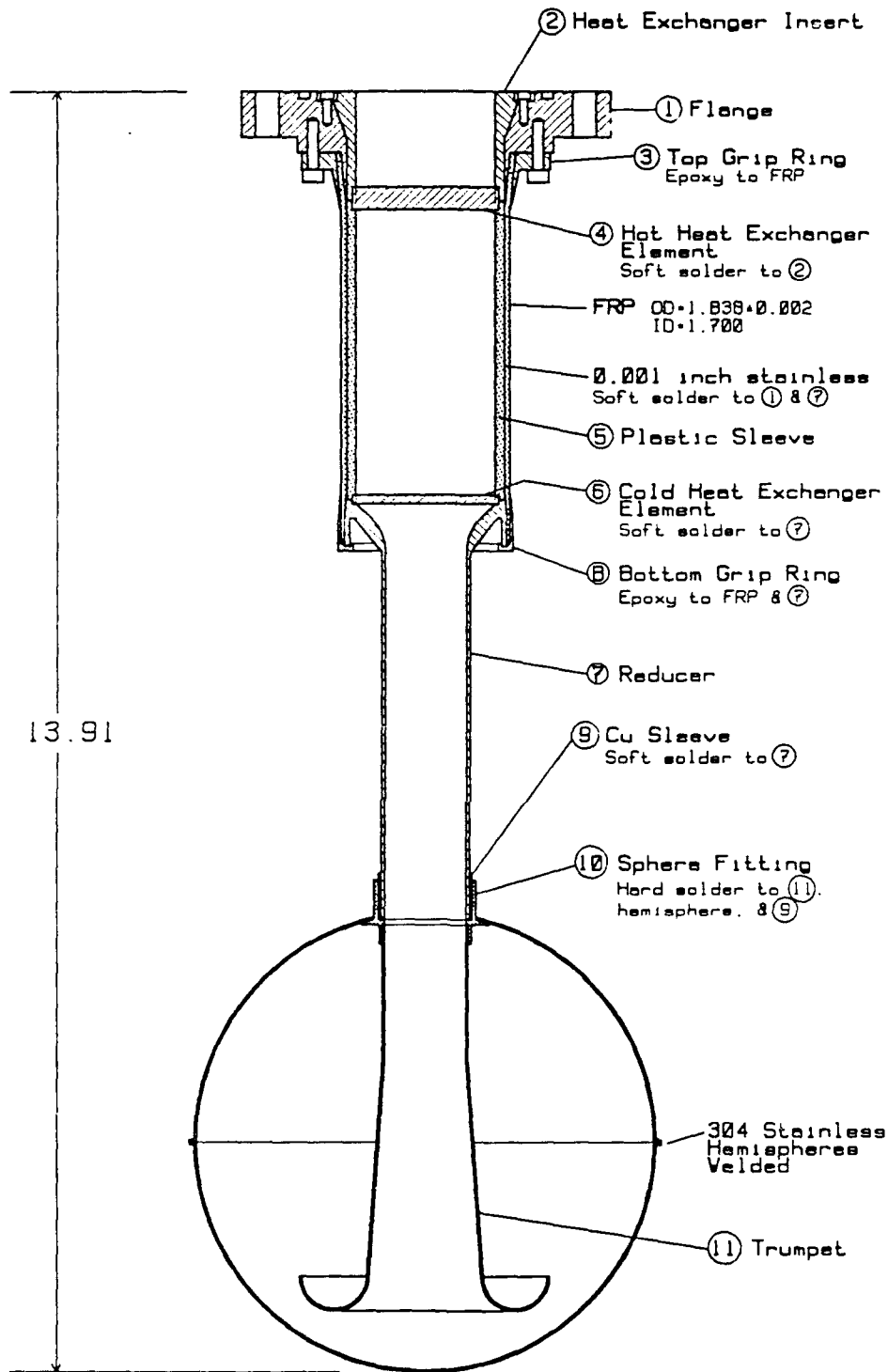


Figure D-1. Resonator Parts Identification Drawing

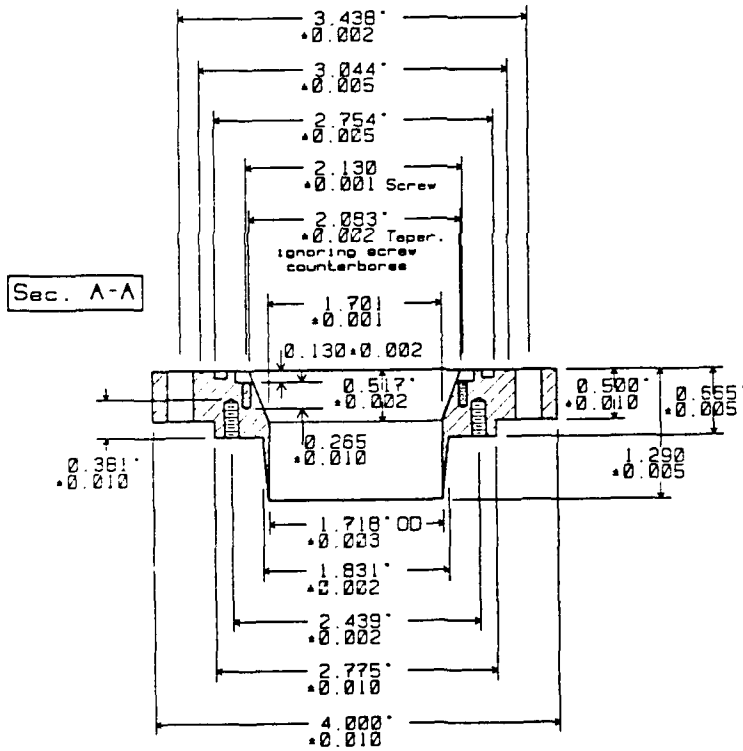
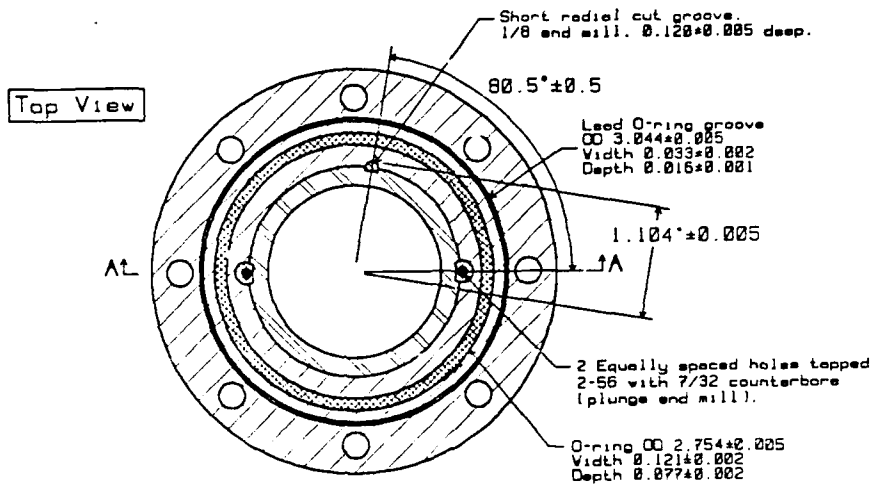


Figure D-2. Resonator Flange

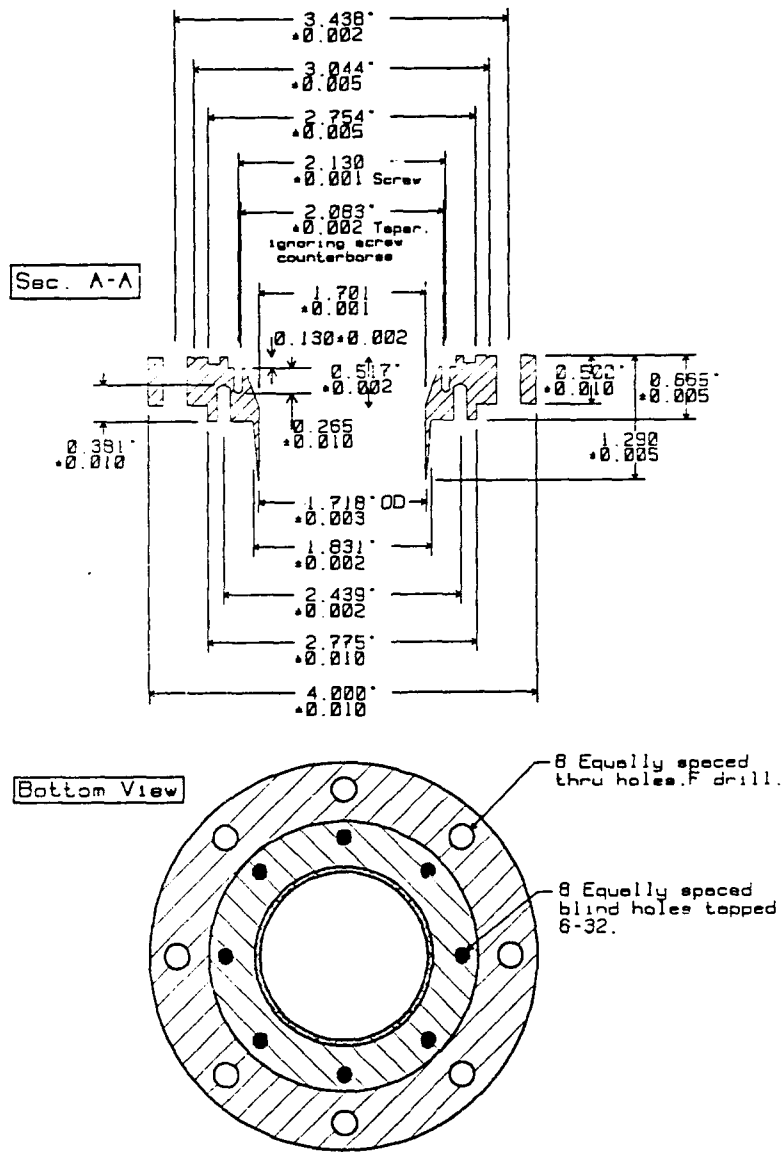


Figure D-3. Resonator Flange

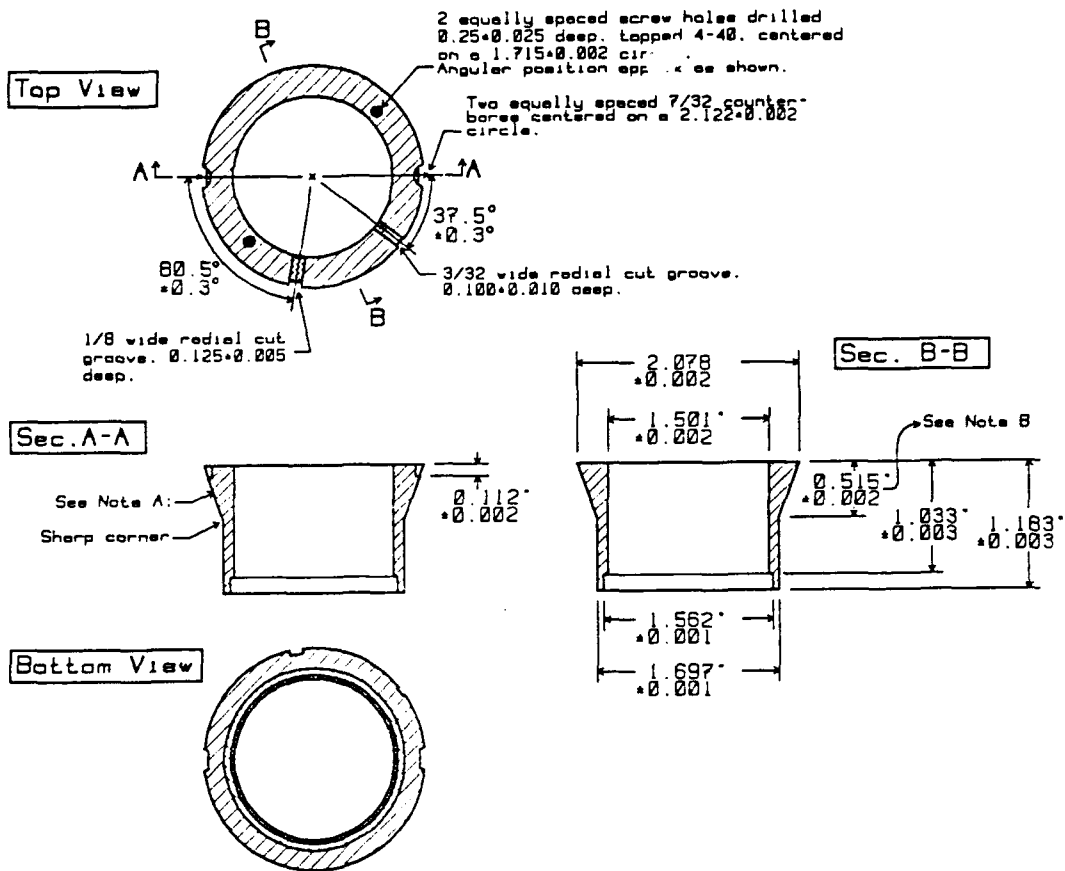


Figure D-4. Hot Heat Exchanger Insert

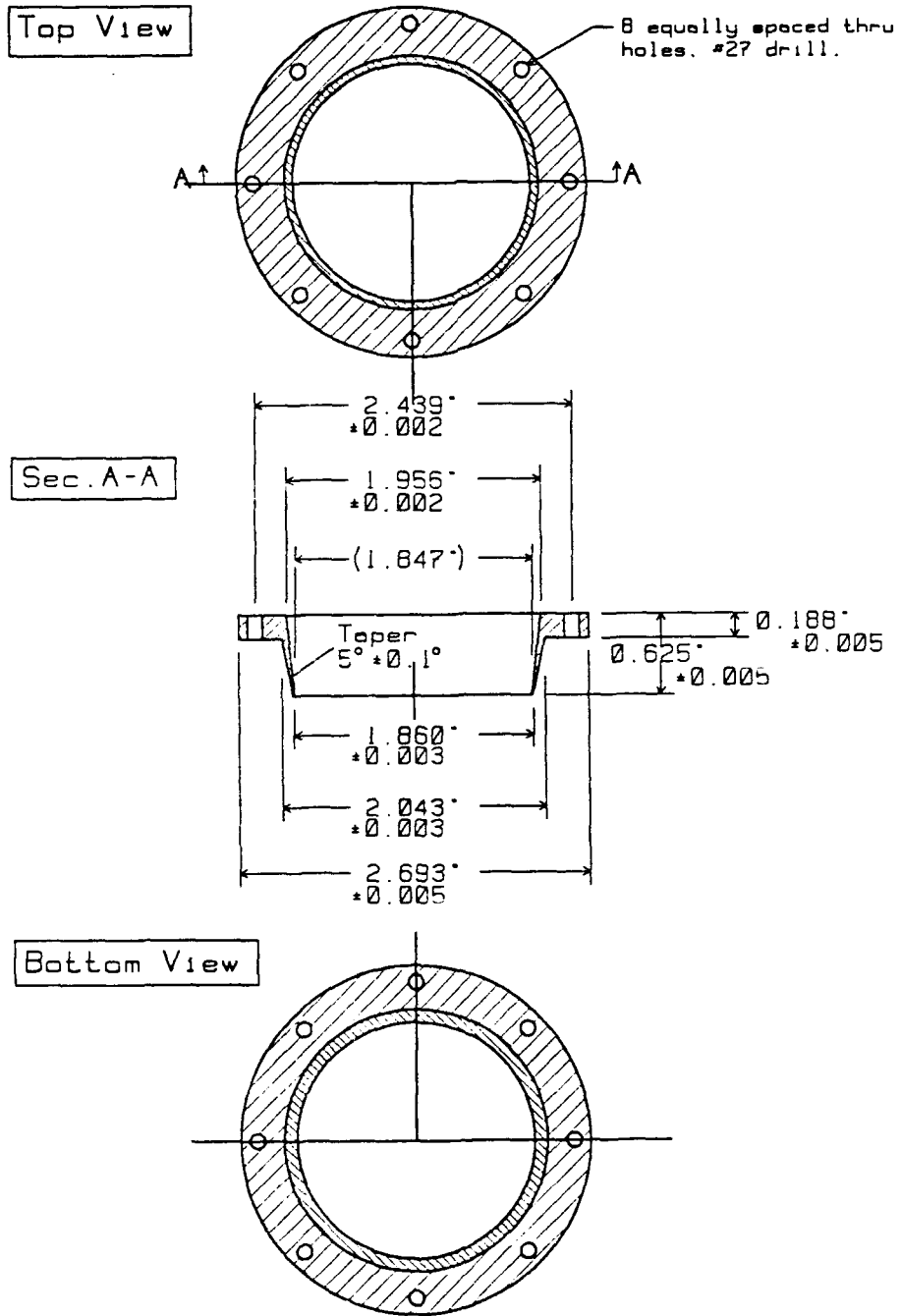


Figure D-5. Top Grip Ring

The Hot Element has a width of 0.250 ± 0.001 as shown & the Cold Element has a width of 0.100 ± 0.001 .

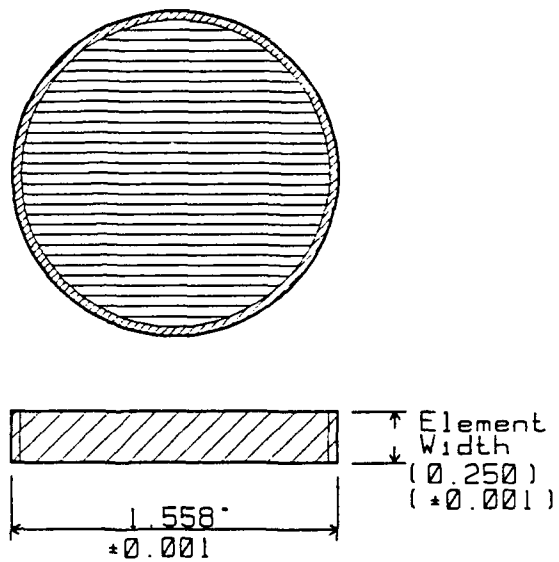
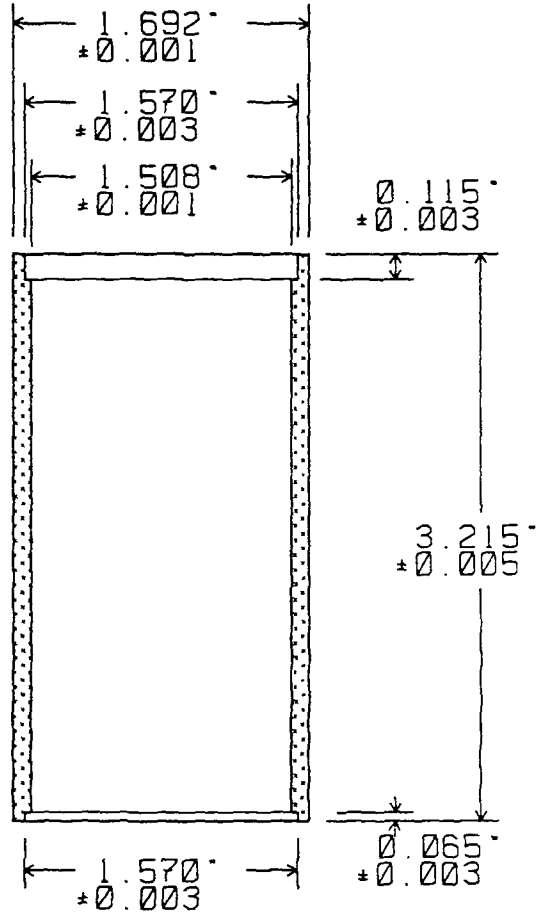


Figure D-6. Heat Exchangers

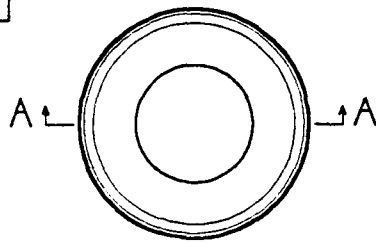
Section



Bottom View

Figure D-7. Phenolic Sleeve

Top View



Sec. A-A

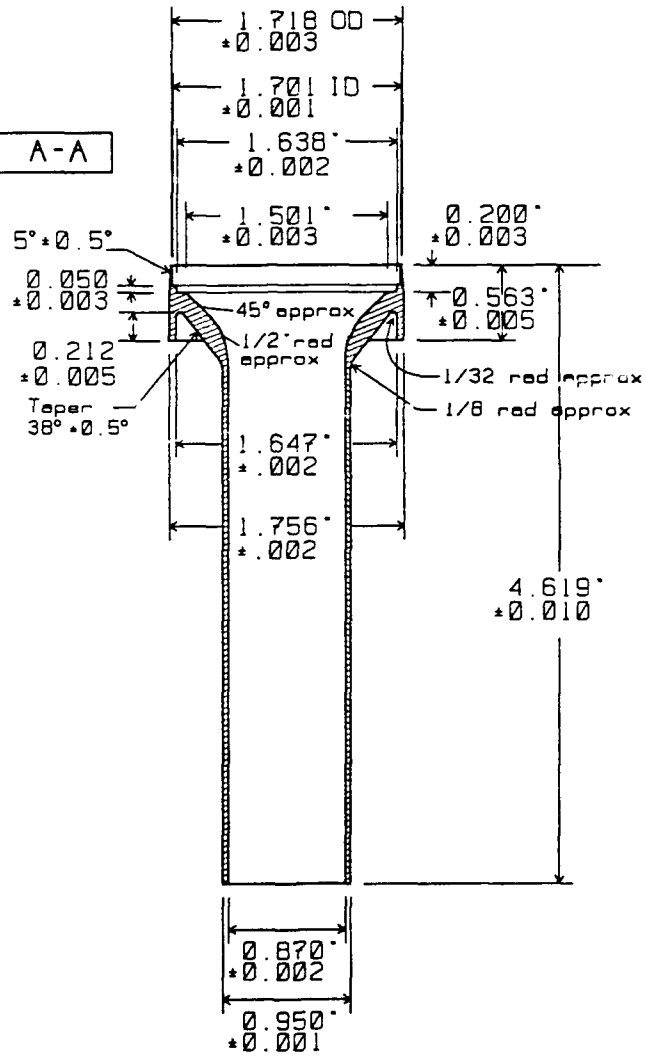
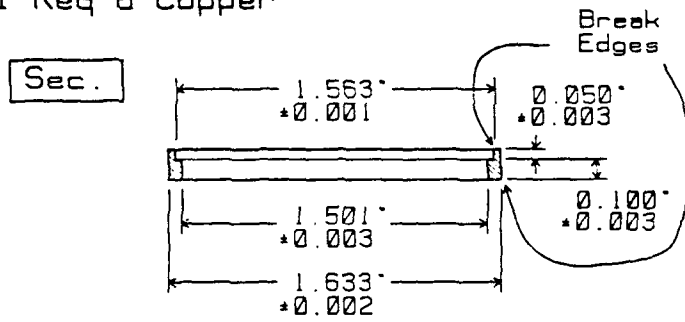


Figure D-8. Reducer

Cold Heat Exchanger Mounting Ring (12)
 1 Req'd Copper



Filler Ring (13)
 1 Req'd Copper

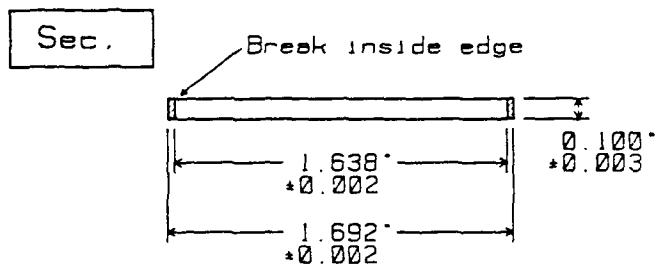
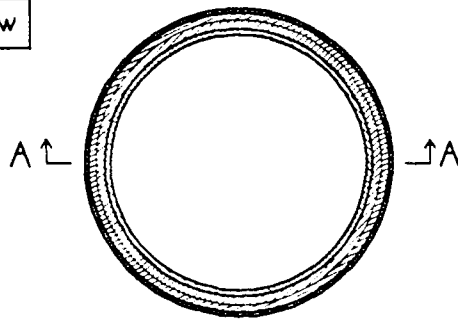
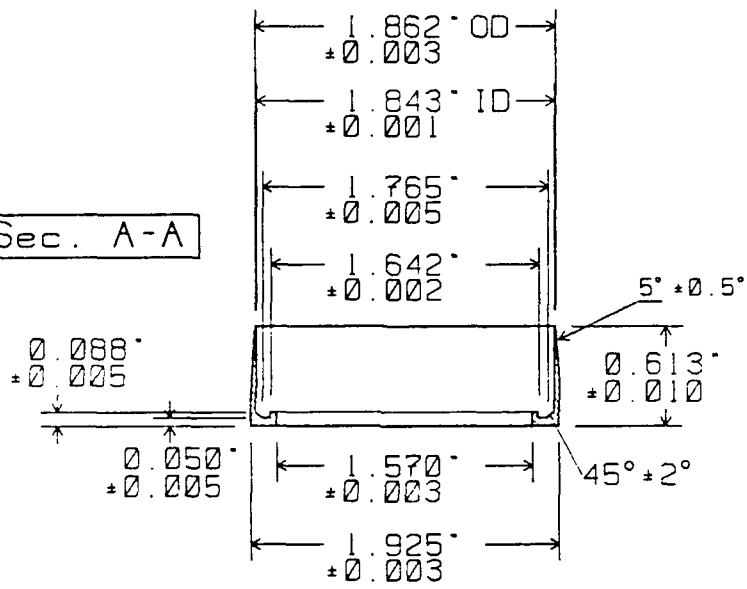


Figure D-9. Cold Heat Exchanger Mounting Ring and Filler

Top View



Sec. A-A



Bottom View

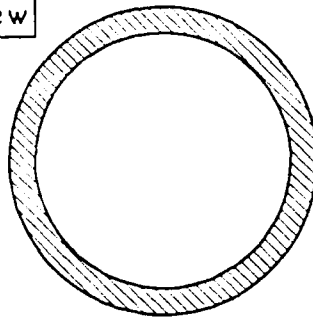


Figure D-10. Bottom Grip Ring

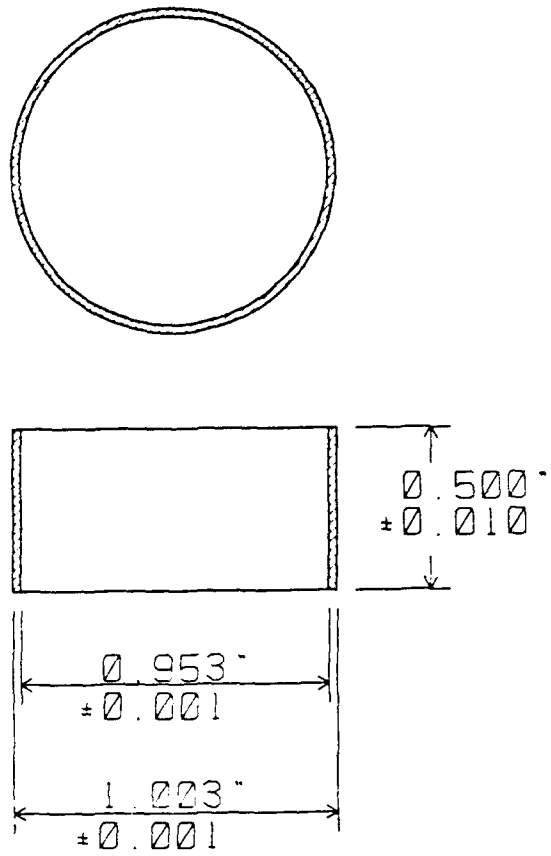
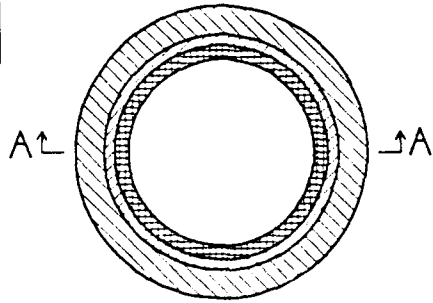
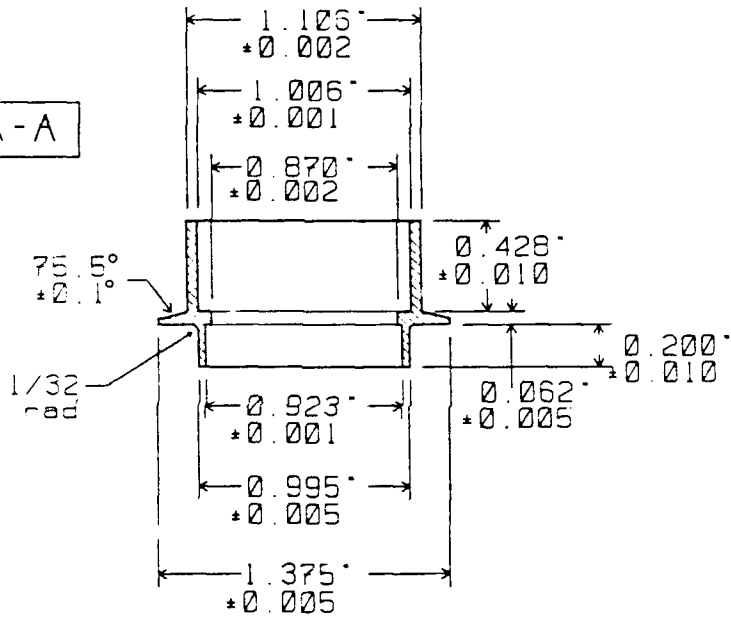


Figure D-11. Copper Sleeve

Top View



Sec. A-A



Bottom View

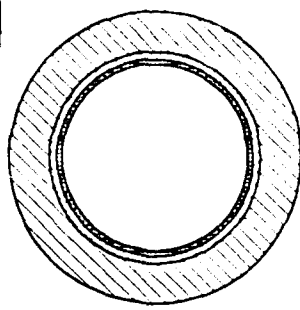


Figure D-12. Sphere Fitting

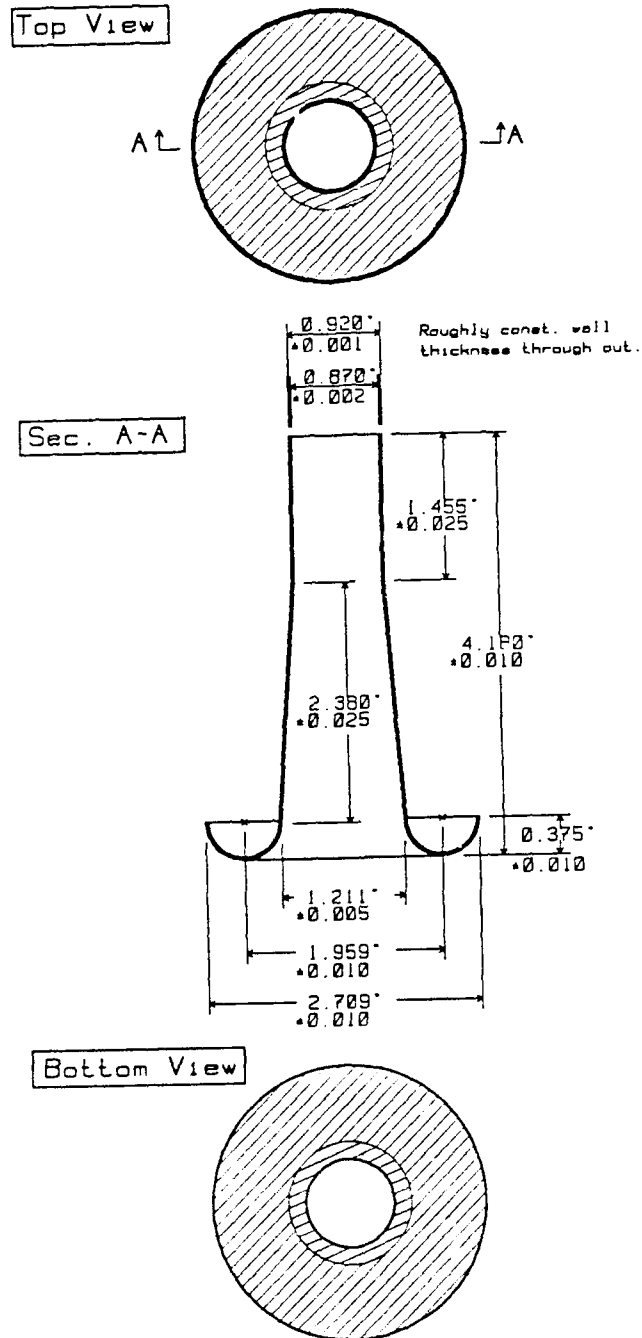
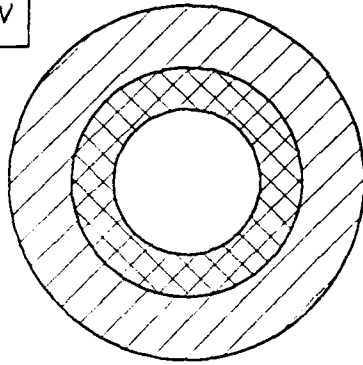


Figure D-13. Trumpet

Top View



Section

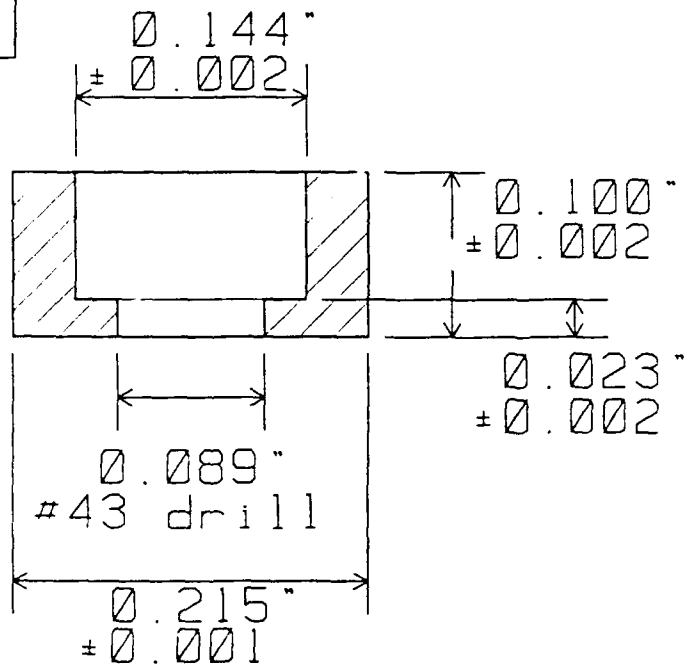


Figure D-14. Screw Head Enlargement

1 Aluminum Base Plate Req'd
 6x11 in. (or 6x15 in. for 2 Corning Hot Plates)

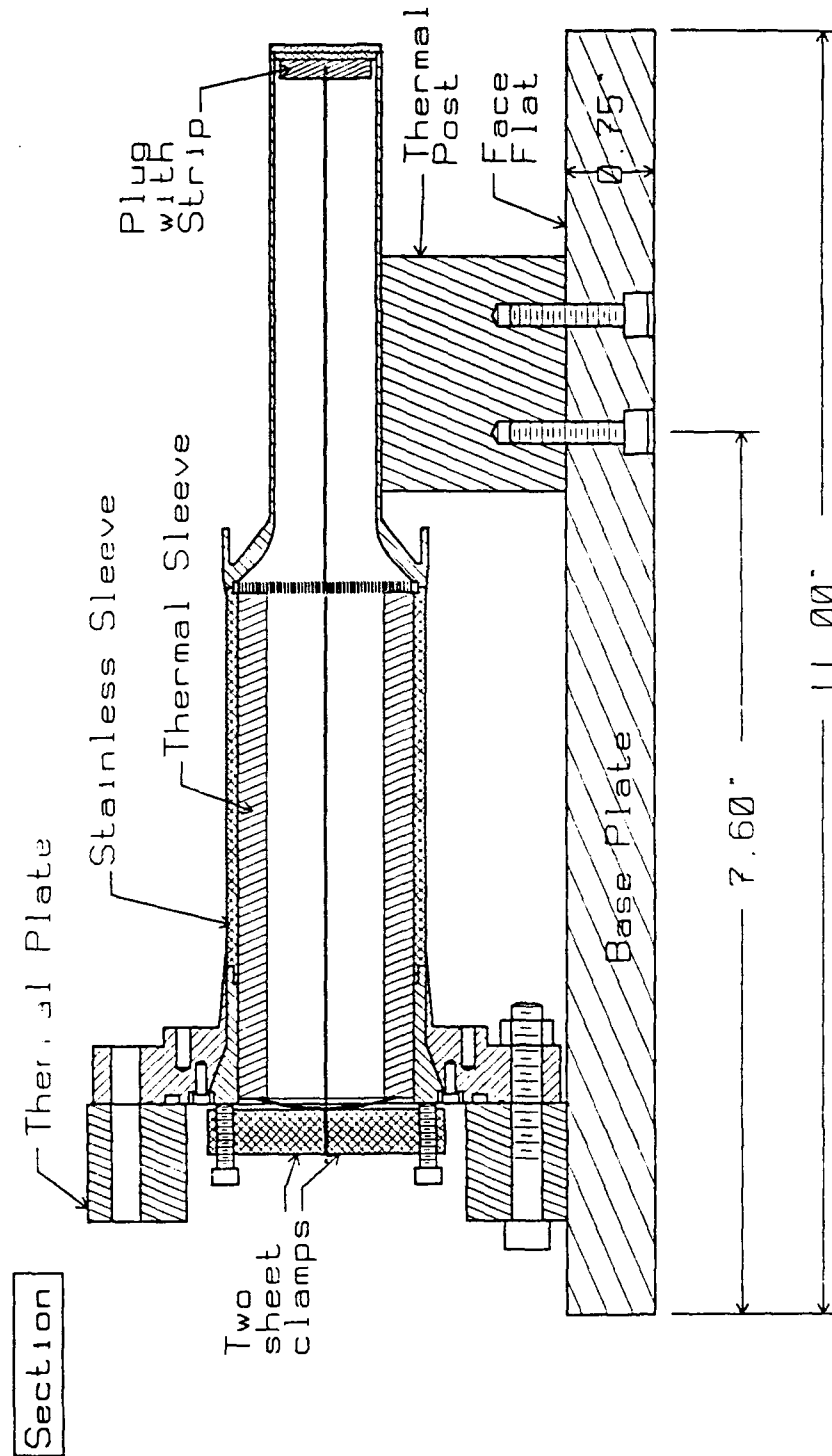


Figure D-15. Stainless Foil Soldering Assembly

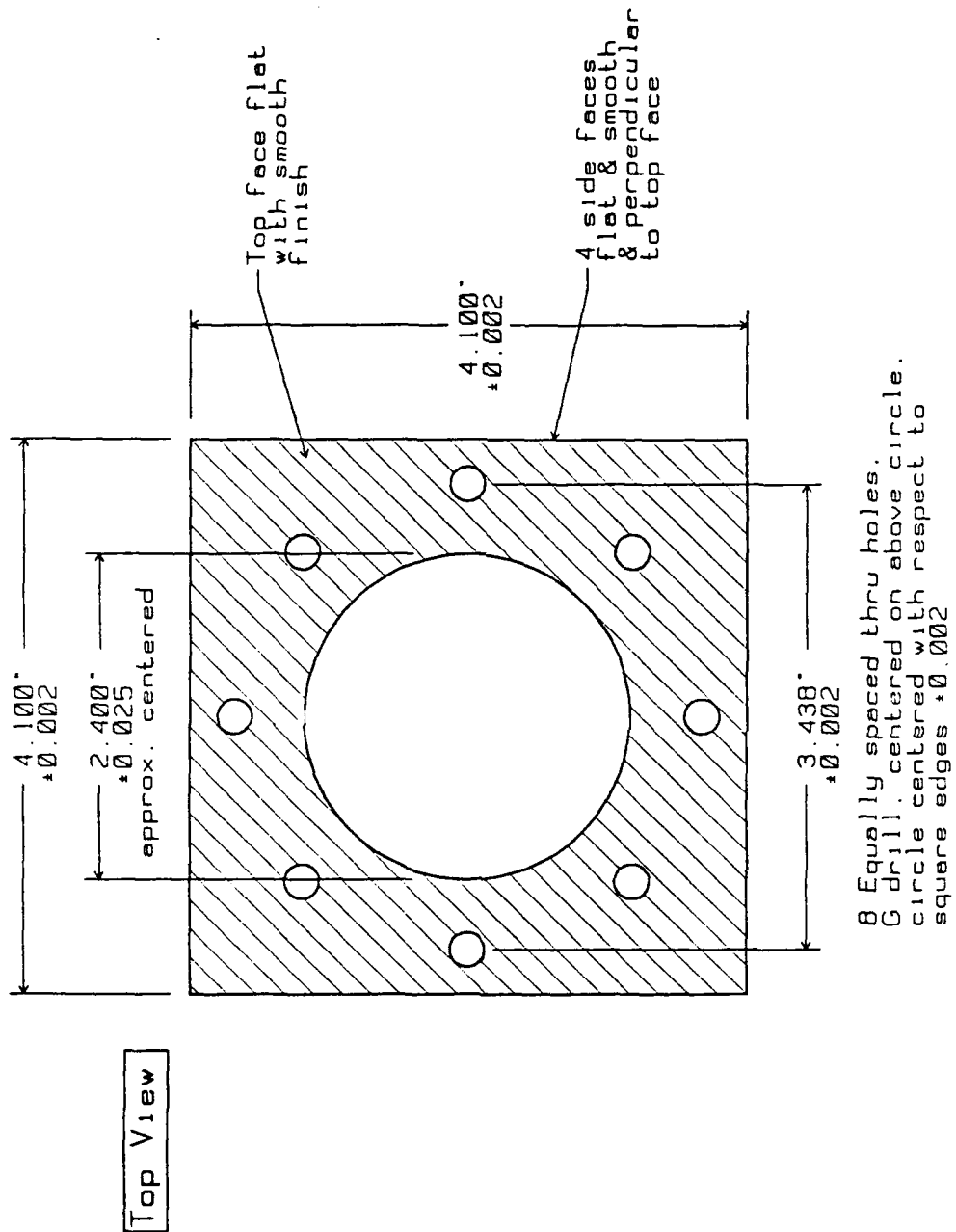


Figure D-16. Thermal Plate

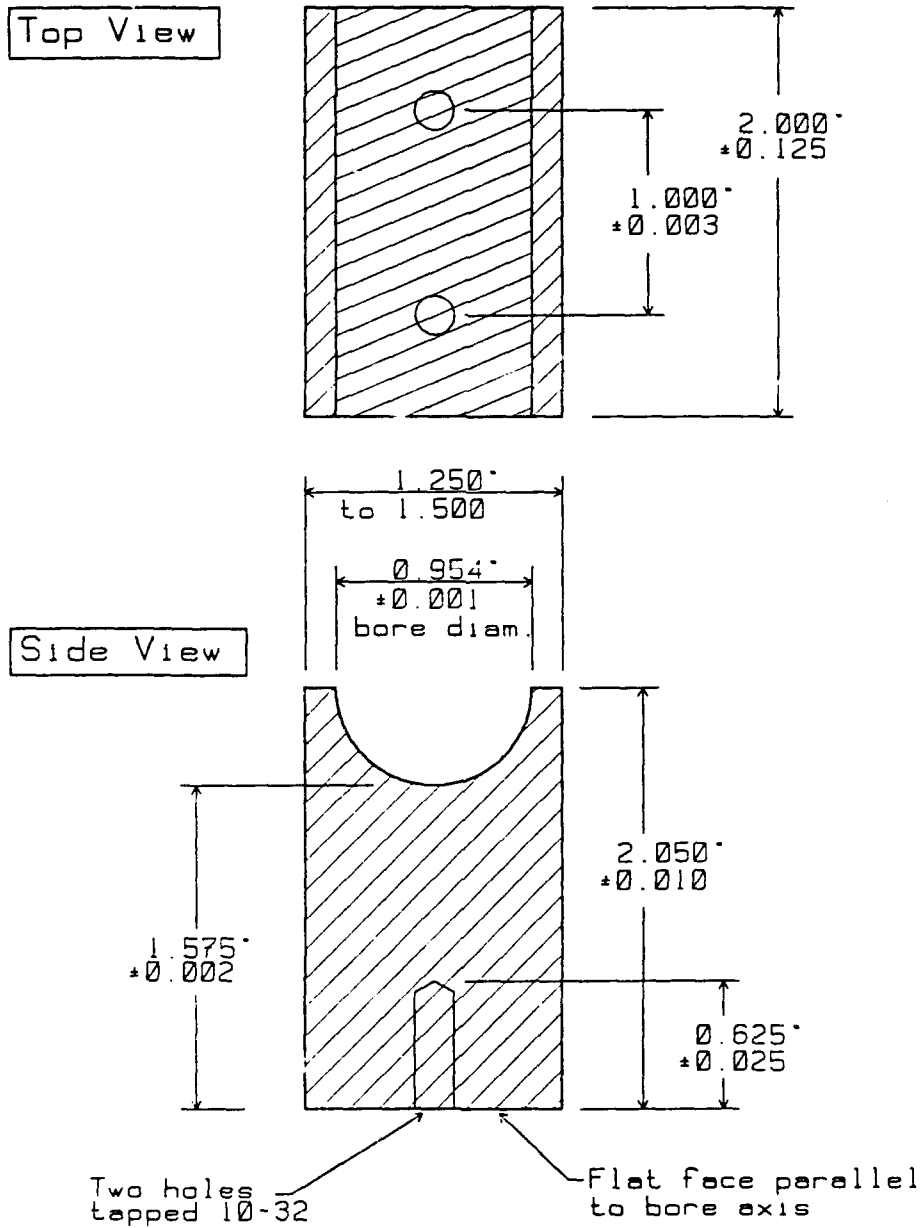


Figure D-17. Thermal Post

2 Req'd Stainless Steel except
 replace the 2 clearance holes
 with 6-32 tapped thru holes on
 part #2.

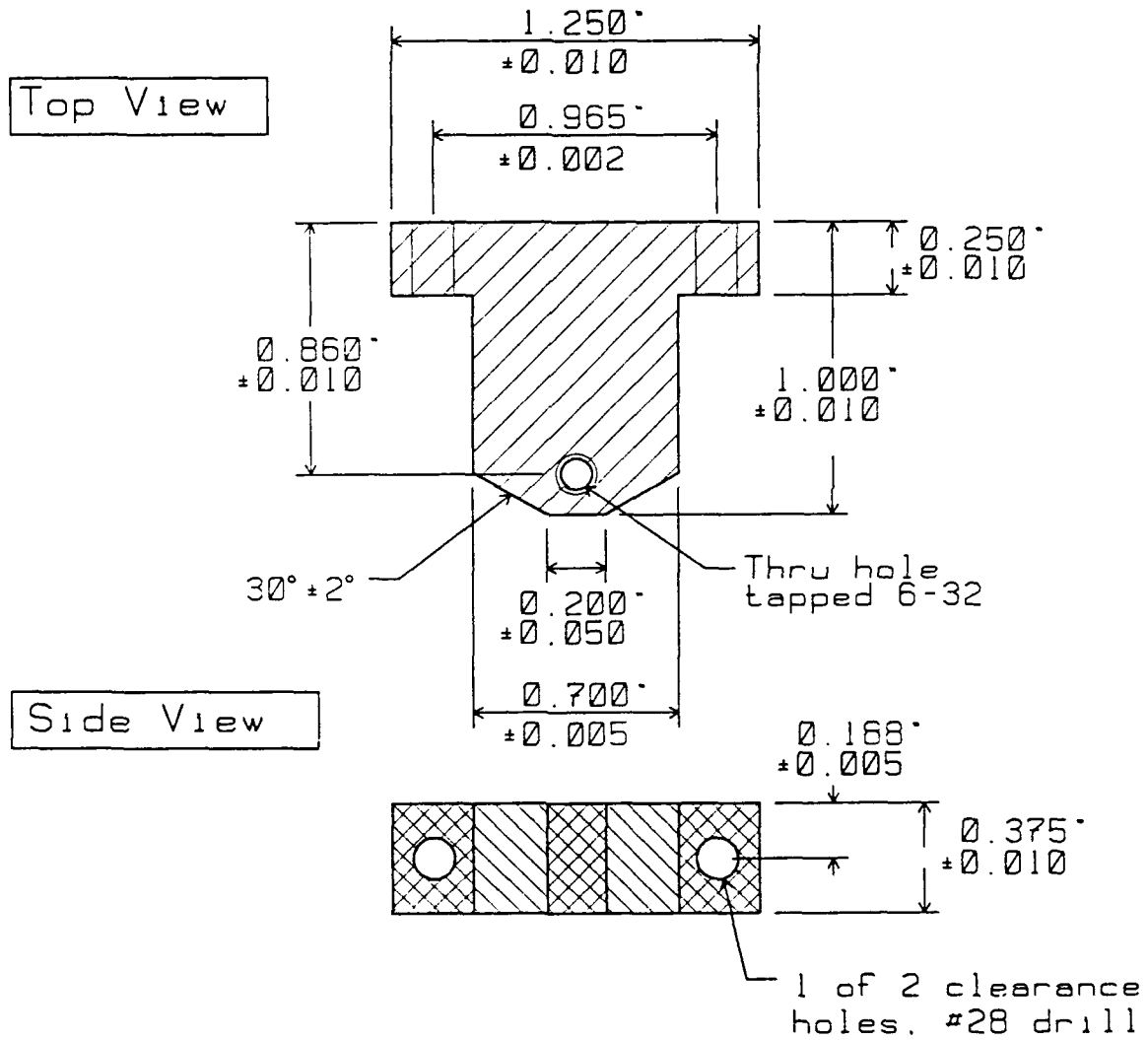
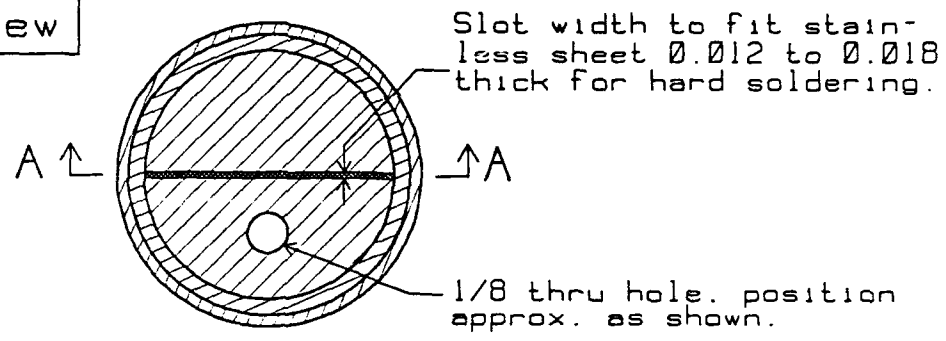


Figure D-18. Sheet Clamp

Top View



Sec. A-A

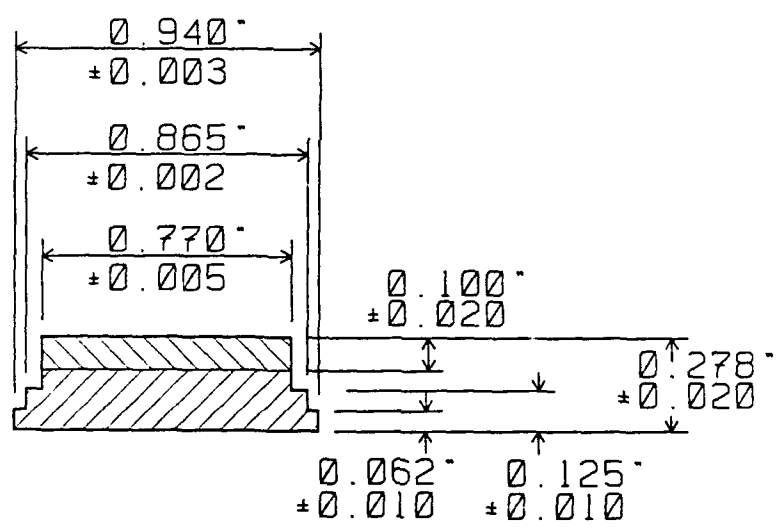


Figure D-19. Assembly Plug

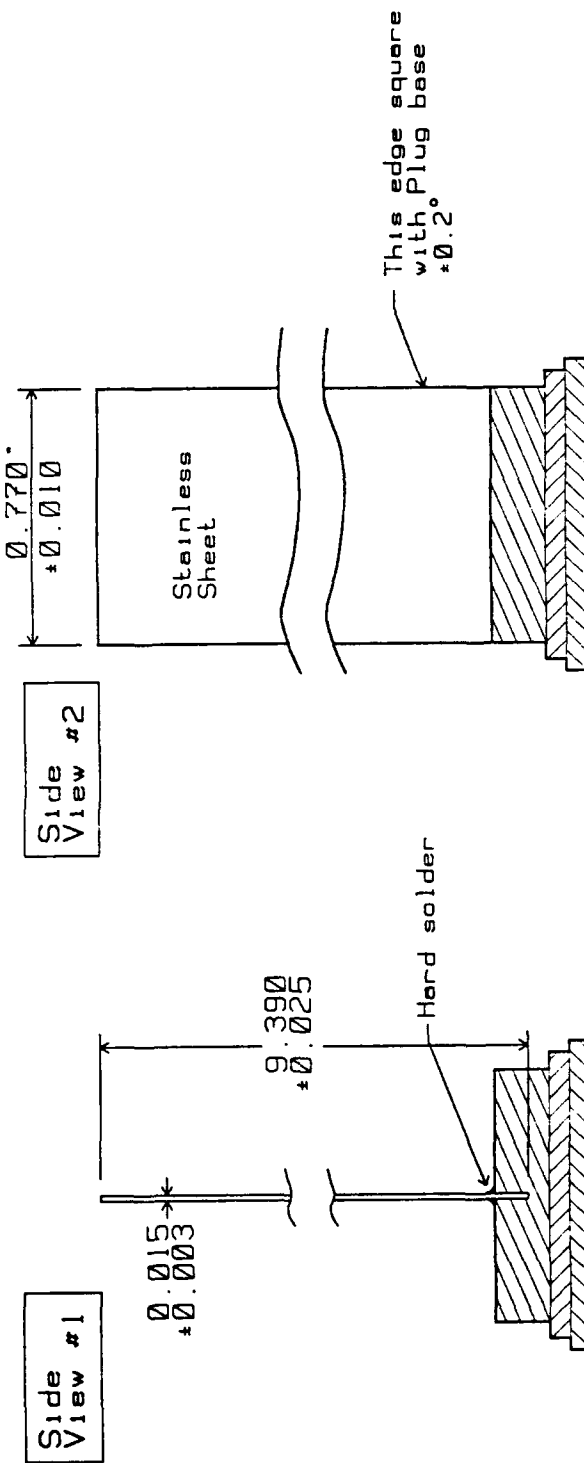
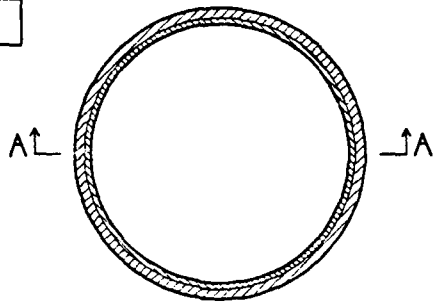


Figure D-20. Plug With Strip

Top View



Sec. A-A

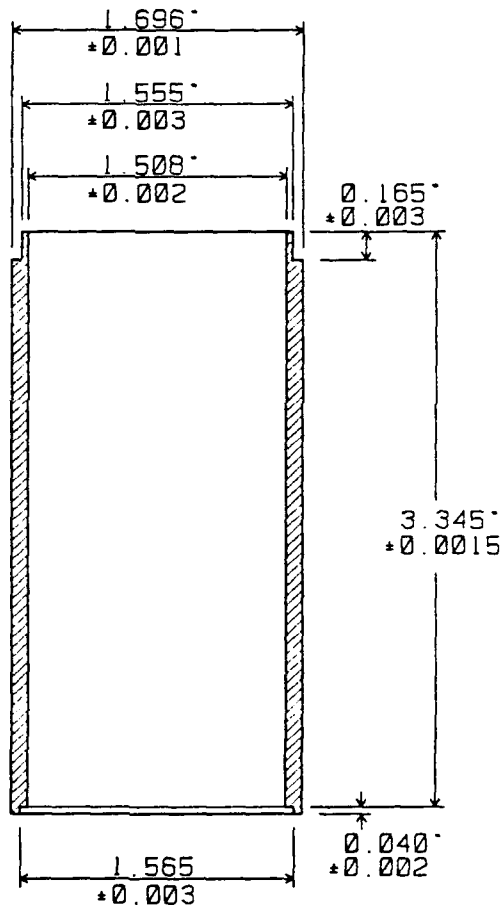
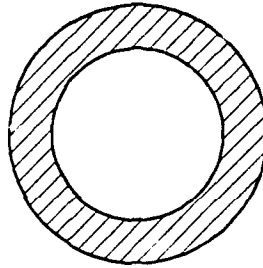


Figure D-21. Stainless Sleeve

Top View



Section

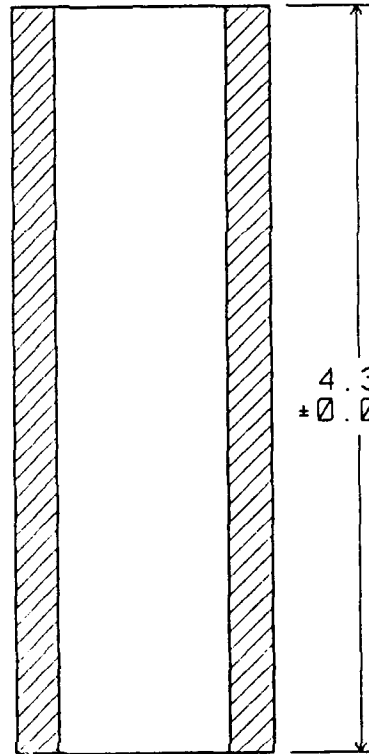
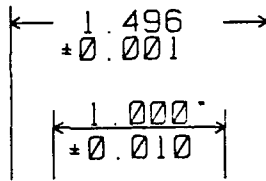


Figure D-22. Thermal Sleeve

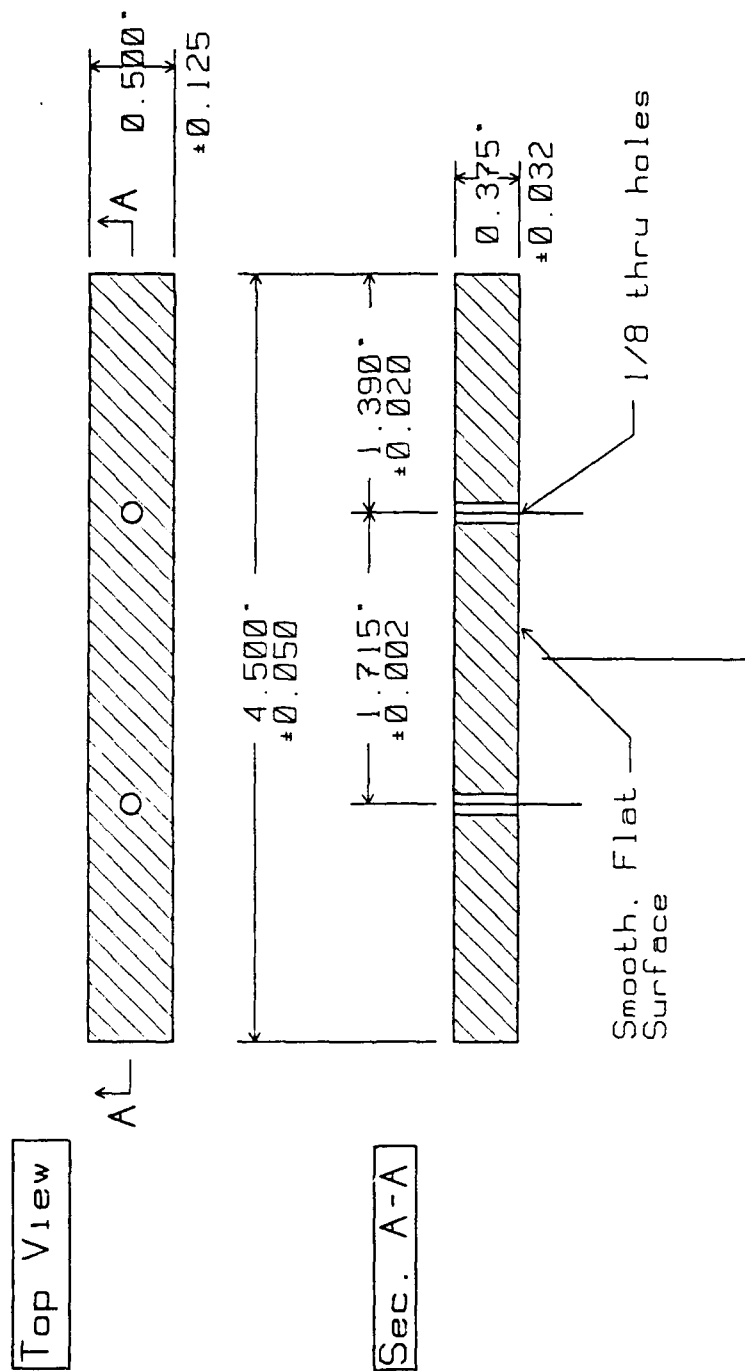


Figure D-23. Heat Exchanger Insert Extractor Tool

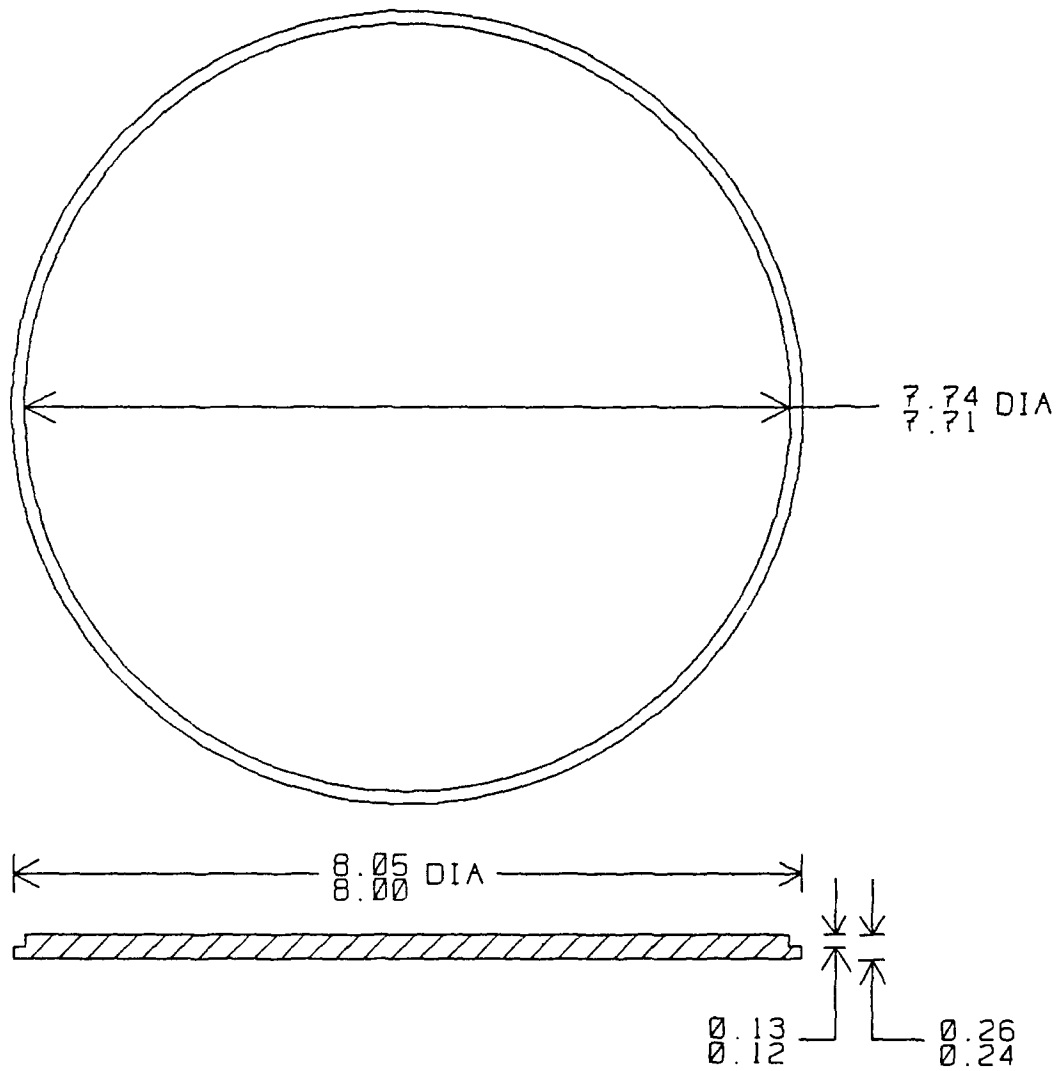


Figure D-25. Vacuum Cannister Base Plate

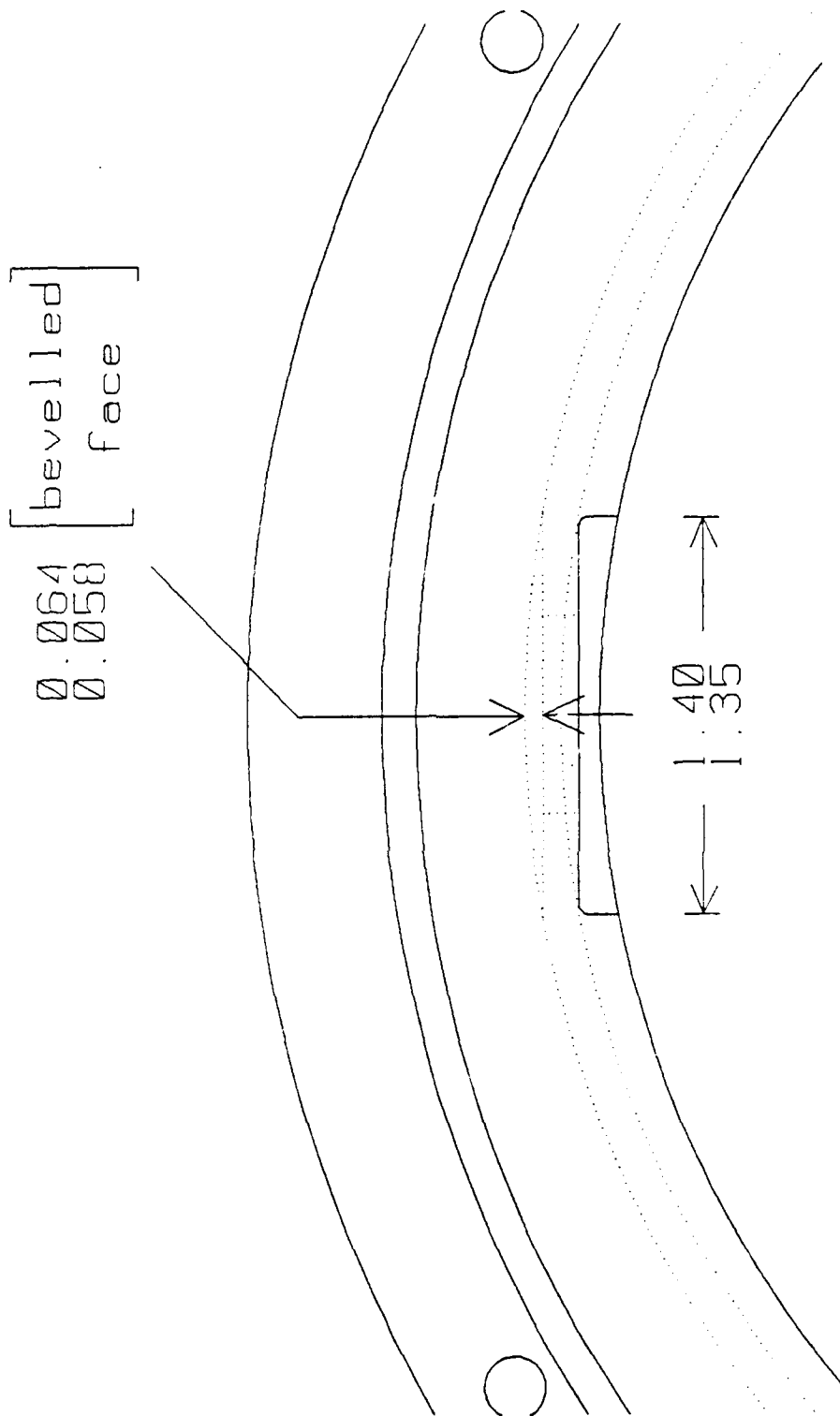


Figure D-26. Top View of Feed-Through

APPENDIX E

MANUFACTURER'S SPECIFICATIONS

This section contains specifications for the Omega E-type thermocouples used on the resonator, and the Dexter-Hysol EA 9396 two-part epoxy used on the fiberglass reinforced plastic (FRP) layer around the stainless steel helium diffusion shield.

GENERAL DESCRIPTION

The OMEGA™ Self-Adhesive thermocouples are designed for fast surface temperature measurements. These sensors are manufactured from 30 awg teflon coated thermocouple wire, with a ribbon type hot junction secured between a high temperature polymer and a high temperature, fiber-reinforced polymer, for good thermal conductivity and fast response. For easy installation, the probes have a self-adhesive backing, no epoxy or cement is required. SA1 thermocouples are supplied in a convenient 5 pack, for multiple applications, or for experimental uses.

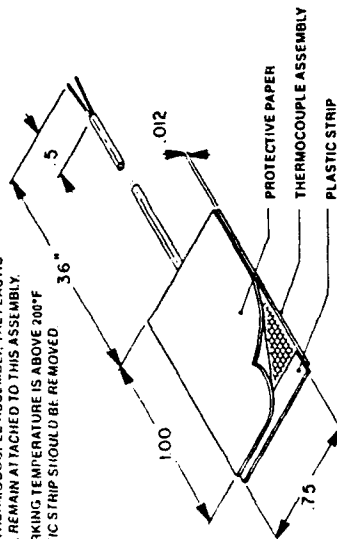
MODEL	THERMOCOUPLE TYPE
SA1 J	J Iron Constantan
SA1 K	K Chromel Alumel
SA1 E	E Chromel-Constantan
SA1 T	T Copper-Constantan

SPECIFICATIONS

T/C CALIBRATIONS:
 J (Iron-Constantan), K (Chromel-Alumel), T (Copper-Constantan), E (Chromel-Constantan)
ADHESIVE:
 Pressure sensitive silicone polymer
MAX. TEMPERATURE:
 500°F, continuous; 600°F for 1 hour
MIN. TEMPERATURE:
 -75°F, continuous
LAMINATES:
 High temperature polymer, and fiberglass reinforced polymer layers
WIRE:
 36" leads, 30 awg Teflon coated

OPERATION

AFTER PEELING THE PROTECTIVE PAPER FROM THE THERMOCOUPLE ASSEMBLY, THE PLASTIC STRIP WILL REMAIN ATTACHED TO THIS ASSEMBLY. IF THE WORKING TEMPERATURE IS ABOVE 200°F THE PLASTIC STRIP SHOULD BE REMOVED.



DEXTER HYSOL

EA 9396

AEROSPACE ADHESIVE PRODUCTS

DESCRIPTION

EA 9396 is a low viscosity, room temperature curing adhesive system with excellent strength properties at temperatures from -67°F to 350°F. EA 9396 has a shelf life of ten months when stored at 77°F for separate components.

FEATURES

- Low Viscosity
- Long Shelf Life at 77°F
- Cures at Room Temperature
- High Strength at Low and High Temperatures

UNCURED ADHESIVE PROPERTIES

	Part A	Part B	Mixed
Viscosity @ 77°F	800-1200 Poise	1 Poise	30-40 Poise
Shelf Life @ 77°F ($\bar{M}_w > 40,000$)	1 year 10 months	1 year 1 year	

This material will normally be shipped at ambient conditions, which will not affect our standard warranty, provided that the material is placed into its intended storage upon receipt. Premium shipment is available upon request.

HANDLING

Mixing - This product requires mixing two components together just prior to application to the parts to be bonded. Complete mixing is necessary. The temperature of the separate components prior to mixing is not critical, but should be close to room temperature.

Mix Ratio	Part A	Part B
By Weight	100	30

Note: Volume measurement is not recommended for structural applications unless special precautions are taken to assure proper ratios.

Pot Life (450 gm mass) 75-90 minutes
Method - ASTM D 2471 in water bath

APPLICATION

Mixing - Combine Part A and Part B in the correct ratio and mix thoroughly. **THIS IS IMPORTANT!** Heat buildup during or after mixing is normal. Do not mix quantities greater than 250 grams as dangerous heat buildup can occur causing uncontrolled decomposition of the mixed adhesive. **TOXIC FUMES CAN OCCUR, RESULTING IN PERSONAL INJURY.** Mixing smaller quantities will minimize the heat buildup.

Applying - Bonding surfaces should be clean, dry and properly prepared. For optimum surface preparation consult Hysol Bulletin G1-600 "Preparing the Surface for Adhesive Bonding". The bonded parts should be held in contact until the adhesive is set. Handling strength for this adhesive will occur in 24 hours at 77°F after which the support tooling or pressure used during cure may be removed. Since full bond strength has not yet been attained, load application should be small at this time.

Curing - EA 9396 may be cured for 5-7 days at 77°F to achieve normal performance. Accelerated cures of 1 hour at 150°F or at 180°F may be used.

Cleanup - It is important to remove excess adhesive from the work area and application equipment before it hardens. Denatured alcohol and many common industrial solvents are suitable for removing uncured adhesive. Consult with your supplier's information pertaining to the safe and proper use of solvents.

BOND STRENGTH PERFORMANCE

Tensile Lap Shear Strength Tensile lap shear strength tested per ASTM D 1002. Adherends are 2024-T3 clad aluminum treated with phosphoric acid anodize per BAC 5555. Values are expressed in PSI.

Test Temperature, °F	-67	75	180	300	350
Cure: 5 days @ 77°F	3300	4000	3200	1800	1500
1 hour @ 150°F	3300	4200	3300	1800	1200
30 min. @ 180°F	3500	4200	3300	1900	1200

Peel Strength

Bell Peel strength tested per ASTM D 3167 after curing for 5 days at 77°F. Adherends are 2024-T3 clad aluminum treated with phosphoric acid anodize per BAC 5555.

Test Temperature, °F	Typical Results (PLI)
77	25
180	20

Service Temperature

Service temperature is defined as that temperature at which this adhesive still retains 1000 PSI using test method ASTM D 1002 and is 300°F.

HAZARD WARNING

For Industrial Use Only!

PART A

CAUTION! The uncured adhesive causes eye irritation and may cause skin irritation as allergic dermatitis. Contains epoxy resins. Use good ventilation. Avoid contact with eyes or skin. Wash thoroughly with soap and water after handling. Do not handle or use until the Safety Data Sheet has been read and understood. Do not cut or weld empty container.

PART B

DANGER! Causes severe skin and eye burns. Do not get in eyes, on skin or on clothing. Wash thoroughly after handling. Vapors may be irritating to the respiratory tract. Avoid breathing vapor. Keep container tightly closed. Use only with adequate ventilation. Do not cut or weld empty container. Do not handle or use until Safety Data Sheet has been read and understood. These warnings are based on *Guides for Classifying and Labeling Epoxy Products According to Their Hazardous Potentialities* prepared by the Epoxy Resin Formulators Division and the Society of the Plastics Industry, Inc., and based on ANSI Z129 standard.

AVAILABILITY

This product is available from Hysol Aerospace and Industrial Products Division, 2850 Willow Pass Road, P.O. Box 312, Pittsburg, CA 94565-3299. Telephone 415 687-4201. TWX 910 387-0363

Revised 2-88

Properties listed are typical values and are not intended for use in engineering specifications. Actual values may vary. Recommendations and suggestions contained herein are intended as reasonable commercial use. No express warranties are intended by any representation and there are no warranties which extend beyond the description on the face hereof. The user is advised to use appropriate test and cure conditions when evaluating the adhesive and to be as representative as possible of those used in the actual manufactured item.

HYSOL

AEROSPACE & INDUSTRIAL PRODUCTS DIVISION

2850 Willow Pass Road, P.O. Box 312, Pittsburg, CA 94565
Phone (415) 687-4201, TWX 910 387-0363

A DIVISION OF THE SPECIALTY CHEMICALS & SERVICES GROUP
THE DEXTER CORPORATION

5 88 1M

REFERENCES

1. Harris, D.A., and Volkert, R.E., Design and Calibration of and Electrodynamic Driver for the Space Thermoacoustic Refrigerator, Masters Thesis, Naval Postgraduate School, Monterey, California, December 1989.
2. Byrnes, R.B., Electronics for Autonomous Measurement and Control of a Thermoacoustic Refrigerator in a Space Environment, Masters Thesis, Naval Postgraduate School, Monterey, California, December 1989.
3. Susalla, M.P., Thermodynamic Improvements for the Space Thermoacoustic Refrigerator, Masters Thesis, Naval Postgraduate School, Monterey, California, June 1986.
4. Hofler, T.J., Thermoacoustic Refrigeration Design and Performance, Ph.D. Dissertation, University of California, San Diego, California, 1986.
5. Swift, G.W., "Thermoacoustic Engines", Pages 1149-1160, The Journal of the Acoustical Society of America Vol. 84, No. 4, October 1988.
6. Reference Four, Figure 2.
7. Reference Five, Pages 1162-1164.
8. Reference Four, Chapter Two Part C.
9. Reference Four, Appendix C.
10. Reference One, Figures II-19, C-16, C-17, and C-18.
11. Fitzpatrick, M., Electrodynamic Driver for the Space Thermoacoustic Refrigerator (STAR), Masters Thesis, Postgraduate School, Monterey, California, March 1988. [DTIC Report No. ADA 192 337]
12. Reference Two, Figure B-1.
13. Reference Two, Chapter Three.
14. Reference One, Table II-2.

15. Polturak, E., Garrett, S.L., and Lipson, S.G.,
"Precision Acoustic Gas Analyzer for Binary Mixtures",
Review of Science Instrumentation, 57(11), November
1986.
16. Reference One, Figure IV-13.
17. Reference Three, Page 101.
18. Reference Four, Chapter VI Part A.
19. Reference Four, Chapter VI Part B.
20. Reference Three, Chapter five.
21. Reference Four, Figure 12A.

BIBLIOGRAPHY

Byrnes, R.B., Electronics for Autonomous Measurement and Control of a Thermoacoustic Refrigerator in a Space Environment, Masters Thesis, Naval Postgraduate School, Monterey, California, June 1989. [DTIC Report No. ADB 141 388]

Callen, H.B., Thermodynamics, John Wiley & Sons, Inc., 1962.

Fitzpatrick, M., Electrodynamic Driver for the Space Thermoacoustic Refrigerator (STAR), Masters Thesis, Naval Postgraduate School, Monterey, California, March 1988. [DTIC Report No. ADA 192 337]

Harris, D.A., Volkert, R.E., Design and Calibration of an Electrodynamic Driver for the Space Thermoacoustic Refrigerator, Masters Thesis, Naval Postgraduate School, Monterey, California, December 1989. [DTIC Report No. ADA 212 022]

Hofler, T.J., Thermoacoustic Refrigeration Design and Performance, Ph.D. Dissertation, University of California, San Diego, California, 1986.

Horowitz, P., and Hill, W., The Art of Electronics, Cambridge University Press, 1980.

Kinsler, L.E., Frey, A.R., Coppens, A.B., and Sanders, J.V., Fundamentals of Acoustics, Third Edition, John Wiley & Sons, Inc., 1982.

Lee, J.F., and Sears, F.W., Thermodynamics, Addison-Wesley Publishing Company, Inc., 1955.

Susalla, M.P., Thermodynamic Improvements for the Space Thermoacoustic Refrigerator (STAR), Masters Thesis, Naval Postgraduate School, Monterey, California, June 1988. [DTIC Report No. ADA 196 958]

Swift, G.W., "Thermoacoustic engines", The Journal of the Acoustical Society of America, Vol. 84, No. 4, October 1988.

Wheatley, J.C., Swift, G.W., and Migliori, A., "The Natural Heat Engine", Los Alamos Science, Number 14, Fall 1986.

INITIAL DISTRIBUTION LIST

1. Defense Technical Information Center 2
Cameron Station
Alexandria, Virginia 22304-6145
2. Library, Code 0142 2
Naval Postgraduate School
Monterey, California 93943-5002
3. Professor S.L. Garrett, Code Ph/Gx 6
Naval Postgraduate School
Monterey, California 93943-5002
4. Professor T.J. Hofler, Code Ph/Hf 3
Naval Postgraduate School
Monterey, California 93943-5002
5. Professor A.A. Atchley, Code Ph/Ay 1
Naval Postgraduate School
Monterey, California 93943-5002
6. Professor R. Panholzer, Code Sp/Pz 1
Naval Postgraduate School
Monterey, California 93943-5002
7. Mr. D. Rigmaiden, Space Systems 1
Naval Postgraduate School
Monterey, California 93943-5002
8. Mr. J. Adeff, Code Ph 3
Naval Postgraduate School
Monterey, California 93943-5002
9. Los Alamos National Laboratories
Condensed Matter and Thermal Physics (Group P-10)
ATTN; Dr. G.W. Swift 1
P.O. Box 1663/MS 764
Los Alamos, New Mexico 87545
10. Director 1
Navy Space Systems Division (OP-943)
Washington, District of Columbia 20350-2000
11. United States Space Command 1
ATTN: Technical Library
Peterson AFB, Colorado 80914

- | | | |
|-----|------------------------------------------------------------------------------------------------------------------------------------------------------------------------------------------------------------------------------------|---|
| 12. | Commanding Officer
Naval Research Laboratory
ATTN: E. Senasack (Code 8220)
P. Hastman (Code 8222)
T. Kawecki (Code 8222)
C. Merk (Code 8221)
4555 Overlook Avenue
Washington, District of Columbia 20375-5000 | 4 |
| 13. | Lt. S. Cobb
Space Test Program Office (SSD/CLFP)
HQ, Space Division
P.O. Box 92960
Los Angeles, California 90009-2960 | 1 |
| 14. | Office of Naval Research
Physics Division - Code 1112
ATTN: Dr. L.E. Hargrove
800 N. Quincy Street
Arlington, Virginia 22217 | 1 |
| 15. | Commander
Naval Space Command
ATTN: Code N155
Dahlgren, Virginia 22448 | 1 |
| 16. | United States Space Command
ATTN: Technical Library
Peterson AFB, Colorado 80914 | 1 |
| 17. | National Center for Physical Acoustics
ATTN: Librarian
Professor H.E. Bass
P.O. Box 847
Fraternity Row
University, Mississippi 38677 | 2 |